

Targeting DNA damage repair pathways in breast and ovarian cancers

Reem A. S. M. Ali

Thesis presented to

The University of Nottingham

For the degree of

Doctor of Philosophy

August 2019

Acknowledgements

I would like to express my deep gratitude to my supervisor Prof. Srinivasan Madhusudan for his advice and guidance throughout my research. He provided me with invaluable encouragement and support in various ways. I am really indebted to him.

I am also very grateful to Dr Abdolrahman Shams Nateri - I have learned a lot from him during my time in his lab. He generously gave me some of his invaluable time for training and advice.

I also want to express my sincere gratitude to Prof. Emad Rakha for all his invaluable advice and support. He never closes his door for any student who seeks advice.

My gratitude to those great scientists not only for their support to me during my research, but also because I learned from them research ethics and incredible enthusiasm and a lot of other things that enlightened my path.

I also would like to thank the Breast Pathology Group members, Dr Eslam Miligy, Dr Michael Toss and Mr. Abdoulbaqui Hawaz for the fruitful collaborations and collecting the DCIS cohort data.

I want to thank my colleagues in the Translational DNA Repair Group for their friendship and support.

Finally, I wish to express my deep gratitude to my lovely husband for taking a load off my shoulders during tough times and my family for their support and patience during this long research journey. I really appreciate it and could not have done it without their support.

Abstract

Background

DNA damage repair pathways are responsible for repairing DNA lesions and thus maintaining genomic integrity. Deficit in the DNA damage response is one of the hallmarks of cancers. Thus, drugs targeting DNA repair relying on this concept are rapidly under development. Targeting PARP1 for synthetic lethality is a novel strategy for *BRCA* germ-line mutated breast and ovarian cancers. However, *BRCA* germ-line mutations are rare and reactivation of BRCA mediated pathways may result in eventual resistance to PARP1 inhibitor therapy. Hence, developing alternative synthetic lethality approaches is an exciting area for future research.

Methods

In this study, we investigated XRCC1 and PARP1 expression in an invasive breast cancer cohort (n=1011) and pre-invasive ductal carcinoma *in situ* (DCIS) (n=776). We evaluated Olaparib and Talazoparib (PARP inhibitors) sensitivity in a panel of XRCC1 deficient and proficient breast cancer cell lines. In the MCF10-DCIS model we evaluated XRCC1 down regulation and epithelial to mesenchymal transition phenotype. We explored XRCC1 KO and Olaparib sensitivity. In the ovarian cancer cohort (n=525) we investigated the correlations between XRCC1 as well as PARP1 expression and clinicopathological outcomes. XRCC1 KO and Olaparib/Talazoparib sensitivity were tested in platinum sensitive and platinum resistant ovarian cancer cell lines in 2D and 3D models. Additionally, polβ and PARG protein expression and correlation with clinicopathological outcomes were investigated in our ovarian cancer cohort. We evaluated polβ depletion and platinum sensitivity in platinum-sensitive and platinum-resistant ovarian cancer cell lines. We tested polβ small molecule inhibitors (Pamoic acid & NSC666719) toxicity in BRCA2 deficient cells. We assessed Olaparib and PARG inhibitor (PDD00017273) lethality in polβ deficient ovarian cancer cells.

Results:

Low XRCC1/high PARP1 expression is associated with aggressive phenotype and poor breast cancer prognosis. In DCIS XRCC1 downregulation is an early event in human breast cancer pathogenesis. In XRCC1 deficient cell lines, Olaparib and Talazoparib were synthetically lethal in XRCC1 deficient breast cancer cell lines as well as MCF10-DCIS cells. PARPi induced cell cycle arrest at S-phase or G2/M phases in XRCC1 deficient breast cancer cells. Cell cycle arrest was dependent on p53 status. Additionally, PARP inhibition selectively induced DNA damage and apoptosis in XRCC1 deficient cells. In MCF10-DCIS XRCC1 knock out induced epithelial to mesenchymal transition phenotype. In 3D spheroids PARP inhibition abolished spheroid forming capacity in MCF10-DCIS(XRCC1_KO) but not in control cells. In ovarian cancers, high XRCC1 or high PARP1 levels were associated with aggressive phenotype and were significantly linked to poor progression free survival (PFS). PARP inhibitors remained selectively toxic in XRCC1 deficient platinum- sensitive ovarian cancer cell lines. PARPi cytotoxicity was associated with DSBs formation, cell cycle arrest and apoptosis in XRCC1 deficient cells. Polβ expression was a predictor of platinum sensitivity in ovarian cancer patients. Polβ depletion not only increased platinum sensitivity but also reduced invasion and migration in ovarian cancer cell lines. Polβ small molecule inhibitors were selectively toxic in BRCA2 deficient cells in 2D as well as 3D spheroids models. High polβ and high PARG co-expression correlated with poor PFS as well as overall survival in ovarian cancer. PARG inhibitor but not Olaparib were selectively toxic in polβ deficient ovarian cancer cells. Polβ-PARG co-expression adversely impacted survival in patients.

Conclusions:

PARP1 targeting is an attractive synthetic lethality strategy and chemoprevention in XRCC1 deficient breast cancers and pre-invasive DCIS lesions. In ovarian cancers XRCC1 deficiency is a biomarker for PARP inhibitor sensitivity. Targeting PARP1 in XRCC1 deficient ovarian cancers is an alternative synthetic lethality approach for PARPi in clinics. Similarly,, our data demonstrates that development of polβ inhibitors could be of clinical benefit to ovarian cancer patients. Polβ depletion

can re-sensitize ovarian cancer patients to platinum. Polβ targeting in BRCA2 deficient ovarian cancers is an attractive synthetic lethality. PARG inhibitors could have a clinical application in targeting Polβ deficient ovarian tumours. Our results could have a valuable therapeutic potential in personalizing breast and ovarian cancers' therapy.

Thesis Related Publications

Ali R, Al-Kawaz A, Toss MS, Green AR, Miligy IM, Mesquita KA, Seedhouse C, Mirza S, Band V, Rakha EA, Madhusudan S (2018) 'Targeting PARP1 in XRCC1-Deficient Sporadic Invasive Breast Cancer or Preinvasive Ductal Carcinoma In Situ Induces Synthetic Lethality and Chemoprevention.', *Cancer Research,* 78(24), pp. 6818-6827.

Ali, R.*, Alabdullah, M.*, Alblihy, A., Miligy, I., Mesquita, K., Chan, S., Moseley, P., Rakha, E. and Madhusudan, S. (2019). PARP1 blockade is synthetically lethal in XRCC1 deficient sporadic epithelial ovarian cancers. *Cancer Letters*, 469, pp.124-133.

Ali R., Alblihy A., Miligy I.,Alabdullah M., Alsaleem M., Toss M., Abdel-Fatah T., Moseley T., ChanS.,Mongan N., Narayan S., Rakha E., and Madhusudan S. 'Distruption of DNA polymerase β for platinum sensitization and synthetic lethality in epithelial ovarian cancers' Oncogene (accepted, *in press*)

Other Publications

Ali, R., Alabdullah, M., Miligy, I., Normatova, M., Babaei-Jadidi, R., S. Nateri, A., Rakha, E. and Madhusudan, S. (2019). ATM Regulated PTEN Degradation Is XIAP E3 Ubiquitin Ligase Mediated in p85α Deficient Cancer Cells and Influence Platinum Sensitivity. *Cells*, 8(10), p.1271.

Abdel-Fatah, T., **Ali, R.,** Sadiq, M., Moseley, P., Mesquita, K., Ball, G., Green, A., Rakha, E., Chan, S. and Madhusudan, S. (2019). ERCC1 Is a Predictor of Anthracycline Resistance and Taxane Sensitivity in Early Stage or Locally Advanced Breast Cancers. *Cancers*, 11(8), p.1149.

Ali R., Rakha E., Madhusudan S., and Bryant H., (2017)'DNA damage repair in breast cancer and its therapeutic implications' Pathology, 49(2), pp.156-165.

Savva C, De Souza K, **Ali R.**, Rakha E., Green A., and Madhusudan S(2019). ‘Clinicopathological significance of ataxia telangiectasia-mutated (ATM) kinase andataxia telangiectasia-mutated and Rad3-related (ATR) kinase in MYC overexpressed breast cancers'. *Breast Cancer Research and Treatment*.

Barone G., Arora A., Ganesh A., Abdel-Fatah T., Moseley P., **Ali R.**, Chan SY., Savva C., Schiavone K., Carmell N., Myers KN., Rakha EA., Madhusudan S., Collis SJ. (2018) 'The relationship of CDK18 expression in breast cancer to clinicopathological parameters and therapeutic response', *Oncotarget,* 9(50), pp. 29508-29524.

Al-Subhi N., **Ali R.**, Abdel-Fatah T., Moseley PM., Chan SYT., Green AR., Ellis IO., Rakha EA., Madhusudan S. (2017) 'Targeting ataxia telangiectasia-mutated- and Rad3-related kinase (ATR) in PTEN-deficient breast cancers for personalized therapy', *Breast Cancer ResTreat.,* 162(2), pp. 277-286.

Green AR., Aleskandarany MA., **Ali R.**, Hodgson EG., Atabani S., De Souza K., Rakha EA., Ellis IO., Madhusudan S. (2017) 'Clinical Impact of Tumor DNA Repair Expression and T-cell Infiltration in Breast Cancers.', *Cancer Immunol Res.,* 5(4), pp. 292-299.

Reem Ali & Srinivasan Madhusudan (2017) 'Prognostic and Predictive Significance of Base Excision Repair in Human Cancers: Molecular Mechanisms and Role in Disease Development and Therapeutic Design', in David.M.Wilson III (ed.) *The Base Excision Repair pathway*.

Abbreviations

Abbreviation	Definition
ARID1A	AT-rich interactive domain containing protein 1A.
BARD1	BRCA Associated Ring Domain 1
BER	Base excision repair
BRCA1/2	Breast cancer susceptibility gene 1/2
BRCT	BRCA1 C-terminal
BRIP1	BRCA Interacting Protein C-terminal Helicase1
CHEK1/2	Checkpoint kinase 1/2
CSA/ CSB	Cockayne syndrome proteins A/B
DCIS	Ductal carcinoma *in-situ*
ER	Estrogen receptor
FAM175A	Family with sequence similarity 175, member A
FEN1	Flap endonuclease 1
GGR-NER	Global genome repair
GRB7	Growth factor receptor bound protein 7
HDR	Homology-directed Fanconi Anaemia pathway
HER	Human epidermal growth factor receptor 2
HR	Homologous recombination
LDLRAP1	Low density lipoprotein receptor adaptor protein 1
MMR	Mismatch repair pathway
MRE11	Meiotic Recombination Homolog 11
NAD	Nicotinamide adenine dinucleotide
NCOR1	Nuclear receptor co-repressor 1
NER	Nucleotide excision repair
NFKβ	Nuclear factor kappa beta
NHEJ	Non-homologous end-joining
NPI	Nottingham prognostic index
OS	Overall survival

PALB2	Partner and localizer of BRCA2
PARG	Poly (ADP-ribose) glycohydrolase
PARP	Poly (ADP-ribose) polymerases
PDGFRβ	Platelet derived growth factor receptor -beta
PFS	Progression free survival
PIK3CA	Phosphoinositide -3 kinase/ catalytic alpha polypeptide
Polβ	DNA polymerase β
PR	Progesterone receptor
RFC	Replication factor C
RUNX1	RUNT- related transcription factor 1
SMARCD1	SWI/SNF related matrix associated actin dependent regulator of chromatin subfamily D1
TBX3	T-box transcription factor3
TCR-NER	Transcription-coupled repair
TFIIH	Transcription factor II H
TIMP1	Tissue inhibitor of metalloproteinases 1
TNBC	Triple negative breast cancer
TNK1/2	Tankyrase 1 /2
TNM	Tumour, lymph node and metastasis.
XL1	XRCC1 linker 1
XPG/XPF	Xeroderma pimentossum G/F
XRCC1	X-ray repair cross-complementing protein 1

Table of Contents

Acknowledgement..... 2

Abstract..... 3

Thesis related publications..... 6

Abbreviations 8

1 Introduction 20

1.1 Breast cancer 21

1.1.1 Epidemiology of breast cancer 21

1.1.2 Breast cancer mortality and risk factors 22

1.1.3 Molecular intrinsic subtypes of breast cancer 24

1.1.4 Breast cancer staging 25

1.1.5 Molecular profiling of breast cancer 25

1.2 Ductal carcinoma *in situ* 27

1.2.1 Epidemiology of DCIS 27

1.2.2 Prognostic markers for DCIS recurrence 28

1.2.3 Oncotype DX for DCIS risk stratification 29

1.3 Ovarian Cancer 31

1.3.1 Epidemiology of ovarian cancer 31

1.3.2 Ovarian cancer subtypes 31

1.3.3 Ovarian cancer staging 34

1.3.4 Molecular profile of ovarian cancer 35

1.4 Overview of DNA damage response 39

1.4.1 DNA damage response signalling 40

1.5 Overview of DNA repair pathways 44

1.5.1 Mismatch repair pathway 44

1.5.2 Double strand breaks repair pathways 46

1.5.3 BRCA role in DDR and cancers 49

1.5.4 Overview of the Base excision repair pathway 51

1.5.5 XRCC1 structure and function 54

1.5.6 XRCC1 polymorphism and cancers 56

1.6 Nucleotide excision repair pathway 58

1.7 Poly (ADP-ribose) polymerases (PARPs) and their inhibition 61

1.7.1 Structure and functions of PARP1 61
1.7.2 Other members of the PARP family 63
1.7.3 Mechanisms of resistance to PARP inhibitors 65
1.7.3.1 Other mechanisms for PARPi resistance 67
1.8 DNA polymerases: 70
1.8.1 Translesion polymerases 70
1.8.2 DNA polymerase Beta (Polβ) 72
1.9 Hypothesis 76
1.10 Objectives 78
2 Materials and Methods 80
2.1 Materials: 80
2.1.1 Compounds 81
2.1.2 Cell lines: 82
2.2 Methods 83
2.2.1 Clinical studies 84
2.2.1.1 Breast cancer study 84
2.2.1.2 DCIS study cohort 86
2.2.1.3 Ovarian cancer study cohort 88
2.2.2 Tissue microarray construction 91
2.2.3 Immunohistochemical staining 92
2.2.3.1 Antigen retrieval and staining 92
2.2.4 Optimisation of immunostaining conditions 95
2.2.5 Evaluation of immune staining 95
2.2.6 Statistical analysis of immunohistochemical data 96
2.2.7 Sub-culturing of cell lines: 96
2.2.8 Cryopreservation of cell lines: 97
2.2.9 Transient transfection of cell lines by siRNA: 97
2.2.10 Generation of CRISPR Cas-9 knock out 99
2.2.11 Preparation of cell lysates: 100
2.2.12 BCA protein quantification assay 100
2.2.13 Western blotting 101
2.2.13.1 Transfer 102
2.2.13.2 Blocking 102
2.2.13.3 Primary antibody incubation 102
2.2.13.4 Secondary antibody incubation 103

2.2.13.5 Detection and analysis 103
2.2.14 Cell proliferation assay (MTS assay) 104
2.2.15 Clonogenic survival assay 105
2.2.15.1 Assay principle 105
2.2.15.2 Plating efficiency 105
2.2.15.3 Clonogenic assay protocol 106
2.2.16 Cell cycle analysis and γ H2AX assay 106
2.2.16.1 Assay principle 106
2.2.16.2 Assay protocol 107
2.2.17 Apoptosis detection by Annexin V assay 110
2.2.17.1 Assay principle 110
2.2.17.2 Assay protocol 110
2.2.18 Invasion assay 112
2.2.19 Migration assay 113
2.2.20 Immunofluorescence staining 114
2.2.21 Generation of 3D Spheroids 117
2.2.21.1 Spheroids staining 117
2.2.22 NAD assay 118
2.2.22.1 Assay principle 118
2.2.22.2 Assay protocol 119
2.2.23 Statistical analysis 120
3 XRCC1 in invasive breast cancers 121
3.1 Introduction 122
3.2 Methodology 126
3.3 Results 128
3.3.1 Clinical Data 128
3.3.1.1 XRCC1-PARP1 co-expression influences the outcome of breast cancer prognosis 128
3.3.2 Selective Olaparib toxicity in XRCC1 deficient cell lines 133
3.3.3 Methylation of XRCC1 gene in MDA-MB-157 cell line 134
3.3.4 Olaparib affects cell cycle progression in XRCC1 deficient cell lines 137
3.3.5 Nutlin3a can influence cell cycle arrest in p53 mutant cell lines treated with Olaparib 139
3.3.6 Accumulation of DSBs and apoptotic cells upon Olaparib treatment 142

3.3.7 Immunofluorescence for PARP1 and γH2AX foci formation in XRCC1 deficient and proficient cells upon Olaparib treatment. 144
3.3.8 Olaparib induces lethality in XRCC1 deficient spheres 146
3.3.9 Sensitivity of XRCC1 deficient cells to other PARP1 inhibitors..... 147
3.3.10 Immunefluoresence for PARP1 trapping in Talazoparib treated cells 149
3.4 Discussion 153
4 Chapter 4: Olaparib as a chemo-preventative strategy for treatment of Ductal carcinoma in-situ..... 159
4.1 Introduction 160
4.2 Methodology 164
4.3 Results..... 165
4.3.1 Clinical Data 165
4.3.1.1 XRCC1 expression in DCIS..... 165
4.3.2 Pre-clinical data: 170
4.3.2.1 XRCC1 in breast cell lines 170
4.3.2.2 Generation of XRCC1 CRISPR knock–out..... 172
4.3.2.3 MCF10-DCIS_XRCC1_KO is sensitive to Olaparib 174
4.3.2.4 Functional studies for Olaparib sensitivity in MCF10-DCIS (XRCC1_KO)..... 175
4.3.2.5 Loss of XRCC1 expression affected the phenotype of MCF10-DCIS..... 176
4.3.2.6 Evaluation of epithelial to mesenchymal phenotype in MCF10-DCIS (XRCC1_KO) 177
4.3.2.7 Morphology of MCF10-DCIS(XRCC1_KO) 187
4.3.2.8 Olaparib as a chemo preventative in MCF10-DCIS(XRCC1_KO) 3D spheres 188
4.4 Discussion 189
5 Chapter 5 XRCC1 in Ovarian cancers 194
5.1 Introduction 195
5.2 Methodology 199
5.3 Results..... 201
5.3.1 Clinical Data 201
5.3.1.1 XRCC1 expression influences patient survival in ovarian cancers..... 201
5.3.1.2 PARP1 expression affects ovarian cancer patients' survival in the platinum sensitive cohort. 208
5.3.2 Pre-clinical data 214
5.3.2.1 XRCC1 SiRNA in ovarian cancer cell lines 214
5.3.2.2 Olaparib is toxic in XRCC1 deficient cisplatin sensitive ovarian cell lines..... 216

5.3.2.3 XRCC1 CRISPR knock out in A2780 cells 219
5.3.3 Validation of cytotoxicity of PARP inhibitors in XRCC1 deficient ovarian cells using Talazoparib. 221
5.4 Discussion 227
6 Chapter6: Targeting DNA polymerase Beta in ovarian cancers 231
6.1 Introduction 232
6.2 Methodology 235
6.3 Results 237
6.3.1 Clinical Data 237
6.3.1.1 Polβ expression in ovarian tumours 237
6.3.2 Pre-clinical Data 242
6.3.2.1 Polβ expression in ovarian cell lines 242
6.3.2.2 Polβ knock-down in A2780cis cells 245
6.3.2.3 Mesenchymal to epithelial transition phenotype in polβ_knock out cells. 256
6.3.2.4 Polβ depletion induces synthetic lethality in BRCA2 deficient ovarian cells 262
6.3.2.5 Synthetic lethality of pamoic acid in BRCA2 deficient PE01 cells 264
6.3.2.6 Evaluation of pamoic acid synthetic lethality in HeLa BRCA2 deficient cells 265
6.3.2.7 Evaluation of NSC666719 polβ small molecule inhibitor for synthetic lethality in BRCA2 deficient cells 267
6.3.2.8 Synthetic lethality of polβ inhibitors in 3D spheroid models of BRCA2 deficient cells 268
6.3.2.9 Evaluation of Olaparib effect in polβ deficient ovarian cancer cells 270
6.3.2.10 Clinicopathological significance of PARG expression in human ovarian tumours 277
6.4 Discussion 283
7 General Discussion 288
7.1 Future directions 297
8 References 300

List of Figures

Figure 1-1: DNA damage response signalling……..42
Figure 1-2: MMR pathway……45
Figure 1-7: An overview of PARP family functions.....65
Figure 2-1: pLV-U6g-EPCG map. 100
Figure 2-2: γH2AX analysis by weasel software. 108
Figure 2-3: Representative figures of cell cycle analysis in weasel software.....109
Figure 3-1: Representative photo micrographic image of XRCC1 & PARP1 expression in tumours. 129
Figure 3-2: Kaplan-Meier curve for breast cancer-specific survival.....129
Figure 3-3: Kaplan-Meier curve for breast cancer-specific survival.....132
Figure 3-4: XRCC1expression by western blot. 134
Figure 3-5: Olaparib sensitivity in XRCC1 deficient cell lines. 134
Figure 3-6: XRCC1 levels in 157 and 231. 136
Figure 3-7: Cell cycle analysis by flow cytometry. 136
Figure 3-8: Cell cycle synchronization in the various cell lines. 138
Figure 3-9: p53 mutations and post-translational modification profiling 139
Figure 3-10: Cell cycle analysis in Nutlin treated cells. 140
Figure 3-11: γH2AX analysis by flow cytometry 141
Figure 3-12: the percentage of apoptotic cells analysed by flow cytometry. 142
Figure 3-13: Immunofluorescence for γH2AX and PARP1 levels in 231, 231_XRCC1_KO cells and 157 treated with Olaparib. 144
Figure 3-14: Mean fluorescence intensity quantification by ImageJ for PARP1 and γH2AX at the indicated time points. 145
Figure 3-15: Olaparib sensitivity in 3D spheroids of XRCC1 deficient cells. 146
Figure 3-16: Clonogenic survival assay for XRCC1 deficient cells with Niraparib and Talazoparib. 147
Figure 3-18: PARP1 and γH2AX nuclear fluorescence quantification by ImageJ software. 150
Figure 3-19: 3D spheroids of XRCC1 deficient cells treated with Talazoparib. 151

Figure 3-20: Functional studies of Talazoparib treatment in MDA-MB-231 control and XRCC1_KO. 152
Figure 4-1: XRCC1 expression in TMAs. 165
Figure 4-2: XRCC1 expression and local recurrence free interval in DCIS. 169
Figure 4-3: Box plot showing XRCC1 expression. 170
Figure 4-4: XRCC1 expression in breast cell lines. 170
Figure 4-5: Invasion assay in MCF10-DCIS, MCF-10A and MDA-MB-231. 171
Figure 4-6: Western blot for XRCC1 CRISPR _KO. 172
Figure 4-7: PARP1 expression in MCF10-DCIS(XRCC1_KO). 173
Figure 4-8: Olaparib sensitivity in MCF10-DCIS(XRCC1_KO). 174
Figure 4-9: Functional studies for Olaparib in MCF10-DCIS (XRCC1_KO). 175
Figure 4-10: Cell proliferation assay for MCF10-DCIS control and XRCC1_KO. 176
Figure 4-11: Representative images of Invasion assay in MCF10-DCIS control and XRCC1_KO. 177
Figure 4-13: Morphology of MCF10-DCIS (control) and MCF10-DCIS (XRCC1_KO). 187
Figure 4-14: Representative photomicrographic images of 3D spheroids. 188
Figure 5-1: Kaplan Meier curve for XRCC1 expression. 201
Figure 5-2: Immunohistochemical expression of XRCC1 and PARP1 in ovarian cancers. . 201
Figure 5-3: Kaplan Meier curve for XRCC1 expression in platinum sensitive patients. 202
Figure 5-4: Kaplan Meier curve for PARP1 expression. 208
Figure 5-6: Kaplan Meier curve for PARP1 expression in platinum resistant patients. 209
Figure 5-9: PARP1 expression in XRCC1_KD cells. 215
Figure 5-10: Clonogenic survival assay for Cisplatin and Olaparib in ovarian cells. 216
Figure 5-11: Clonogenic survival assay for Cisplatin and Olaparib in OVCAR3 cells. 217
Figure 5-12: Functional studies of Olaparib sensitivity in XRCC1_KD ovarian cells. 218
Figure 5-13: Western blot for XRCC1_KO and quantification in A2780 cells. 219
Figure 5-14: Clonogenic survival assay for A2780 (XRCC1_KO) in different doses of Olaparib. 220
Figure 5-15: Functional studies for Olaparib sensitivity in A2780 (XRCC1_KO). 220
Figure 5-17: Functional studies for Talazoparib sensitivity in A2780 (XRCC1_KO). 222
Figure 5-18: Clonogenic survival assay for PARG inhibitor sensitivity in A2780(XRCC1_KO) cells. 223
Figure 5-19: Functional studies for PARG inhibitor in A2780 (XRCC1_KO). 224
Figure 5-20: Spheroids of ovarian cells treated with Olaparib, Talazoparib and PDD00017273. 225

Figure 5-21: Invasion and migration assay in A2780 (XRCC1_KO). 226
Figure 6-1: Polβ immunohistochemical expression in ovarian tumours. 237
Figure 6-2: Kaplan Meier curve for polβ expression in ovarian tumours. 237
Figure 6-3: Kaplan Meier curve for polβ expression in platinum sensitive tumours. 238
Figure 6-4: Kaplan Meier curve and Polβ expression in platinum resistant tumours. 239
Figure 6-5: *polβ* mRNA expression in ovarian tumours. 241
Figure 6-6: *Polβ* mRNA expression and overall survival in ovarian tumours. 241
Figure 6-7: Polβ protein expression in A2780 and A2780cis ovarian cell lines. 242
Figure 6-8: *Polβ* mRNA expression in A2780 and A2780cis cells treated with cisplatin. .. 243
Figure 6-9: Nuclear and cytoplasmic extraction of A2780 and A2780cis cells. 244
Figure 6-10:Polβ nuclear localization by immunofluorescence. 244
Figure 6-11: Polβ siRNA knock-down. 245
Figure 6-12: Cisplatin sensitivity in A2780cis control and polβ _KD. 246
Figure 6-13: Functional studies of cisplatin response in polβ knockdown cells. 248
Figure 6-14: Replication stress in A2780cis_polβ _KD cells. 248
Figure 6-15: Clonogenic survival assay for ATRi and CHK1i in polβ _KD cells. 249
Figure 6-16: Polβ knock-out in A2780cis cells. 249
Figure 6-18: Immunofluorescence staining for γH2AX and 53BP1 in A2780cis cells. 250
Figure 6-20: Functional studies for cisplatin sensitivity in PEO4_polβ_KD cells. 252
Figure 6-22: Polβ siRNA knockdown in A2780 cells. 253
Figure 6-23: Functional studies for cisplatin sensitivity in A2780_polβ_KD cells. 254
Figure 6-24: Polβ CRISPR_KO in A2780 cells. 255
Figure 6-25: Functional studies of cisplatin sensitivity in A2780_polβ _KO cells. 255
Figure 6-26: Immunofluorescence for γH2AX and 53BP1 nuclear staining in A2780 cells. 256
Figure 6-28: Migration assay in polβ _KO cells. 258
Figure 6-29: Western blots for E-cadherin, N-cadherin, TGFβ and MMP-9 in A2780 and A2780cis control and polβ _KO cells. 259
Figure 6-30: RT2 PCR profiler for EMT genes in A2780 control and polβ_KO. 259
Figure 6-32: Synthetic lethality of polβ knockdown in BRCA2 deficient cells. 262
Figure 6-33: Functional studies of polβ synthetic lethality with BRCA2. 263
Figure 6-34: Pamoic acid sensitivity in PE01 and PE04. 264
Figure 6-35: Functional study of pamoic acid synthetic lethality in PE01 cells. 265
Figure 6-36: Pamoic acid sensitivity in HeLa BRCA2 deficient cells. 265

Figure 6-37: Functional studies for pamoic acid sensitivity in HeLa BRCA2 deficient cells. 266
Figure 6-38: NSC666719 sensitivity in PE01 and PE04 cells. 267
Figure 6-39: Functional study of NSC666719 synthetic lethality in PE01 cells. 268
Figure 6-40: Polβ inhibitors in 3D spheroids of PE01 and PE04 cells. 268
Figure 6-41: polβ inhibitors in 3D spheroids of HeLa control and HeLa_BRCA2_KD. 269
Figure 6-42: Olaparib treatment in polβ _KO cells. 271
Figure 6-43: PDD0017273 sensitivity in Polβ deficient cells. 271
Figure 6-44: PAR and PARP1 protein levels in polβ _KO cells. 272
Figure 6-45: Western blot for PAR levels in treated polβ _KO cells. 273
Figure 6-46: Immunofluorescence of PAR in A2780 control and A2780(polβ _KO) cells. 274
Figure 6-47: NAD+ assay in polβ deficient and proficient cells treated with PARGi. 275
Figure 6-48: Functional studies of PARGi sensitivity in A2780 control and polβ _KO cells. 276
Figure 6-49: Functional studies for PARGi sensitivity in A2780cis (polβ_KO) cells. 276
Figure 6-51: PARG expression in human ovarian cancers. 277
Figure 6-52: Kaplan Meier curve for PARG expression in the whole cohort. 279
Figure 6-53: Kaplan Meier curve and PARG expression in the platinum sensitive cohort. 280
Figure 6-54: Kaplan Meier curve and PARG expression in the platinum resistant cohort. 280

List of tables

Table 1-1: List of genes in the Oncotype DX DCIS and their score. 30
Table 1-2: Histological subtypes of epithelial ovarian cancers. 32
Table 1-3: FIGO staging for ovarian cancers. 34
Table 1-5. Recent clinical trials of PARP inhibitors 68
Table 2-1: Cell lines and their culture conditions. 82
Table 2-2: Clinicopathological characteristics of breast cancer patients' cohort. 85
Table 2-3: Patient demographics in the DCIS cohort. 87
Table 2-4: Ovarian cancer cohort patients demographics 89
Table 2-5: Antibodies for immunohistochemistry. 94
Table 2-6: siRNA constructs and their sequences. 98
Table 2-7: Antibodies used in western blot and immunofluorescence studies. 115
Table 3-1. Clinicopathological significance of XRCC1and PARP1in breast cancers 130
Table 3-2: LD50 for PARP1 inhibitor sensitivity in XRCC1 deficient cells. 148
Table 4-1: Patients demographics in DCIS cohort. 166
Table 4-2: XRCC1 and clinicopathological associations in pure DCIS cohort. 167
Table 4-3: List of EMT PCR array gene layout. 179
Table 5-1: Ovarian cancer patient demographics. 203
Table 5-2: XRCC1 expression and ovarian cancer. 206
Table 5-3: PARP1 expression and ovarian cancer. 210
Table 5-4: XRCC1/PARP1 co-expression in ovarian cancer. 212
Table 5-5: XRCC1/ PARP1 multivariate analysis. 214
Table 6-1: Polβ expression and clinico-pathological associations. 240
Table 6-2:Polβ /PARG co-expression and clinicopathological associations. 278
Table 6-3: Multivariate analysis for polβ , PARG and platinum sensitivity. 279
Table 6-4: PARG expression and clinico-pathological associations. 282

1 Introduction

1.1 Breast cancer

1.1.1 Epidemiology of breast cancer

Breast cancer is the most common cancer targeting women worldwide. It is also the leading cause of cancer- related deaths in women. The incidence of new diagnosed cases was 127.5 per 100,000 women per year according to the National Cancer Institute Surveillance, Epidemiology and End Result program (SEER) data base report on 2012-2016. The rate of breast cancer diagnosis is approximately 12.8 percent of women per year based on 2014-2016 SEER data (https://seer.cancer.gov). In the US, the prevalence of breast cancer was estimated to be 3,477,866 women in 2016. While in Europe the incidence was 562,500 cases in 2018 (Ferlay *et al.*, 2010). Although it is universally reported in every country around the globe, the prevalence, mortality rates and patient outcomes vary between regions and ethnicities. Breast cancer is more common in Caucasian females than in Asian or Black females (De Angelis *et al.*, 2014). The incidence rate is 27 per 100,000 in Central Africa and Eastern Asia but increases up to 96 per 100,000 in Western Europe (Ferlay *et al.*, 2015).

Importantly, the incidence of breast cancer in the UK is among the highest. It accounts for thirty percent of cancers in women. In 2007 the incidence of new cases reached 45,695 which corresponds to 89 per 100,000. Hence, it is the second most common cause of death in females in the UK with approximately 11,500 reported deaths in 2016 & (Cancer Research UK breast cancer incidence statistics).

1.1.2 Breast cancer mortality and risk factors

Breast cancer mortality accounts for 522,000 deaths worldwide which is equivalent to 6.4% of cancer related deaths. Although breast cancer is the second most common cancer in the world, it is ranked the fifth in terms of cause of death. That is attributed to the significant improvement in treatment modalities and early detection as well as the screening programmes in developed countries (Ferlay *et al.*, 2015).

The risk factors for breast cancer include age, genetic predisposition, oestrogen exposure, late parity, and radiation exposure. Other lifestyle related factors like alcohol consumption and obesity are considered risk factors for breast cancer (Shah, Rosso and Nathanson, 2014). Proliferative breast lesions with hyperplasia like pathology confer a risk factor for breast cancer onset while atypical hyperplasia confers an increased risk of breast cancer representing 4.3 times that of normal breast pathology (Shah, Rosso and Nathanson, 2014). Atypical hyperplasia is usually identified in mammographic screening and its incidence increased significantly after the introduction of the mammographic screening programme in the UK.

1.1.3 Breast cancer staging

The TNM (primary tumour [T], regional lymph nodes [N], distant metastases [M]) staging system was first introduced in 1959 by the American Joint Committee for Cancer (AJCC) which published its first edition of the staging manual in 1977. The TNM staging system is being reviewed annually to include advanced findings on

prognostic markers that develop through extensive research and guide clinicians to more efficient therapy (Giuliano *et al.*, 2017). According to the TNM, staging diagnosed breast cancers can be grouped into 4 different stages that can predict five-year survival rates for patients. The rate of survival for stage I, IIA, IIB, IIIA, IIIB, and IV disease correspond to 95, 85, 70, 52, 48, and 18 percent respectively. The latest (eighth) edition has been updated to include prognostic markers such as ER, PgR, HER2 expression, histological grade, and recurrence score (Amin *et al.*, 2017; Giuliano *et al.*, 2017). The eighth edition has acknowledged other prognostic factors that are supported by level I evidence and are more likely to be included in other editions such as the well-established proliferation marker Ki67. Other multigene assays including Mamaprint, EndoPredict, PAM50 Risk of Recurrence (ROR), and the Breast Cancer Index were recognised by the report as reliable assays for staging that could be officially incorporated into following editions (Amin *et al.*, 2017; Brandão, Pondé and Piccart-Gebhart, 2019).

Another powerful prognostic tool is the Nottingham Prognostic Index (NPI) which is a well-established prognostic model for breast cancer. NPI has been validated in multiple cohorts of patients (Blamey *et al.*, 2007; Winzer *et al.*, 2016; Green, 2017). The three factors of lymph node (LN), stage and tumour size are considered to produce the index. The latest version of NPI proposed five cut points to create six categories of variable prognosis (Blamey *et al.*, 2007).

NPI calculation = LN (1 - 3) + Grade (1 -3) + maximum diameter (cm) *0.2.

1.1.4 Molecular intrinsic subtypes of breast cancer

The work by Perou *et al.* on the analysis of gene expression of breast cancers has led to comprehensive characterisation of the intrinsic subtypes of breast cancers (Perou *et al.*, 2000; Rakha, Reis-Filho and Ellis, 2008). In their early study they analysed cDNA arrays of 65 surgical specimens of breast tumours from 45 different patients before and after chemotherapy treatment. The analysis of matching samples identified an intrinsic gene list of 550 genes (Perou *et al.*, 2000; Sørlie *et al.*, 2001). Clustering analysis of these genes classified the samples into two main subtypes with respect to ER status: ER positive and ER negative tumours. The ER positive cluster can be classified into two main subtypes: luminal A which accounts for about 40 percent of breast tumours and has a favourable prognosis and luminal B represents 20 percent of breast tumours and has a higher expression of genes involved in mitosis and cell proliferation. Luminal B breast cancers have a worse outcome compared to luminal A tumours. The other main cluster (ER negative) can be sub-divided into two main subtypes. The first is characterised by low or negative expression of hormonal receptors (ER, PgR, and HER2) and thus named as triple negative breast cancers (TNBCs). Those tumours represent 20 percent of diagnosed breast cancers. TNBCs have the worst outcome as they usually manifest as high grade, infiltrating ductal carcinoma. TNBCs show the expression of a "basal gene cluster" which shows HER1 expression, basal cytokaratins 5/6 and c-Kit (the proliferation cluster) expression as well as low expression of HER2 and hormone receptor genes. The second subtype in the ER negative cluster is characterised by overexpression of HER2 related genes (called HER2 enriched subtype). HER2 related genes are located on 17q21 and include

HER-2 and growth factor receptor-bound protein 7 (GRB7). There is a high expression of nuclear factor (NF-kB), GATA4, and a lack of expression of ER and GATA3 (Perou *et al.*, 2000; Rakha, Reis-Filho and Ellis, 2008). The third and last subtype in the ER negative cluster is noted as the normal breast-like group which has a similar genetic profile to normal breast tissue. That subtype is characterised by the expression of adipose cells and non-epithelial cells with a low expression of epithelial markers (Sørlie *et al.*, 2001; Rakha, Reis-Filho and Ellis, 2008; Russnes *et al.*, 2017).

1.1.5 Molecular profiling of breast cancer

The rapid advances in genomic and transcriptomic assays have aided to better understand the molecular and genetic signatures of breast cancer. Several important studies have led to the characterisation of genomic aberrations and tumour heterogeneity of breast cancer. Stephens and colleagues looked at gene copy number and mutations from 100 breast tumours. They identified novel driver mutations in key genes including *AKT2, ARID1B, CASP8, CDKN1B, MAP3K1, MAP3K13, NCOR1, SMARCD1* and *TBX3* (Stephens *et al.*, 2012). Another important study in the same year by Ellis *et al.* aimed at utilizing whole genome sequencing (WGS) to characterise the genetic signature associated with the response to neo-adjuvant therapy. The study which comprised 46 tumour samples from 31 cases and included two trials of aromatase inhibitor therapy described mutations in novel genes such as *TBX3, RUNX1, LDLRAP1, MYH9, AGTR2, STMN2, SF3B1* and *CBFB.* The study was able to correlate some mutational profiles to tumour behaviour. Whereas luminal A, low grade tumours were associated with *MAPK3K1* mutations, the response to aromatase

inhibitor therapy was more associated with *GATA3* mutations (Ellis *et al.*, 2012). Of note here is the largest genomic study by Curtis *et al.* on a comprehensive set of 1000 primary tumours from the Molecular Taxonomy of Breast Cancer International Consortium (METABRIC) cohort. This study grouped patients into ten molecular subgroups with distinct genetic profile and clinical outcome. The authors validated that classification on a further 1000 cases. Other groups have adopted similar genomic analysis and proposed further sub-classification including other molecular entities (Aure *et al.*, 2017; Alba *et al.*, 2018). Nevertheless, the recent understanding of the heterogeneity of breast cancer required incorporation of molecular identified markers into NPI to develop a more comprehensive prognostic tool that is more tailored to the genomic profiling era. The updated NPI plus incorporated other markers such as cytokeratin (CK) 5/6, CK18, EGFR, ER , PgR, HER2, HER3, HER4, Mucin1 and p53 expression to provide a more progressive tool for personalised breast cancer management (Rakha *et al.*, 2014; Green *et al.*, 2016). The molecular prognostic models described have been subsequently validated in several studies. However, the intrinsic subtyping for breast cancer based on immunohistochemical characterisation of (ER, PgR & HER2) remains the gold standard for breast cancer management and prognosis.

1.2 Ductal carcinoma *in situ*

Ductal carcinoma in situ (DCIS) represents a heterogeneous group of diseases which is characterised by increased proliferation of epithelial cells within the myoepithelial of ducto-lobular lineage with no invasion to the adjacent stromal tissue. DCIS was revealed to have high heterogeneity underlying differential genomic profiles, morphology and prognostic outcomes. It is considered a major risk factor for subsequent recurrence into invasive breast carcinoma (Bane, 2013).

1.2.1 Epidemiology of DCIS

The incidence of DCIS increased dramatically after the introduction of the mammographic screening programme. The incidence of DCIS in the UK was estimated to be 7,984 cases in 2016. In the US, according to the latest cancer statistics of the Surveillance, Epidemiology and End Result programme (SEER) the DCIS incidence in 2016 was expected to be 61,000 cases. The prevalence of DCIS in menopausal women has decreased remarkably in recent years. Meanwhile, there is an increase in DCIS incidence in young women which presents with more aggressive forms of DCIS associated with higher recurrence rate and progression into invasive carcinoma (Li, 2003; Li, Daling and Malone, 2005).

The risk factors of DCIS are similar to invasive breast cancer including history of familial breast cancer, age above 50 years, nulliparity and increased mammographic breast density. Several studies have revealed the similarities between DCIS and breast cancer genetic abnormalities suggesting common molecular mechanisms (Bane, 2013). Importantly, BRCA mutations confer major

risk for both DCIS lesions and invasive carcinoma. The loss of tumour suppressor genes such as p53 and p16 are also associated with DCIS onset.

1.2.2 Prognostic markers for DCIS recurrence

Despite the recent advances in proteomic and genomic profiling, current prognostic markers are unable to predict DCIS recurrence (Pang, Dobrovic and Fox, 2013). In one study, included samples from 1162 DCIS patients and matching subsequent recurrence samples of DCIS or invasive tumours revealed that p16, COX-2, and Ki67 triple positive ($p16^{+}COX\text{-}2^{+}Ki67^{+}$) initial DCIS lesions are associated with high recurrence risk into invasive breast cancer (Kerlikowske *et al.*, 2010). Another study investigated the epigenetic changes between DCIS and adjacent invasive tissue in 33 breast cancer patients concluded that promotor hypermethylation of *PAX6, BRCA2, PAX5, WT1, CDH13* and *MSH6* is elevated in both DCIS and invasive carcinoma (Moelans, Verschuur-Maes and van Diest, 2011). The data suggests that epigenetics regulation plays a role in breast cancer early pathogenesis. Several studies revealed that low ER expression is significantly associated with increased risk of DCIS local recurrence (Ringberg *et al.*, 2001; Provenzano *et al.*, 2003; Roka *et al.*, 2004). Additionally, ER negative status combined with either HER2 expression or Ki67 expression was associated with DCIS recurrence. Zhou *et al.* concluded that triple negative DCIS (DCIS negative for ER, PgR and HER2) confers a higher risk of local recurrence (Zhou *et al.*, 2010). Not only has ER expression been studied as a prognostic biomarker for DCIS recurrence, but also clinical trials have investigated ER expression as a predictor of tamoxifen and aromatase inhibitor therapy. The results of those trials are controversial, whereas tamoxifen reduced the incidence of breast carcinoma in

DCIS patients. However, the trials failed to conclude whether tamoxifen efficacy is solely linked to ER expression status (Eng-Wong, Costantino and Swain, 2010; Cuzick *et al.*, 2011).

Other studies have explored the expression of cyclins and DCIS recurrence. The role of cyclins in cell cycle regulation is well described. Overexpression of cyclins in cancers including breast cancer have been previously reported. Overexpression of cyclin A , D1 and cyclin E have been suggested to correlate with ipsilateral local recurrence (Chasle *et al.*, 2003; Jirström *et al.*, 2003; Sutherland and Musgrove, 2004) .

Although these reports unravelled some of the molecular profiles of DCIS, there are some limitations that conflicted with the conclusions. The number of pure DCIS patients in individual cohorts are limited. Also, the treatment regimens for patients are variable between endocrine therapy and/or radiotherapy which affected the clinical outcome. Thus, the investigation of novel prognostic markers for DCIS recurrence is still an area of un-met need (Lari and Kuerer, 2011).

1.2.3 Oncotype DX for DCIS risk stratification

The incidence of DCIS has increased with screening mammography which can detect DCIS in asymptomatic women. Management of DCIS is currently variable. The guidelines recommend breast conservation surgery and adjuvant radiotherapy to reduce the risk of local recurrence. However, a lot of DCIS lesions will not recur if treated with conservation surgery alone which raises concerns over overtreatment. Contrariwise, a small group of patients are at risk of developing invasive carcinoma and therefore being undertreated with surgery alone (Solin *et al.*, 2013; Lalani and Rakovitch, 2017). Available pathological

markers and clinical features have tried to define risks of DCIS recurrence. However, reproducible methods for risk stratification of recurrence are not yet established. The Oncotype DX DCIS score is a multigene assay to predict risk of recurrence within a ten-year estimate for patients. The assay provides a DCIS score with continuous output ranges from 0-100 combined with categorical output (low, intermediate and high-risk groups). The list of genes tested in the assay is summarised in (Table 1-1). The Oncotype DX was initially validated in two cohorts: the Eastern Cooperative Oncology group (ECOG) of 327 DCIS patients and another cohort of 571 patients (Lalani and Rakovitch, 2017). In both groups the Oncotype DX score was independently associated with the risk of local recurrence. Although the assay provides a personalised recurrence risk for patients, limitations such as the high cost and further validation prevented incorporation of such a tool in routine clinical practice (Lalani and Rakovitch, 2017).

Table 1-1: List of genes in the Oncotype DX DCIS and their score.

Genes tested in the Oncotype DX DCIS			
Proliferation genes	**Hormone receptor**	**Tumour metabolism**	**Reference genes**
Ki67- STK15 - Survivin- CCNB1 - MYBL2	*PR*	*GSTM1*	*ACTB- GADPH- RPLPO – GUS -TRFC*
Scores and risk group Low risk group<39 Intermediate group 39-54 High risk group 55-100			

1.3 Ovarian Cancer

1.3.1 Epidemiology of ovarian cancer

Ovarian cancer is the seventh most diagnosed cancer in females worldwide. It accounts for most of the gynaecological tumours related deaths in the US. In 2008 ovarian cancer incidence was 5.0 per 100,000 and the mortality rate was 3.1 per 100,000. In the US there are 22,000 newly diagnosed cases annually and 14,000 ovarian cancer deaths every year. According to the GLOBOCAN 2018 cancer estimates, the incidence of ovarian cancer worldwide for 2018 was estimated to be 295,414 cases and the related deaths were estimated at 184,799 cases which represent 1.9% of all deaths. 1.3 percent of women will be diagnosed with ovarian cancer in their lifetime. Very few cases (about 15%) are presented with localised tumours with a good prognosis and a high 5-year survival rate above 90 percent, whilst the majority of patients are diagnosed at later stages with a survival rate below 30 percent. The percentage of 5-year survival rate was as low as 47.6% in 2016. Therefore, it is a major public health problem (Reid, Permuth and Sellers, 2017; Bray *et al.*, 2018).

1.3.2 Ovarian cancer subtypes

The majority of ovarian cancers are derived from epithelial cell origins about (90%). Only 5-6% are sex cord-stromal tumours and 2-3% derive from germ cell origin. Thus, epithelial ovarian cancers are the main focus of ovarian cancer research.

Ovarian cancer is not a single neoplasm - in fact it is a heterogeneous group of diseases with different histological subtypes. Some studies have suggested that

high and low-grade serous carcinomas originate from the fallopian tubes (Reid, Permuth and Sellers, 2017), while clear cell and endometroid carcinomas are derived from endometriotic cysts. Mucinous carcinomas are believed to be derived from mesothelial cell junctions (Ricci *et al.*, 2018). Epithelial ovarian carcinoma has five main subtypes that differ in their pathological and clinical behaviour - these are summarised in (Table 1-2).

Table 1-2: Histological subtypes of epithelial ovarian cancers.

Histological subtype	**Prevalence**	**Pathological markers**	**Molecular Markers**
High grade serous carcinoma (HGSOC)	70%	P53, P16, WT1, ER, PAX8 and high Ki67	*BRCA1, BRCA2, TP53*
Endometroid carcinoma (ENOC)	10%	vimentin, ER, PR, PAX-8, and CA125. Low p16 &p53. Negative WT-1 & calretinin.	*CTNNB-1, PTEN, PIK3CA & ARID1A*
Clear cell carcinoma (CCOC)	10%	HIF-1α, glypican, HNF-1β	*KRAS, PTEN & PIK3CA.*
Mucinous carcinoma (MOC)	3%	CK20, CDX2, CK7, P16. Negative ER, PR, WT-1 &CA125.	*KRAS, MUCINS (MUC2, MUC3&MUC17). TP53, c-MYC*
Low-grade serous carcinoma (LGSOC)	5%	WT-1, ER &PR. Low Ki67&p53. Negative HNF-1& Calretinin	*BRAF, KRAS*

Shih and Kurman proposed in 2004 their first dualistic model to classify epithelial ovarian cancers into two subclasses based on the pathological and molecular features. Type I tumours include low-grade serous, mucinous, endometrioid and clear cell carcinomas and generally have a better prognosis when diagnosed at an early stage. Type I tumours account for 10% of epithelial ovarian cancers. Controversially, Type II tumours confine the high-grade serous carcinoma which commonly present at higher aggressive stage and they represent the majority of epithelial ovarian cancers (Shih and Kurman, 2004). Not only do these two types differ in their incidence and clinical outcome, but also, they differ in their molecular and mutational profiles. Whereas type I tumours are often associated with *BRAF* and *KRAS* mutations in serous and mucinous carcinomas, PTEN mutations are profound in endometrial carcinomas. Meanwhile Type II tumours are characterised by p53 mutations which are predominant in HGSOC malignancies and believed to play a role in their aetiology (Shih and Kurman, 2004; Reid, Permuth and Sellers, 2017). Numerous studies have tried to explore the histological and molecular markers of ovarian cancer and provide a better insight into the aggressiveness of that disease. Therefore, a revised version of the dualistic model was published to account for the genetic characteristics and incorporate it with histological features (Kurman and Shih, 2016). In The revised model Type I has been divided further into three subtypes: I) endometriosis sub-group; including endometrioid, clear cell and mullerian neoplasms. II) Fallopian tube related tumours. III) Germ cell and transitional cell related neoplasms. The main molecular difference between both main subtypes is the genetic stability of type I which appears to be associated with relatively less aggressive

ovarian neoplasms and the genomic instability of type II whereas homologous recombination defects and p53 mutations are predominant (Kurman and Shih, 2016; Reid, Permuth and Sellers, 2017).

1.3.3 Ovarian cancer staging

Ovarian cancers are staged according to the International Federation of Gynecology and Obstetrics (FIGO). The staging system account for Tumour, node and Metastasis (TNM) in the classification and is followed for staging tumours of the ovary, fallopian tubes and peritoneum (Prat, 2015). A summary of the FIGO staging system for ovarian cancers is shown in (Table1-3).

Table 1-3: FIGO staging for ovarian cancers.

Stage I: Tumour confined to the ovary	
IA	Tumour limited to 1 ovary, no tumour on the surface.
IB	Tumour involves both ovaries, no tumour on the surface.
IC1	Tumour limited to one or both ovaries with surgical spill.
IC2	Tumour limited to one or both ovaries with capsule rupture before surgery.
IC3	Tumour limited to one or both ovaries with malignant cells in the ascites.
Stage II: Tumour involves one or two ovaries with pelvic extension	

IIA	Extension and /or implant on uterus and fallopian tubes.
IIB	Extension to other pelvic intraperitoneal tissues.
Stage III: Tumour involves one or two ovaries	
IIIA i	Positive retro-peritoneal lymph nodes≤10 mm.
IIIA ii	Positive retro-peritoneal lymph nodes>10 mm.
IIIA2	Microscopic extra peritoneal metastasis≤2cm + positive lymph nodes.
IIIB	Macroscopic extra peritoneal metastasis>2cm + positive lymph nodes.
IIIC	Macroscopic extra peritoneal metastasis>2cm + positive lymph nodes with extension to capsule of liver or spleen.
Stage IV: distant metastasis excluding peritoneal metastasis	
IVA	Pleural effusion with positive cytology.
IVB	Hepatic or splenic metastasis, metastasis to extra abdominal organs.

1.3.4 Molecular profile of ovarian cancer

Over the years, cancer treatment has shifted dramatically from conventional use of cytotoxic chemotherapeutics to molecular targeted therapies that are personalized to a patient's gene signature. In ovarian cancer, this approach is really lagging compared to breast cancer for instance, due to less identification of driver mutations for ovarian carcinoma. The standardised treatment for *BRCA* non-mutated ovarian cancers remains surgical management combined with systemic chemotherapy like cisplatin/ carboplatin with or without taxanes drugs such as Paclitaxel and Docetaxel (Armstrong *et al.*, 2006; Tewari *et al.*, 2016). There are some large studies that have attempted to subclass ovarian cancer based on molecular signatures. The previously described model by Kurman and Shih shed light on the commonality of TP53 mutations in type II ovarian tumours

i.e. high grade serous adenocarcinoma, conversely the involvement of KRAS and BRAF mutations in type I tumours (Kurman and Shih, 2016). Another important study by the TCGA identified four molecular subclasses within 489 high grade serous ovarian carcinoma. Those are immunoreactive, differentiated, proliferative and mesenchymal subtypes. Importantly, this study confirmed the predominance of TP53 mutations in type II tumours (Cancer Genome Atlas Research Network, 2011), in addition to the high association between BRCA mutations and type II tumours (Bowtell, 2010). That led to re-evaluation of TP53 wild type ovarian tumours within the TCGA that have been classified as high-grade serous carcinoma suggesting that alternative diagnosis should be denoted for those tumours (Previs *et al.*, 2016).

DNA repair mutations have been suggested to play a role in ovarian cancer pathogenesis. A comprehensive study of 360 ovarian cancer tumours has revealed mutations in some key DNA repair genes other than BRCA signature. The study showed mutations in *BARD1, BRIP1, CHEK2, MRE11A, MSH6, NBN, PALB2, RAD50,* and *RAD51C* within the cohort suggesting that homologous recombination defects can contribute to ovarian cancer aggressiveness (Stephens *et al.*, 2012).

Another DNA repair key player is *ARID1A*, a SWI-SNF chromatin remodelling complex subunit. ARID1A coordinates double strand break repairs through interaction with ATR (Shen *et al.*, 2015). Two recent studies have explored inducing synthetic lethality in ARID1A deficient cells by targeted therapy (Bitler *et al.*, 2015; Shen *et al.*, 2015). The first study showed the synthetic lethality of PARP inhibitors in ARID1A deficient cells (Shen *et al.*, 2015). The second study investigated targeting ARID1A mutated cells with EZH2 methyltransferase

inhibitors for synthetic lethality approach in clear cell ovarian carcinoma. ARID1A and EZH2 respectively belong to the SWI/SNF and polycomb complexes. They play antagonistic functions in regulating *PIK3IP1* transcription (Bitler *et al.*, 2015).

Other reports have tried to use genotyping approaches to identify predictive markers for therapy. Whereas a lot of ovarian tumours are refractory for platinum-based chemotherapy, amplification of 19q12, which contains cyclin E (CCNE1), is associated with platinum primary resistance in high grade serous carcinoma (Nakayama *et al.*, 2010). Multivariate analysis showed 19q12 amplification to be an independent prognostic factor of patients' survival post platinum- taxane therapy (Etemadmoghadam *et al.*, 2009). Additionally, TP53 mutations have been suggested to be a predictor for response to VEGFR inhibitors (Wheler *et al.*, 2016).

Other established prognostic factors for ovarian cancer are CA125 (Previs *et al.*, 2016) and EphA2 (Landen, Kinch and Sood, 2005).

DNA copy number and genomic sequencing analysis has shed light on the prevalence on genomic instability in ovarian cancer and its implications in molecular subtyping of the disease. Collectively, these data highlighted DNA repair aberration in ovarian cancers as we have already pointed out here. However, the role of DNA repair defects in ovarian cancer pathogenesis and response to therapy is still poorly understood.

In the literature, BRCA mutated ovarian cancers have been extensively investigated. Lots of lessons learned from breast cancer have been useful in underlying the molecular mechanisms of BRCA mutation in ovarian tumours. The success of PARP inhibitors in BRCA deficient high-grade serous carcinoma represents the first validation of precision medicine in ovarian cancer. But BRCA mutated ovarian tumours represent less than 30% in most of the studied cohort. Further investigations are required to stratify molecular subtypes with consequential targeted therapy (Previs *et al.*, 2016; Wang *et al.*, 2017).

1.4 Overview of DNA damage response

DNA damage repair is a complex process that involves the activation of various cellular activities. Genomic DNA is under constant bombardment from several stimuli that cause genomic instability (O'Connor, 2015). There is a range of genomic insults that can damage the DNA leading to various forms of damages such as small base damage, methylation events and intra/ inter-strand crosslinks. DNA can harbour more serious forms of damage such as double-strand breaks (Robertson *et al.*, 2009). Suboptimal repair of these lesions will lead to genomic instability. The main pathways required for DNA repair include base excision repair (BER), Mismatch repair pathway (MMR), nucleotide excision repair (NER), single strand break repair, homologous recombination (HR), non-homologous end-joining (NHEJ) and the homology-directed Fanconi Anaemia pathway (HDR). These pathways interplay with one another to provide genomic stability (Saldivar, Wu and Gershenson, 2007; O'Connor, 2015).

An established hallmark of cancers is genomic instability and the tendency for increased mutational load accompanied with impaired DNA damage response (Dianov and Hübscher, 2013). Conventional therapeutic regimes for cancers by radiotherapy or chemotherapy rely on this principle (Gavande *et al.*, 2016), though it is proven to be associated with severe toxicities of normal tissue. Over-expression of DNA repair enzymes is frequently seen in tumours.

A proportion of cancer cells shows an increase in BER enzymes which lead to resistance of those tumours to alkylating agents (Curtin, 2012) ,(Dianov and Lindahl, 1994).Therefore, more research and efforts have been dedicated toward

developing DNA repair targeted drugs that can enhance conventional chemotherapy sensitivities (Robertson *et al.*, 2009). These approaches for choosing the optimal DNA damage drug target have led to the exploration of more specified targets and the development of more personalised therapies. Here, we will shed light on previous resistance to some DNA repair targeted therapy. We will discuss the recent advances, particularly in the PARP inhibitor research field in the context of synthetic lethality approaches and personalised DNA repair targeted therapy as well as their clinical significance for cancer patients (O'Connor, 2015).

1.4.1 DNA damage response signalling

The response to DNA damage involves the activation of signal transduction cascade comprising sensors, transducers and effectors. They have the multiple role of delaying cell cycle progression and mediating DNA repair. On the other hand, DNA damage response signalling can initiate apoptosis upon extensive DNA damage (Zhou and Elledge, 2000). The DNA damage response (DDR) is initiated by the ATM, ATR and DNA PKcs transducers which belong to the phospho-inositide kinase (PIK) family. Signalling of ATM and ATR kinases activates their downstream effectors ChK1 and ChK2 which act as cell cycle checkpoints through the regulation of CDC25C and WEE1 kinase levels (Maréchal and Zou, 2013). ChK1 and ChK2 are serine threonine kinases that are phosphorylated by ATR and ATM respectively. ChK2 phosphorylation at threonine 68 in response to ionizing radiation (IR), methyl methane sulphonate and hydroxyurea is proven to be ATM dependent. A previous study showed that ChK2 can phosphorylate p53 on serine

20 and prevent it from binding to its antagonist Mdm2 (Chehab *et al.*, 2000). However, other studies have contradicted these findings (Jallepalli *et al.*, 2003). So, it is not clear whether ChK2-p53 interaction is independent from ATM activation (Zannini, Delia and Buscemi, 2014). The role of ATR- ChK1 phosphorylation is more profound in genotoxic insults that compromise DNA replication. ATR abundantly phosphorylates ChK1 on serine 345 in response to hydroxyurea and UV radiation but moderately in IR damage. ATR- ChK1 signalling regulates origin firing and protects replication forks from cleavage by nucleases in replication stress conditions (Zhang and Hunter, 2014). Thus, ChK kinases play a crucial role in coordinating cell cycle progression in DNA repair. Other effector proteins such as BRCA1, Nbs1 and p53 are activated in DNA damage response signalling. The interaction between BRCA1, ATM and the MRN complex is thought to play a complementary role in recognising DNA damage (Zhou and Elledge, 2000). A summary of DNA damage signalling is illustrated in (Figure 1-1). On the other hand, they are components of the BRCA1-associated genome surveillance complex comprising BRCA1, ATM, the MRN complex, mismatch proteins (MSH2 /6 and MLH2), Bloom's helicase (BLM) and replication factor C (Deng and Wang, 2003). The commonality between those different sensors is their ability to recognize various forms of DNA aberrations such as DSBs, stalled replication forks or mismatched DNA (Deng and Wang, 2003).

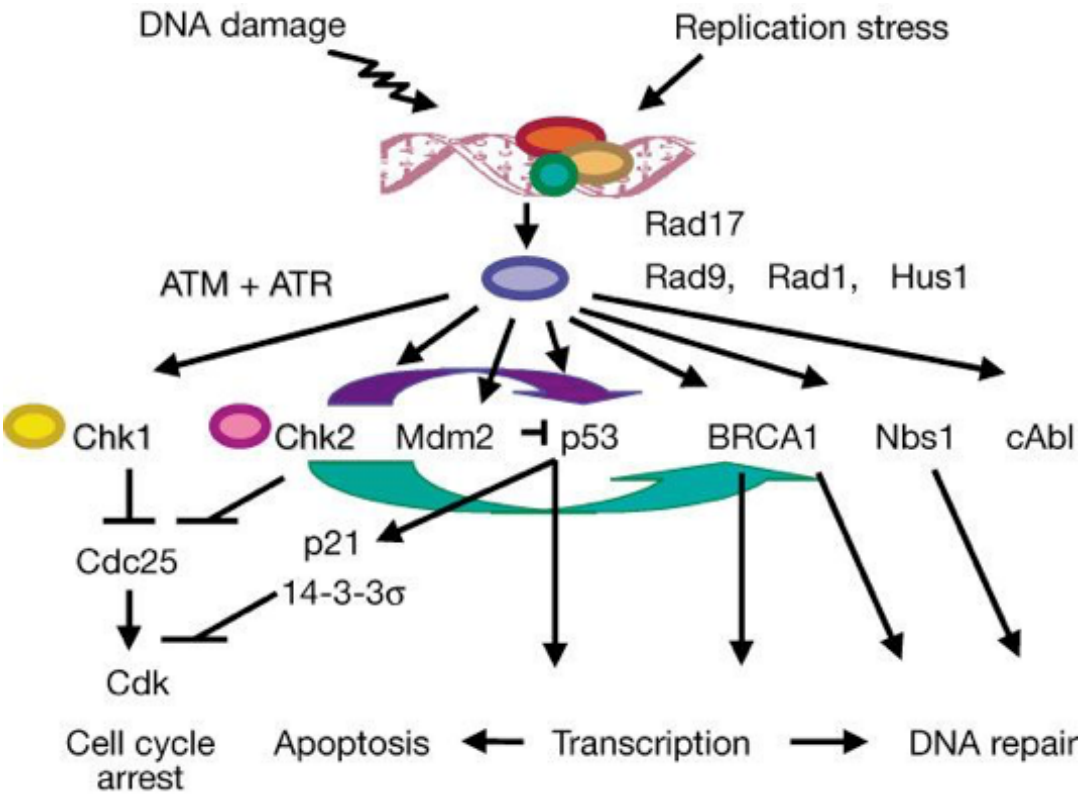


Figure 1-1: DNA damage response signalling.

Arrow heads represent activating steps. Perpendicular ends represent inhibitory steps. Adapted from (Zhou and Elledge, 2000)

Better understanding of ATM functions in DNA repair have been learned from the Ataxia telangiectasia disorder where mutations of ATM in patients lead to defects in ionizing radiation response and G1 cell cycle arrest (McKinnon, 2004). Activation of ATM and other transducer kinases lead to activation of the tumour suppressor gene p53. P53 controls the transcription of other target genes regulating cell cycle progression, senescence and apoptosis. P53 exerts its functions through p21 and BH3-only protein signalling. P21 inhibits cyclin dependant kinases to delay cell cycle progression allowing more time for DNA repair, while BH3-only proteins regulate PUMA, BAX and Bak pro-apoptotic

effectors (Zhou and Elledge, 2000). These mechanisms act as surveillance systems to inhibit the proliferation of cells with DNA damage. P53 mutations are almost predominant in 50% of cancers. This frequency reflects the key role of DNA damage response aberrations in tumour aetiology (Reinhardt and Schumacher, 2012).

The complexity of DNA damage response at the molecular level emphasises that its importance is beyond the signalling of cell death or survival. It is directly involved in controlling DNA repair. DNA repair pathways are highly conserved processes, and each pathway is activated in response to different types of lesions. However, studies referring to the interplay between the pathways through their key regulators are emerging (Pearl *et al.*, 2015). The network of genomic maintenance implies six main pathways for DNA repair: the base excision repair (BER), nucleotide excision repair (NER), homologous recombination (HR), non-homologous end joining (NHEJ), mismatch repair (MMR) and Fanconi anaemia pathway (FA) (Dietlein, Thelen and Reinhardt, 2014). Defects in DNA repair pathways have been suggested to be drivers of genomic alterations in cancer cells. It was proved that tumour cells at early stages inactivate DDR and overcome senescence, suggesting that defective DDR is a prerequisite for tumour genesis. On the other hand, tumours rely on DNA repair abilities to bypass the damage induced by cytotoxic drugs. Accordingly, pre-clinical studies are now focused on augmenting conventional chemotherapies with DNA repair inhibitors (Dietlein, Thelen and Reinhardt, 2014).

1.5 Overview of DNA repair pathways

1.5.1 Mismatch repair pathway

The MMR pathway is a conserved pathway between bacteria and humans. It has been widely studied in *E-coli* using purified enzymes through which resemblance with the human analogues has been understood. The pathway is responsible for base substitution mismatches as well as insertion deletions (IDLs) that arise due to the low fidelity of DNA polymerases, thus improving their proofreading role by an estimate of 50-1000-fold (Martin, 2016). The pathway can be accomplished through three individual steps: mismatch recognition, excision, and repaired DNA synthesis. Eukaryotic MMR can be initiated by the MutSα complex consisting of the MSH2-MSH6 heterodimer which can recognise the mismatch lesion of up to 1-2 base IDLs. In the case of 2> base lesions, the MutSβ complex can be activated to process the multiple base recognition. Activation of MutS helps recruit MutLα (MLH1·PMS2 heterodimer) which in turn activates EXO1 excision activity. The DNA synthesis function is mainly completed by polymerase δ and DNA ligase I (Figure1-2)(Modrich, 2006; Hsieh and Yamane, 2008).

There are key differences between prokaryotic and mammalian MMR. The substitution of MutSβ for MutSα allows repair of IDLs of more than 2 bases, a feature which is absent from the prokaryotic system. Additionally, a bi-directional repair system is only supported in mammalian MMR orchestrated by seven key players, namely MutSα, MutLα, RPA, EXO1, PCNA, RFC, and DNA polymerase δ.

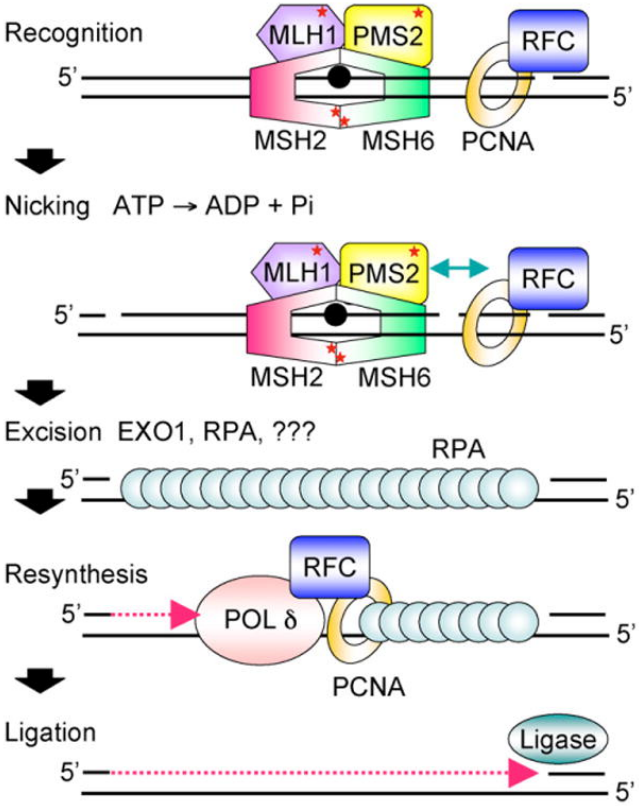


Figure 1-2: MMR pathway

Recognition of the mismatch by MutSα or MutSβ and MutLα in an ATP dependent manner. PCNA plays a role in the recruitment of the MMR proteins. Nicking of the DNA by PMS2 endonuclease activity prmoted by PCNA and RFC. Excision of the mismatched base by EXO1 and the formation of RPA coated SS DNA. synthesis is accomplished by polymerase δ and DNA ligase I.
Adapted from (Hsieh and Yamane, 2008)

PCNA and RFC can function when the strand break is located 3'or 5' to the mismatch (Constantin *et al.*, 2005; Hsieh and Yamane, 2008), while in E-coli a 5' to 3' hydrolytic activity is required to process strand break located 5' to the mispair (Constantin *et al.*, 2005). MMR germline mutations are known as Lynch syndrome which is frequently seen in familial colorectal cancer cases. Additionally, MMR deficiency is seen in 15-20% of sporadic colorectal cancers (Li and Martin, 2016).

Loss of MMR functions are known to generate a mutator phenotype. It is also associated with microsatellite instability which describes the presence of shortened tandem nucleotide repeats in the genome (Hsieh and Yamane, 2008). MMR is also responsible for recognising mismatched lesions formed by cytotoxic drugs including *O*^{6}methylguanine (*O* ^{6}meG) lesions formed by SN1 alkylators, 5-flurouracil and cisplatin adducts. Moreover, MMR mutated cells are more tolerant to 6-thioguanine drug which inhibits cellular replication in S-phase, which is known to be regulated by ATR-ChK1 signalling (Jiricny, 2006). That finding might indicate that MMR deficiency also modulates ATR-ChK1 activation. Thus, MMR mutations directly play a role in chemotherapeutic drug resistance. The MMR proteins MutSα and MutLα are involved in apoptosis signalling and activate DDR cascade including p53, Chk1, Chk2, and CDC25A (Hsieh and Yamane, 2008). Taken together, those findings suggest a complex role for MMR proteins in DDR signalling side by side to mismatch lesion repair functions.

1.5.2 Double strand breaks repair pathways

Double strand breaks (DSBs) are the more deleterious forms of DNA damage that arise due to genotoxic agents, ionising radiation and stalled replication forks that encounter unrepaired single strand breaks (SSBs) during replication. If unrepaired, DSBs can lead to severe aberrations or ultimately to cell death. DSB repair is mainly processed by HR interrelated pathways including high fidelity (HR) and error prone (NHEJ) and Holliday junction (HJ) pathways (Li and Heyer, 2008).

The main effector in the HR pathway is RAD51 which is the homolog of RecA in prokaryotes. RAD51 binds to 3'ssDNA in an ATP dependant manner. RAD51 has a core function in the three phases of HR: pre-synapsis, synapsis and post-synapsis. In the pre-synapsis phase RAD51 recognises and binds to RPA coated ssDNA creating a pre-synaptic filament (Krejci *et al.*, 2012). The ssDNA filament can be stretched to allow efficient strand invasion into a homologous DNA template. In the synapsis phase, RAD51 generates a DNA (D-loop) to assist the interaction between the ssDNA in the filament and the duplex DNA template. A new DNA is synthesized using the invading ssDNA at the 3'-end in the so-called post synapsis stage. Finally, RAD51 will dissociate from the DNA to allow completion of the synthesis process (Prakash *et al.*, 2015).

The formed D-loop and intermediate products can be processed differently according to the nature of the products. In the case of non-cross over products, the newly synthesised DNA will dissociate from the D-loop to anneal with the other DNA end and DNA ligation will proceed in the synthesis- dependent strand-annealing (SDSA) pathway of HR (Li and Heyer, 2008). While in the case of crossover or non-crossover products, the D-loops are generated on double-Holliday structures and rely on the resolution of these structures (Matos and West, 2014). In the case of DNA blunted ends, HR can be completed through non-homologous end joining (NHEJ) in which the DNA ends can be resected before joining (Krejci *et al.*, 2012).

Although RAD51 activation is the rate limiting step to HR initiation, other signalling cascades play a crucial role in DSB sensing and repair by HR pathways.

ATM, ATR and DNA-PK kinases are the early sensors of DSB that get activated at early events in HR repair. ATM signalling phosphorylates the serine 139 residue of histone H2AX at the site of the break. Another early event player is the MRN complex formed of the MRE11, RAD50 and NBS1 proteins which are activated and recruited to the site of damage. Mutations or inhibitions of the proteins of the MRN complex modulate the ATM signalling cascade (Lamarche, Orazio and Weitzman, 2010). ATM kinase signalling activates other key proteins and histones that are recruited to the DSB site. Among those are MDC-1, 53BP1, BRCA1, BRCA2 and PALB2. In addition, the ChK1 and ChK2 cell cycle check points are activated to modulate cell cycle progression (Wyman and Kanaar, 2006).

In NHEJ, the DNA ends are detected by the Ku70/80 heterodimer which activates another kinase DNA protein kinase C (DNA PKcs) which in turn recruits other proteins including nuclease artemis, DNA polymerases and MRE11 to bind to the DNA. Then XRCC4 and DNA ligase IV complete the DNA ligation step (Chang *et al.*, 2017).

The exact mechanism for selecting the pathway of choice is unknown. But the structure of the DSB substrate certainly plays a role. DNA blunted ends or complementary 3’ or 5’ strands can be a substrate for NHEJ repair. Radiation induced lesions cannot be processed by DNA ligases - they require DNA synthesis steps as in the HR pathway. Another key aspect is that the DSB pathways are highly controlled by the cell cycle, whereas HR is known to be operating predominantly in the S phase through the G2 phase. This is because of the presence of the sister chromatid required for the progression of the HR repair (Zhao *et al.*, 2017). NHEJ can be activated throughout the cell cycle but it is mostly

active in the G1 phase. Control cyclin dependent kinases (CDK) are suggested to have a role as studies have shown that RPA binding to the ssDNA is partially activated by CDK. Moreover, the inhibition of CDK activity leads to the aberration of DSB repair (Zhao *et al.*, 2017). Thus, DSB repairs are tightly controlled mechanisms that are highly orchestrated up to the level of the more hazardous form of damage to the genome integrity.

1.5.3 BRCA role in DDR and cancers

The breast cancer susceptibility genes 1&2 (BRCA1& BRCA2) are core proteins in the DDR. The direct link established between BRCA gene mutations and hereditary breast and ovarian cancer syndrome (HBOC) made them subject for investigation in most breast and ovarian cancer genomic and proteomic studies. Inheritance of one allelic mutation in one or both BRCA genes increase breast cancer predisposition by 60%. HBOC accounts for 5-7% of breast cancers. BRCA genes have central roles in HR pathways. They have distinctive structures that facilitate their functions (Roy, Chun and Powell, 2011). The BRCA1 protein has three main regions, as discussed in the following. The (RING) domain interacts with BARD1. A coiled domain binds to the bridging protein PALB2 and establishes a connection with BRCA2. The BRCA1-PALB2-BRCA2 complex is crucial for HR activation and RAD51 recruitment to DSB sites. The third domain is BRCA1 carboxy-terminal repeats (BRCTs) which communicates BRCA1 with other important proteins such as Abraxas/FAM175A, BRIP1/BACH1, and CtIP/RBBP8 thereby forming complexes with BRCT domain (Prakash *et al.*, 2015). In HR, BRCA1 co-localises with the MRN complex and particularly with RAD50. BRCA1 promotes end-resection through interaction with the resection factor CtIP, thus favouring HR repair for DSB.

Besides end resection, BRCA1 antagonises 53BP1 levels at the S-phase to allow the completion of the repair process (Powell and Kachnic, 2003; Lamarche, Orazio and Weitzman, 2010).

Similar to BRCA1, BRCA2 has conserved domains called BRC repeats and a carboxy terminal. BRC repeats are essential for RAD51 pre-synapsis steps and DSB repair. However, BRC domains appear to have other functions in genome integrity. That hypothesis is supported by mice knock out studies for BRC encoding exon 11 which show embryonic lethality. Of note is that RAD51 binding to the carboxy terminal is exclusive from BRC repeats and is regulated by CDK suggesting a role for BRCA2 in cell cycle regulation (Powell and Kachnic, 2003).

The obvious roles for BRCA1 and BRCA2 in DDR and maintaining genomic stability explain the frequency of *BRCA* mutations in cancers. The loss of wild type *BRCA* allele (LOH) was reported in HBOC syndrome. Additionally, mutations in TP53 and or ATM /ChK2 are also shown to be associated with *BRCA* mutated tumours contributing to the genetic instability characterizing those malignancies (Powell and Kachnic, 2003). However, that phenotype does not explain the direct link between *BRCA* mutations and breast /ovarian cancers. Few hypotheses have tried to explain that feature (Roy, Chun and Powell, 2011). The first one is the role of *BRCA1* in ER signalling. The BRCA1-BARD1 complex regulates oestrogen receptor ERα activity through ubiquitination in a negative feedback loop. Furthermore, if exposed to tamoxifen*, BRCA1* deficient cells are hypersensitive to oestrogen and they would secrete additional growth factors that would enhance proliferation of

other receptor negative cells. Most *BRCA1* deficient tumours are ER negative sub type which can support that hypothesis (Manavathi *et al.*, 2013). Another explanation is the increase in reactive oxygen species after each menstruation which leads to oxidative DNA damage (Roy, Chun and Powell, 2011). BRCA1 deficient cells are proven to be defective in HR and thus cannot repair those lesions. A recent report showed that oestrogen treatment induced proliferation of ER positive *Brca-1* proficient and ER negative *Brca-1* mutant mice. Oestrogen treatment activated the AKT pathway in *Brca1* deficient cells confirming the feedback loop between BRCA1 and ER signalling (C. Wang *et al.*, 2018).

1.5.4 Overview of the Base excision repair pathway

The (BER) pathway is critical for the repair of oxidised base damage and alkylated base damage. The pathway is initiated by DNA glycosylases that recognise the damaged base and excise it thereby creating a basic site (Dianov and Hübscher, 2013). There are eleven different human DNA glycosylases that differ according to the type of damaged base (David, O'Shea and Kundu, 2007). A basic site or AP site can be processed by the endonuclease activity of APE1 which cleaves the phosphodiester bond 5' to the nicked DNA. The generated SSB has a 3' hydroxyl residue and 5'-deoxyribosephosphate that is recognised by the DRP lyase activity of DNA polymerase β (Pol β). Pol β then inserts a new nucleotide and then XRCC1–DNA ligase IIIα heterodimer seals the DNA ends and accomplish the classical short-batch BER pathway (Dianov and Hübscher, 2013).

If the 5' end is blocked and cannot be removed from the nick, then alternatively a replicative polymerase such as Pol δ or pol λ along with proliferating cell nuclear antigen and replication factor C (RFC) can displace the strand. FEN1 can excise the

resulting flap of 2–12 nucleotides and finally DNA ligase I can seal the DNA nick and complete the long-batch base excision repair (Figure 1-3).

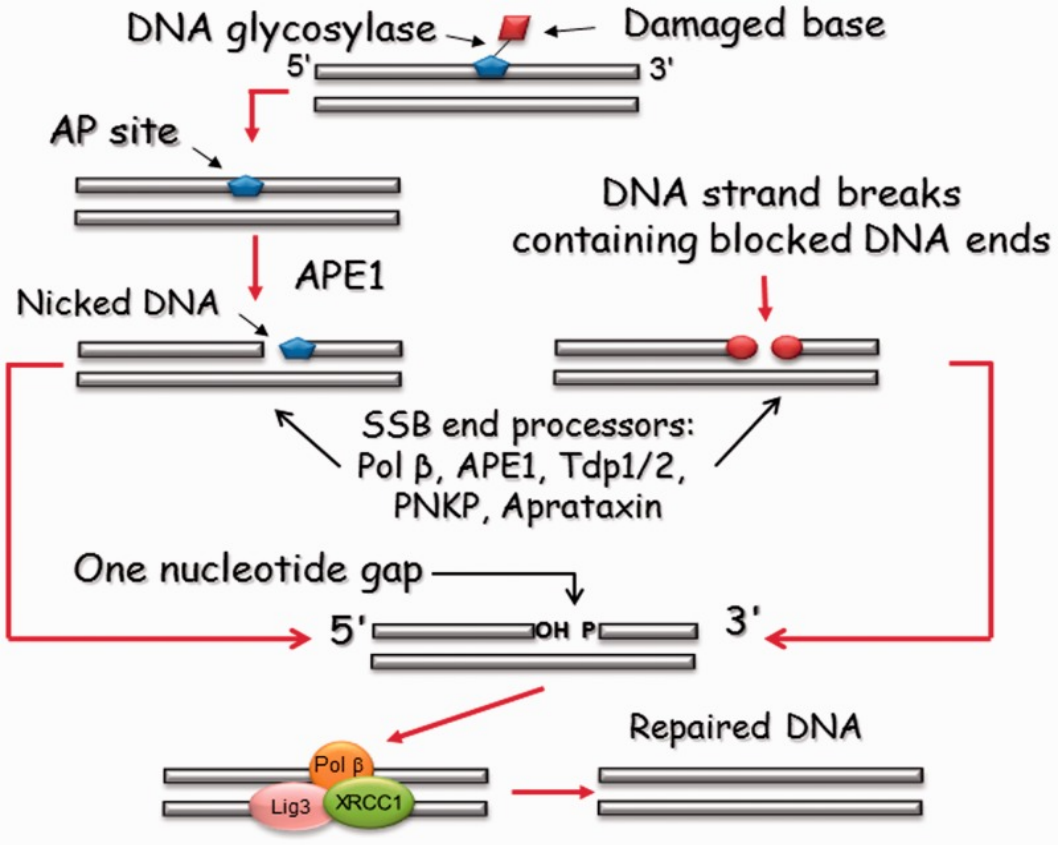


Figure 1-3: BER pathway

Damaged base is recognised by DNA glycosylase which nick the DNA and create AP site that is processed by APE1 endonuclease activity. Polβ insert single nucleotide in the SP-BER and ligase 3α-XRCC1 heterodimer seals the DNA. Adapted from (Dianov and Hübscher, 2013).

BER functions preferably in the G1 phase of the cell cycle, where it can screen the DNA for lesions and repair them before transcription. That process of repair is tightly controlled by check points such as p53 which directly control the DNA damage response by activation of cell cycle regulators or apoptosis signalling if the DNA lesion is beyond repair (Wallace, Murphy and Sweasy, 2012). However, cancer cells can also use BER as a mechanism of resistance for cytotoxic agents. A number of studies have explored overexpression of base excision repair enzymes in cancers, besides the validity of using them as drug targets. APE1 enzyme is a good example. Cleavage of the A basic site by the endonuclease activity is a rate limiting step in BER. Additionally, APE1 is a redox regulator to other transcription factors including Fos, Jun, paired box containing genes (PAX), nuclear factor-kappa B, hypoxia-inducible factor alpha (HIF-1alpha), HIF-like factor (HLF) and p53 (Al-Attar *et al.*, 2010). Overexpression of APE1 has been reported in several neoplasms including prostate cancer (Kelley *et al.*, 2001), osteosarcoma (Wang, Luo and Kelley, 2004) and ovarian cancers (Moore *et al.*, 2000). Our group previously investigated APE1 expression as a prognostic factor in ovarian, gastro-oesophageal, and pancreatic-biliary tumour micro arrays from patient tissues. APE1 high expression was associated with aggressive clinicopathological features of tumours, indicating that APE1 is a potential drug target for inhibition of tumour aggressiveness (Al-Attar *et al.*, 2010). Similarly, a number of studies tried to isolate APE1 inhibitors through drug screening assays. CRT0044876 is an early developed APE1 inhibitor (Madhusudan *et al.*, 2005). It has been validated for synergic effects with HSP90 in non-small cell lung cancer

(Koll *et al.*, 2008). Another APE1 inhibitor is APX3330, with a licence recently being granted for testing in clinical trials (Shah *et al.*, 2017).

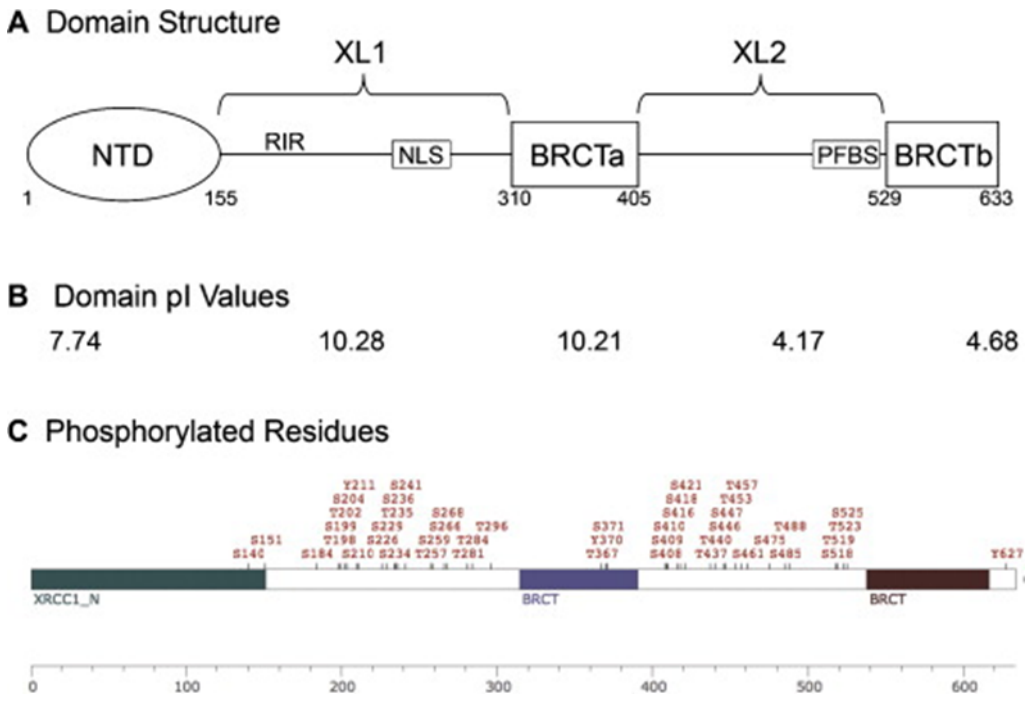
Other DNA repair enzymes like DNA glycosylases, DNA polymerases and DNA ligases have been explored through in vitro inhibition or knock out studies as potential candidates for drug targeting in cancer. However, more research is needed to take these hypothesises to clinical trials (Dianov, 2011).

Perhaps the best example for the feasibility of targeting BER in cancer therapy is the poly (ADP) ribose polymerase (PARP)inhibitors. PARPi inhibit PARP enzyme ability to synthesis poly ADP ribose polymers from NAD+ by competing with the NAD + at the binding site (Gavande *et al.*, 2016). Olaparib is the first FDA approved PARPi for treatment of *BRCA* mutant ovarian cancers. The success of Olaparib in clinic has triggered a number of studies and drug discovery programs trying to expand the use of Olaparib as a single agent or in combination with other drugs for different tumour types (Underhill, Toulmonde and Bonnefoi, 2011). PARP inhibitors and their resistance mechanisms will be reviewed later.

1.5.5 XRCC1 structure and function

Among the core enzymes of BER is the scaffold protein X-ray cross-complementing group 1 protein (XRCC1). Scaffold proteins have been shown to largely coordinate DNA repair pathways. These enzymes function mainly by binding to the DNA repair intermediates and preventing them from being released to create further damage (London, 2015). Mice with xrcc1 deficiency have embryonic lethality (Tebbs *et al.*, 1999). XRCC1 was shown to be involved in protection from alkylating agents and UV induced damage. XRCC1 does not possess any intrinsic enzymatic activities. Understanding the structure of XRCC1 and its distinct domains aided the

elucidation of its functions (London, 2015). Three discrete domains of XRCC1 have been described: the XRCC1 N-terminal domain (X1NTD) which is the site of interaction with DNA polymerase beta β (POLβ). The central domain (X1BRCTa) which has a poly (ADP-ribose) (PAR)-binding motif and enables XRCC1/ PARP1 interactions in the BER pathway. The second (BRCTb) domain that interacts with forkhead associated (FHA) domains. There are two inter-domain linkers that participate significantly in XRCC1 functions. Linker 1(XL1) and linker 2(XL2) both facilitate XRCC1 nuclear localization and recruitment of DNA polymerases (Figure 1-4). Importantly, both linkers are highly phosphorylated and their phosphorylation activities block degradation of the XRCC1-Ligase3α complex through the proteasome machinery (London, 2015; Yuan *et al.*, 2015) and the accomplishment of the BER pathway.



F**igure 1-4**: XRCC1 domain structure
(A) domain structure of XRCC1 showing N-terminal domain (NTD), and BRCT domains a &b. In between X-linker domains.
REV1 interacting region (RIR) and Nuclear localisation signal (NLS). (B) domain pI value adapted from Expasy site. (C) potential phosphorylated residues from phosphositePlus.
Adapted from (London, 2015)**.**

1.5.6 XRCC1 polymorphism and cancers

The most extensively studied polymorphisms of *XRCC1* are Arg194Trp, Arg280His, Arg399Gln, Pro161Leu and Tyr576Ser. Associations between *XRCC1* and breast cancers have been heavily studied in the literature. Polymorphisms in Arg399Gln and Arg280His were concluded to be associated with breast cancer risk in two recent meta-analysis studies by Bu *et al.* (Bu *et al.*, 2014) and Moghaddam *et al.* (Sanjari Moghaddam *et al.*, 2016). However, another study concluded that polymorphism in Arg194Trp is not associated with breast cancer risk (Huang, Li

and Yu, 2009). These findings are contradictory, with another study confirming that conclusion and showing no association between Arg194Trp *XRCC1* variant and cancer onset risk. On the contrary, the study by Moghaddam *et al.* showed potential increased breast cancer risks with Arg194Trp polymorphism (Sanjari Moghaddam *et al.*, 2016). The studies show that there is an impact for those polymorphisms but more detailed stratification for cases based on patient ethnicity and genetic background could give more meaningful conclusions. Not only have *XRCC1* genetic variants been associated with breast cancer risk but also evidence on the link between *XRCC1* variants and response to therapy have been emerging (Yuan *et al.*, 2015). Radiation therapy is very common in breast cancer treatment. Importantly, in a 2-stage designed study with discovery and replication phases involving 2600 breast cancer patients, the *XRCC1* genetic variant rs2682585 was highly associated with severe radiation toxicity (Seibold *et al.*, 2015). Another meta-analysis study investigated the pharmacogenetics of the *XRCC1* gene on platinum response in lung cancer patients. Patients bearing the favourable Arg194Trp have a better response to platinum than Arg399Gln, which predict poor response and worse outcome for patients (Yuan *et al.*, 2015).

1.6 Nucleotide excision repair pathway

Nucleotide excision repair (NER) is another crucial pathway for SSBR. NER is mainly responsible for the repair of the DNA lesions arising from UV radiation. Additionally, it is implied in the repair of bulky DNA adduct damage produced by platinum compounds (Saldivar, Wu and Gershenson, 2007).

The pathway can be broken down into four or five main steps and two different subpathways, the global genome repair (GGR-NER) and the transcription-coupled repair (TCR-NER) (Moser *et al.*, 2007). (TC-NER) lesions located in the transcribed genes on the DNA strand are recognised by RNA polymerase II, which is aided by Cockayne syndrome proteins, CSA and CSB. While in (GGR- NER) the recognition step is initiated by sensor proteins that scan the genomic DNA for chemical distortions. Thus, the protein complex XPC- hHR23B together with XPE recognise the DNA damage (Friedberg, 2003). The NER Pathway is illustrated in (Figure 1-6). When the XPC–hHR23B complex recruits TFIIH to the site of the damage, the second step, the unwinding of the DNA helix around the lesion, is then performed by TFIIH and its subunit helicases XPB and XPD along with the XPA–RPA complex. The incision step is then accomplished by the endonuclease activity of XPG and XPF-ERCC1 hydrolysing the phosphodiester bonds of the damaged strand at the 3’ and 5’ of the adduct respectively (Marteijn *et al.*, 2014). This rate limiting step requires the presence of XPG and the XPA–RPA complex for the right positioning of the XPG and the XPF-ERCC1 endonucleases. Excision and DNA re-synthesis are then performed by DNA polymerases δ and/or ε and ligation of the DNA is accomplished by DNA ligase I (Saldivar, Wu and Gershenson, 2007).

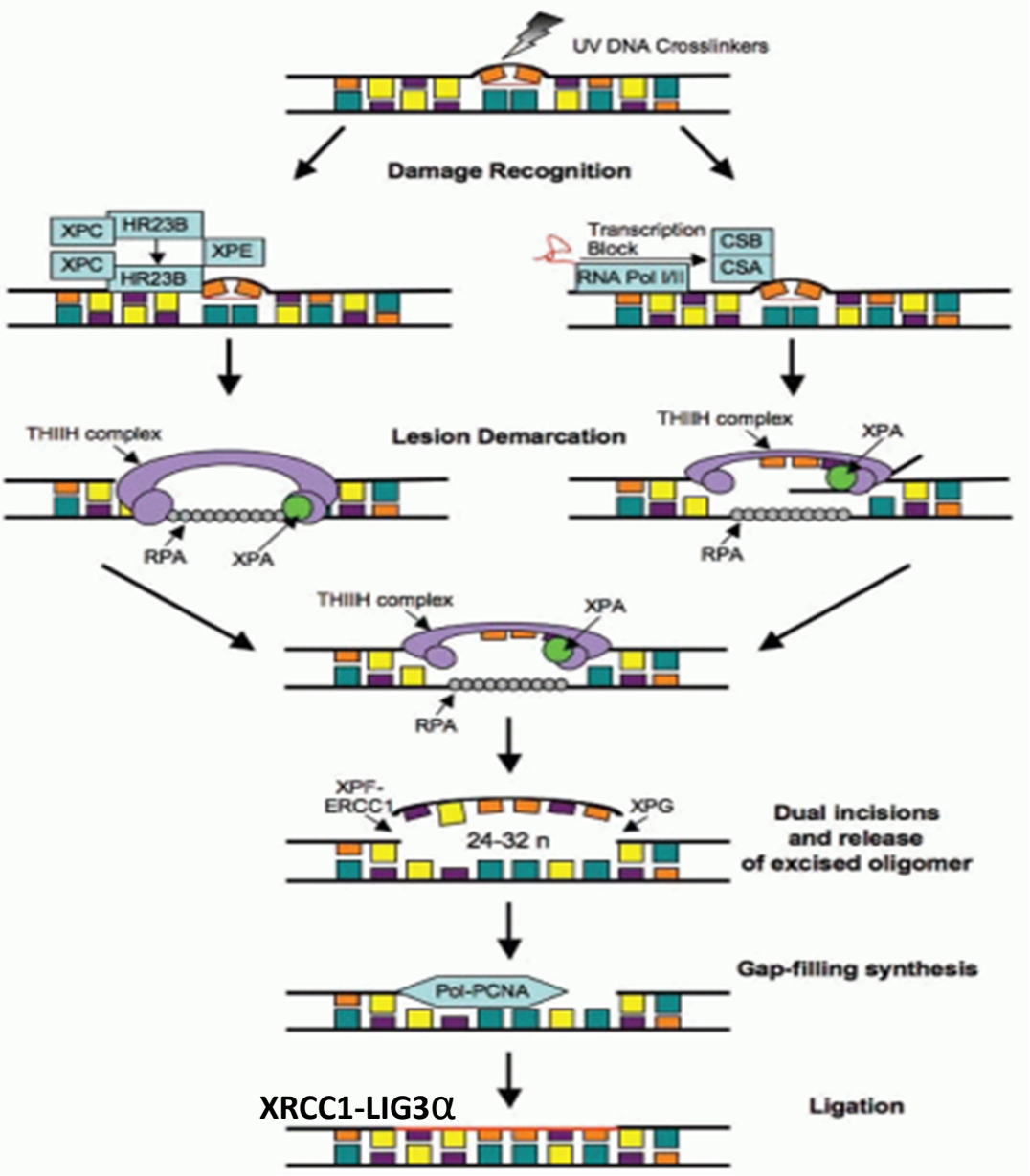


Figure 1-5: NER Pathway.

DNA damage recognition by XPC- hHR23B together with XPE in the GG-NER. In the TC-NER RNA pol II with CSA/CSB recognise the damage. TFIIH with XRA-RPA unwinds the DNA. XRCC1-LIG3α role was recognised in NER of UV induced lesions. Adapted from (Saldivar, Wu and Gershenson, 2007)

Interestingly, XRCC1-Ligase3α interactions have been described as being indispensable for the NER repair of UV induced lesions. XRCC1 and Ligase3α are recruited to the UV damage sites and co-localized with ERCC3 in both cycling and quiescent cells. Although XRCC1 has limited enzymatic activity these results demonstrated a new functional interaction between XRCC1 and DNA repair enzymes to orchestrate a DNA damage response (Moser *et al.*, 2007).

1.7 Poly (ADP-ribose) polymerases (PARPs) and their inhibition

1.7.1 Structure and functions of PARP1

PARP1 was initially introduced in 1963 (Kim, Wilson and III, 2012). Currently, the PARP superfamily includes 17 enzyme members. However, PARP1 is the most extensively studied member due to its well-defined functions in processing the SSB repair (Underhill, Toulmonde and Bonnefoi, 2011). PARP1, through the PARylation (poly [ADP-ribose] polymerization) process, catalyses the formation of poly (ADP) - ribosylated forms of its substrate molecule (NAD+). Parylation aids recruitment of other proteins to the site of DNA damage (Kim, Zhang and Kraus, 2005; Underhill, Toulmonde and Bonnefoi, 2011). This enzymatic activity is conserved in different organisms but not in yeast. PARP1 molecules have highly conserved motifs that play a role in its catalytic functions; The BRCA1 C-terminus-like domain (BRCT) and the N-terminal double zinc finger DNA-binding domain. PARP1 can bind to different forms of DNA such as single and double-strand breaks to some extent (Kim, Zhang and Kraus, 2005). Also, it has affinity to different DNA conformations like supercoils and cruciforms. Although the enzymatic activity of PARP1 is low at basal levels, DNA damage can activate PARP1 activity, trapping it at the sites of DNA damage and stimulating its catalysed PARylation (Figure 1-6) (Gavande *et al.*, 2016).

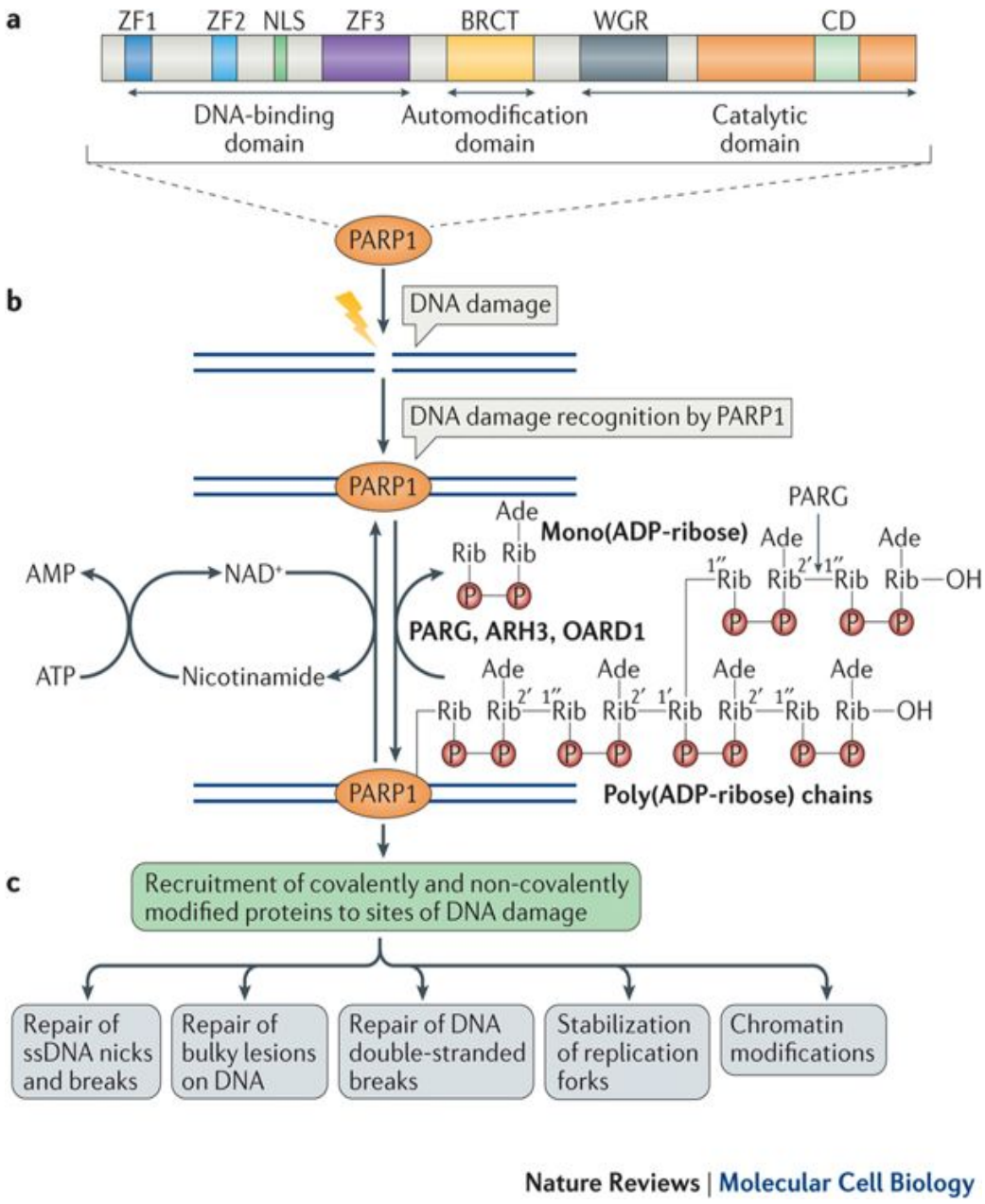


Figure 1-6: Structure and functions of PARP1.

(A) domains of PARP1 are shown here. (B) PARP1 recognises the DNA damage through its DNA binding domain. PARP1
catalyses the formation of Poly ADP ribose polymers (PAR) using NAD as a substrate. (C) Parylation of PARP1 and other target proteins is essential for repairing of different forms of DNA damage.
Adapted from (Ray Chaudhuri and Nussenzweig, 2017).

In addition to its role in DNA damage repair, in the presence of excessive DNA damage, NAD+ levels decrease significantly which can promote cell death. PARP1 depletion by genetic deletion or systemic inhibition is argued to induce the same lethal effect independently from NAD+ depletion. PARP1 activation induces the translocation of the apoptosis-inducing factor (AIF) from the mitochondria to the nucleus. Thus, in severe DNA damage, PARP activation is indispensable for efficient DNA repair as well as for triggering PARP1 dependent cell death mechanisms (Alano *et al.*, 2010).

1.7.2 Other members of the PARP family

Although PARP1 is the most crucial DNA repair player of the PARP family, attention should be given to other members. PARP-1, PARP-2, tankyrase 1 (TNK1), and tankyrase 2 (TNK2) form branched poly (ADP-ribose) (PAR) polymers; the rest of the PARPs are either mono or oligo ADPR-transferases (Bai, 2015). Similar to PARP1, PARP-2 and PARP-3 are also involved in some forms of double-stranded break (DSB) repair, which are mainly processed either by the non-homologous end joining pathway in the G1-phase or the homologous recombination pathway which operates mainly in the G2-phase of the cell cycle. PARP-1 and PARP-2 recruit other key proteins to process the (HR) pathway. However, PARP3 and TNK1 together with PARP1 are involved in NHEJ pathway events, though the exact mechanisms for these contributions remain unclear (Sajish and Schimmel, 2015). PARP family members are illustrated in (Figure 1-7).

PARP1, 2 and 3 can be regulated by various post-translational modifications such as phosphorylation, acetylation and ubiquitination. Nevertheless, self-parylation and sumoylation inhibit PARP activity. Micro RNA (miRNA) can also regulate PARP activity. In one such case, miRNA223 was reported to regulate PARP1, and miRNA149 similarly is involved in PARP2 regulation (Bai, 2015). The majority of PARP family enzymatic activity is exerted by PARP1 and to a minimal extent by PARP2. There is no doubt that PARP1 is the focus of extensive study in the PARP family (Szántó *et al.*, 2012).

Another important enzyme that is not considered a member of the PARP family is poly (ADP-ribose) glycohydrolase (PARG) which cleaves the poly ADP-ribose polymers and releases free ADPR molecules. PARG isoform co-localisation is different in the cellular compartments, whereas full-length PARG 111 is mainly located in the nucleus. PARG 102 and PARG 99 are present in the cytoplasm, whereas shorter isoforms (PARG 60, PARG 55) are localised in the mitochondria (Shirai *et al.*, 2013). PARG knock-out sensitized cells to the alkylating agent MMS indicating that PARG plays a role in the repair of alkylated DNA lesions such as the 3-methyladenine lesions and the O6-methyl guanine lesions induced by MMS. Hence, PARG could be essential in mismatch repair (MMR) and (HR) pathways (Shirai *et al.*, 2013).

PARG inhibitors are currently of interest to some researchers. The small molecule inhibitor PDDOOO17273 was recently reported to be synthetically lethal with BRCA1, BRCA2, PALB2, BRCA1 complex subunit (FAM175A) and the BRCA1-associated RING domain protein1 (BARD1) (Gravells, Grant, Kate M. Smith, *et al.*, 2017).

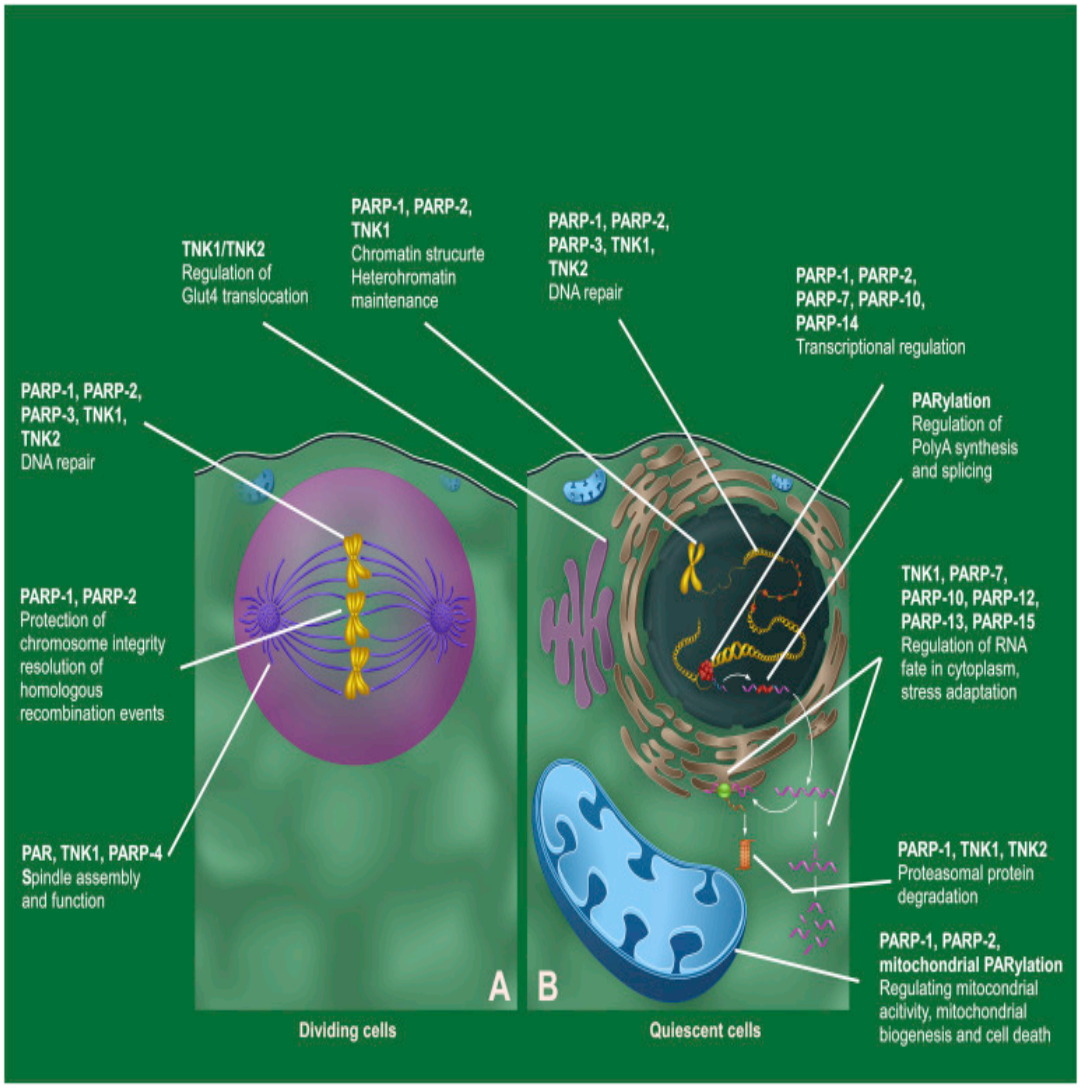


Figure 1-7: An overview of PARP family functions.

PARP1and PARP2 plays multiple roles in DNA repair, chromatin remodelling and transcription regulation (A) dividing cells. (B) Quiescent cells.
Adapted from (Bai, 2015).

1.7.3 Mechanisms of resistance to PARP inhibitors

Despite the promising results with PARP inhibitors (Here after PARPi) and the fact

1.7.3

that many PARPi are currently in clinical trials, tumours often can develop

resistance to PARPi. Olaparib, a well investigated PARPi, is the main focus of our

study. Olaparib has previously shown efficacy in breast, ovarian and other cancer models. However, reports of resistance to Olaparib have been emerging and therefore designed studies to understand the underlying mechanisms of resistance are crucial. It has been reported that truncated forms of the BRCA C-terminal (BRCT) domain of BRCA1 frequently give rise to protein products that are unable to fold and cannot be candidates for the proteasome machinery. The study by Johnsons et al. described a two-step mechanism for BRCA1 mediated resistance for Olaparib. The first step involves stabilization of the mutant forms of the (BRCT) by the heat shock protein (HSP) 90. Secondly, mutations in BRCT are also coupled with TP53BP1 mutation. These two mutant forms facilitated DNA end resection and thus they restored partial function and managed to accomplish RAD51 loading and HR pathway and hence PARP inhibitor resistance as well as platinum resistance (Johnson *et al.*, 2013).

Moreover, mutations occur in the BRCA1 RING domain like the BRCA1 (C61G) mutation which is a common missense variant and reduces the binding between BRCA1 and its heterodimer BARD1. Dimerization of BRCA1/BARD1 is essential for DSB repairs. BRCA1 (C61G) mutations cause failure in the interaction of BRCA1 with E2 ubiquitin-conjugating enzymes and thereby inhibit the E3 ubiquitin ligase activity of this heterodimer (Drost *et al.*, 2011). Thus, it is unclear which of the BRCA1 functions are required for therapy resistance.

The epigenetic re-expression of BRCA1 by the loss of methylation in the BRCA1 promoter may confer resistance to PARPi. That hypothesis was studied in a patient-derived xenograft (PDX) model in which 73% of the Olaparib resistant mice were BRCA1 positive due to re-expression of BRCA1 (Johnson *et al.*, 2013).

Another theory is that Pax2 transactivates domain-interacting protein (PTIP) deficiency which can stabilize MRE11 at the stalled replication fork and could restore HR activity in BRCA2 deficient cells (Ding *et al.*, 2016). Perhaps the mTOR pathway is another potential player in the PARPi resistance mechanisms. It has been reported that phosphorylation of the ribosomal protein S6 (an m -TOR downstream effector) contributes to PARPi resistance thereby restoring HR functions in the BRCA deficient context (Sun *et al.*, 2014).

1.7.3.1 Other mechanisms for PARPi resistance

Apart from the indirect restoration of homologous recombination or restoring BRCA function and disturbing the synthetic lethality relation between PARP1 and BRCA, there are other reports about the resistance to PARP inhibitors that can produce PARPi resistance regardless of BRCA status. At transcriptomic levels, mi-RNA can mediate PARPi resistance. Overexpression of the miR-622 can lead to reduced expression of several key effector molecules such as 53BP1, Ku70, and Ku80 and thereby inhibit the consequent NHEJ repair pathway (Choi *et al.*, 2016). Also, overexpression of c-Met in the cells predicts high resistance to PARPi. That was confirmed in the c-met mice knock out studies which are more sensitive to PARPi than the wild type cells. The receptor tyrosine kinase (c-Met) phosphorylates PARP1 at Tyr907. PARP1 Py907 increases PARP1 activity and decreases its binding affinity to PARPi. In fact, combining c-Met inhibitors and PARPi synergized PARPi in a xenograft model was an attempt to re-sensitize the cells to PARPi (Du *et al.*, 2016).

The HOX genes are a family of transcription factors that are important in embryonic development. Different isoforms of HOXs have been proposed to play

a role in epithelial differentiation in ovarian cancers. In DSB repair, HOXs were shown to have some functions through induction of TGF-β signalling that in turn recruit ATM to the sites of DSBs. Accumulation of RAD51 foci in HOXA9 amplified tumours suggests that HOX upregulation could be a mechanism for PARPi resistance (Kelly *et al.*, 2011).

Table 1-4: Recent clinical trials of PARP inhibitors

PARP inhibitor	**Target**	**Clinical trial**	**Inclusion criteria**
CEP-9722	PARP1&PARP 2	NCT01311713	Advanced or metastatic solid tumours.
Talazoparib	PARP1	NCT01989546	Advanced solid tumours and deleterious BRCA mutations.
2X-121	PARP 1/2 and Tankyrase 1/2.	NCT03562832	Metastatic breast cancers.
Veliparib	PARP1	NCT03044795	HR defective cancers that expressRAD51 foci.
Talazoparib	PARP1	NCT02049593	BMN-673 with temozolomide or irinotecan hydrochloride in treating patients with advanced or metastatic solid tumours
Olaparib	PARP1	NCT03575078	ARQ761 combination with Olaparib for treatment of

			lymphoma.
Talazoparib	PARP1	NCT02326844	Deleterious BRCA1/2 mutation associated ovarian cancers with previous PARP inhibitor treatment.
Rucaparib	PARP	NCT01074970	Breast cancer patients treated with cisplatin as a mono-agent or a cisplatin and Rucaparib combination.
Veliaparib	PARP1/PARP 2	NCT02723864	Cisplatin in combination with veliparib and VX-970 (ATR inhibitor) for treatment of solid tumours.

1.8 DNA polymerases:

1.8.1 Translesion polymerases

DNA polymerases are crucial enzymes for replication and DNA repair pathways. There are about fifteen studied DNA polymerases to date that have been grouped into different families (A, B, C, D, Y and X). The main function of these enzymes is to synthesize DNA and ensure accurate replication of the genome. Besides, DNA polymerases have other roles in DNA damage response (Albertella, Lau and O'Connor, 2005). In BER and NER, DNA polymerases are responsible for DNA gap filling by inserting nucleotides to replace damaged bases (Dianov, 2011). Some of these polymerases participate in DNA damage tolerance by performing a process called translesion DNA synthesis (TLS). When the replication fork encounters DNA lesions on the leading strand, replication is stalled. Although the lagging strand can still go through the replication mechanism, normal base pairing cannot progress and eventually replication will be blocked. The cells develop mechanisms to prevent this hazardous form of DNA damage and continue replication (H. Nicolay, Helleday and A. Sharma, 2012). TLS is an adaptive mechanism in which the cell switches to specific polymerases to insert a base in the lesion. However, that mechanism is done with very low fidelity and leads to mutations. There are seven identified polymerases that exhibit TLS activity in DNA replication; Polη, POLι, POLκ, POLη, POLθ and POLν (Albertella, Lau and O'Connor, 2005). Polη mutations are associated with increased predisposition to xeroderma pigmentosum and increased risk of squamous cell carcinoma (Lehmann *et al.*, 1975). Polη knock out mice cannot bypass light-induced cyclobutane pyrimidine

dimer lesions. In addition, Polη can bypass 8-oxoG lesions induced by radiation (Albertella, Lau and O'Connor, 2005). POLκ is suggested to be responsible for bypassing bulky DNA adducts. Previous reports have shown that POLκ are able to incorporate nucleotides opposite to N(2)-guanine lesions which is the same lesion induced by mitomycin C (Lehmann *et al.*, 1975). On the other hand, Polη was shown to have the ability to bypass cisplatin-GG adducts. Abasic sites are usually formed during BER due to oxidised and alkylated bases damage (Lange, Takata and Wood, 2011). Although Polη and POLκ have the capability to incorporate a base in Apurine or apyrimidine lesions, POLθ is the only polymerase known to insert nucleotides opposite to Abasic sites and continue extending the DNA template, though with very low fidelity (Seki *et al.*, 2004). POLν was shown to bypass thymine glycol lesions which are formed due to ROS (Yamtich and Sweasy, 2010). The exact mechanisms that trigger loading the polymerase of choice is still not fully understood, but the specificity of polymerases to particular lesions seems to play a role. Nevertheless, some studies described other factors. Blocking replication fork stimulates mono ubiquitination of PCNA by the E3 ubiquitin ligase activity of RAD51. The structure of the Y family of polymerases which comprises Polη, POLι and POLκ have a ubiquitin binding domain which can enable binding with ubiquitinated forms of PCNA and thus better loading onto the DNA. Rev1 is a DNA polymerase that has limited DNA synthesis ability compared to other polymerases. It is only proved to bypass UV induced DNA damage. Rev1 can interact with ubiquitinated PCNA and the Y-family of polymerases, and thus, it is suggested to have a role in binding the polymerase of choice (Yamtich and Sweasy, 2010). Understanding the roles and functions of TLS polymerases is a

crucial aspect in future cancer therapy as they contribute to DNA damage tolerance.

1.8.2 DNA polymerase Beta (Polβ)

DNA polymerase Beta (Polβ) is the most extensively studied member of the DNA polymerases, perhaps due to earlier reports showing the direct link between Polβ mutations and cancers. Polβ is a member of the X family of polymerases. Polβ sequence is conserved in mammalians; its enzymatic activity is a rate limiting step in the BER pathway. *Polβ* gene encodes a 39 KDa protein which comprises two domains enabling it to exert its enzymatic functions (H. Nicolay, Helleday and A. Sharma, 2012). The lyase activity functions through its N-terminal (8 KDa), while the nucleotidyl transferase functions through its c-terminal domain (31 KDa). Unlike other replicative polymerases, Polβ lacks 3'-5' exonuclease activity and therefore has lower fidelity compared to replicative polymerases (Dalal *et al.*, 2007).

Polβ deficiency in mice leads to embryonic lethality. Polβ deficient embryonic fibroblasts are exquisitely sensitive to methylating drugs. In normal human tissue, abundant polβ levels are only seen in testicular tissue. The pattern of polβ expression is relatively stable throughout the cell cycle. Due to its role in nucleotide gap filling during BER, polβ is required to be activated in the cells but in lower levels compared to replicative polymerases. Thus, this ensures better fidelity during replication (H. Nicolay, Helleday and A. Sharma, 2012). Overexpression of polβ leads to resistance to methyl methane-sulphonate (Chen *et al.*, 1998). High polβ expression was shown to trigger a mutator phenotype

(Canitrot *et al.*, 1998). Additionally, It can lead to frame shift mutations during the BER pathway (Chan *et al.*, 2007). A number of studies have investigated aberrations of polβ expression in tumours. A previous report showed polβ overexpression compared to other polymerases in tumour tissues of ovarian, uterine, prostate and stomach cancers (Albertella, Lau and O'Connor, 2005). Polβ variants have been reported in colorectal cancers (Donigan *et al.*, 2012), prostate cancer (Alnajjar *et al.*, 2017) and gastric cancer (Lang *et al.*, 2007). On the other hand, our group previously showed that low polβ expression at mRNA levels and protein levels is associated with high histological grade, triple negative phenotype and poor breast cancer prognosis (Tarek M.A. Abdel-Fatah *et al.*, 2014), suggesting a complex but key role for polβ dysregulations in genetic instability and tumorigenesis.

Recently, Polβ has been suggested to have a TLS activity at the AP sites leading to base substitution errors. Biochemical studies showed that polβ can bypass lesions formed by chemotherapeutic drugs. For instance, it can replicate past 1,2GG and 1,2AG adducts formed by cisplatin (Uchiyama *et al.*, 2009). Also, it can insert nucleotides opposite cyclobutene pyrimidine dimers formed by UV radiation with low fidelity error prone ability leading to mutagenesis (Uchiyama *et al.*, 2009).

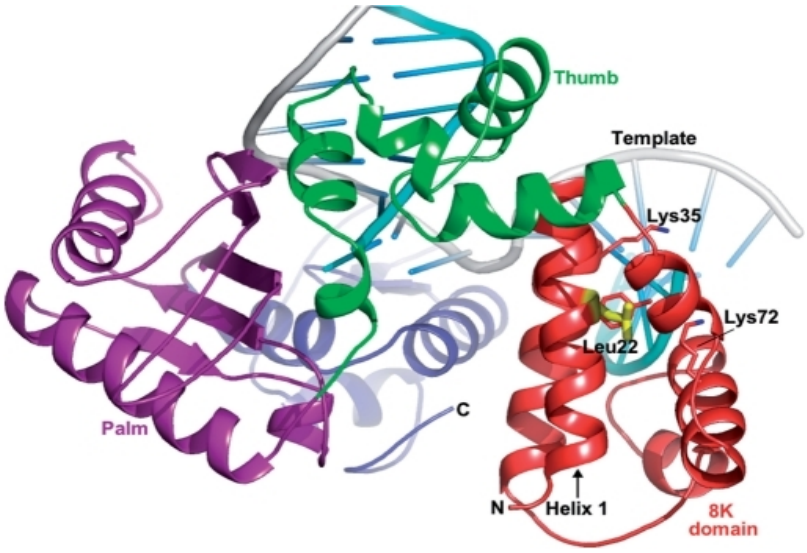


Figure 1-8: Polβ structural domains.

A ribbon representation of Polβ showing its dRP lyase domain (8KDa) and its nucleotide transferase domain (36KDa).
Adapted from (Dalal *et al.*, 2007)

Studies suggesting that polβ plays a role in mitochondrial DNA repair have been emerging (Prakash and Doublié, 2015; Prasad *et al.*, 2017). The levels of reactive oxygen species in the mitochondrial DNA is substantially high compared to that in nuclear DNA that is attributed to the increase in oxidative phosphorylation in its electron transport system. Theories proposing an efficient BER system for mitochondrial DNA have been put forward (Prakash and Doublié, 2015). The presence of functional key BER enzymes in the mitochondria was confirmed using several biochemical studies. DNA glycosylases and APE1 initiate the BER through excising the damaged base and creating Abasic sites that become a substrate to the function of the exonuclease activity of APE1. A similar mechanism is required to process the oxidized base lesions created in mitochondrial DNA. The presence of polynucleotide kinase phosphate (PNKP) enzyme is also crucial in mitochondrial

DNA for gap margins on the DNA before polymerase docking and gap filling. However, the nucleotide gap insertion function exerted by polβ in nuclear DNA repair is suggested to be performed by another polymerase (polϒ) in mitochondrial BER (Prakash and Doublié, 2015), although studies in that aspect are ambiguous. polϒ purified enzyme is able to process 5' DNA intermediates through its lyase activity, insert nucleotides in the gap and accomplish BER. However, polϒ dRP lyase activity is up to 20 times slower than polβ. Hence, it is doubtful that polϒ is efficient for the uprunning BER machinery to preserve mitochondrial DNA (Prasad *et al.*, 2017). Hansen and colleagues presented evidence to contradict this theory. In their study they isolated both polϒ and polβ from mitochondrial DNA. Their analysis of mutated polϒ and polβ activity on mitochondrial BER could not conclude the exact role of polβ (Hansen *et al.*, 2006). However, Earlier work isolated polβ like enzyme from bovine heart mitochondria (Nielsen-Preiss and Low, 2000). Another recent study investigated polβ expression in mitochondrial mice fibroblasts and revealed that polβ deficient mice fibroblasts have defective mitochondrial BER in response to hydrogen peroxide treatments (Prasad *et al.*, 2017). Taken together, these data suggest that polβ plays a role in mitochondrial BER. However, more work is needed to understand the exact mechanism of the interplay and switch between polymerases in mitochondrial BER machinery (Prasad *et al.*, 2017).

1.9 Hypothesis

In this study, we aimed to maximize the benefit of the synthetic lethality of PARP inhibitors beyond BRCA deficient tumours. We hypothesised that there is a synthetic lethality relationship between XRCC1 and PARP1. We postulated that XRCC1 deficient breast and ovarian cancers could be targeted with PARP1 inhibitors (Olaparib, Talazoparib and Niraparib). That new application will offer personalised therapies for new cohorts of patients with XRCC1 deficient tumours. In addition, we hypothesised that DNA repair dysregulation in DCIS is an early event in the progression to invasive breast carcinoma. Low XRCC1 expression in DCIS tumours is associated with local recurrence. We postulated that Olaparib could be a possible chemo preventative management for XRCC1 deficient DCIS lesions.

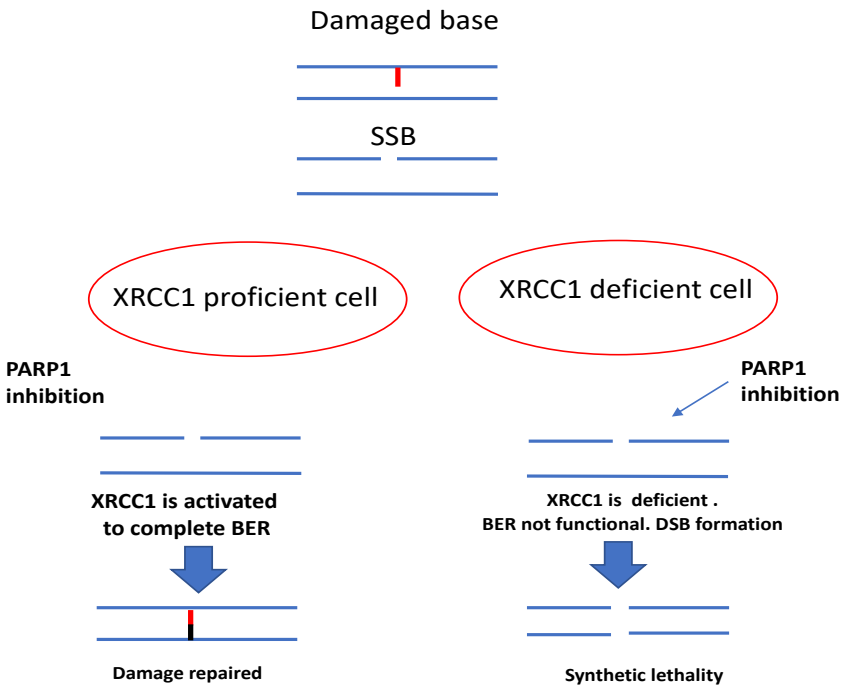


Figure 1-9: Diagram represents PARPi synthetic lethality.

In presence of PARPi, XRCC1 proficient cells can repair the SSB produced by PARPi. While XRCC1 deficient cells are unable to repair the SSB by the BER pathway and DSBs are formed resulting in synthetic lethality and cell death.

In the context of dysregulation of the base excision repair pathway in cancer, we hypothesised that overexpression of Polβ expression is associated with poor survival and platinum resistance in ovarian cancer patients. We postulated that Polβ inhibition can be a novel approach for Platinum chemo sensitization in ovarian cancers and that Polβ inhibitors can induce synthetic lethality in BRCA2 deficient ovarian cancers.

1.10 Objectives

I. Investigating the correlation between XRCC1 and PARP1 expression in breast tumours and patients' clinicopathological features and survival outcomes. We employed immunohistochemical staining of XRCC1 and PARP1 in a large cohort of invasive breast cancer patients (n= 1011).

II. Investigating the effect PARP1 inhibition in XRCC1 deficient cell lines. XRCC1 deficient and proficient cell line models are used. The generation of XRCC1 CRISPR-Cas9 knock out in MDA-MB-231 triple negative cells was performed to study this approach.

III. Exploring XRCC1 and PARP1 expression in a pure DCIS cohort (n=776) and correlating this with disease local recurrence and survival outcome for patients.

IV. Investigating Olaparib sensitivity in a XRCC1 deficient DCIS cell line model. To achieve that we generated XRCC1 CRISPR-Cas9 knock out in MCF10-DCIS cells. We explored the effect of XRCC1 deficiency on cell proliferation, spheroid forming ability, epithelial to mesenchymal transition as well as sensitivity to Olaparib.

V. Investigation of XRCC1 and PARP1 expression in ovarian cancers and correlation of their expression to clinicopathological features and Platinum sensitivity in patients. We approached that by immunohistochemical staining of XRCC1 and PARP1 in a cohort of ovarian cancer patients (n=525).

VI. Exploring PARP1 inhibitor (Olaparib and Talazoparib) sensitivity in XRCC1 deficient ovarian cell lines. XRCC1 transient knock down by siRNA was assayed in A2780, A2780cis and OVCAR3 ovarian cancer cells. XRCC1 CRISPR-cas9 knock out was generated in A2780 cells.

VII. Investigating Polβ and PARG expression in ovarian cancers and correlation of their expression to clinicopathological features and survival outcome in ovarian cancers. Immunohistochemical staining of Polβ and PARG was conducted in an ovarian cancer cohort (n=525).

VIII. Investigating the effect of Polβ inhibition and cisplatin sensitisation in ovarian cancer cell lines (A2780, A2780cis and PE04). Exploring Polβ small molecule inhibitors for synthetic lethality in BRCA2 deficient cells (HeLa BRCA2_KD &PE01).

IX. Exploring PARG inhibitor (PDD00017273) sensitivity in Polβ knock out cells.

2 Materials and Methods

2.1 Compounds

Olaparib (AZD2281) and ATR inhibitor AZD6738 were kindly provided by AstraZeneca Pharmaceuticals. Both were suspended in 100 % v/v dimethyl sulphoxide (DMSO) (Sigma, UK) and stored at 10mM concentration at-20 °C. p-ChK1 inhibitor (Chir-124) was purchased from (Selleckchem, UK). This compound was suspended in 100 % v/v dimethyl sulphoxide (DMSO) and stored at 10 mM concentration at-20 °C. Polβ small molecule inhibitor NSC666719 [4-chloro-5-methyl-N-[5-(naphthalen-2-ylamino)-1H1,2,4-triazol-3-yl]-2-sulfanylbenzenesulfonamide] was obtained from the Developmental Therapeutics Program of the National Cancer Institute of the National Institutes of Health and validated before in (Jaiswal *et al.*, 2009, 2011, 2015). Pamoic acid was purchased from Sigma Aldrich (UK). Compounds were stored at 50mM concentration and stored at 20 °C. Cisplatin was obtained as a solution (3.3mM concentration) from the pharmacy at Nottingham University Hospitals and stored at room temperature. Nutlin 3a and Azacytidine were purchased from (Sigma, UK). PARG inhibitor PDD00017273 was purchased from (Tocris, UK). Inhibitors were dissolved in DMSO at 10 mM concentration and stored at -20 °C.

2.2 Cell lines:

Cell lines used were purchased from the American Type Culture Collection (ATCC) and cultured as per ATCC recommendations. Hela scrambled control and HeLa SilenciX were purchased from Tebu-Bio. Culture media are shown in (Table 2-1). Cell line authentication was performed with AuthentiFiler™ PCR Amplification Kit. All cells were tested for mycoplasma routinely every 6 months using a MycoProbe Mycoplasma Detection Kit (R&D systems). All cell lines were used up to 15 passages.

Table 2-1: Cell lines and their culture conditions.

Cell Line	Culture media
MDA-MB-231 Triple negative breast cancer cells	Minimum Essential Medium Eagle (MEM) supplemented with 2mM L-glutamine + 10% FBS+ 1% penicillin/streptomycin.
MDA-MB-157 Triple negative breast cancer cells	Iscove's Modified Dulbecco's Medium (IMDM) supplemented with 15% FBS + 1% penicillin/streptomycin.
Chinese Hamster Ovary (CHO9) Murine breast cancer cells	Ham's Nutrient Mixture F12 supplemented with 10% FBS + 1% penicillin/streptomycin.
EMC-11 Murine breast cancer cells	Ham's Nutrient Mixture F12 supplemented with 10% FBS + 1% penicillin/streptomycin.
EMC-12 Murine breast cancer cells	Ham's Nutrient Mixture F12 supplemented with 10% FBS + 1% penicillin/streptomycin.
A2780 Ovarian cancer	RPMI -1640 supplemented with 10% FBS + 1%

cells	penicillin/streptomycin.
A2780-Cis Ovarian cancer cells	RPMI -1640 supplemented with 10% FBS + 1% penicillin/streptomycin.
PE01 Ovarian cancer cells	RPMI -1640 supplemented with 10% FBS + 1% penicillin/streptomycin.
PE04 Ovarian cancer cells	RPMI -1640 supplemented with 10% FBS + 1% penicillin/streptomycin.
OVCAR3 Ovarian cancer cells	RPMI -1640 supplemented with 10% FBS + 1% penicillin/streptomycin.
OVCAR4 Ovarian cancer cells	RPMI -1640 supplemented with 10% FBS + 1% penicillin/streptomycin.
SKOV3 Ovarian cancer cells	RPMI -1640 supplemented with 10% FBS + 1% penicillin/streptomycin.
HeLa (Control) Cervical cancer cells	Dulbecco's Modified Eagle Medium (DMEM) supplemented with 10% FBS + 1% penicillin/streptomycin.
Hela SilenciX Cervical cancer cells	DMEM supplemented with 125 µg/ml Hygromycin B + 10% FBS + 1% penicillin/streptomycin.
MCF10 DCIS Dcis breast cells	DMEM -F12 supplemented with 10% horse serum, insulin, cholera toxin, and Epidermal growth factor EGFR, hydrochortisone and 1% penicillin-streptomycin.

2.3 Clinical studies

2.3.1 Breast cancer study

The clinical study of XRCC1 and PARP1 expression was conducted on a consecutive series of 1650 patients with invasive breast cancers. Tumour samples were taken during surgery from the primary tumour site. The patients included in our study were diagnosed between 1986 and 1999 and were included into the Nottingham Tenovus Primary Breast Carcinoma series. All patients were treated in a single institution and their tumours have been well characterised with the evaluation of a series of biomarkers in previous publications (Elston and Ellis, 1991; Galea *et al.*, 1992; ELLIS *et al.*, 2007). Patients' demographics are summarised in (Table 2-2). Additionally, XRCC1 /PARP1 expression was evaluated in a separate cohort of 281 ER negative invasive breast cancers. Patients were treated in Nottingham University between 1999 and 2007. The patients were treated uniformly whereas breast surgery, followed by radiotherapy and anthracycline chemotherapy were the standard treatment regimen for all ER negative patients. ER negative cohort demographics are summarised in (Table 2-3.)

The Reporting Recommendations for Tumour Marker Prognostic Studies (REMARK) criteria, recommended by McShane *et al*. (McShane *et al.*, 2005), were followed throughout this study. The ethical approval for the study was granted by the Nottingham Research Ethics Committee in accordance with the Declaration of Helsinki and ethical approval (C202313). Written informed consent from patients was obtained where applicable.

Table 2-2: Clinicopathological characteristics of breast cancer patients' cohort.

Variable	**n***	**Cases**	**(%)**
Menopausal status	1650		
Pre-menopausal		612	(37.0)
postmenopausal		1038	(63.0)
Tumour Grade (NGS)	1650		
Grade1		306	(18.5)
Grade2		531	(32.2)
Grade3		813	(49.3)
Lymph node stage	1650		
Negative		1056	(64.0)
Positive (1-3 nodes)		486	(29.5)
Positive (>3 nodes)		108	(6.5)
Tumour size (cm)	1650		
TNM1a+1b (⩽1.0)		187	(11.0)
TNM c (>1.0 -2.0)		868	(53.0)
TNM2 (>2.0-5)		5729	(35.0)
TNM3 (>5)		16	(1.0)
Tumour type	1650		
IDC-NST		941	(57)
Tubular		349	(21)
ILC		160	(10)
Medullary (typical/atypical)		41	(2.5)
Others		159	(9.5)
NPI subgroups	1650		
Excellent PG(2.08-2.40)	Low risk	207	(12.5)
Good PG(2.42-3.40)		331	(20.1)
Moderate I PG(3.42 to 4.4)	High risk	488	(29.6)
Moderate II PG(4.42 to 5.4)		395	(23.9)
Poor PG(5.42 to 6.4)		170	(10.3)
Very poor PG(6.5–6.8)		59	(3.6)

Survival at 20 years	1650		
Alive and well		1055	(64.0)
Dead from disease		468	(28.4)
Dead from other causes		127	(7.6)
Adjuvant systemic therapy (AT)	1602		
No AT		665	(42.0)
Hormone therapy (HT)		642	(41.0)
Chemotherapy		307	(20.0)
Hormone + chemotherapy		46	(3.0)

* Number of cases for which data were available. TNM; tumour, lymph node, metastasis breast cancer staging. IDC-NST: invasive ductal carcinoma, no special type. ILC: invasive lobular carcinoma. NPI; Nottingham prognostic index, PG; prognostic group.

2.3.2 DCIS study cohort

The investigation of XRCC1 and PARP1 expression in DCIS was performed in a pure non-invasive DCIS cohort of 776 patients diagnosed between 1987 and 2012. The patients were identified from the National Health System (NHS) database of the Nottingham University Hospitals. The newly constructed cohort was reviewed by colleagues in the Breast Pathology Group. Patient demographics are summarised in (Table2-4). The samples were assessed with haematoxylin and eosin (H&E) staining. H&E staining is usually performed to select the most representative area of the whole tissue and to avoid haemorrhagic and necrotic tumour zones. The slides were digitally scanned using a high-resolution slide scanner (PANNORAMIC 250 FLASH III, 3DHISTECH) at 20x magnification. Formalin-fixed paraffin

embedded (FFPE) tissue blocks for the pure DCIS cases were retrieved and evaluated for selection of DCIS representative blocks. Subsequently, further H&E staining was prepared from the selected DCIS blocks for the assessment of tumour burden and suitability for the construction of Tissue Microarrays (TMAs) as a representative of the original block. Another cohort of 239 cases of IBC with a DCIS component was also identified from the NHS database. The patients were diagnosed between 2000 and 2007 only as other cases before 2000 were included in the invasive cohort. The suitable blocks were similarly assessed with H&E staining and retrieved for inclusion in the study. Another 50 normal breast tissues were also identified from the NHS databases and included in the study for the purpose of comparison with the DCIS cohort.

Table 2-3: Patient demographics in the DCIS cohort.

Parameter	**Groups**	**Number**
Age	≤45 years	57
	>45 years	396
Presentation	Screening	217
	symptomatic	236
Extent	Localized	305
	Diffused	67
Size	≤20mm	195
	>20mm	255

Grade	Low	60
	Moderate	117
	High	276
Comedo/ Necrosis	No.	154
	Yes	299
DCIS type	Pure DCIS	453
	DCIS + invasive	196
LCIS	No	411
	Yes	42
Paget's.	No	276
	Yes	21
ER* status	Negative	109
	Positive	308
PR status	Negative	177
	Positive	246
Treatment	Mastectomy	260
	Breast conserving surgery +RT	193
	Breast conserving surgery	123

ER: Estrogen receptor.PR: Progestogen receptor.

2.3.3 Ovarian cancer study cohort

Investigation of the expression of XRCC1, PARP1, Polβ and PARG in epithelial ovarian cancers was carried out on tissue microarrays of 525 consecutive ovarian epithelial cancer cases treated at Nottingham University Hospitals (NUH) between

1997 and 2010. Patients staging wasere conducted according to the International Federation of Obstetricians and Gynaecologists (FIGO) Staging System for Ovarian Cancer. Overall survival for patients was calculated from the operation date until the 1st of October 2016 when any remaining survivors were censored. Progression-free survival was calculated from the date of the initial surgery to disease progression or from the date of the initial surgery to the last date known to be progression-free for those censored. Platinum resistance was defined as patients who had progression during first-line platinum chemotherapy or relapse within 6 months after completion of chemotherapy. Patient demographics are summarized in (Table 2-4).

Table 2-4: Ovarian cancer cohort patients demographics

Characteristics	**Number**	**Percentages**
Pathology		
Serous cystadenocarcinoma	290	55.2%
Endometrioid	82	15.6%
Clear cell carcinoma	48	9.1%
Mucinous cystadenocarcinoma	60	11.4%
Others	18	3.4%
Mixed	17	3.2%
Unknown	10	2.1%
Grade		
1	68	12.9%
2	87	16.5%

3	306	58.2%
Unknown	64	12.4%
Residual tumour		
None/Microscopic	265	50.4%
<1cm	82	15.6%
>1-2 cm	29	5.5%
>2cm	110	20.9%
FIGO Stage		
I	182	34.6%
II	76	14.4%
III	213	40.5%
IV	32	6%
Unknown	22	4.5%
Chemotherapy		
Carboplatin monotherapy	163	31%
Carboplatin + Paclitaxel	177	34%
Other platinum-based regimes*	121	23%
No chemotherapy	25	5%
Unknown	39	7%
Platinum sensitivity		
Sensitive	376	71.6%
Resistant	85	16.1%
Unknown	64	11.8%

Relapse status		
Progression-free	238	45.3%
Progressed/relapsed	243	46.2%
Unknown	44	8.3%
Survival status		
Living	199	37.9%
Dead	286	54.4%
Unknown	40	7.6%

*= CAP (Cyclophosphamide, Adriamycin and Cisplatin), ICON5 Trial, SOCTROC Trial, Carboplatin and Endoxan

2.3.4 Tissue microarray construction

The FFPE blocks with abundant tumour burden and suitable thickness for arraying were selected for TMA construction. TMAs were constructed with 2 replicate 0.6-mm cores on paraffin wax receipt blocks. Samples were taken from the centre and periphery of the tumours or other lesions for comprehensive evaluation of tumour and surrounding stroma. The automated TMA arrayer machine (Beecher Instruments) was used to load up to 60 donor blocks at a time on the recipient blocks. For preserving the orientation of the tissue cores, three normal kidney cores were loaded at the start of the first row and two more at the end of the last row were used to mark the orientation. The constructed TMAs were then

sectioned at 4 μM thickness on clean glass slides for immunohistochemical staining (Kononen *et al.*, 1998).

2.3.5 Immunohistochemical staining

Immunohistochemistry was conducted as per the protocol validated and published previously (R. Sultana *et al.*, 2013; Green *et al.*, 2015). Slides containing TMAs were stained using a Novolink Polymer Detection System Kit (Leica Biosystems, RE7150-K). Initially, the slides were heated at 60°C for 10 min. The slides were deparaffinised and re-hydrated using a Leica autostainer machine. The slides were automatically processed through immersion in two racks of Xylene for 5 min each, followed by washing three times (2 mins each wash) with 100% industrial methylated spirit (IMS). The slides are then rehydrated in water racks three times for 5 mins each.

2.3.5.1 Antigen retrieval and staining

Antigen retrieval steps were performed for all biomarkers except EGFR and HER2. Slides were heated in 0.1M sodium citrate buffer (PH 6.0) using a microwave oven for 20 min. After cooling of the slides using running tap water, primary antibodies were added at the indicated dilutions (Table 2-6).

Blocking of endogenous peroxidase activity was performed by incubating the slides with 100 μL of the supplied peroxidase block solution (Novolink kit) for 5 mins. The slides were then washed with Tween phosphate buffer saline (TBS) three times for 5 mins each. Post primary block followed by Novolink polymer incubation were performed for 30 mins incubation time each followed by washing

with TBS three times for 5 mins each. Peroxidise reaction was visualised using freshly prepared solution of 3-3' Diaminobenzidine tetrahydrochloride (DAB). 100 μL of diluted DAB chromogen was diluted at (1:20) dilution in DAB substrate provided by the kit. Finally, the slides were counterstained with Novolink haematoxylin for 6 min, then dehydrated in the Leica autostainer machine. The slides were then covered with coverslips and left in the fume cupboard to dry overnight.

Negative controls were included in each run by omission of the primary antibody incubation step. Positive control tissues with known reactivity to stained antibodies as suggested by the suppliers' recommendations were included accordingly for each antibody. Antibody staining conditions and cut-off points for analysis are summarised in (Table 2-5).

Table 2-5: Antibodies for immunohistochemistry.

Antibody	**Supplier**	**Dilution**	**H-score cut-off**
Anti-XRCC1 mouse monoclonal antibody (Breast TMAs)	Thermofisher Scientific. Clone (33-2-5)	1: 200. incubation for 15 mins room temperature	≤100
Anti-PARP1 mouse monoclonal antibody (Breast TMAs)	BD Pharmingen, USA, catalog. no.7D3-6	1: 1000 incubation for 15 mins room temperature	≤10
Anti-XRCC1 mouse monoclonal antibody (Ovarian TMAs)	Thermofisher Scientific. Clone (33-2-5	1: 250. incubation for 30 mins room temperature	≤100
Anti-PARP1 mouse monoclonal antibody (Ovarian TMAs)	BD Pharmingen, USA, catalog. no.7D3-6	1:600 incubation for 60 mins room temperature	≤80
Anti-polβ rabbit polyclonal antibody (Ovarian TMAs)	Abcam, catalog no. ab26343	1:200 incubation for 60 mins room temperature	≤180
Anti-PARG rabbit polyclonal antibody (Ovarian TMAs)	Thermofisher Scientific, catalog no: PA514158	1:100 incubation for 60 mins room temperature	≤105

2.3.6 Optimisation of immunostaining conditions

Optimisation of the staining conditions for each antibody was approached by incubating consecutive slides with three different dilutions of the antibody starting with the suggested dilution range by the antibody supplier. Additionally, incubation time and temperature were evaluated by testing room temperature incubation and overnight incubation. Optimisation slides were reviewed by a pathologist for choosing the optimum conditions. Optimum staining will indicate the sub-cellular localisation of the antibody of interest (nuclear, cytoplasmic or membranous). Antibody dilutions which achieve specific immune staining with minimal background were chosen for staining the slides of the whole cohorts. The studied biomarkers were evaluated previously in our group for homogeneity staining in full-face sections (Rebeka Sultana *et al.*, 2013; Tarek M A Abdel-Fatah *et al.*, 2014; Green *et al.*, 2015). The concordance between the expression in full-face and the TMAs was high. Therefore, TMA staining was suitable for assessment of the biomarkers.

2.3.7 Evaluation of immune staining

Two individual cores from each tumour case were evaluated separately and the mean of the two histochemical scores (H-score) was calculated. The H-score evaluates both the intensity and the positivity of the immune staining and combines both into one score. The intensity of the staining is allocated a score of 0, 1, 2 or 3 corresponding to negative, weak, moderate or strong, respectively. The percentage of the positive cells is estimated in a range of 0-100%. The final score is calculate using the formula: 3 x percentage of strongly staining nuclei + 2 x percentage of moderately staining nuclei + percentage of weakly staining nuclei to

give a score between 0-300. There was an excellent intra and inter-observer agreement between my scoring and the expert pathologist scoring according to the Cohen Kappa concordance which was calculated (K > 0.7).

2.3.8 Statistical analysis of immunohistochemical data

Statistical analysis was performed using SPSS software ver.21. The cut-off points for negative H-scores were chosen based on the median according to the pattern of distribution of the data. Chi-squared tests were used for univariate correlation between the biomarker expression and each of the clinicopathological parameters. Cox regression analysis was performed for multivariate analysis. Survival curves were analysed by the Kaplan-Meier method. P-values of <0.01 were considered a significant result. Adjusted p-values were calculated using the Benjamini and Hochberg method (Benjamini and Yekutieli, 2005).

2.3.9 Sub-culturing of cell lines:

All cell lines were cultured at 37ºC in a humidified incubator with 5% CO2 and 95% air. Cells were handled under sterile conditions. For sub-culturing cells, the medium was removed and they were washed with phosphate buffered saline (PBS) (without Ca2+ and Mg2+). Adherent cells were detached from the flask by addition of 0.5mg/ml trypsin EDTA (Sigma, UK) 2ml or less and incubated for 3-5 minutes at 37ºC. Flasks were gently shaken to aid disruption of the monolayer. The medium was used at a 4:1 ratio to trypsin to deactivate its enzymatic activity. Cells were collected by centrifugation at 1000 rpm. The formed cell pellet was

resuspended in fresh medium and split into a new flask for re-growing. All cells were tested for mycoplasma regularly.

2.3.10 Cryopreservation of cell lines:

Cells were cryopreserved in the liquid nitrogen bank at a low passage number for future use. Cells were collected by trypsinization as described. To perform cell counts, cells were resuspended and mixed well in fresh medium and 10 µL of the suspension was pipetted into a Neubauer Chamber. The suspension sat for 1 minute before counting. $1x10^6$cells were resuspended in 1 ml of freezing medium. Freezing medium consisted of complete culture medium for the cell line + 10% DMSO. Cells were stored in a freezing container (Mr frosty) at -80 ºC overnight and then transferred to liquid nitrogen for long-term storage. Cells were sub-cultured for experiments for 10-15 passages and then discarded and fresh vials were thawed for use. For recovering cells from liquid nitrogen, cells were rapidly thawed in the water bath at 37°C. Cells were resuspended in fresh culture medium and transferred to tissue culture flasks to adhere overnight. The following day, the medium was changed to fresh medium to remove the traces of DMSO.

2.3.11 Transient transfection of cell lines by siRNA:

Two siRNA constructs were used for polβ knock down. A pre-validated siRNA construct was used for XRCC1 in this study (R. Sultana *et al.*, 2013). Silencer select siRNA constructs, as well as a negative scrambled control construct, were purchased from Thermofisher (UK). Constructs were resuspended in 50 µL nuclease-free water to make a stock solution of 100 µM and diluted to 10µM

working dilution at the time of transfection as per manufacturer recommendations. Lipofectamine 3000 transfection reagent (Thermofisher, UK) was used to deliver siRNA to the cells in Opti-MEM low serum media (Sigma, UK). Lipofectamine proportions were used as recommended in the manufacturer's protocol. To transfect cells with siRNA, 1-1.5 $x10^6$ cells were seeded in T25 flasks overnight to achieve 60-70% confluency the following day for transfection. 20.8 µl Lipofectamine 3000 were diluted in 0.75 ml Opti-MEM medium. Then 9.4µl of 10µM working siRNA solution or negative control (catalogue no. 4390843 Thermofisher, UK) was diluted in 0.75 ml Opti-MEM for 2-3 minutes. Then diluted lipofectamine was added to the diluted siRNA tube and incubated for 15 minutes. Meanwhile, cells were washed with Opti-Mem media before the addition of transfection master mix. Transfected flasks were incubated at 37°C overnight. The next day the transfection medium was replaced with fresh culture medium supplemented with 10% FBS. Transfection efficiency was checked by western blotting at day 3 and day 5.

Table 2-6: siRNA constructs and their sequences.

Construct	**Sequences**
XRCC1 siRNA (ID s14942)	5'GCUUGAGUUUUGUACGGUUtt 3'-sensesequence 3'acCGAACUCAAAACAUGCCAA5' –antisense sequence
Polβ siRNA_1 (ID s10776)	5' CGUGAAGAGAUGUUACAAAtt 3' sense sequence 3' UUUGUAACAUCUCUUCACGag 5' antisense sequence
Polβ siRNA _2 (ID s10775)	5' CAACUGGAAAAUUACGUAAtt 3' sense sequence 3' UUACGUAAUUUUCCAGUUGct 5' antisense sequence

2.3.12 Generation of CRISPR Cas-9 knock out

Oligonucleotides carrying silencing gRNA for XRCC1 or Polβ cloned into a Plv-U6g-EPCG plasmid (Figure 2-1) expressing Cas-9 and carrying the puromycin resistance gene were purchased from Sigma (UK). Transfection cells were seeded at 60-70% confluency in 6 well plates overnight. The following day 7.5 µL lipofectamine 3000 were diluted into 500µl Opti-MeM medium and 2-3 µg of CRISPR plasmid were diluted in 500µl Opti-MeM and p3000 reagent. Diluted lipofectamine was added into diluted DNA tubes and incubated for 15 minutes at room temperature. Meanwhile, the cells were washed with Opti-MeM and the transfection mixture was added and left overnight. The transfection medium was changed to complete culture medium the next day. After 48 hours, the selection of desired clones started with puromycin. MDA-MB-231(XRCC1_KO) cells were selected in 10µg/ml puromycin. A2780, A2780cis, and MCF10DCIS cells were selected in 5µg/ml of puromycin. Selection doses were determined pre-transfection using the puromycin kill curve experiment in the parental cells. After 2 weeks stable transfected colonies were amplified, and transfection efficiency was checked by western blotting.

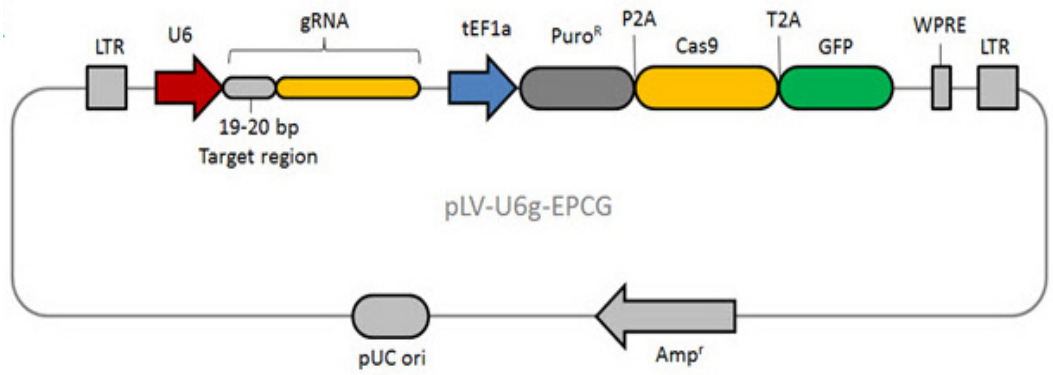


Figure 2-1: pLV-U6g-EPCG map.

Plv-U6G-EPCG plasmid incorporating g-RNA for silencing XRCC1 or POLβ was used.

2.3.13 Preparation of cell lysates:

To prepare cell lysate for western blotting experiments, cells were collected by trypsinization as described. They were then counted in the Neubauer chamber, 1x106 were lysed by resuspending the pellet in 100 µl of RIPA buffer (20 mM Tris, 150 mM NaCl, 0.5% sodium deoxycholate, 1mM EDTA, 0.1% SDS) purchased from Sigma(UK) supplemented with 1% of protease inhibitor (Sigma, UK), 1% of phosphatase inhibitor cocktails 2 and 3 (Sigma, UK). The cell lysate was incubated on ice for 30 minutes then repeatedly aspirated with a fine-gauge needle to break all the cellular membranes. Lysates were centrifuged at 13000 rpm for 20 minutes in a 4°C pre-setup microcentrifuge. The supernatant was stored at -20°C.

2.3.14 BCA protein quantification assay

The Pierce™ BCA Protein Assay Kit was used to quantify proteins in the cell lysate using the standard curve method of pre-determined protein concentrations of

BSA (bovine serum albumin). The dilutions of BSA were prepared in nuclease-free water to obtain the following concentrations: 2000 µg/ml, 1500 µg/ml, 1000 µg/ml, 750 µg/ml, 500 µg/ml, 250 µg/ml, 125 µg/ml, 25 µg/ml and 0 which is the blank. 8 µl of diluted protein samples (diluted 1:5 in nuclease free water), as well as the standards, were pipetted in triplicates in a 96-well plate. They were then mixed with 200 µl of the working solution of BCA reagent and incubated at 37°C for 30 minutes before reading on a FLUOstar OPTIMA, UK/ Infinite® F50 (UK) microplate reader at a wavelength of 595 nm.

2.3.15 Western blotting

Western blotting is a semi-quantitative technique widely accepted to determine relative protein levels in cell or tissue lysate. The assay usually involves two steps: separation of protein according to their electrophoretic mobility on sodium dodecyl sulfate (SDS)-polyacrylamide gel, and electrophoretic transfer of proteins on nitrocellulose or polyvinylidene difluoride PVDF membranes to enable detection by relevant antibodies. In this protocol, ready-made, SDS 4X sample buffer from Thermo Fisher (UK) was used. SDS is an anionic detergent which breaks the hydrogen bonds between molecules and aids protein unfolding. Dithiothreitol (DTT) reducing agent 10x (Thermofisher, UK) was added to the sample to break disulphide linkages between cysteine molecules. 20 µg of cell lysates were diluted in sample buffer and reducing agents and then proteins were totally denaturated by heating at 100°C for 5 minutes. Precast SDS 4-12% gels (Thermofisher, UK) were used for loading the denaturated protein samples in a

propanesulfonic acid-sodium dodecyl sulfate (MOPS-SDS) sample buffer at 150 constant volts for approximately 90 minutes.

The detection of proteins separated on the SDS-PAGE gel involved five main steps: transfer, blocking, primary antibody incubation, secondary antibody incubation and protein detection and analysis.

2.3.15.1 Transfer

Proteins were transferred to a nitrocellulose membrane (Whatman, GE Healthcare) in a transfer buffer containing 20% (v/v) methanol, 50 mM Tris-HCl, and 380 mM glycine. The SDS-PAGE gel containing the proteins was blotted in a Xcell II Blot Module (Invitrogen) in a semi-dry transfer using a gel-Membrane-Filter sandwich running at 25 volts for 90 minutes.

2.3.15.2 Blocking

The unreacted sites on membranes should be blocked after the protein transferring step to reduce non-specific binding with the subsequent antibodies. 5% non-fat milk in phosphate buffered saline (PBS) solution + 0.05% Tween-20 was used to block the membranes for 1 hour at room temperature.

2.3.15.3 Primary antibody incubation

The primary antibody against the target protein was incubated at 4°C overnight or 1 hour at room temperature. After the primary antibody incubation steps the membranes were washed with PBS + 0.05% Tween-20 wash buffer three times for 5 minutes each to remove unbound primary antibodies. The membranes were then incubated with an antibody against the abundantly expressed protein

(housekeeper protein) to be used in relative protein quantification and analysis. The housekeeper antibodies used are the anti-β-actin antibody (Sigma, UK), β-tubulin and GADPH (Abcam, UK). All primary antibodies have been diluted in 1% BSA (bovine serum albumin). The same washing step was repeated after the housekeeper antibody incubation.

2.3.15.4 Secondary antibody incubation

The membranes were exposed to HRP (horseradish peroxidase) conjugated secondary antibodies to enable detection of the primary antibodies. The secondary antibodies used are IRDye® 680RD Donkey anti-Mouse IgG and IRDye® 800CW Donkey anti-Rabbit IgG. Both were used at 1:10,000 dilutions in 1% BSA. The membranes were incubated with the secondary antibodies for 1 hour at room temperature then washed with PBS/0.05% Tween three times for 5 minutes each before drying and scanning.

2.3.15.5 Detection and analysis

The LI-COR Odyssey Imaging System was used to detect the antibody reacted bands on the membranes. The Image Studio Lite software (Ver 3.1) (Li-Cor, USA) was used for quantification of the bands. The readings for the protein of interest were normalized against the housekeeper readings. The assay was performed in three independent experiments. The student t-test or one way-ANOVA test was used to calculate statistical significance between samples. Graphs were produced and statistical analysis was performed using GraphPad Prism software.

2.3.16 Cell proliferation assay (MTS assay)

This assay used a colourimetric method for determining the viability of cells in proliferation, cytotoxicity or chemosensitivity assays. The CellTiter 96® AQ_{ueous} One Solution Reagent (Promega, UK) used here contains a tetrazolium compound [3-(4,5-dimethylthiazol-2-yl)-5-(3-carboxy methoxy phenyl)-2-(4-sulfophenyl)-2H-tetrazolium, inner salt; MTS] and an electron coupling reagent (phenazine ethosulfate; PES). Tetrazolium can be only reduced by the viable cells with the aid of NADPH or NADH dehydrogenases to form a stable coloured formazan solution. This coloured formazan product can be measured at 490nm absorbance in a 96-well plate reader and its concentration will be relative to the cells' viability. To perform the MTS assay, 1000 cells/ well in a 100µl were seeded in a flat-bottom 96-well plate overnight. The following day the drug to be tested was added at the indicated doses to the cells in triplicates. The control cells were incubated with a DMSO negative control diluted in culture medium. Then cells were incubated with the drug at 37°C for 5 days. On day 6, 20 µl of the CellTiter 96® Aqueous One Solution Reagent was added to each well. Then the cells were incubated for 1-4 hours before reading using a FLUOstar OPTIMA, UK/ Infinite® plate reader at 490nm (recommended absorbance). To determine the proliferation of treated cells, the average readings of each dose treated cells were normalized against the average readings of the control wells. The data was plotted as a survival curve in GraphPad Prism.

2.3.17 Clonogenic survival assay

2.3.17.1 Assay principle

The clonogenic assay is a well described in vitro method to test the ability of every single cell in the assay for division and colony formation. The assay can measure drug cytotoxicity or ionizing radiation efficacy after allowing the cells to perform at least 5-6 replication rounds. Each colony will contain at least 50 cells and can be seen by the naked eye at the end point of the experiment. Colonies can be stained with crystal violet stain and counted for estimating the survival relative to the control.

2.3.17.2 Plating efficiency

Prior to performing the clonogenic survival assay with the cytotoxic drugs, the plating efficiency of each individual cell line should be determined. Plating efficiency can be defined by the ability of individual cells to form a colony. To test the plating efficiency of a cell line, cells were seeded at various seeding densities in 6-well plates in triplicates and left to grow under normal incubation conditions for 14 days. At the end of the incubation period, the media were removed, and the cells were fixed (with methanol and acetic acid mixture) for 10 minutes. Plates were stained with crystal violet and colonies counted manually. Plating efficiency was calculated from (number of colonies formed/number of cells seeded) x 100.

2.3.17.3 Clonogenic assay protocol

Cells were seeded in 6-well plates and left to adhere overnight. The following day the tested drugs were added to the cells at the indicated concentration in complete culture media. Each condition was tested in triplicates and control cells were exposed to DMSO diluted in culture medium. The plates were left in the incubator at 37°C for 14 days. At the end of incubation, the media were removed, and the cells were fixed (with a methanol and acetic acid mixture) for 10 minutes. Plates were stained with crystal violet and colonies counted manually. Blue stained visible colonies with ≥ 50 cells were counted manually, and the survival fraction was calculated as follows:

Surviving Fraction = [No. of colonies formed / (No. of cells seeded x Plating efficiency)]. The assay was performed three times and graphs were generated using GraphPad software.

2.3.18 Cell cycle analysis and γ H2AX assay

2.3.18.1 Assay principle

Phosphorylation of the histone H2AX is a rapid and sensitive way of measuring double-strand break (DSB) formation. There are three types of histone H2A protein, although the H2AX variant is the most protein sensitive to DSB formation. DNA damage response is primarily mediated by proteins of the phosphatidylinositol 3-kinase-like protein kinase (PIKKs) family, ATM, ATR, and DNA-PK and by members of the poly (ADP-ribose) polymerase (PARP) family. Upon DSB ATM, (DNA-PK) and ATR proteins are activated. PARP1 mediate the initial recruitment of the MRE11-NBS1-RAD50 complex to the sites of the DSB. The

ATM and MRN complex initiate the phosphorylation of H2AX on ser139 which further stabilize the MRN complex in a positive feedback loop. Each focus of γH2AX is thought to correspond to a double strand break within the cell. Histone H2A.X phosphorylated at serine 139 can be detected by labelling the cells with the anti-phospho-Histone H2A.X, FITC conjugate antibody and can be detected on a flow cytometer (Sharma, Singh and Almasan, 2012). (Figure 2-2) shows an example of the raw data output in Weasel software. We co-stained the cells with Propidium iodide (PI) stain, which is a stoichiometric DNA binding stain that binds proportionally to the amount of the DNA present in the cells. PI stain allows the staining of the DNA content in each phase of the cell cycle and thus progression of cells through the cell cycle can be assessed (Figure 2-3).

2.3.18.2 Assay protocol

To perform the assay, 1x 10^5 cells per well were seeded in 6-well plates overnight. The following day, cells were treated with the indicated doses of the drugs for 24 hours or 48 hours. Cells were then washed with PBS and collected by trypsinization in rounded bottom 5ml falcon flow cytometry tubes. Cells were washed twice by PBS and centrifuged at 1000rpm for 5 minutes and then fixed with ice-cold 70% ethanol for at least 30 minutes. Fixed cells can be stored at -20°C for a few weeks before analysis. To remove the fixation, cells were centrifuged and the supernatant containing ethanol was carefully discarded. The small cell pellet was washed twice with cold PBS and then permeabilized by

resuspending the pellet in 50 µl of 1X permeabilization solution. Cells were incubated for 15 minutes with 3.5 µl of anti-phospho-Histone H2A.X (Ser139) (γH2AX), FITC conjugate (Merck, UK). After incubation, the cells were washed with 100 µl 1X saponin wash solution to aid washing non-bound FITC. The cells were pelleted by centrifugation and incubated with 5µg/ml RNAase solution (Invitrogen, UK) for 15 minutes. The cells were then stained with 400 µl of 1µg/ml propidium iodide solution (Sigma, UK). The cells were analyzed on a FC500 flow cytometer (Beckman Coulter, USA) using a 488nm laser for excitation and a 620nm bandpass filter. Weasel software (Walter and Elisa Hall, Australia) was used for data analysis.

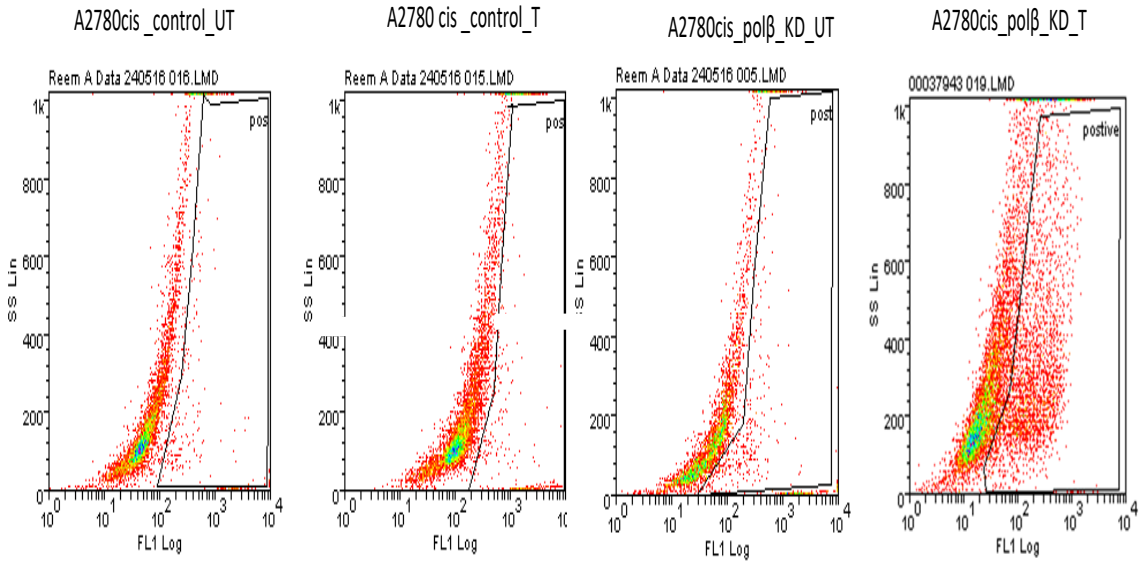


Figure 2-2: γH2AX analysis by weasel software.
γH2AX analysis in A2780cis control and polβ_KO cells untreated or cisplatin treated. Cisplatin treated A2780cis_ polβ_KO cells show substantial accumulation of γH2AX positive cells. FL1 Log: FACS fluorescence channel used for measuring FITC annexin V staining.

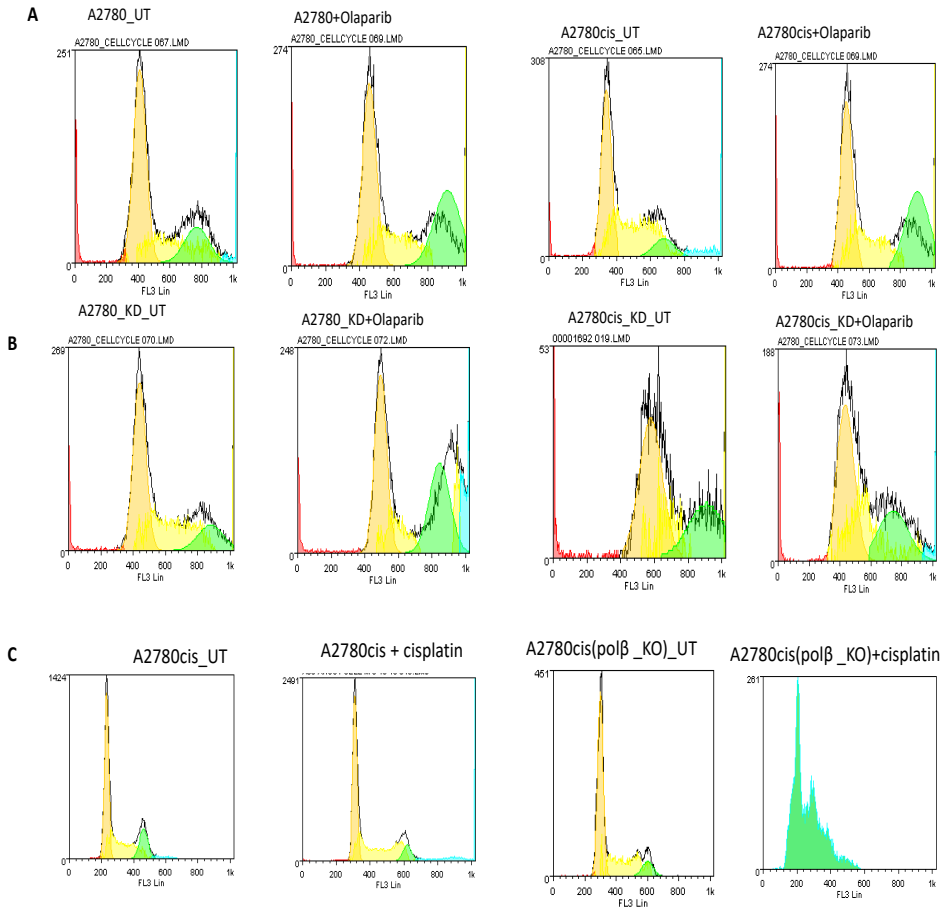


Figure 2-3: Representative figures of cell cycle analysis in weasel software.

(A)Representative images of cell cycle analysis in A2780 and A2780cis control cells, untreated and Olaparib treated. Olaparib treated cells show G2/M cell cycle arrest. (B) Representative images of cell cycle analysis in A2780 and A2780cis XRCC1_KD cells untreated and Olaparib treated. Olaparib treated cells show substantial G2/M cell cycle arrest compared to control cells. (C) Representative images of cell cycle analysis in A2780cis control and polβ_KO untreated and cisplatin treated cells showing S-phase cell cycle arrest in polβ_KO cells treated with cisplatin. FL3 Lin: FACS fluorescence channel used for measuring PI staining.

2.3.19 Apoptosis detection by Annexin V assay

2.3.19.1 Assay principle

Programmed cell death (Apoptosis) is a process that helps maintain tissue homeostasis. The apoptosis process is characterized by certain morphologic features, including loss of plasma membrane asymmetry and adherence, and chromatin condensation. Translocation of the membrane phospholipid phosphatidylserine (PS) from the inner plasma membrane to the outer side is among the early features in the apoptosis process (Andree *et al.*, 1990). Annexin V is a 35-36 kDa Ca2+ dependent phospholipid-binding protein that has a high affinity for PS. Thus, it can bind to the cells with translocated PS outside the plasma membrane and detect early apoptosis. AnnexinV staining in combination with another dye such as propidium iodide (PI) or 7-Amino-Actinomycin (7-AAD) will aid detection of cells undergoing the apoptosis process. Viable cells with intact plasma membranes are not stained for AnnexinV or PI. Early apoptotic cells are positive for AnnexinV staining but not PI. Late apoptotic cells are Annexin V and PI positive and necrotic cells are PI positive and AnnexinV negative (Koopman *et al.*, 1994).

2.3.19.2 Assay protocol

To perform the assay, 1x 10^5 cells per well were plated into 6-well plates overnight. The following day, cells were treated with the inhibitory drugs at the indicated doses for 24 or 48 hours. At the end of the incubation, cells were harvested by trypsinization, washed twice with ice-cold PBS and resuspended in 100 µl 1X annexin V binding buffer (BD Pharmingen, USA). Cells were incubated

with a 2.5µl fluorescein isothiocyanate (FITC) conjugated AnnexinV antibody and 2.5 µl propidium iodide for 15 minutes on ice in a dark room. Then cells were analyzed on a FC500 flow cytometer (Beckman Coulter, USA) using a 488nm laser for excitation and a 575nm bandpass filter. At least 10x10 ^{5} cells were analyzed for each tube. Weasel software (Walter and Elisa Hall, Australia) was used for the output flow cytometry data analysis.

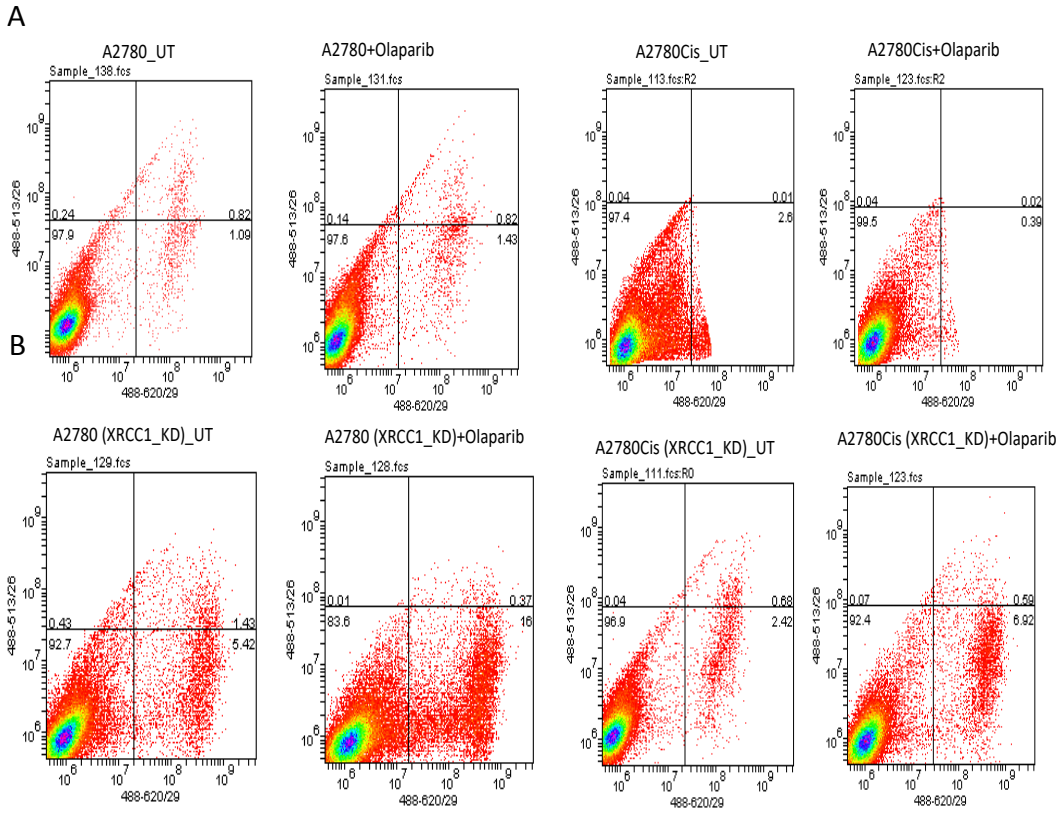


Figure 2-4: Representative images of annexin V analysis in weasel software.

(A)AnnexinV apoptosis analysis in A2780 and A2780cis control cells untreated and Olaparib treated. (B) Annexin V apoptosis analysis in A2780 and A2780cis XRCC1_KD cells untreated and Olaparib treated. A2780 and A2780cis XRCC1 _KD cells treated with Olaparib showing significant apoptotic cell accumulation. FACS fluorescence Channels are FL1 Log for measuring annexin V staining (horizontal) and FL3 Log for measuring PI staining (vertical).

2.3.20 Invasion assay

The ability of cells to invade was investigated using the Cell Biolabs CytoSelect cell invasion assay kit (catalogue no. CBA-110) as per the supplier protocol. The kit provides polycarbonate membrane inserts of 8µm pore size for seeding the cells. The upper layer of the inserts is coated with basal matrix, whereas invasive cells can invade through the matrix by degradation of the matrix proteins. Later, invasive cells can be dissociated from the polycarbonate membrane for quantification. To perform the assay, the cell lines to be tested were trypsinised from the culture flasks and counted. Cell suspensions of 0.6- 1x10^6 were prepared in serum-free culture media. Then 300 µL of cell suspension was added to the inserts. The lower wells of the invasion plate were topped with 500 µL of complete culture media supplemented with 10% fetal bovine serum (FBS). The cells in the inserts are left to invade toward the serum for 24 hours at 37 ºC in the incubator. After 24 hours, media containing non-invasive cells were aspirated. The inside of the inserts was wiped with the provided wetted cotton swaps to remove all non-invasive cells. The bottoms of the inserts containing invasive cells were stained in crystal violet for 10 mins at room temperature. Images of the invasive cells were taken with a Nikon microscope camera at 20X magnification. For quantification of the invasive cells, the stained inserts were placed into a new 24-well plate containing 200 µL per well of the provided cell extraction solution. Inserts were incubated with extraction solution for 10 mins on an orbital shaker. Then 100µL of the dissociated cells were transferred to a 96-well plate to measure the optical density (OD) at 560 nm using a microtiter plate reader. Statistical analysis and data plotting were performed in GraphPad Prism7 software.

2.3.21 Migration assay

Migration assays were performed using the Radius96-well cell migration assay (Cell Biolabs, catalog. no CBA-126) as per the supplier protocol. The kit provides a 96-well plate, and each well contains a hydrogel spot of 0.68 mm. The radius pre-coated hydrogel spot prevents adherent cells from attaching to it. The gel area can be removed later with the supplied non-toxic gel removal solution to allow cells to migrate in the radius spot and be evaluated for their migration ability. To perform the assay, the plate has to be moisture free by incubation for 1 hour at room temperature inside the sterile cabinet. The cells to be tested are trypsinised and counted as described before. Cells are re-suspended at 0.3 $x10^6$ cells/ml concentration in complete culture media. Then 100 µL of the cell suspension is added to each of the tested wells. It is important that the number of cells seeded can form a monolayer of 90% confluency at the time of plating, so they occupy all the well but not the hydrogel spot and start migrating after the spot is dissolved. Thus, previous optimisation of cell seeding density was performed separately in 96-well cell culture plates. The migration plate was transferred to the incubator to allow cells to adhere overnight. The following day, media were aspirated from the tested wells and the cells were washed with 100 µL fresh media to remove debris and non-attached cells. 1X Radius Gel Removal solution was prepared by diluting the provided 100X solution 1:100 in fresh media. Then 100 µL of the working 1X solution was added to each well and transferred to the incubator for 30 minutes to allow removal of the gel spot. After incubation, the Gel Removal solution was aspirated, and the cells were washed with 100 µL of fresh media three times. Finally, the wells were topped with 200 µL fresh media. At that point of time, pre-

migration images were taken with a Nikon microscope camera at 20X magnification. Then the plate was left in the incubator for 15 hours to allow cells to migrate. After incubation, the media were aspirated from the wells and the cells were fixed for 10 mins with 100 µL of cell fixation solution (provided). The cells were washed with 100 µL of PBS three times before taking the post-migration images. Each experiment was performed in triplicate wells simultaneously and then repeated two more times on different biological replicates. The analysis of the migration images was carried out using ImageJ software. Percentage closure was calculated from the formula: % of wound closure = [(At = 0 h – At = Δ h)/At = 0 h] × 100% as described by Yue *et al.* where (At = 0 h) is the area measured in the pre-migration images and (At = Δ h) is the area measured in post-migration images (Yue *et al.*, 2010). The statistical analysis and data plotting were performed in GraphPad Prism7 software.

2.3.22 Immunofluorescence staining

Cells were trypsinised from culture flasks and counted as described before. $1x10^5$cells per well were seeded overnight on autoclaved coverslips pre-layered in 6-well plates. Cells were treated with the indicated concentrations of the drugs for the incubation time described in the figure legends later in the results sections. After incubation, cells were stained as per the described protocol (Ibrahim *et al.*, 2012). Briefly, cells were fixed in 4% paraformaldehyde for 30 mins, then permeabilised with 300 µL per well of 0.1% Triton (Thermofisher, UK) for another 30 mins. Non-specific binding was blocked using the blocking buffer consisting of 3% bovine serum albumin solution (BSA) diluted in PBS. Cells were incubated with the blocking buffer for 1 hour at room temperature. During that time, the working

dilution of primary antibodies was prepared in 1% BSA solution and then 300 µL of diluted primary antibody solution was added to each well. Cells were incubated with primary antibodies overnight at 4^{o} C. The following day, cells were washed three times for 5 mins each with a wash buffer consisting of 1 %BSA and 0.1% Tween-20 in PBS. Cells were incubated with the secondary antibodies diluted in 1% BSA for 1 hour at room temperature in the dark. After incubation with the secondary antibodies, the cells were washed in a dark room with the wash buffer three times for 5 mins each. The coverslips are then removed from the 6-well plates using a fine tweezers and layered on microscopic slides containing one drop of mounting medium with DAPI (Vector Labs). The edges of the coverslips are then sealed with nail varnish to ensure firm adhesion to the slides. Slides were prepared in duplicates. Imaging was performed using a Leica SP2 confocal laser scanning microscope. Images were analysed in ImageJ software. For analysis, a minimum of 100 cells per slide were counted. Data were analysed in Graphpad Prism 7 software.

Table 2-7: Antibodies used in western blot and immunofluorescence studies.

Antibody	**Supplier**	**Dilution for WB**	**Dilution for IF**
Anti-XRCC1 mouse monoclonal antibody	Thermofisher Scientific. Clone (33-2-5).	1: 500	NA
Anti-PARP1 rabbit monoclonal antibody	Cell Signalling, clone 46D11.	1:1000	1:800
Anti- CyclinE1 rabbit monoclonal antibody	Abcam, catalogue no. ab33911.	1:500	NA
Anti- p-CyclinB1 (ser126) rabbit polyclonal antibody	Abcam, catalogue.no ab55184	1:500	NA

Anti-ATM rabbit monoclonal antibody	Abcam, clone Y170 catalogue no. ab32420	1:1000	NA
Anti-p-ChK1(ser345) rabbit polyclonal antibody	Abcam, catalogue no. ab47318	1:1000	NA
Anti ATR rabbit monoclonal antibody	Cell Signalling, catalog.no. 2790	1:1000	NA
Anti Polβ rabbit polyclonal antibody	Abcam, catalogue no. ab26343	1:1000	1:200
Anti poly (ADP)ribose polymers (PAR),	Abcam, catalogue no. ab14459	1:500	1: 500
Anti-E-cadherin	Abcam, catalogue no ab1416.	1:500	NA
Anti-N-cadherin rabbit monoclonal antibody	Cell Signalling, clone (D4R1h), catalogue no.13116	1:500	NA
Anti-MMP-9 rabbit monoclonal antibody	Abcam, catalogue no. ab76003	1:500	NA
Anti-TGFβ mouse monoclonal antibody	Abcam, catalogue no. ab27969	1:1000	NA
Anti-p21 rabbit monoclonal antibody	Abcam, catalogue no. ab218311	1:200	NA
Anti γH2AX mouse monoclonal antibody	Merckmillipore, catalogue no. 05-636, clone JBW301	NA	1:500
Anti 53BP1 rabbit monoclonal antibody	Cell Signalling, catalogue no.4937S	NA	1: 200
Anti-β-actin mouse monoclonal antibody	Sigma Aldrich, catalogue no. A5441	1:10,000	NA
Anti-β-tubulin rabbit polyclonal antibody	Abcam, catalogue no. ab6046.	1:2000	NA
Alexa fluor 488 goat anti-Mouse secondary antibody	Thermofisher Catalogue no. A-11029.	NA	1:200
Goat anti-rabbit secondary antibody, TRITC.	Thermofisher Catalogue no. T-2769	NA	1:500

2.3.23 Generation of 3D Spheroids

To generate a 3D model from our adherent monolayer cells we used the Promocell 3D tumoursphere medium xenofree (catalog. no. C-28070) as per the supplier protocol. Briefly, adherent cells were trypsinised, centrifuged and the pellet was re-suspended in a small volume of the 3D tumoursphere medium (i.e. 3-5 ml). After counting the cells, a suspension of $4x10^4$ cells/ml was prepared and each one ml was seeded in a Nunclon Sphera ultra-low attachment 6-well plate (Thermofisher, catalogue no.174932). The cells were then topped up with another one ml of tumoursphere medium. Every three days cells were topped up with 0.5 ml of the tumousphere medium. Spheroid structure formation was checked under the microscope regularly. After an average of three weeks, spheroids can be passaged before they form a dark centre of dead cells. Spheroid passaging can be performed by collecting the cell suspension containing the structures into a falcon and precipitating them by centrifugation. Structures can be washed with PBS and dissociated by resuspending in trypsin for three minutes. Pipetting the spheres up and down aids in dissociating the structure aggregates and obtaining a single cell suspension. Cells can be counted and divided into new ultra -low attachment culture plates to form new spheroid structures.

2.3.23.1 Spheroids staining

3D spheroid structures were treated with the indicated concentrations of the inhibitors as described in the figure legends in the results section. To perform staining, spheres were fixed in 37% formaldehyde at a 1:10 ratio for 30 mins. They

were then stained with 2µM of calcein AM and 1.5µM of ethidium homodimer-1 (Live dead assay, Thermofisher), with the protocol adapted from (Debnath, Muthuswamy and Brugge, 2003). Imaging was carried out using a Leica SP2 confocal laser scanning microscope. At least 30 spheroids were analyzed per cell line. Images were analyzed in ImageJ software. For quantification of cell viability by flow cytometry, spheres were collected after treatment and dissociated by trypsinization as described in the passaging protocol. Dissociated cells were resuspended in 0.05µM of calcein AM and 2.5 µM of ethidium homodimer 1. Cells were analysed on a FC-500 flow cytometer (Beckman Coulter). Analysis was performed in Weasel flow cytometry software.

2.3.24 NAD assay

2.3.24.1 Assay principle

PARP1 catalyses the formation of poly (ADP) ribose polymers on PARP1 itself and on key DNA repair molecules and histones that trigger DNA repair signalling. The parylation process is transient and requires NAD molecules. Poly (ADP) ribose polymers can be hydrolysed by Poly (ADP) ribose glycohydrolase activity. We measured NAD+ levels in Olaparib treated or PARGi treated polβ deficient and proficient cells using the NAD+/NADH colorimetric assay kit (catalogue no: ab221821, Abcam, UK) as per the supplier recommendations. The assay is based on alcohol dehydrogenase (ADH) and diaphorase coupled-reaction that convers WST-1 to WST-1 formazan, which can be easily detected at OD 450 nm.

2.3.24.2 Assay protocol

A2780 and A2780cis control and polβ knock out cells were plated in t25 flasks overnight then treated with Olaparib (10μM) or PARGi PDD00017273 (25μM). The following day, cells were collected by trypsinisation and washed with ice-cold PBS. NAD+ was then extracted from the cells under acidic conditions using a prepared 0.5 M percloric acid solution. Samples were incubated on ice for 30 mins. The acidic conditions were neutralized by adding 100μL of NAD+ neutralization solution (0.55 M K_2CO_3). The PH of the supernatant is adjusted to 7.5-8.5 by adding a few drops of NAD+ Neutralization solution.

Protein content in the sample was quantified via a BCA protein quantification kit (Thermofisher, UK). Standard wells were prepared by serial dilutions from A2780 control cell extracts according to the supplier protocol. The reaction is initiated by adding 60 μL of the reaction mix (shown below in the table provided by the supplier). Outputs were measured after 60 minutes on a TECAN microplate reader at 450 nm.

Component	NAD^+/NADH Reaction Mix (μL)
20X NAD/NADH Assay Buffer	5
WST-1	5
ADH	5
Diaphorase	5
Ethanol Solution	5
ddH_2O	35

2.3.25 Statistical analysis

Statistical analysis was performed on GraphPad Prism7 software. Student- T-tests were used for comparison between two groups as in the western blot quantifications, clonogenics cell survival assay and immunofluorescence quantification. One-way ANOVA was used for comparison between three or more groups as in the western blot and γH2AX assay. The two-way ANOVA test was used for multiple comparisons in cell cycle analysis and Annexin V assays. Error bars represent standard error of mean between experiments. P-values <0.05 =*, p-value <0.01 =** & p-value <0.001=***.

3 XRCC1 in Invasive Breast Cancers

3.1 Introduction

The comprehensive understanding of tumour cell vulnerabilities has led to the development of novel therapeutic strategies that are far more selective to cancer cells. That is achieved by identifying targets that are more predominant in tumour cells and hence essential for tumour cell survival. Targeting such proteins will have minimal toxicity to normal cells (Zecchini and Frezza, 2017).

The concept of synthetic lethality was observed for the first time in Drosophila studies where certain non-allelic genes became lethal only when present combined while the homozygous alleles in the parents did not affect viability (Trowbridge *et al.*, 2007). That concept explained how a mutation in one gene does not affect cell viability however when present combined with another mutation causes lethality (Beijersbergen, Wessels and Bernards, 2017). Given the increase in mutational load in cancer cells, there have been multiple approaches to the concept of synthetic lethality to improve cancer therapeutics through enhancing specific tumour cell death and cause less damage to normal tissues (Brunen and Bernards, 2017). Although synthetic lethality is known to be induced through simultaneous loss of functional genes, it can also be applied to mutations that cause a gain of functional alleles. This phenomenon is known as synthetic dosage lethal (SDL). Cancer cells often accumulate oncogenic mutations that increase tumour aggressiveness and increase resistance to conventional chemotherapies (Reid *et al.*, 2016). Thus, screening for synthetic dosage lethal partners is an interesting approach to specifically eliminate those cells (Zecchini and Frezza, 2017). A very successful example of that approach is demonstrated in

the sensitization of chronic myelogenous leukaemia (CML) to imatinib. On the other hand, the translocation of the ABL tyrosine kinase gene from chromosome 9 to the breakpoint cluster region (BCR) gene on chromosome 22 leads to the formation of the oncogenic BCR-ABL protein. A constitutively active BCR-ABL protein kinase is a major cause of (CML) (Sherbenou and Druker, 2007). Inhibition of BCR-ABL tyrosine kinase activity with imatinib proved the dependence of CML cells on BCR-ABL activity for their survival (Sherbenou and Druker, 2007). A recent study showed a synthetic lethality interaction between STAT3 and BCR-ABL that could be useful in targeting resistant forms of CML (Eiring *et al.*, 2015). Another model is the overexpression of the oncogenic c-MYC gene which is widely reported in different types of tumours (Zecchini and Frezza, 2017). Dimerization of MYC with its partner MAX is crucial for its activation and regulation of cell cycle progression and DNA repair (Kiessling *et al.*, 2006). Therefore small molecule inhibitors targeting MYC-MAX heterodimers like Mycros (Kiessling *et al.*, 2006) and 10058-F4 (Huang *et al.*, 2006) were useful approaches toward induction of MYC synthetic lethality.

Other genomic studies tried to identify crucial genes for the survival of MYC amplified tumour cells. Among those are GSK3β, FBXW7, and PTK2 which were reported to be MYC synthetic lethality partners (King *et al.*, 2013). Furthermore, an RNAi screening study revealed SUMO-activating enzymes (SAE) 1&2 to be synthetically lethal with MYC (Huang *et al.*, 2006).

Another promising aspect of synthetic lethality is the model of cancer metabolism. Genomic studies of cancer metabolism have identified unexpected metabolic liabilities that are selective to cancer cells (Zecchini and Frezza, 2017).

Targeting tumour metabolism is another exciting path to tackling tumours. The first metabolic change obvious in cancer cells is the increase in glucose uptake and upregulation of the glycolysis pathway (Dörr *et al.*, 2013). However, this feature is not solely exclusive from normal cells leading to significant cytotoxicity to cells utilizing these glycolytic enzymes (McLornan, List and Mufti, 2014). An increase in amino acid production like glutamine, serine, glycine, proline, and arginine is also noted. Inhibitors of lipid metabolism like Orlistat (a fatty acid synthase inhibitor) and SB-204990 (an inhibitor of ATP citrate lyase) demonstrated some success (Facchetti, Zampieri and Altafini, 2012). However, recent studies focused on finding synthetic lethality partners in cancer metabolism. Succinate dehydrogenase is a mitochondrial enzyme involved in the tricarboxylic acid cycle and the electron transport chain (Facchetti, Zampieri and Altafini, 2012). The loss of heterozygosity in the succinate dehydrogenase (SDH) allele leading to loss of its enzymatic function was denoted as an early sign of neoplasia. SDH deficient tumours will upregulate hypoxia-inducible factors (HIF) and generate a hypoxic like the situation in tumours (Teicher, Linehan and Helman, 2012). Importantly, succinate dehydrogenase deficient cells secrete more pyruvate carboxylase as they are labile on pyruvate metabolism. Therefore, recently inhibition of pyruvate carboxylase has been proved to have a synthetic lethality relation with SDH (Metallo, 2013). Similarly, fumarate hydratase heterozygosity and loss of function are profound in neoplastic cells. Extensive research has revealed that FH deficient cells are dependent on the Haem pathway to secrete higher levels of bilirubin. Further, inhibition of Haem oxygenase 1 which is the rate limiting enzyme in the

Haem pathway leads to cell death in FH deficient cells with minimum effect on the control cells (Frezza *et al.*, 2011).

The advances in tackling tumour cell liability with synthetic lethality applications made it an area of research interest for us and many other groups. The success of PARP1 inhibitors in inducing synthetic lethality in BRCA deficient tumours has led to FDA approval for Olaparib in the treatment of BRCA germline mutated ovarian cancers (Lee and Gulley, 2017). However, BRCA re-expression and activation of homologous recombination pathways directly or indirectly leading to Olaparib resistance have been extensively reported (Drost *et al.*, 2011). The XRCC1 enzyme has a fundamental role in single strand break repair (SSBR). XRCC1 interacts with PARP1 in the base excision repair pathway (Hoch *et al.*, 2017). Our group previously showed XRCC1 to be associated with high grade, triple negative phenotype and more aggressive forms of breast cancer. Additionally, our previous study showed the ATM/ATR inhibitor KU55933 and the DNA-PK inhibitor NU7441 to be synthetically lethal with XRCC1 in breast cancer cell lines (Rebeka Sultana *et al.*, 2013).

In this study, we hypothesised that PARP1 inhibition by Olaparib and Talazoparib can have a synthetic lethality in XRCC1 deficient breast cell lines.

3.2 Methodology

Immunohistochemistry of XRCC1 and PARP1 was performed on TMAs of 1650 patients with invasive breast cancers and a separate cohort of 281 ER negative invasive breast cancers. Patient demographics are summarised in the Methods chapter (Table 2-2). The immunohistochemistry protocol and antibody details are described in the Methods chapter. Evaluation of immune staining was performed by calculation of H-scores (range 0–300). For XRCC1, low/negative nuclear expression was identified by the median cut off ≤ 100. Low/negative nuclear PARP1 staining was defined by a median H score of <80.

Murine cell lines used in this study are CHO9 (xrcc1 proficient) and EMC-12 (xrcc1 deficient). Human cell lines used include HeLa cells (XRCC1 deficient) and HeLa XRCC1 SilenciX cells obtained from Tebu-bio. Triple negative breast cancer human cell lines are MDA-MB-231 (XRCC1 proficient), MDA-MB-231 _XRCC1_KO, and MDA-MB-157 (XRCC1 deficient). XRCC1 knock out was performed using the CRISPR- Cas-9 technique. Single cell cloning was performed to obtain a pure population as described in the Materials and Methods chapter. Media used to maintain all the cell lines as well as cell passaging, and storage are described in the Materials and Methods chapter. Assays used in this study include the clonogenic survival assay, western blotting, flow cytometry analysis, and immunofluorescence as detailed in the Methods section.

All experiments were repeated 3 or 4 times. Immunofluorescence was done on different biological replicates and the slides were fixed and stained together. Data analysis was performed on GraphPad Prism-7 software. Error bars represent standard error of mean between experiments. P-values are indicated as P-values <0.05 =*, p-value <0.01 =** & p-value <0.001=***.

3.3 Results

3.3.1 Clinical Data

3.3.1.1 XRCC1-PARP1 co-expression influences the outcome of breast cancer prognosis

Impaired DNA repair can promote tumour aggressiveness and poor prognosis. In breast cancer, loss of DNA repair mechanisms is associated with poor prognosis (Rebeka Sultana *et al.*, 2013; Albarakati *et al.*, 2015). XRCC1 loss has been reported previously by our group and by others to be associated with high grade, an absence of hormonal receptors (ER-/PgR -/AR-) and poor breast cancer-specific survival (Abdel-Fatah *et al.*, 2013; Rebeka Sultana *et al.*, 2013). Additionally, the loss of XRCC1 expression was significantly associated with the loss of expression of other key DNA repair proteins, such as BRCA1 and TOP2A, as well as the deregulation of tumour suppressor proteins such as p53, p16 as well as the downstream genes of p53 such as p21,MDM2, MDM4 BCL2 and BAX leading to a high level of genomic instability (Rebeka Sultana *et al.*, 2013). Moreover, previously published data by our group have proven the correlation between PARP1 expression and the aggressiveness of breast cancers (Green *et al.*, 2015). Given the interaction between XRCC1 and PARP1 in the BER pathway, we proceeded to investigate XRCC1 and PARP1 co-expression in a large cohort of breast cancers.

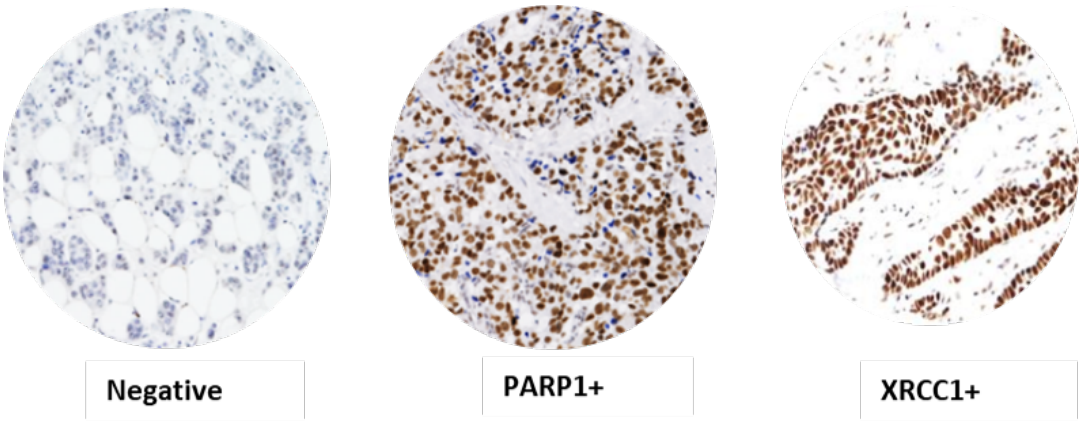


Figure 3-1: Representative photo micrographic image of XRCC1 & PARP1 expression in tumours.

Representation of TMA's of negative expression, PARP1+ nuclear expression and

XRCC1 nuclear expression respectively are shown here.

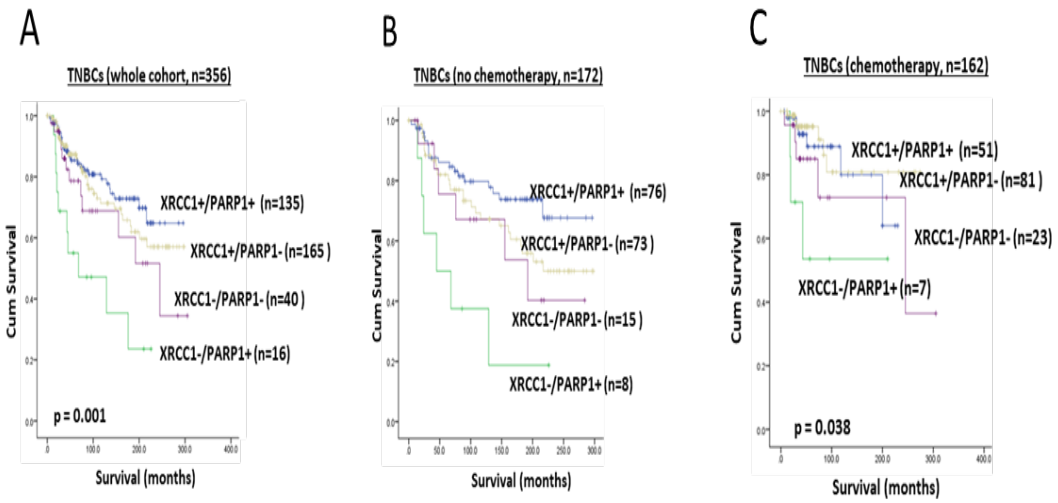


Figure 3-2: Kaplan-Meier curve for breast cancer-specific survival.

Kaplan-Meier showing the correlation between XRCC1 and PARP1 expression in (A) Triple-negative breast cancers (TNBCs), whole cohort. (B) TNBCs that received no chemotherapy. (C) TNBCs treated with chemotherapy.

Table 3-1: Clinicopathological significance of XRCC1and PARP1in breast cancers

	PARP1 and XRCC1 co-expression				**P- value**	***P -Value** (Adjusted)
	PARP1+ /XRCC1+	PARP1+ /XRCC1-	PARP1- /XRCC1+	PARP1- /XRCC1-		
Tumour Type						
IDC-NST*	272(44.3%)	46(7.5%)	225(36.6)	71(11.6%)	0.007	**0.0110**
Tubular	81 (42.0%)	10 (5.2%)	88 (45.6%)	14(7.3%)		
Medullary	10 (38.5%)	3 (11.5%)	7 (26.9%)	6 (23.1%)		
ILC	57(54.8%)	0 (0%)	42 (40.4%)	5 (4.8%)		
Others	3 (25.0%)	0 (0%)	7 (58.3%)	2 (16.7%)		
Mixed NST & Lobular/special type	28(45.2%)	2 (3.2%)	27(43.5%)	5 (8.1%)		
Tumour Size						
<1cm	41(45.1%)	7 (7.7%)	37(40.7%)	6 (6.6%)	0.332	0.3652
>1-2cm	225(44.2%)	21(4.1%)	212(41.7)	51(10.0%)		
>2-5cm	186(45.8%)	31(7.6%)	145(35.7)	44(10.8%)		
>5cm	8 (47.1%)	2 (11.8%)	5(29.4%)	2 (11.8%)		
Tumour Stage						
1	278(45.4%)	26(4.2%)	242(39.5)	66(10.8%)	0.171	0.2090
2	140(43.8%)	28(8.8%)	123(38.4)	29(9.1%)		
3	43(46.2%)	7 (7.5%)	7 (7.5%)	7 (7.5%)		
Tumour Grade						
Grade1	60(36.6%)	5(3.0%)	85(51.8%)	14(8.5%)	$1.7x10^{-9}$	**<0.0001**
Grade2	180(52.5%)	6(1.7%)	136(39.7)	21(6.1%)		
Grade3	220(42.6%)	50(9.7%)	179(34.6)	68(13.2%)		
NPI						
≤ 3.4	135(46.2%)	6(2.1%)	131(44.9)	20(6.8%)	$3.7x10^{-4}$	**<0.0001**
>3.4	301(44.2%)	50(7.3%)	250(36.7)	80(11.7%)		
Mitotic Index						
M1 (low; mitoses < 10)	164(47.8%)	7(2.0%)	150(43.7)	22(6.4%)	$6.1x10^{-6}$	**<0.0001**
M2 (medium; mitoses 10-18)	93(50.0%)	9(4.8%)	64(34.4%)	20(10.8%)		
M3 (high; mitosis >18)	198(42.8%)	45(9.7%)	161(34.8)	59(12.7%)		
Tubule Formation	20(40.0%)	2(4.0%)	24(48.0%)	4(8.0%)	0.068	0.0935
1 (>75% definite tubule)	147(44.3%)	14(4.2%)	142(42.8)	29(8.7%)		
	288(47.2%)	45(7.4%)	209(34.3)	68(11.1%)		

2 (10%-75% definite tubule) 3 (<10% definite tubule)						
Pleomorphism 1 (small-regular uniform) 2 (Moderate variation) 3 (Marked variation)	6(37.5%) 177(45.5%) 271(46.4%)	1(6.3%) 8(2.1%) 52(8.9%)	8(50.0%) 175(45.0) 190(32.5)	1(6.3%) 29(7.5%) 71(12.2%)	$8.04x10^{-6}$	**<0.0001**
Her2 overexpression No Yes	391(44.8%) 62 (45.3%)	50(5.7%) 11(8.0%)	349(40.0) 48(35.0%)	83(9.5%) 16(11.7%)	0.503	5.5330
ER* status Negative Positive	98(38.1%) 355(47.7%)	31(12.1%) 29(3.9%)	84(32.7%) 307(41.3)	44(17.1%) 53(7.1%)	$1.7x10^{-10}$	**<0.0001**
PR* Negative Positive	152(37.8%) 285(49.7%)	38(9.5%) 22(3.8%)	153(38.1) 229(39.9)	59(14.7%) 38(6.6%)	$1.1x10^{-7}$	**<0.0001**

*IDC-NST: Invasive ductal carcinoma -no specific type. ER: Estrogen receptor. PR: progestogen receptor. NPI: Nottingham prognostic index.

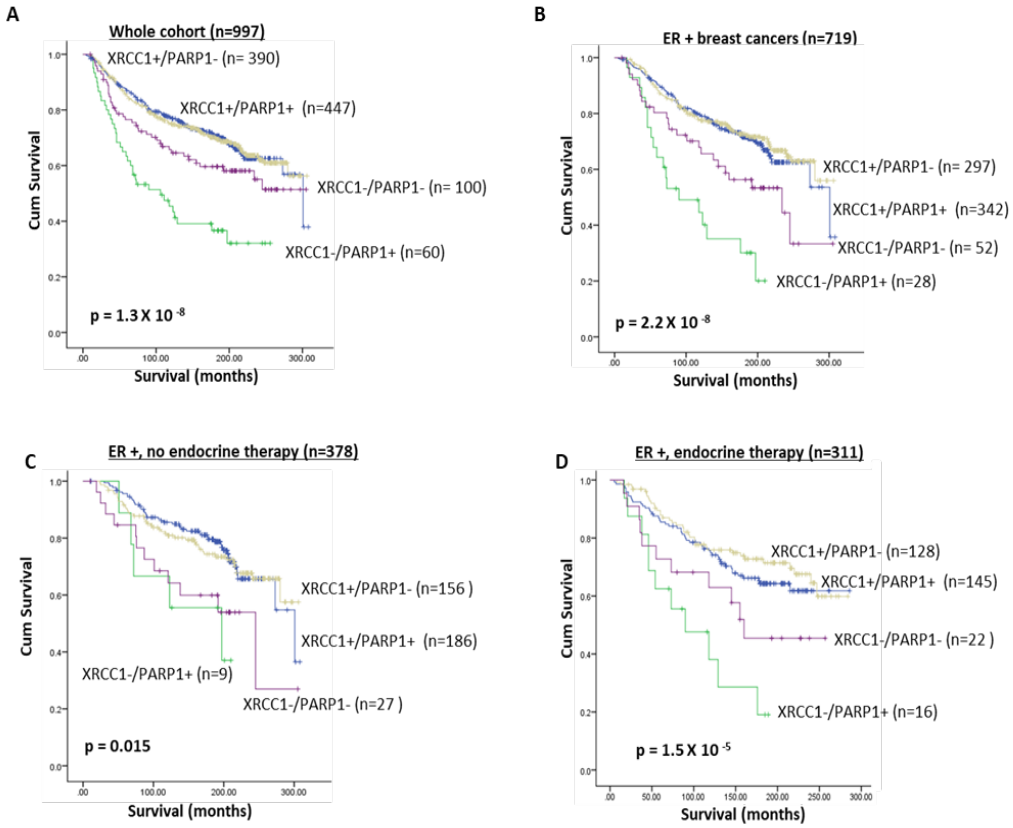


Figure 3-3: Kaplan-Meier curve for breast cancer-specific survival.

Kaplan-Meier curve showing the correlation between XRCC1 and PARP1 in (A) Whole cohort, (B) ER+ breast cancers, (C) ER+ breast cancers that received no endocrine therapy and (D) ER+ breast cancers that received endocrine therapy.

We found that a total of 1011 breast tumours were suitable for XRCC1-PARP1 co-expression analyses (Figure 3-1). 451/1011 (44.6%) were XRCC1+/PARP1+, 61/1011 (6%) were XRCC1-/PARP1+, 396/1011(39.1%) were XRCC1+/PARP1- and 103/1011 (10.1 %) were XRCC1-/PARP1-. As shown in (Table 3-1), tumours that are XRCC1-/PARP+ are likely to be high grade, high mitotic index, high pleomorphism, ER-/PR- and high-risk Nottingham Prognostic Index (NPI >3.4) (all adjusted p values <0.0001). In the whole cohort (n=997), XRCC1-/PARP+ tumours had the worst breast cancer-specific survival (p<0.0001) (Figure 3-2 A).

In ER+ breast cancers, XRCC1-/PARP+ tumours had the worst survival outcome ($p<0.0001$) (Figure 3-2B) including in patients who had no endocrine therapy ($p=0.015$) (Figure 3-2C) or endocrine therapy ($p<0.0001$) (Figure 3-2D). In TNBCs (n=356), similarly, XRCC1-/PARP+ tumours had the worst survival outcome in the whole cohort ($p=0.001$) (Figure 3-3A) including in patients who had no chemotherapy ($p=0.003$) (Figure 3-3B) or chemotherapy (Figure 3-3C) ($p=0.038$). Taken together, these data indicate that high expression of PARP1 in XRCC1 deficient tumours is associated with poor breast cancer prognosis and provide the rationale that targeting PARP1 in XRCC1 deficient breast cancers by synthetic lethality could have clinical potential. To explore this hypothesis further we validated these findings through in vitro studies.

3.3.2 Selective Olaparib toxicity in XRCC1 deficient cell lines

We utilized in this study a panel of murine and human cell lines. As shown in (Figure3-4), Chinese hamster ovary CHO9 cells (XRCC1 proficient), EMC-12 (XRCC1 deficient), HeLa control cells (XRCC1 proficient), HeLa (XRCC1_KD) by Sh-RNA, MDA-MB-231 control (XRCC1 proficient), and MDA-MB-231 (XRCC1_KO) that we generated by CRISPR-Cas-9 for the purpose of this study. MDA-MB-231(XRCC1: KO) have been single-cell cloned to obtain a pure KO population as shown in (Figure 3-4). All the synthetic lethality experiments have been conducted on the single cell cloned 231: KO population. We observed sensitivity to Olaparib in the XRCC1 deficient cell line models tested (Figure 3-5).

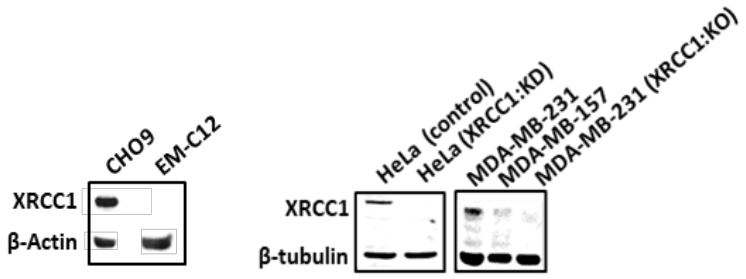


Figure 3-4: XRCC1expression by western blot.

Representative image for XRCC1 levels by western blot In HeLa control, HeLa (XRCC1_KD), MDA-MB-231 control, MDA-MB-231(XRCC1_KO) and MDA-MB-157 cells.

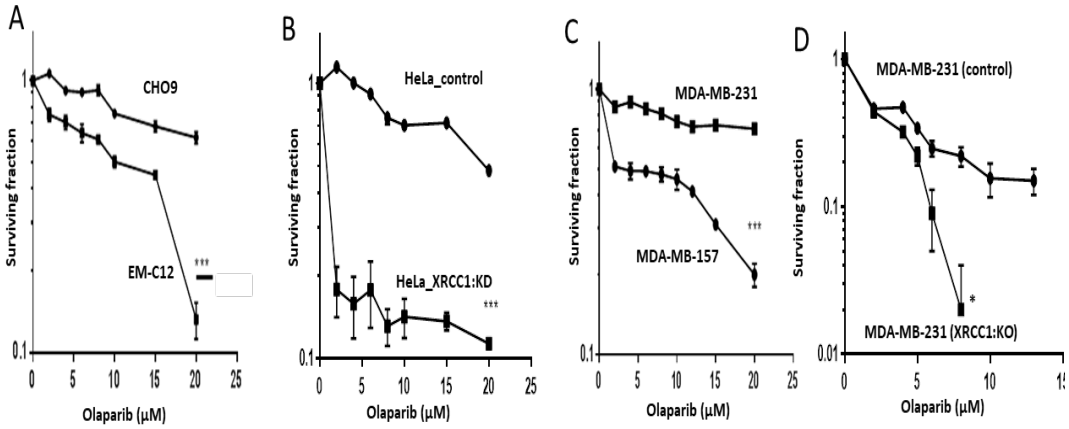


Figure 3-5: Olaparib sensitivity in XRCC1 deficient cell lines.

Clonogenic survival assay. With different doses of Olaparib for (A) CHO9 and EMC-12. (B) HeLa control and HeLa (XRCC1_KD). (C) MDA-MB-231 and MDA-MB-157. (D) MDA-MB-231 and MDA-MB-231(XRCC1_KO).

3.3.3 Methylation of XRCC1 gene in MDA-MB-157 cell line

We then investigated the mechanism of XRCC1 downregulation in MDA-MB-157

breast cancer cells. As shown in (Figure 3-6A), qRT-PCR analysis indicated that XRCC1 mRNA expression was significantly low in MDA-MB-157 cells compared to MDA-MB-231 cells. Upon treatment with Azacytidine (a hypomethylating agent), XRCC1 mRNA expression increased in MDA-MB-157 cells and was comparable to XRCC1 mRNA expression in MDA-MB-231 (Figure 3-6B). We checked XRCC1 protein levels after Azacytidine treatment by western blotting and we found that the previously low expressed XRCC1 increased significantly (Figure 3-6C).

To then confirm that the observed Olaparib sensitivity in MDA-MB-157 is dependent on XRCC1 deficiency, we compared Olaparib sensitivity in control MDA-MB-157and MDA-MB-157 treated with Azacytidine in the clonogenic survival assay (Figure 3-6D). MDA-MB157 treated with Azacytidine was resistant to Olaparib treatment in comparison to XRCC1 deficient MDA-MB-157.

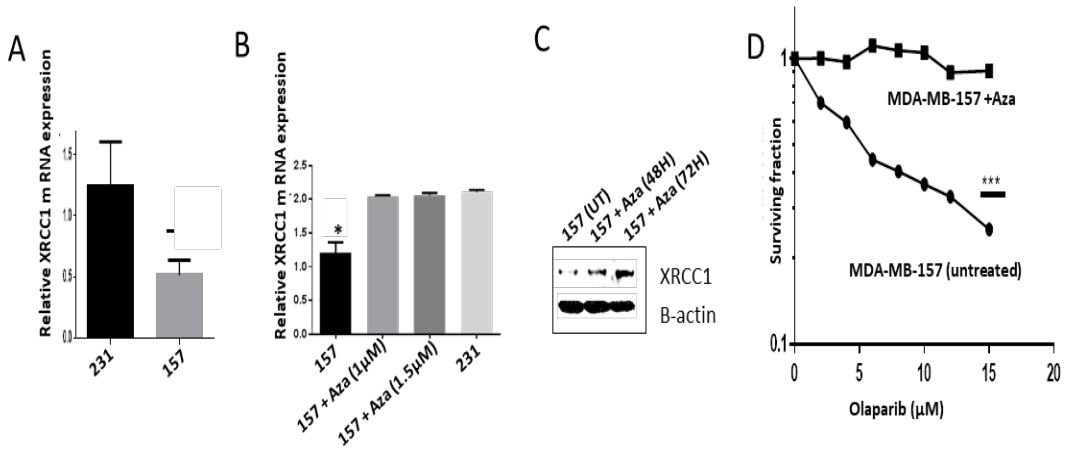


Figure 3-6: XRCC1 levels in 157 and 231.
(A) *XRCC1* mRNA expression in MDA-MB-157 and MDA-MB-231. (B) *XRCC1* mRNA expression in MDA-MB-157 treated with Azacytidine compared to MDA-MB157 untreated cells and MDA-MB-231. (C) XRCC1 protein levels by western blotting in MDA-MB-157 treated with Azacytidine. β-actin was used as a loading control. (D) Clonogenic survival assay with different doses of Olaparib in MDA-MB-157 treated with Azacytidine compared to untreated cells.

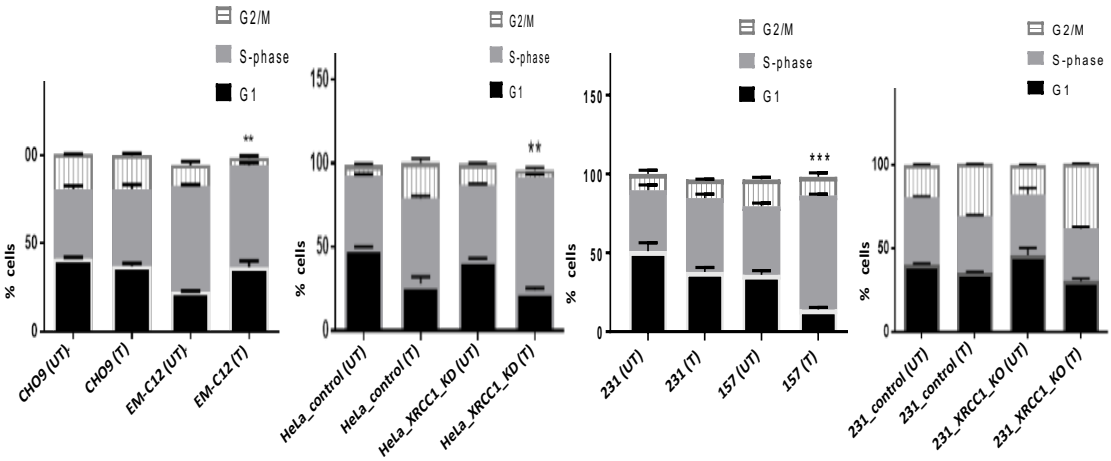


Figure 3-7: Cell cycle analysis by flow cytometry.
(A)CHO9 cells and EMC-12 treated with 10μM of Olaparib for 24 hrs. (B)HeLa control and HeLa (XRCC1_KD) cells treated with Olaparib (10μM) for 24 hrs. (C) MDA-MB-231 control and MDA-MB-157 treated with Olaparib (10 μM) for 24 hrs. (D) MDA-MB-231 control and MDA-MB-231 (XRCC1_KO) treated with Olaparib (10 μM) for 24 hrs. All experiments were done in triplicates.

3.3.4 Olaparib affects cell cycle progression in XRCC1 deficient cell lines

The role of PARP1 in cell cycle progression has been previously described (Yang *et al.*, 2013; Jelinic and Levine, 2014). Jelinic and Levine have also reported that Olaparib but not Veliparib influences cell cycle progression through regulating the levels of p53 and p21 (Jelinic and Levine, 2014). Therefore, we investigated the effect of Olaparib treatment on cell cycle progression. CH09, EMC12, HeLa control, HeLa_XRCC1_KD, MDA-MB-231 control, MDA-MB-157, and MDA-MB-231: XRCC1_KO were seeded in 6-well plates overnight and treated with Olaparib (10µM) for 24 hours. Then cells were collected by trypsinization, washed with ice-cold PBS and fixed with 70% ethanol for at least 30 minutes. Then cells were stained with propidium iodide for analyzing DNA content as described in the Methodology section. An interesting observation that we found was that Olaparib treated HeLa_XRCC1_KD, MDA-MB-157 arrest in S-phase, while MDA-MB-231: XRCC1_KO arrest in G2/M-phase (Figure 3-7).

To confirm this differential Olaparib response, we aimed to test Olaparib effect on cell cycle progression in a synchronized population of cells. Cells were synchronized at G1 by serum starvation for 16 hours (Figure 3-8A). Flow cytometry analysis confirmed that <85% of the tested cell lines arrest in G1 by serum starvation for 16 hours. Thus, we seeded the cells overnight and synchronized them by serum starvation for 16 hours and then they were released in complete culture media with or without 10µM of Olaparib. After 24 hrs, cells were collected and fixed in 70% ethanol and stained with propidium iodide

following the same cell cycle analysis protocol. As expected, similar to the asynchronous population, we observed a substantial S-phase arrest in HeLa XRCC1_KD and MDA-MB-157 upon Olaparib treatment (Figure 3-8B). While in MDA-MB-231 :(XRCC1_KO) a very significant population was arrested in G2/M (Figure 3-8 C).

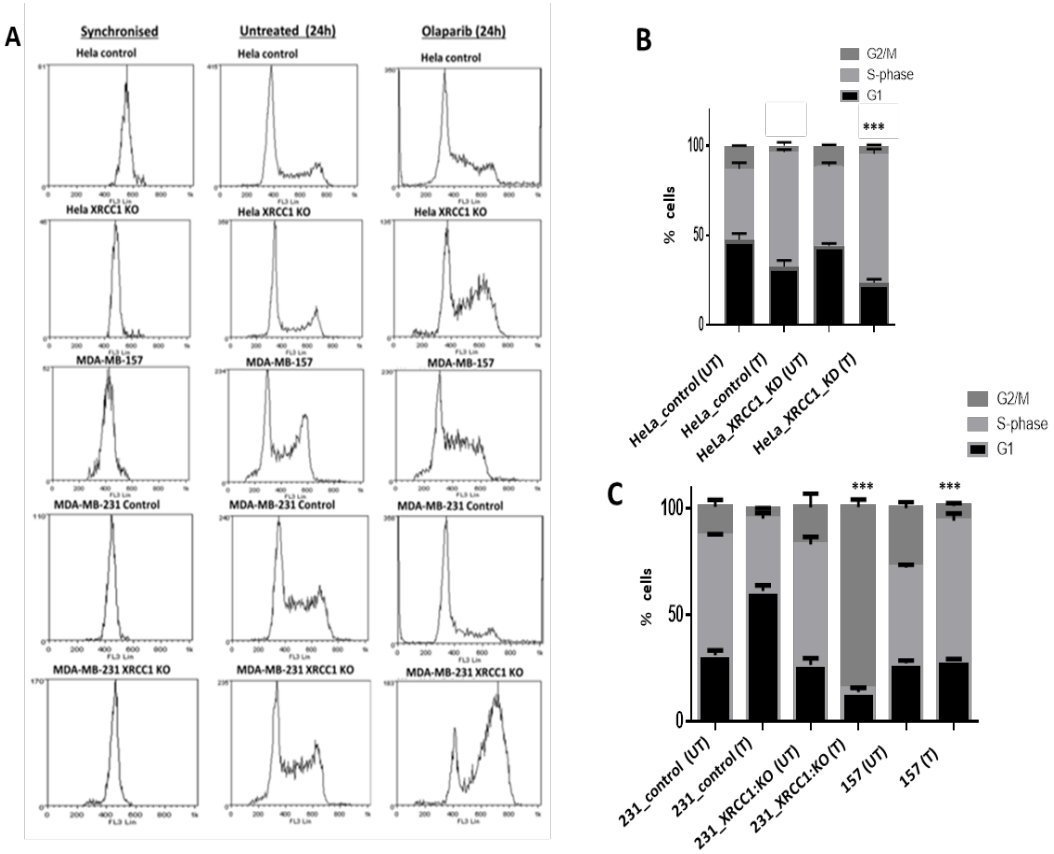


Figure 3-8: Cell cycle synchronization in the various cell lines.
(A)Representative images for cell synchronization in untreated and Olaparib treated cells. FACS analysis in synchronized Olaparib treated HeLa control and HeLa XRCC1_KD cells (B). 231 control and 231: XRCC1_KO and 157 cells (C). All experiments were done in triplicates.

Given the difference in the p53 status of those cell lines, HeLa cells are known to be p53 wild-type and MDA-MB-231 and MDA-MB-157 are known to be a p53

mutant. As shown in (Figure 3-9). We screened the cells for various pre-defined p53 mutations to understand the activity of p53 in those cell lines. MDA-MB-157 and MDA-MB-231 but not HeLa cells had mutant p53 and active forms of phosphorylated p53 at serine 46, serine 392, and serine 20. However, none of the cells has acetylation of p53 at lysine 382, which is known to have a role in the regulation of apoptosis (Liu *et al.*, 2017).

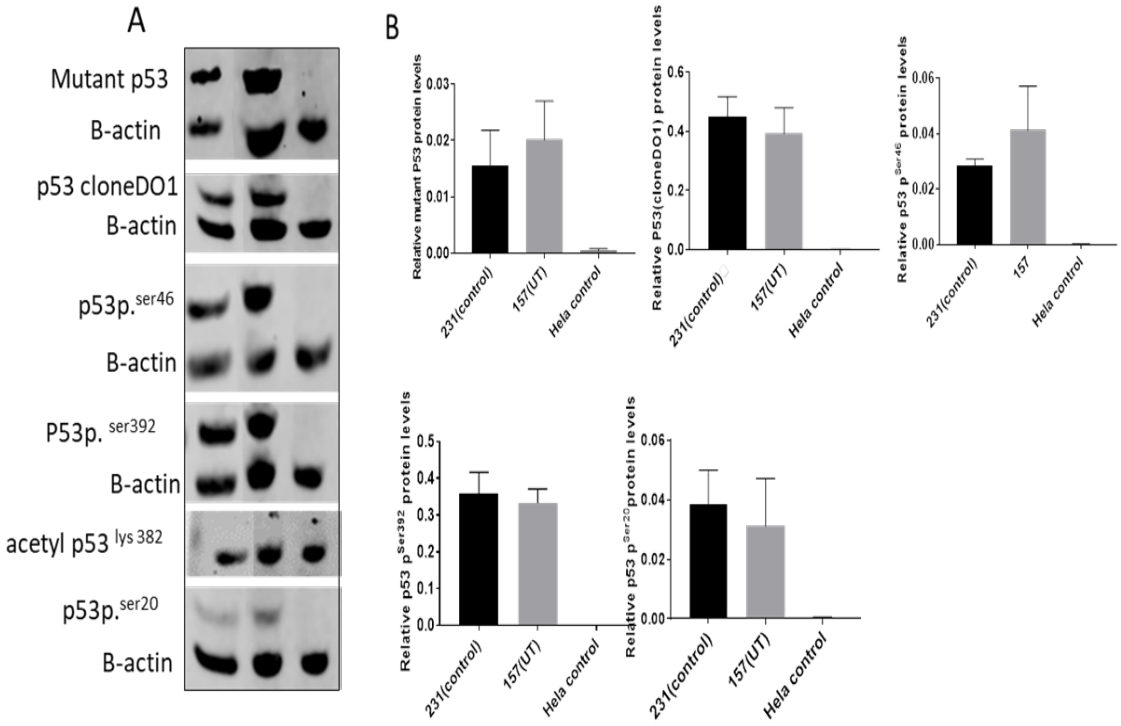


Figure 3-9: p53 mutations and post-translational modification profiling
(A). Quantification of p53 protein levels by western blotting. β-actin was used as a loading control (B).

3.3.5 Nutlin3a can influence cell cycle arrest in p53 mutant cell lines treated with Olaparib

Nutlin-3a is a potent antagonizing small molecule inhibitor of MDM2 (murine double minute 2) that binds to MDM2 in the p53 binding pocket leading to p53

activation (Kojima *et al.*, 2006; Villalonga-Planells *et al.*, 2011). To determine if the cell cycle response observed in Olaparib treated cells is p53 pathway dependent, we treated the cells with Nutlin3a (10µM) for 72 hours. At 48 hours, the cells were treated with Olaparib (10µM) or left treated with Nutlin alone. Interestingly, the Nutlin /Olaparib combination resulted in G2/M arrest in MDA-MB-157 in comparison to S-phase arrest induced in Olaparib treated MDA-MB-157 (Figure 3-10A). However, the Nutlin /Olaparib combination in MDA-MB-231: XRCC1_KO leads to S-phase arrest compared to the previously observed G2/M in Olaparib alone treated cells (Figure 3-10A).

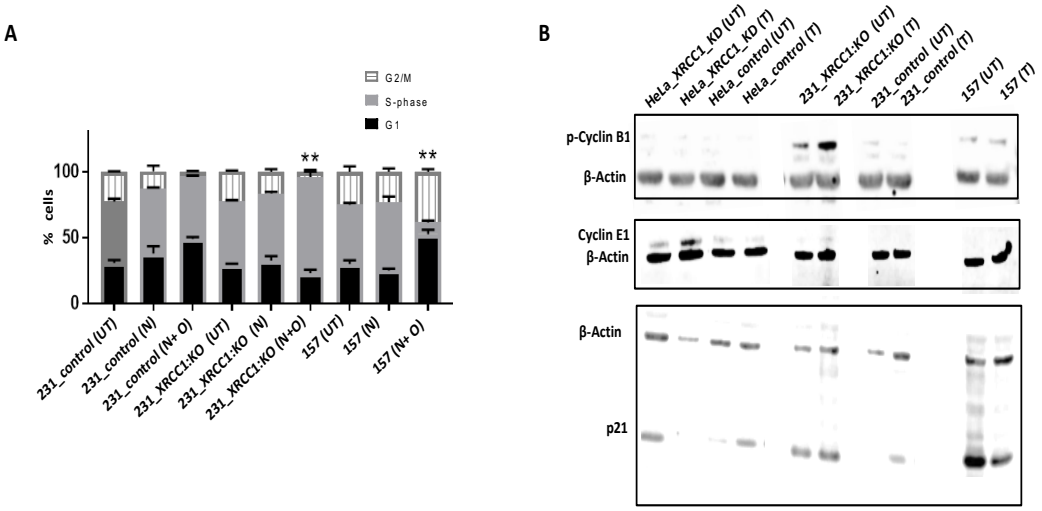


Figure 3-10: Cell cycle analysis in Nutlin treated cells.
(A) Cell cycle analysis of MDA-MB-231, MDA-MB-231: XRCC1_KO and MDA-MB-157 treated with Nutlin3a alone or Nutlin3a /Olaparib combination. (B) p-Cyclin B1, CyclinE1 and p21 levels in the cells untreated or treated with Olaparib (10µM) for 24 hours.

Cyclins and cyclin-dependent kinases are a family of proteins that regulate cell cycle progression through its different phases. Cyclin-dependent kinases have a

serine threonine-binding pocket that can be occupied and regulated by the specific cyclins (Lim and Kaldis, 2013). We then evaluated key cyclins that are directly involved in the regulation of the G2/M phase such as p-cyclinB1 at serine 126 (Hagting *et al.*, 1999; Soni *et al.*, 2008). P-cyclinB1 levels were elevated in MDA-MB-231: XRCC1_KO treated with Olaparib which evidences the cell's entry into G2/M as observed in cell cycle analysis. On the other hand, we assessed cyclinE1 levels which are known to facilitate the cell's entry into the S-phase (Caldon and Musgrove, 2010). CyclinE1 levels were up-regulated in HeLa XRCC1_KD treated with Olaparib which arrest in the S-phase as shown previously in cell cycle analysis by flow cytometry (Figure 3-10B).

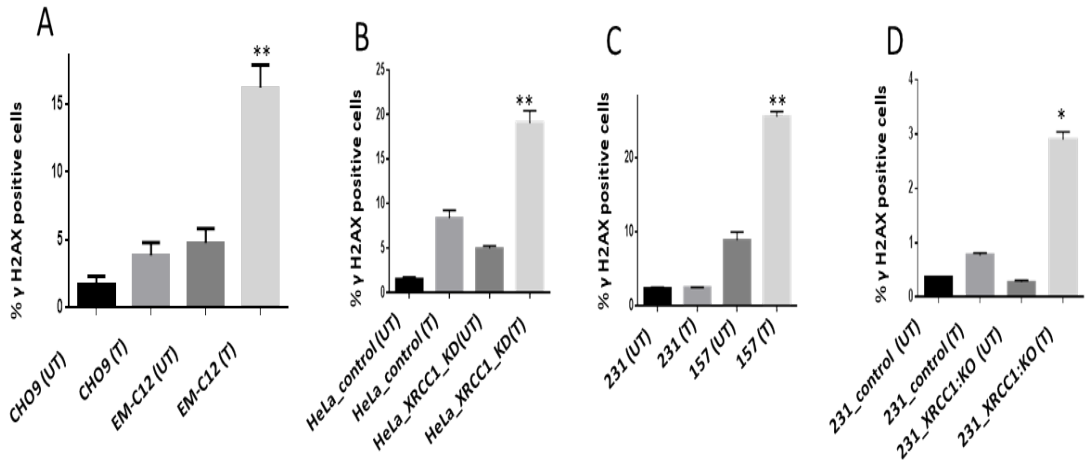


Figure 3-11: γH2AX analysis by flow cytometry
γH2AX positive cell quantification in (A) CHO9 and EMC12 cells treated with Olaparib (10µM) for 24 hrs. (B)HeLa control and HeLa XRCC1_KD treated with Olaparib (10µM) for 24 hrs. (C)MDA-MB-231(control) and MDA-MB-157 treated with Olaparib (10µM) for 24 hrs. (D) MDA-MB-231(control) and MDA-MB-231: XRCC1_KO treated with Olaparib (10µM). All experiments were done in triplicates.

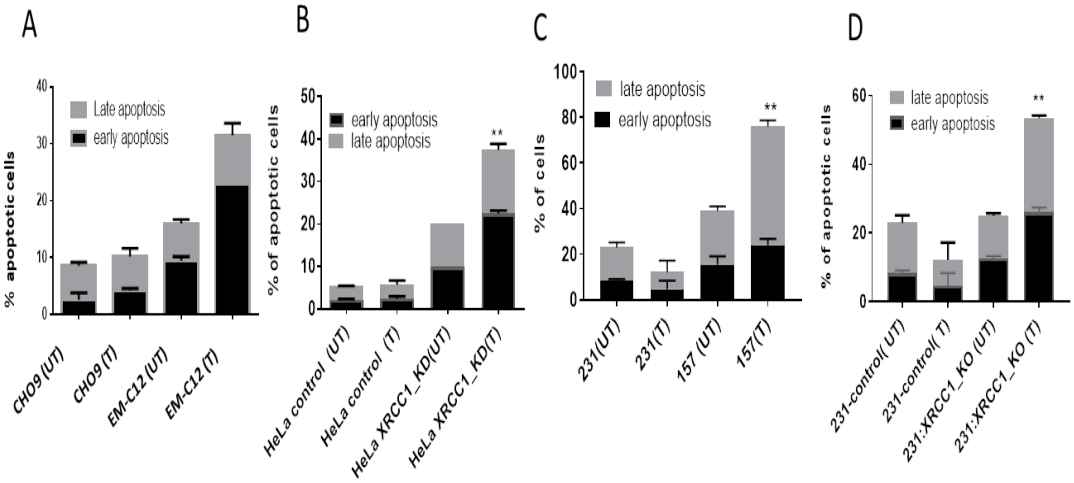


Figure 3-12: the percentage of apoptotic cells analysed by flow cytometry.

AnnexinV apoptosis assay in (A) CHO9 and EMC12 cells treated with Olaparib (10µM) for 24 hrs. (B)HeLa control and HeLa XRCC1_KD treated with Olaparib (10µM) for 24 hrs. (C)MDA-MB-231(control) and MDA-MB-157 treated with Olaparib (10µM) for 24 hrs. (D) MDA-MB-231(control) and MDA-MB-231: XRCC1_KO treated with Olaparib (10µM) for 24 hrs. All experiments were done in triplicates.

3.3.6 Accumulation of DSBs and apoptotic cells upon Olaparib treatment

PARP1 is known to be involved in processing single strand break repairs in various DNA damage repair pathways. Inhibition of PARP1 by Olaparib treatment will not only lead to the accumulation of single-strand breaks but also will result in delayed activation of key DSB proteins, thus, leading to an accumulation of DSBs. ATM recruits SMC1, p53 and p.histone H2AX pser139 in the event of DSB (Ray Chaudhuri and Nussenzweig, 2017). To investigate whether the SSB accumulated upon inhibition of PARP1 activity have retained the ability to be repaired in XRCC1 deficient cells, we measured the levels of histone H2AX phosphorylated on ser139

(γH2AX) which is a marker of DNA damage. The results show an accumulation of γH2AX levels in XRCC1 deficient cells treated with Olaparib: EMC12 (Figure 3-11A), HeLa XRCC1_KD (Figure 3-11B), MDA-MB-157 (Figure 3-11C) and MDA-MB-231: XRCC1_KO (Figure 3-11D).

Modification of PARP1 by caspases is known to be a hallmark of apoptosis (Chaitanya, Steven and Babu, 2010). To investigate whether cell cycle arrest and DNA damage will eventually lead to apoptosis, we conducted annexin-V and PI staining for the different XRCC1 proficient and deficient cell lines treated with Olaparib. As shown in (Figure 3-12), we noticed an accumulation of apoptotic cells in XRCC1 deficient cells EMC12 (Figure 3-12A), HeLa XRCC1_KD (Figure 3-12B), MDA-MB-157 (Figure 3-12C) and MDA-MB-231: XRCC1_KO (Figure 3-12D).

3.3.7 Immunofluorescence for PARP1 and γH2AX foci formation in XRCC1 deficient and proficient cells upon Olaparib treatment.

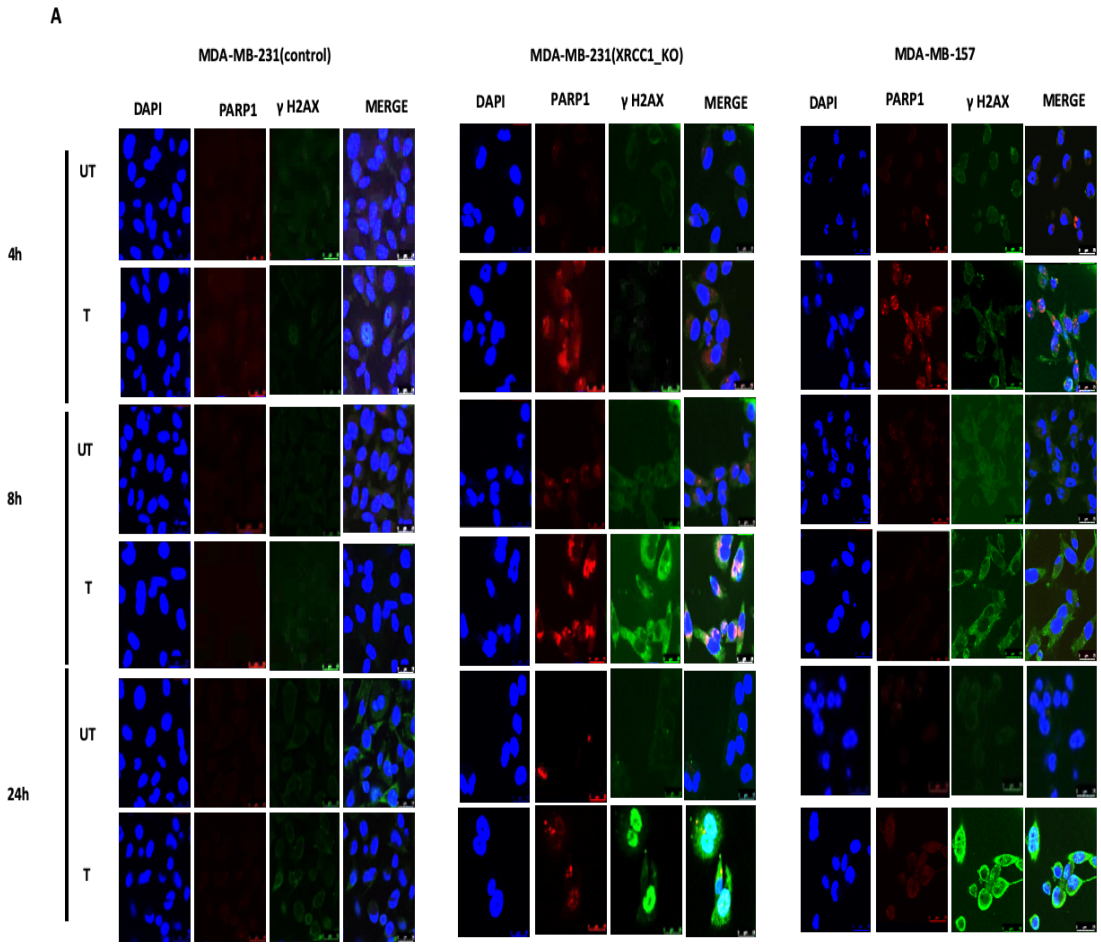


Figure 3-13: Immunofluorescence for γH2AX and PARP1 levels in 231, 231_XRCC1_KO cells and 157 treated with Olaparib.
Cells were seeded on coverslips overnight and then treated with Olaparib (10 μM). Cells were fixed with 4 % paraformaldehyde at 4 hrs, 8 hrs and 24 hrs. Then the cells were stained with γH2AX and PARP1 antibodies as per the immunofluorescence protocol described in the Methods chapter.

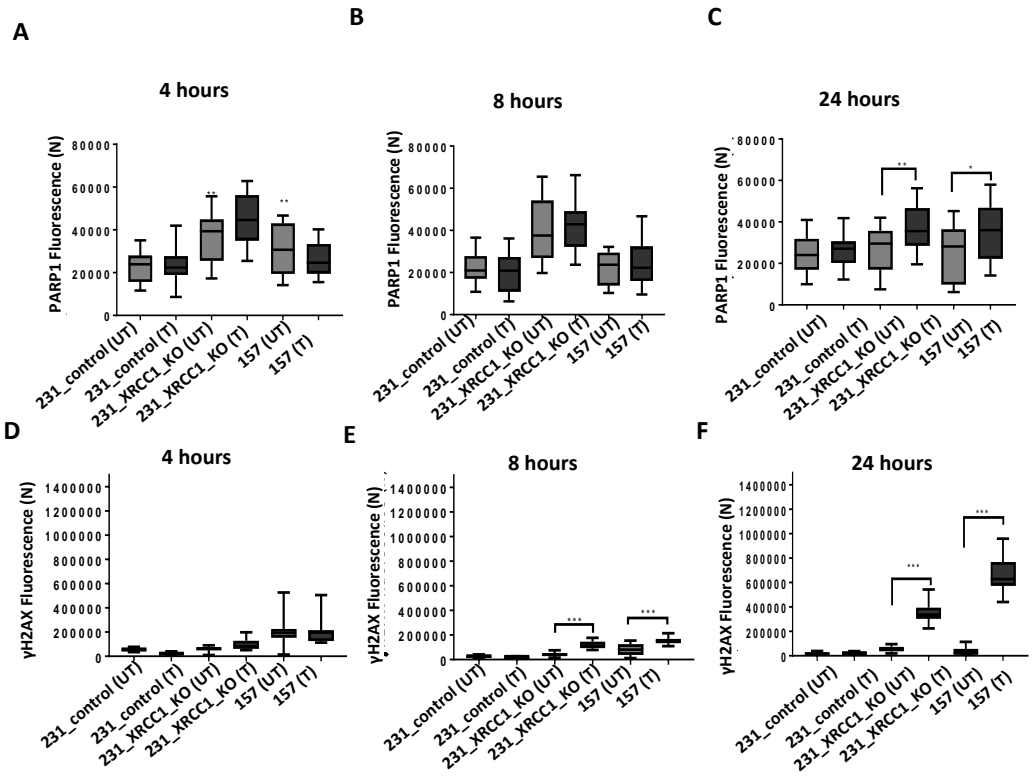


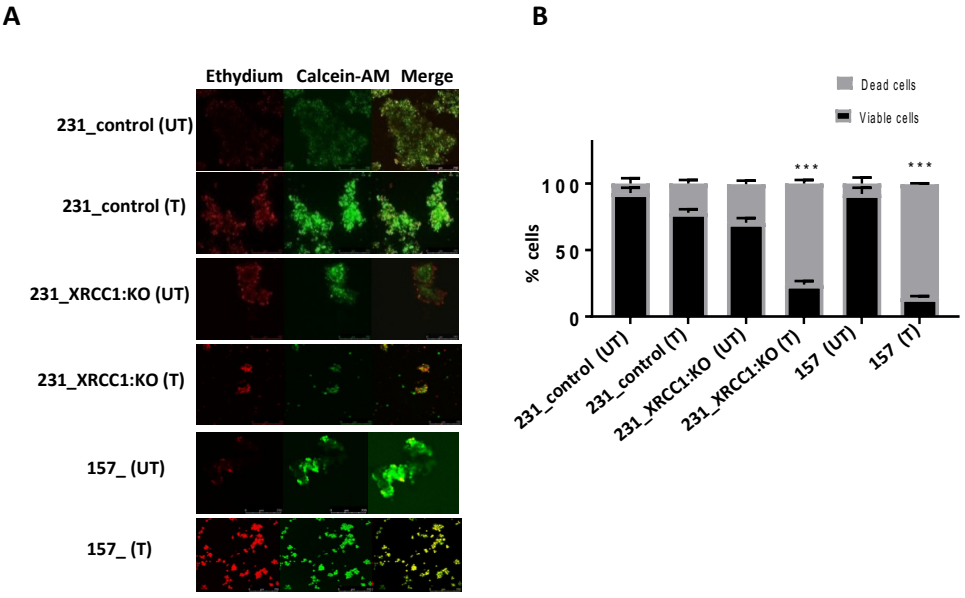
Figure 3-14: Mean fluorescence intensity quantification by ImageJ for PARP1 and γH2AX at the indicated time points.
PARP1 nuclear fluorescence quantification in 231 control, 231_XRCC1_KO & 157 treated with Olaparib (10 μM) for 4hours (A), 8 hours (B) and 24 hours (C). γH2AX nuclear fluorescence quantification in 231 control, 231_XRCC1_KO & 157 treated with Olaparib (10 μM) for 4hours (D), 8 hours (E) and 24 hours (F).

PARP1 interacts with XRCC1 in the base excision repair pathway. XRCC1 deficiency enhances single strand break (SSB) formation which in turn activates PARP1. It has been described that PARP1 inhibitors can enhance cytotoxicity through trapping of PARP-DNA complexes (Murai *et al.*, 2012). Thus, we monitored the formation of PARP1 and γH2AX foci formation upon Olaparib treatment at 4 hrs, 8hrs and 24 hrs (Figure 3-13).

We observed higher PARP1 fluorescence in XRCC1 deficient cells (MDA-MB-231XRCC1_KO & MDA-MB-157) at the basal levels (Figure 3-14 A). Upon Olaparib treatment, PARP1 levels significantly increase at 24 hours in XRCC1 deficient cells

but not in XRCC1 proficient cells which indicates PARP1 trapping in XRCC1 deficient cells by Olaparib (Figure 3-14 C).

On the other hand, analysis of γH2AX foci showed an increase in γH2AX levels in Olaparib treated XRCC1 deficient cells in comparison to control cells at 8 hours which persists after 24 hours (Figure 14 F&G).



3.3.8 Olaparib induces lethality in XRCC1 deficient spheres

Figure 3-15: Olaparib sensitivity in 3D spheroids of XRCC1 deficient cells.

(A)Representative photomicrographic images of 3D spheroids of MDA-MB-231 control, MDA-MB- 231: XRCC1_KO and MDA-MB- 157 treated with Olaparib. (B) Quantification of cell viability by flow cytometry. Cells were grown in the tumour sphere medium for 3 weeks. After formation of spheroid structures, cells were treated with Olaparib for 48 hours. Spheres were fixed in 37% formaldehyde (1:10 concentration) for 30 minutes, then stained with Calcein (AM)(2µM) and ethidium bromide homodimer (1.5µM). For quantification of cell viability, spheres were

dissociated by trypsinization and stained with Calcein (AM), (0.01µM) and ethidium bromide (1µM).

We aimed to further test Olaparib sensitivity in XRCC1 deficient cells in 3D tumour sphere models to mimic an in-vivo system. Upon Olaparib treatment, XRCC1 deficient spheres in MDA-MB-231(XRCC1_KO) and MDA-MB-157 retained a reduction in sphere sizes as well as accumulation of dead cells as evident by the increase in ethidium homodimer staining (Figure 3-15).

3.3.9 Sensitivity of XRCC1 deficient cells to other PARP1 inhibitors

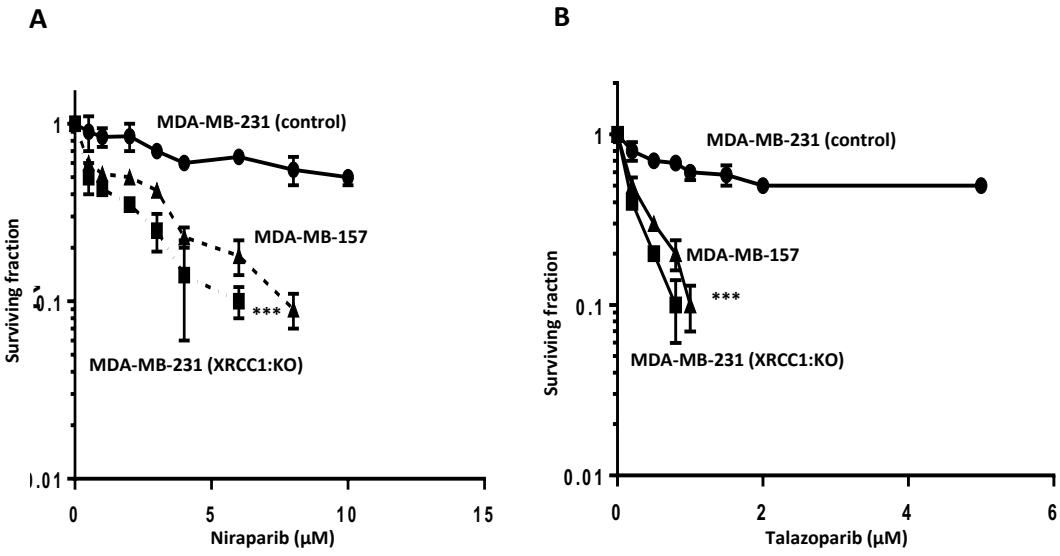


Figure 3-16: Clonogenic survival assay for XRCC1 deficient cells with Niraparib and Talazoparib.

(A) Clonogenic survival assay of MDA-MB-231 and MDA-MB-231(XRCC1_KO) and MDA-MB-157 in different doses of Niraparib. (B) Clonogenic survival assay of MDA-MB-231 and MDA-MB-231(XRCC1_KO) and MDA-MB-157 in different doses of Talazoparib.

Trapped PARP-DNA complexes are known to be more lethal to cells than the single strand breaks that PARP inhibition forms. The immunofluorescence data suggested that PARP trapping is the mechanism of toxicity in XRCC1 deficient cells. We then evaluated the sensitivity of XRCC1 deficient cells to other PARP1 inhibitors. Niraparib are more potent that Olaparib, Talazoparib in turn is 100 times more potent in PARP1 trapping (Lord and Ashworth, 2017). We found that XRCC1 deficient cells MDA-MB-231(XRCC1_KO) & MDA-MB-157 are very sensitive to Niraparib and Talazoparib compared to control cells MDA-MB-231 (Figure 3-16). Calculations of the lethal dose 50% (LD50) revealed that at doses tested, Niraparib was five times more potent than Olaparib. Talazoparib was twenty times more potent than Olaparib (Table 3-2).

Table 3-2: LD50 for PARP1 inhibitor sensitivity in XRCC1 deficient cells.

	MDA-MB-231(XRCC1_KO)	**MDA-MB-157**	
Olaparib	4 μM	4 μM	
Niraparib	1μM	0.9 μM	5x potent than Olaparib

Talazaparib	0.2µM	0.1 µM	20x potent than Olaparib

3.3.10 Immunofluorescence for PARP1 trapping in Talazoparib treated cells

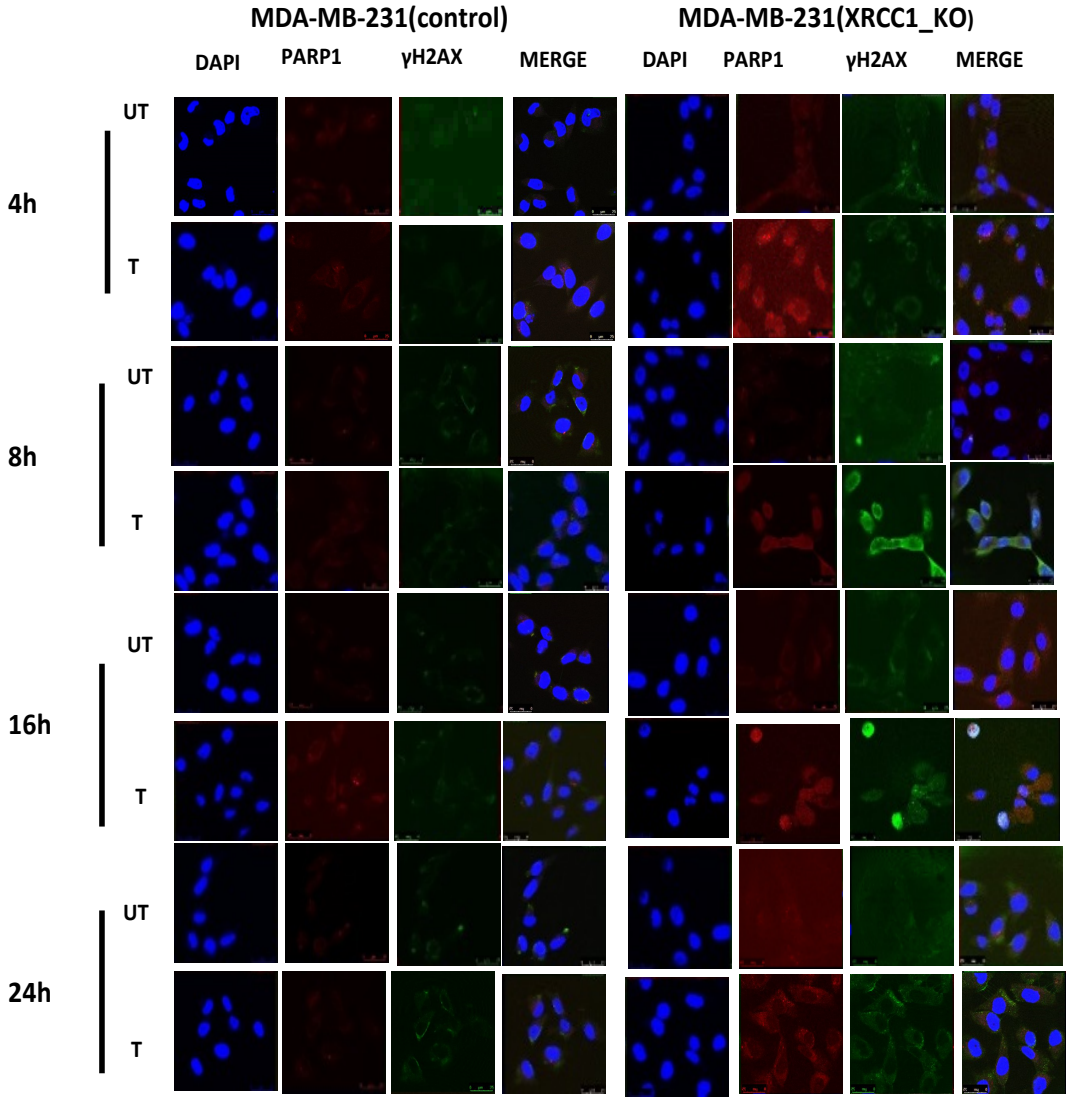


Figure 3-17: Immunofluorescence for PARP1 and γH2AX staining in MDA-MB-231 and MDA-MB-231(XRCC1_KO).
231(control) & 231(XRCC1_KO) were plated on coverslips overnight then treated with 5 µM Talazoparib. Cells were fixed with 4% paraformaldehyde at 4 hrs, 8 hrs, 16 hrs and 24 hrs. Cells were stained with PARP1 and γH2AX as per the immunofluorescence protocol described in the Methods section.

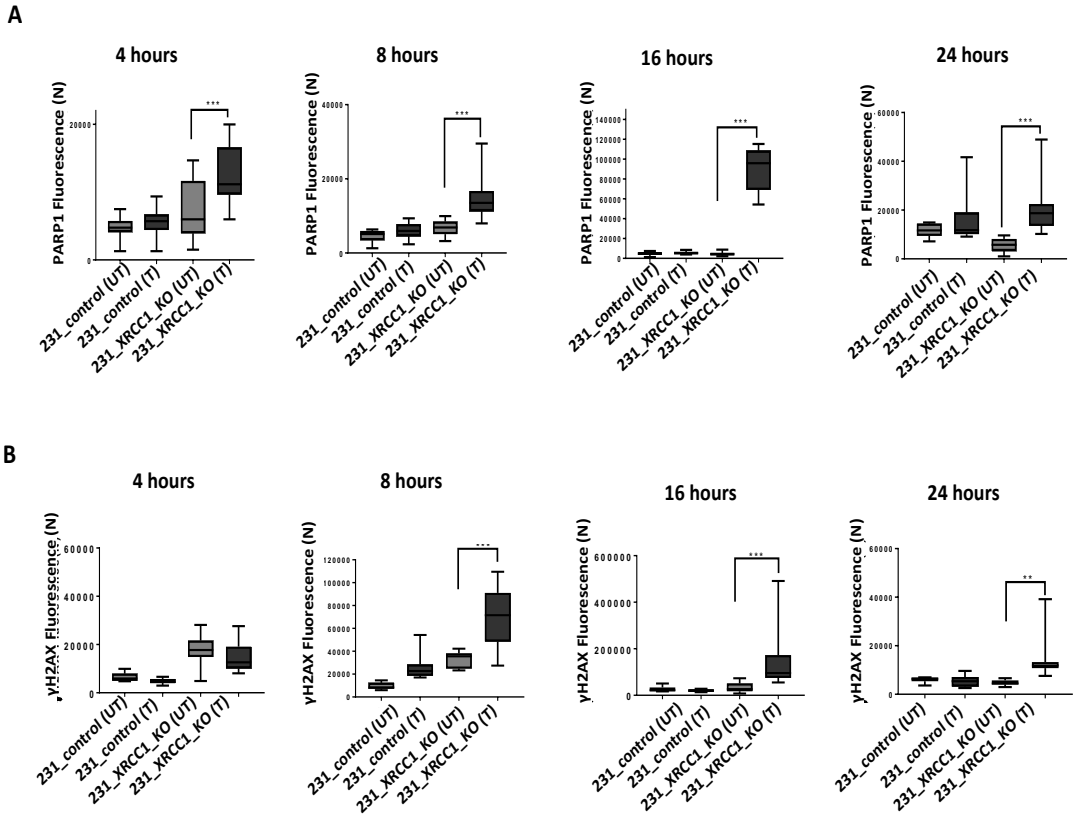


Figure 3-18: PARP1 and γH2AX nuclear fluorescence quantification by ImageJ software.
(A) PARP1 nuclear fluorescence in MDA-MB-231 control, MDA-MB-231(XRCC1_KO) and MDA-MB-157 treated with Talazoparib (5 μM) for 4hrs, 8hrs, 16hrs and 24hrs. (B) γH2AX nuclear fluorescence in MDA-MB-231 control, MDA-MB-231(XRCC1_KO) and MDA-MB-157 treated with Talazoparib (5 μM) for 4hrs, 8hrs, 16hrs and 24hrs.

Talazoparib treatment increased PARP1 fluorescence as early as at 4 hours, increased PARP1 levels which persisted after 24 hours indicates earlier PARP1 trapping in comparison to Olaparib. Talazoparib also induced γH2AX significantly in the XRCC1 deficient cells after 8 hours (Figure 3-18).

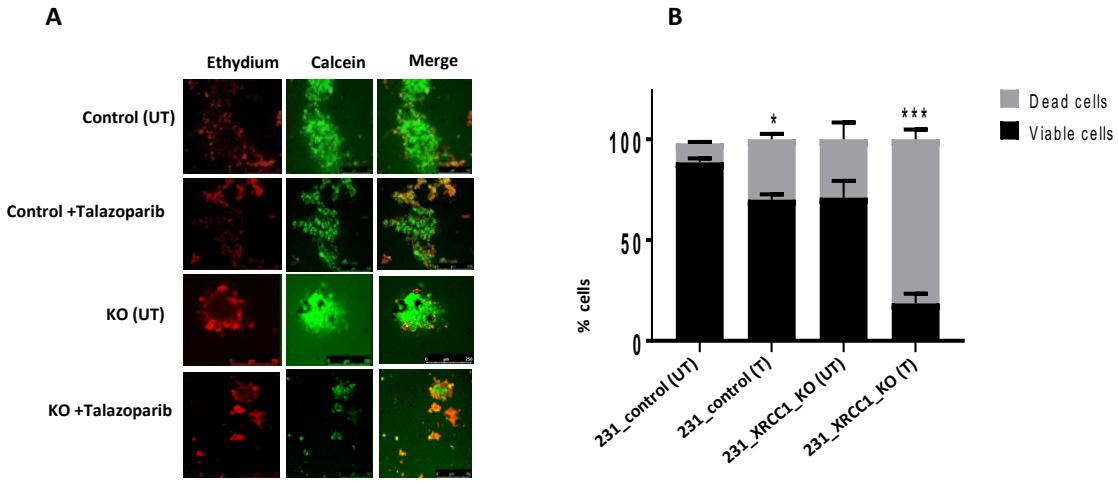


Figure 3-19: 3D spheroids of XRCC1 deficient cells treated with Talazoparib. (A) Representative photo micrographic images of MDA-MB-231 control and MDA-MB-231(XRCC1_KO) 3D spheroids treated with Talazoparib (5μM) for 48 hrs. (B) Quantification of cell viability by flow cytometry.

We tested Talazoparib sensitivity in 3D spheroids of XRCC1 proficient and deficient cells to recapitulate the in vivo model. MDA-MB-231(XRCC1_KO) was really sensitive to Talazoparib and it led to a reduction in sphere size as well as an accumulation in dead cells as evident by the flow cytometry analysis of cell viability (Figure 3-19).

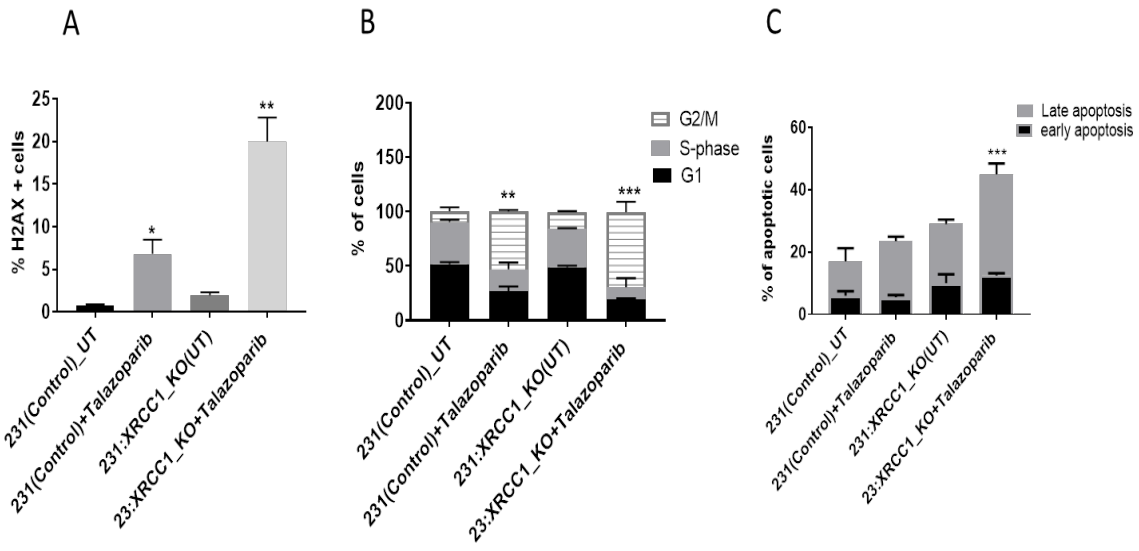


Figure 3-20: Functional studies of Talazoparib treatment in MDA-MB-231 control and XRCC1_KO.
γH2AX analysis by flow cytometry (A), cell cycle analysis by flow cytometry (B) and apoptosis analysis by flow cytometry (C) in MDA-MB-231 control and MDA-MB-231(XRCC1_KO) treated with Talazoparib (5μM) for 24 hrs.

Additionally, we tested the effect of Talazoparib on cell cycle progression, apoptosis and double strand breaks formation. Talazoparib treatment for 24 hours led to DNA damage evident by γH2AX accumulation (Figure 3-20A) which led to striking cell cycle arrest in the G2/M phase (Figure 3-20B) and the accumulation of apoptotic cells which is more profound in XRCC1_KO cells (Figure 3-20C).

3.4 Discussion

XRCC1 is a multi-domain protein with no known catalytic activity (Horton *et al.*, 2014). However, three distinct domains of XRCC1 interact with DNA polymeraseβ, PARP1 and DNA Ligase III to accomplish various SSBR pathways (Sanjari Moghaddam *et al.*, 2016). The link between XRCC1 deficiency and breast cancer aggressiveness has been previously reported by our group (Rebeka Sultana *et al.*, 2013) and by others (Horton *et al.*, 2014). The associations between *XRCC1* gene polymorphisms and breast cancers have been heavily studied; in particular, the variants (Arg194Trp, Arg280His, and Arg399Gln) have been linked to clinical prognostic factors or adverse reactions to radiotherapy in breast cancers in previously published meta-analysis studies (Moullan *et al.*, 2003; Brem *et al.*, 2006; Li, Ha and Tai, 2009).

In our study, we showed the correlation between XRCC1 deficiency and poor prognosis of breast cancers. The clinical data also showed that high PARP1 levels in XRCC1 deficient tumours are linked to high grade, high mitotic index, high pleomorphism, ER-/PR- and high-risk Nottingham Prognostic Index (NPI >3.4) as shown in Table 1 (all adjusted p values <0.0001). This suggests that targeting PARP1 in XRCC1 deficient tumours could have promising clinical potential.

BRCA1 and BRCA2 are components of the HR pathway. BRCA1- and BRCA2-associated cancers can be targeted with PARP1 inhibitors in a synthetic lethality approach (Y. Wang *et al.*, 2016). PARP1 inhibition generates DNA damage that requires functional BRCA1 and BRCA2 genes to be paired (Farmer *et al.*, 2005). That approach opened a large therapeutic window for Olaparib which acquired

FDA approval in 2014 for treatment of advanced ovarian cancers with BRCA mutations. It was also approved for treatment of metastatic breast cancers with BRCA germline mutations in 2018. More PARP inhibitors are in different phases of clinical trials (clinical trials.gov NSC-737664 & NSC-746045). In the current study, we screened Olaparib sensitivity in XRCC1 deficient and proficient breast cancer cell lines and we found a consistent sensitivity in the XRCC1 deficient breast cell lines across the board in the MTS and clonogenic survival assays shown in the results. Accumulation of apoptotic cells after 24 hours of Olaparib treatment in XRCC1 deficient cells revealed the selective Olaparib toxicity in XRCC1 deficiency background. We mechanistically investigated Olaparib influence on cell cycle progression. Olaparib treatment induced cell cycle arrest which appeared to be influenced by p53 genetic background. Additionally, γH2AX analysis by flow cytometry confirmed the extent of DNA damage which reflects that the SSB lesions generated by PARP inhibition failed to be repaired and have been converted to more serious DSB DNA damage lesions. Interestingly, our investigation in MDA-MB-157 confirmed that XRCC1 deficiency is essential for PARP1 inhibitor extreme sensitivity and synthetic lethality. Methylation of the *XRCC1* gene appeared to be the mechanism of down-regulation of XRCC1 in this cell line. Upon treatment with Azacytidine XRCC1 mRNA and protein levels were restored. Comparison of Olaparib sensitivity in MDA-MB-157 untreated and those treated with Azacytidine revealed significant resistance to Olaparib upon XRCC1 re-expression. Du *et al.* reported that combining c-Met blockage and the PARP1 inhibitor would achieve a synergistic effect to suppress breast cancer in vitro and in vivo mouse models (Du *et al.*, 2016). In another study, modulation of the

receptor tyrosine kinase AXL synergized PARP1 inhibition. AXL promotes epithelial to mesenchymal transition phenotype and is linked with aggressive breast cancers. Modulation of AXL causes homologous recombination deficits and thus introduces again the concept of synthetic lethality with the PARP1 inhibitor (Balaji *et al.*, 2017). Here we introduced Olaparib as a single agent to achieve selective toxicity in XRCC1 deficient tumours.

However, there are several studies addressing BRCA mutations as being a mechanism of resistance to PARP inhibitors. BRCA RING domain mutations such as $BRCA1^{185delAG}$ can fail this synthetically lethal pair to function (Drost *et al.*, 2016). The epigenetic re-expression of BRCA1 through the loss of methylation in the BRCA1 promoter was confirmed by in-vivo studies (ter Brugge *et al.*, 2016). Additionally, mutations restore the open reading frame (ORF) of BRCA and thus reactivation of the homologous recombination repair pathway (Edwards *et al.*, 2008).

Thus, finding other targets that would achieve synthetic lethality with PARP inhibitors is an interesting approach at the core of our study.

We showed knock –out of XRCC1 by the CRISPR Cas-9 system in MDA-MB-231 to revert Olaparib resistance in those cells and significantly affect their survival. MDA-MB-231 as well as MDA-MB-157 are derived from triple negative breast cancer origin and therefore represent an *in vitro* model for the most aggressive form of breast cancers. A fairly sizable number of patients in our clinical cohort were a triple negative subtype of breast cancers with low XRCC1 expression (16%) (Rebeka Sultana *et al.*, 2013). Consequently, investigation of targeting XRCC1

deficient tumours with PARP1 inhibitors provide a new therapeutic potential to aggressive breast cancers with limited therapeutic options.

Two mechanisms of action have been proposed to the cytotoxicity of PARP inhibitors: PARP inhibition and PARP trapping. Upon DNA damage response (DDR) PARP1 and PARP2 act as DNA damage sensors that bind to single strand breaks (SSB) and other DNA lesions (Murai *et al.*, 2014). PARP1 synthesises Poly ADP ribose polymers (PAR) on itself and on other DNA repair intermediates like XRCC1. Inhibition of PARP1 catalytic activity (PARylation) leads to persistence of SSBs which become DSBs when encountering the replication fork (Lord and Ashworth, 2017). Thus, PARP inhibition is described as the mechanism of cytotoxicity of PARP inhibitors in homologous recombination deficient cells. However, more studies have suggested trapping of PARP1 and PARP2 at the SSB sites to exert more cytotoxicity than inhibition of PARP catalytic activity (Murai *et al.*, 2012, 2014). The formed PARP-DNA complexes prevent DNA repair completion. We observed selective Olaparib toxicity in XRCC1 deficient breast cell lines and we studied further PARP1 trapping in Olaparib treated cells. Our immunofluorescence studies showed that XRCC1 deficient cells have higher PARP1 at the basal levels. XRCC1 mutations were previously reported to be associated with PARP1 hyper-activation (Hoch *et al.*, 2017). Olaparib treatment increased nuclear PARP1 fluorescence which indicates PARP1 trapping in XRCC1 deficient MDA-MB-157 and MDA-MB-231(XRCC1_KO) cells. That PARP1 trapping was associated with an increase in γH2AX fluorescence after 24 hours of treatment is evidence of the extended DNA damage.

Murai *et al*. demonstrated using a chromatin bound fractions assay that Talazoparib is 100 times more potent than Olaparib and Rucaparib at inducing PARP-DNA complexes (Murai *et al.*, 2014). In clonogenic experiments, we found that the LD50 of Talazoparib is 0.1μM while that of Olaparib and Niraparib is 4 μM and 1μM respectively. Given that hypersensitivity to Talazoparib, we hypothesized that it could be more potent in PARP1 trapping than Olaparib. The immunofluorescence study showed that Talazoparib treatment increased PARP1 fluorescence as early as 4 hours in MDA-MB_231 (XRCC1_KO) which persists at 24 hours. Additionally, Talazoparib treatment induced γH2AX at 8 hours which is earlier than Olaparib.

Detailed functional studies of Talazoparib showed that it induces cell cycle arrest at the G2/M phase of the cell cycle similar to Olaparib. It also increases apoptosis and DSB formation in cells as confirmed by flow cytometry analysis.

A 3D culture model is a better environment to study drug targets as it more closely resembles an in vivo cell system. The interconnection between the cells and the extracellular matrix (ECM) is noted to play a role in drug response (Langhans, 2018). Therefore, we studied Olaparib and Talazoparib in 3D spheres of XRCC1 deficient and proficient cells to observe whether our findings can have more clinical relevance. MDA-MB-231(XRCC1_KO) and MDA-MB-157 spheroids were significantly sensitive to Olaparib. Olaparib not only increased dead cells in XRCC1 deficient spheres but also led to a reduction in sphere size. Similarly, XRCC1 deficient spheres were extremely sensitive to Talazoparib as evident by the flow cytometry quantification of cell viability and immunofluorescence imaging.

The data provides compelling evidence that PARP inhibition in XRCC1 deficient breast cancers is an attractive therapeutic approach for personalized breast cancer treatment. Further clinical trials on PARP inhibitors would benefit from screening breast cancer patients for XRCC1 expression.

4 The Role of XRCC1 as a Therapeutic Target for Ductal Carcinoma In-situ.

4.1 Introduction

Ductal carcinoma *in situ* (DCIS) refers to malignant lesions occurring in the breast ducts and lobules. Similar to invasive breast cancers, DCIS include an heterogeneous group of diseases that differ in their histological and molecular subtypes (Punglia *et al.*, 2018). The incidence of DCIS has increased dramatically due to national mammographic screening in many countries (Lynge *et al.*, 2014). It represents 25 percent of the diagnosed breast cancers in the United States with around 60,000 women annually being diagnosed. The risk factors for DCIS are very similar to those for invasive breast cancers and include age and genetic background. The incidence of DCIS is very low in younger women under 30 (Kerlikowske, 2010). The rate of diagnosis increases with age; in the 40-50 age group, the rate is around 0.6 % per 1000 screening examinations. However, that rate doubles to 1.3% per 1000 screening examinations in women of 70 to 84 years (Sänger *et al.*, 2014). Other risk factors are a family history of breast cancer, nulliparity, history of biopsy, menopause, and prolonged use of oestrogen and progestin hormonal therapy after menopause, elevated body mass index as well as high mammographic breast density (Kerlikowske, 2010).

Although the risk of mortality of DCIS is very minimal, the risk of recurrence into invasive breast cancer is significant. It is estimated that 45–78 % of all invasive breast cancers are associated with DCIS. Therefore more understanding of the recurrence factors is crucial (Sänger *et al.*, 2014).

A recent meta-analysis study evaluated the known prognostic factors for DCIS recurrence including biomarkers and tumour characteristics and concluded that

positive surgical margins, high nuclear grade and non-screening-detected cancers were highly associated with DCIS recurrence into invasive carcinoma (Zhang *et al.*, 2016).

On the other hand, various studies tried to classify DCIS according to their genomic profiles. BRCA1 and BRCA2 mutations have been described as genetic risk factors for DCIS predisposition (Claus *et al.*, 2005; Yang *et al.*, 2015). The role of BRCA1 and BRCA2 in invasive breast cancer (IBC) predisposition is well known and has been extensively studied (Dhillon and Taniguchi, 2015). That could be attributed to the molecular mechanisms by which BRCA mutations influence IBC aggressiveness.

Breast cancers harbouring BRCA1 and BRCA2 mutations are more likely to manifest as high grade poorly differentiated tumours. Moreover, BRCA1 mutated breast cancers are more likely to be oestrogen, progesterone and human epidermal growth factor receptor (HER2) negative (Kroiss *et al.*, 2008). Nevertheless, as DCIS is less profound in BRCA associated tumours, less is understood about the role of BRCA mutations in DCIS pathogenesis. Recent studies have found non-invasive lesions in prophylactic mastectomy specimens from patients with BRCA mutation indicating the onset of high recurrence DCIS in BRCA mutated patients (Kauff *et al.*, 2003; Kroiss *et al.*, 2008). p53 mutations have also been previously reported to be linked to high grade DCIS (Simpson and Page, 2000). Other genetic signatures which are predominant to cancer susceptibility such as ERBB2 overexpression and BCL2 upregulation were also linked to DCIS onset. Those studies suggest that genomic instability is a key driver in DCIS pathogenesis (Simpson and Page, 2000).

Studies of chromosomal instability in DCIS prognosis have revealed controversial outcomes. Some studies concluded that there is no difference in chromosomal alterations between pure DCIS and IBC (Heaphy *et al.*, 2009; Petridis *et al.*, 2016). However, other studies have reported the association of some chromosomal abnormalities with DCIS grading (Hwang *et al.*, 2004; Pan *et al.*, 2016). Hwang *et al*. reported that gain of 17q and loss of 8p is frequently found in high-grade DCIS, while the loss of 16q is more associated with low/intermediate grade DCIS rather than higher grades (Hwang *et al.*, 2004).

The key predictive biomarkers identified for DCIS recurrence are the amplification of *ERBB2* (Vincent-Salomon *et al.*, 2008) and *MYC* genes (Pan *et al.*, 2016). Further, the profound of *PIK3CA* mutations in the DCIS component of lesions but it's absent in the IBC component (Li *et al.*, 2010).

Although most of the studies up till now indicate that the 10-year mortality rate for DCIS patients is less than 2%, the risk of DCIS recurrence is high (Gorringe and Fox, 2017). Patients with DCIS can recur locally as a new DCIS or to invasive carcinoma. Patients with recurrent invasive carcinoma confer a high risk of breast cancer related death (Schwartz *et al.*, 2000). The Canadian National Breast Screening study revealed that 20% of DCIS patients have progressed to invasive carcinoma (To *et al.*, 2014). Therefore, the identification of predictive biomarkers of DCIS recurrence is crucial. Randomized clinical trials concluded that radiotherapy and breast-conserving surgery (BCS) is the optimum treatment strategy for DCIS (Emdin *et al.*, 2006; Holmberg *et al.*, 2008). However, increasing evidence shows that still the risk of recurrence occurs for some patients (Gorringe and Fox, 2017). Hence, the development of prognostic factors for personalised

DCIS treatment for individual patients can reduce the risk of recurrence to aggressive invasive carcinoma.

In this study, we explored the pattern of expression of XRCC1 in a cohort of 776 DCIS patients. Low XRCC1 is associated with high grade DCIS. We tested PARP inhibition in the XRCC1 knock out MCF10-DCIS cell line model. Olaparib was synthetically lethal in MCF10-DCIS (XRCC1_KO). Thus, we hypothesised that Olaparib could be a personalised chemo-preventative treatment for XRCC1 deficient DCIS.

4.2 Methodology

Immunohistochemistry staining of XRCC1 for TMA of DCIS cases (n=776) was performed as detailed in the Methods chapter. The evaluation of immune staining was performed by calculation of the H-score (range 0–300). For XRCC1, low/negative nuclear expression was identified by the median cut off ≤ 100.

Cell lines used in this study are MCF10A (normal breast tissue), MDA-MB-231 (triple negative) and MCF10-DCIS (DCIS model). MCF10-DCIS breast cancer cell line was previously isolated from a xenograft originating from premalignant MCF10AT cells injected into SCID mice. Injection of the MCF10DCIS cells into SCID mice within 22 passages results in a predominantly comedo ductal carcinoma in situ phenotype (Band and Sager, 1989; Miller *et al.*, 2000). XRCC1CRISPR _KO in MCF-10DCIS was performed as described in the Methods section. Invasion, migration and RT2PCR- for epithelial to mesenchymal transition (EMT) profiling, western blotting, clonogenics and 3D-spheroids are all detailed in the methods section. Flow cytometry was performed for cell cycle, γH2AX and apoptosis analysis, which are all described in the Methods section. Data analysis was performed in GraphPad Prism-7 software. Error bars represent standard error of mean between experiments. P-values are indicated as P-values <0.05 =*, p-value <0.01 =** & p-value <0.001=***.

4.3 Results

4.3.1 Clinical Data

4.3.1.1 XRCC1 expression in DCIS

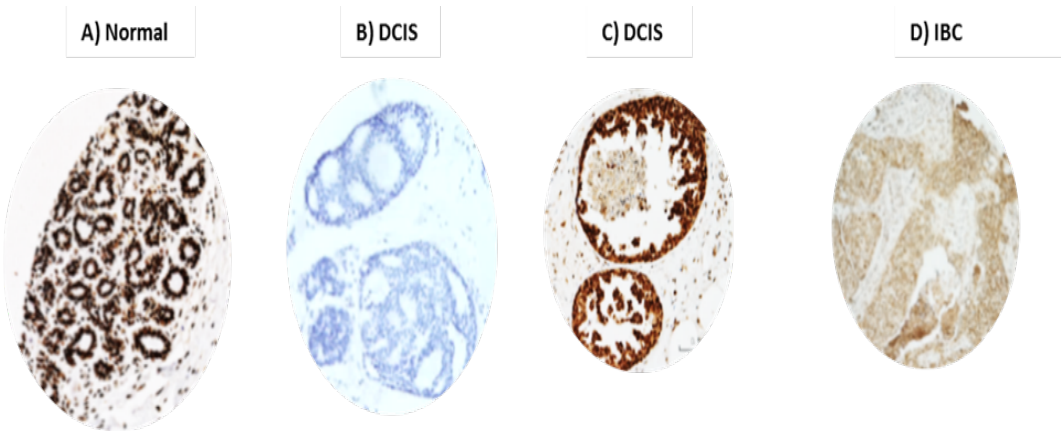


Figure 4-1: XRCC1 expression in TMAs.
Representative for XRCC1 expression by immunohistochemistry staining in normal tissue (A), XRCC1 negative DCIS (B), XRCC1 positive DCIS (C) and invasive breast cancers (D).

We investigated XRCC1 expression in a cohort of 776 pure DCIS patients (Figure 4-1) treated in Nottingham University Hospitals between 1987 and 2012. A cohort of 239 DCIS that co-exist with invasive breast cancer (IBC) as well as 50 normal breast tissues was also identified and assessed for XRCC1 expression.

Table 4-1: Patients demographics in DCIS cohort.

Parameter	**Groups**	**Number**
Age	≤45 years	57
	>45 years	396
Presentation	Screening	217
	Symptomatic	236
Extent	Localized	305
	Diffused	67
Size	≤20mm	195
	>20mm	255
Grade	Low	60
	Moderate	117
	High	276
Comedo/ Necrosis	No.	154
	Yes	299
DCIS type	Pure DCIS	453
	DCIS + invasive	196
LCIS	No	411
	Yes	42
Paget's.	No	276
	Yes	21
ER* status	Negative	109
	Positive	308

PR* status	Negative	177
	Positive	246
Treatment	Mastectomy	260
	Breast conserving surgery +RT	193
	Breast conserving surgery	123

*ER: Estrogen receptor. PR: Progestogen receptor.

Table 4-2: XRCC1 and clinicopathological associations in pure DCIS cohort.

Parameter	Groups	XRCC1 Expression	Number	%	*P value*
Age	≤45 years	Low High	24 33	42.1% 57.9%	**0.048**
	>45 years	Low High	222 174	56.1% 43.9%	
Presentation	Screening	Low High	120 97	55.3% 44.7%	0.684
	Symptomatic	Low High	126 110	53.1% 46.6%	
Size	≤20mm	Low High	100 95	51.3% 48.7%	0.207
	>20mm	Low High	146 109	57.3% 42.7%	
Grade	Non high (low + moderate)	Low High	86 91	48.6% 51.4%	**0.05**

Comedo/ Necrosis	No	Low	75	48.7%	0.086
		High	79	51.3%	
	Yes	Low	171	57.2%	
		High	128	42.8%	
LCIS	No	Low	227	55.2%	0.216
		High	184	44.8%	
	Yes	Low	19	45.2%	
		High	23	54.8%	
Paget's.	No	Low	157	56.9%	0.982
		High	119	43.1%	
	Yes	Low	12	57.1%	
		High	9	42.9%	
ER* status	Negative	Low	72	66.1%	**0.015**
		High	37	33.9%	
	Positive	Low	162	52.6%	
		High	146	47.4%	
PR* status	Negative	Low	105	59.3%	0.137
		High	72	40.7%	
	Positive	Low	128	52.0%	
		High	118	48.0%	

*ER: Estrogen receptor. PR: Progestogen receptor

Low XRCC1 expression was more profound in the older age group >45 years (p-value =0.048). Low XRCC1 was significantly associated with high grade DCIS (p-value=0.05) and comedo necrosis (p-value =0.086) (Table4-2). Additionally, low XRCC1 expression was linked to loss of oestrogen receptor (ER) in 66.1% of the ER negative patients (p-value=0.015). Similarly, low XRCC1 expression was observed in 59.3% of the progesterone receptor (PR) negative patients (p-value=0.13)

(Table 4-2). Therefore, the clinical data postulates that low XRCC1 is linked to the more aggressive phenotypes of DCIS.

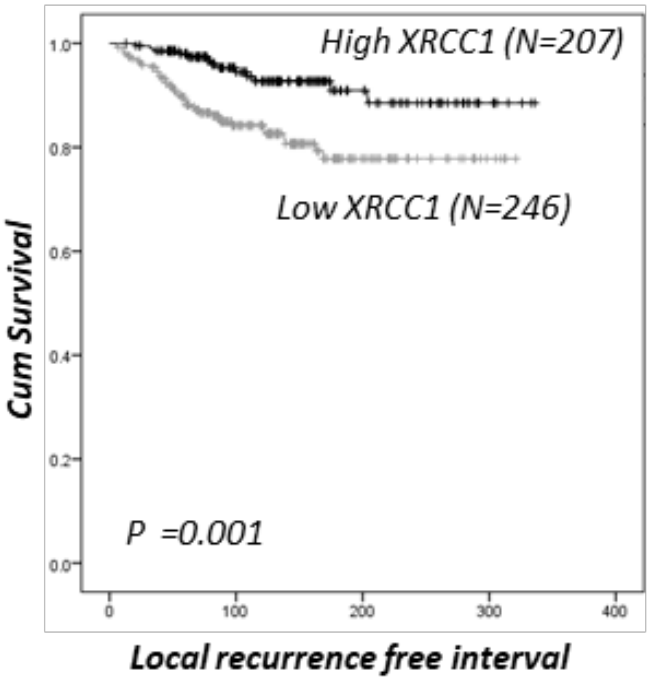


Figure 4-2: XRCC1 expression and local recurrence free interval in DCIS.

An interesting observation was that high XRCC1 expression is found in normal breast tissue. However, XRCC1 expression is significantly decreased in DCIS and invasive breast cancers, which implies that loss of XRCC1 expression could potentiate DCIS aggressiveness and recurrence (Figure 4-3).

Similarly, analysis of XRCC1 expression and local recurrence showed that low XRCC1 was significantly linked to disease local recurrence in DCIS (Figure 4-2). Together, the analysis indicates that loss of XRCC1 expression could be a potential predictor of disease progression to invasive breast cancer.

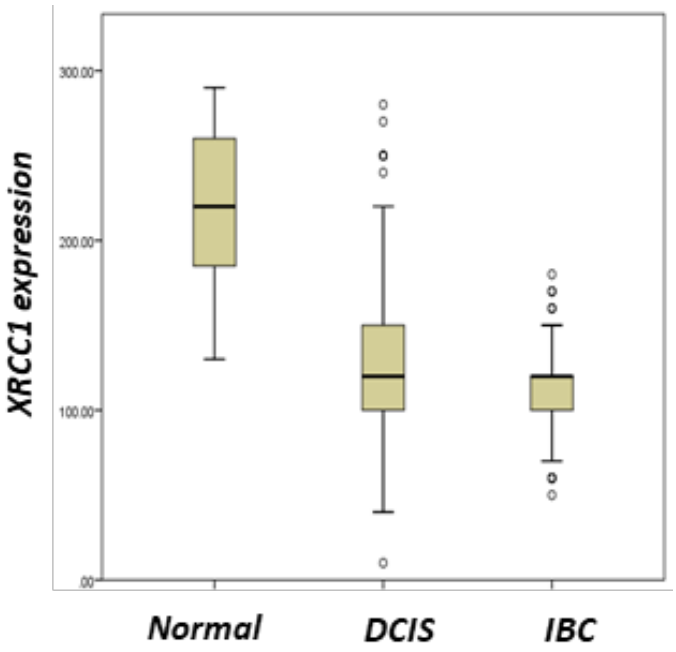


Figure 4-3: Box plot showing XRCC1 expression.
XRCC1 expression in normal breast tissues, DCIS and invasive breast cancers.

4.3.2 Pre-clinical data:

4.3.2.1 XRCC1 in breast cell lines

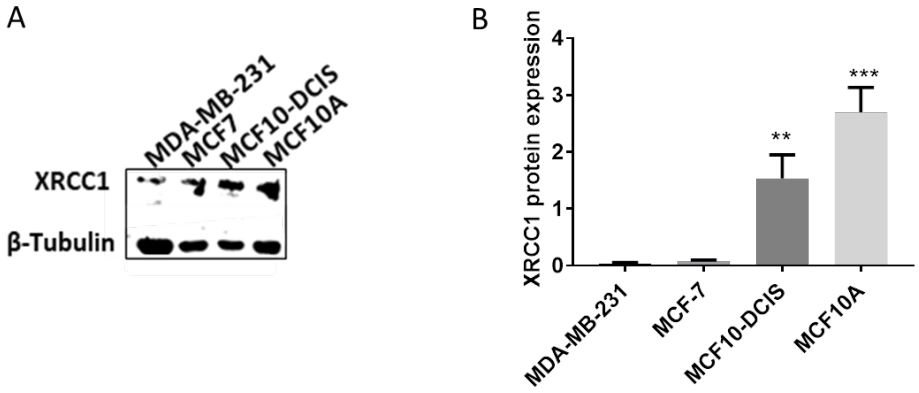


Figure 4-4: XRCC1 expression in breast cell lines.
Western blot image of XRCC1 expression in breast cell lines (MDA-MB-231, MCF7, MCF10DCIS and MCF10A cells) (A). Quantification for XRCC1 levels by western blot relative to β-tubulin (B).

We investigated XRCC1 expression in different breast cell line models; MDA-MB-231(triple negative), MCF-7 (Luminal A), MCF-10DCIS (DCIS) and MCF10A normal breast. There is a robust XRCC1 expression in MCF10-DCIS. However, the levels of expression seem different in the tested cells. Comparison of XRCC1 levels in MCF-DCIS and MCF10A normal tissue shows down-regulation of XRCC1 in MCF10-DCIS in comparison to normal MCF10A. On the other hand, comparison of MCF10-DCIS to MDA-MB-231 (triple negative) demonstrates increased levels of XRCC1 in MCF10-DCIS than triple negative MDA-MB-231. This differential expression of XRCC1 shows that loss of XRCC1 could be associated with breast cancer aggressiveness (Figure 4-4).

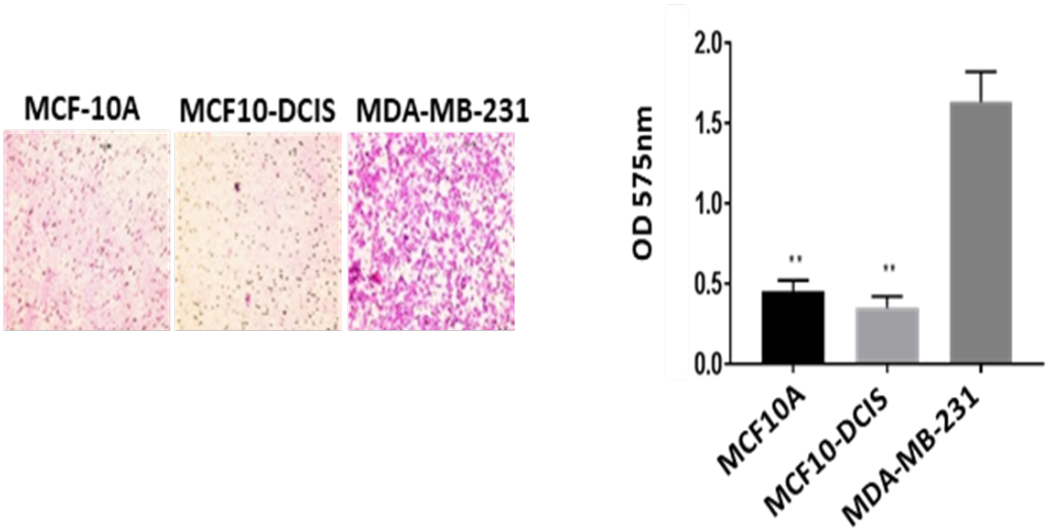


Figure 4-5: Invasion assay in MCF10-DCIS, MCF-10A and MDA-MB-231. MCF10-A, MCF10-DCIS and MDA-MB-231 were seeded in polycarbonate membrane inserts in 24 well plates (Cell Biolabs, USA) in serum free media and left to invade toward serum containing culture media for 24 hours. The bottoms of the inserts were stained with crystal violet. Images were taken with a Nikon camera microscope at 20X magnification. For quantification, invasive cells were dissociated and absorbances were measured at 575 nm.

Pure DCIS is a benign breast tumour with non-invasive phenotype (Gorringe and Fox, 2017). To study MCF10-DCIS as a representative in-vitro model for DCIS, we compared MCF10-DCIS invasion ability to invasive MDA-MB-231. MCF-10A was used as a negative control (Figure 4-5).

As expected, MCF10-DCIS has a very minimal invasion ability comparable to that of the normal breast cell line MCF-10A (Figure 4-5). Thus, it is a suitable model to study the molecular and epigenetic regulations in DCIS.

4.3.2.2 Generation of XRCC1 CRISPR knock–out

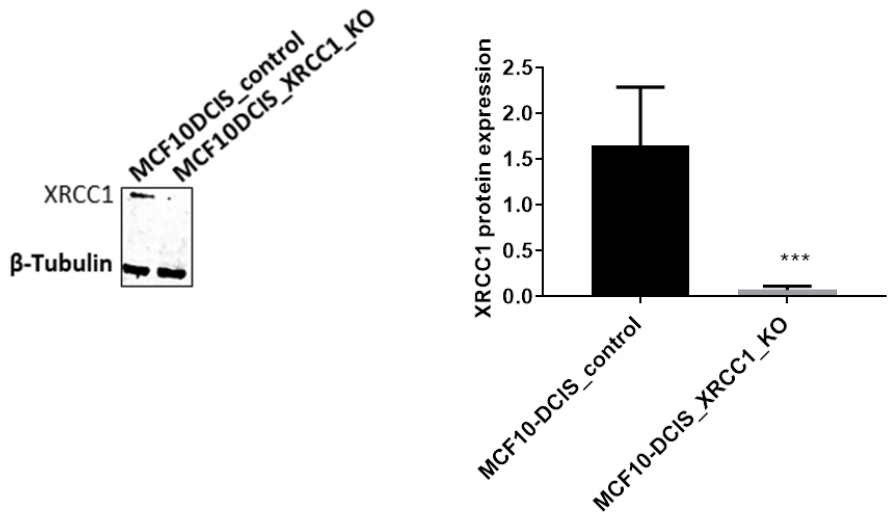


Figure 4-6: Western blot for XRCC1 CRISPR _KO.
Quantification of XRCC1 protein levels relative to β-tubulin in MCF10-DCIS_XRCC1_KO.

Increased mutational load in DCIS is known to be a key player in disease recurrence and invasiveness (Petridis *et al.*, 2016). To study the effect of long-term low expression of XRCC1 in DCIS, we generated XRCC1_KO using CRISPR – cas9 construct as described in the Methodology section. The desired clones were selected in puromycin antibiotic (10µg/ml) (Figure 4-6).

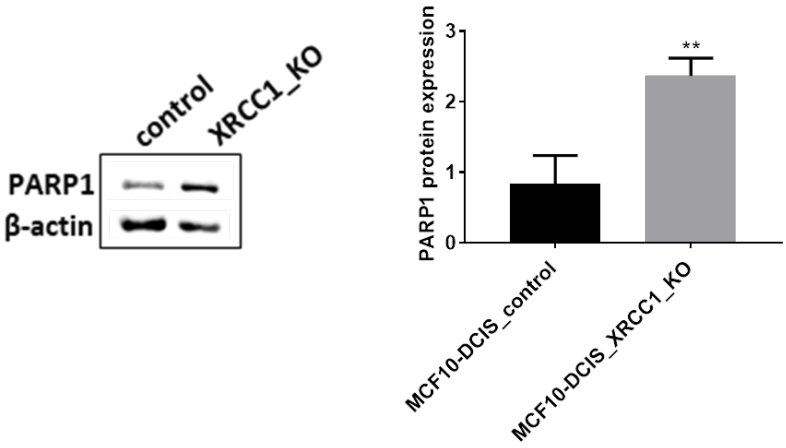


Figure 4-7: PARP1 expression in MCF10-DCIS(XRCC1_KO).
Western blot and protein quantification for PARP1 protein expression in MCF10-DCIS control and MCF10-DCIS _XRCC1_KO. β-actin is used as a loading control.

PARP1 interacts with XRCC1 during the base excision repair pathway. XRCC1 mutations are known to hyper-activate PARP1 (Hoch *et al.*, 2017). We observed previously an increase in PARP1 levels in the XRCC1 deficient cell lines MDA-MB-157 and MDA-MB-231 (XRCC1_KO) (Chapter 3). We hypothesised that XRCC1_KO in MCF10-DCIS could lead to an increase in PARP1 levels. We observed an increase in PARP1 levels in MCF10-DCIS upon XRCC1 knock-out (Figure 4-7). Thus, we anticipated that these cells could be sensitive to Olaparib.

4.3.2.3 MCF10-DCIS_XRCC1_KO is sensitive to Olaparib

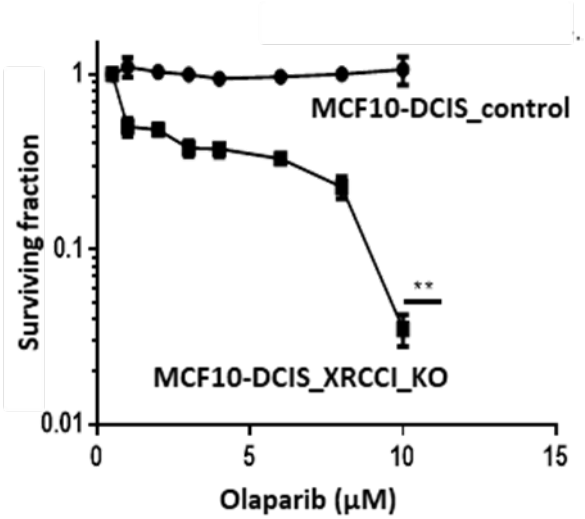


Figure 4-8: Olaparib sensitivity in MCF10-DCIS(XRCC1_KO).
Clonogenics survival assay for MCF10-DCIS (control) and MCF10-DCIS (XRCC1_KO) with different doses of Olaparib.

We tested MCF10-DCIS (control) and MCF10-DCIS (XRCC1_KO) sensitivity to Olaparib in a clonogenic survival assay. MCF10-DCIS (XRCC1_KO) was significantly sensitive to Olaparib which reduced their colony formation ability in comparison to the control cells (Figure 4-8).

4.3.2.4 Functional studies for Olaparib sensitivity in MCF10-DCIS (XRCC1_KO)

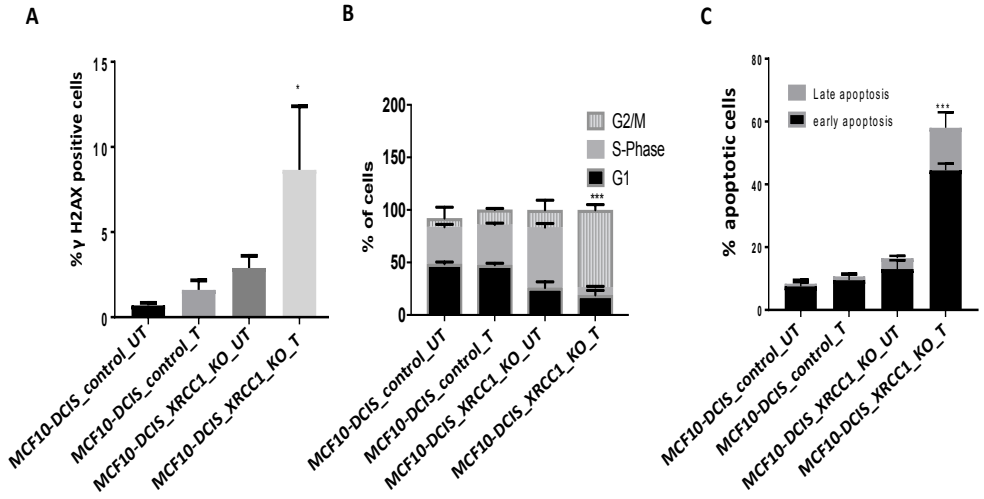


Figure 4-9: Functional studies for Olaparib in MCF10-DCIS (XRCC1_KO). (A) γH2AX quantification by flow cytometry. (B) Cell cycle analysis by flow cytometry. (C) Annexin V analysis by flow cytometry. $2x10^5$ cells of MCF10-DCIS control or XRCC1_KO were plated overnight. The following day cells were treated with 10μM Olaparib for 24 hours. After 24 hours cells were collected by trypsinization and washed with ice cold PBS. For cell cycle and γH2AX analysis, cells were fixed for at least 30 mins before following the PI/ γH2AX staining protocol. For annexinV analysis, cells were resuspended in annexin V binding buffer and stained for flow cytometry as described in the Methodology section.

Olaparib treatment leads to significant cell cycle arrest at G2/M in MCF10-DCIS(XRCC1_KO). We also observed an increase in DNA damage in the XRCC1_KO upon Olaparib treatment. Cell cycle arrest and DNA damage led to apoptosis as confirmed by annexinV apoptosis analysis (Figure 4-9).

4.3.2.5 Loss of XRCC1 expression affected the phenotype of MCF10-DCIS

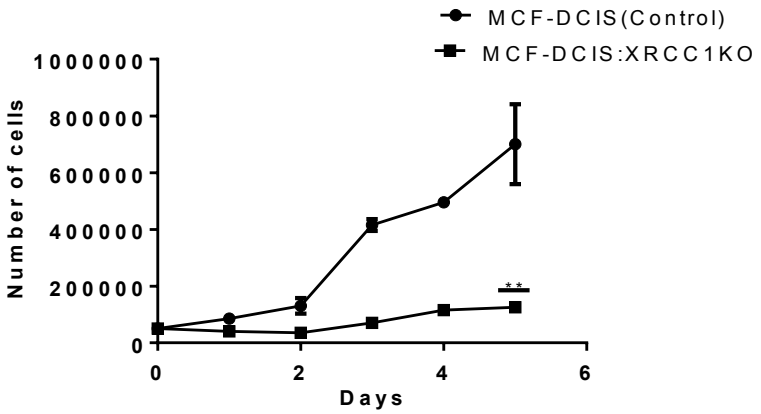


Figure 4-10: Cell proliferation assay for MCF10-DCIS control and XRCC1_KO.

MCF10-DCIS control and XRCC1_KO cells were plated at $2x10^5$ cells density in 6-well plates overnight. Each day cells were trypsinised and counted in duplicates and averages were taken.

We observed in the clinical data that the loss of XRCC1 expression in DCIS was linked to higher grade disease and recurrence. Therefore, we hypothesised that stable knock-out of XRCC1 in MCF10-DCIS could lead to changes in proliferation and invasion ability of those cells.

We assessed the effect of XRCC1 knock-out on MCF10-DCIS cell proliferation. MCF1- DCIS_XRCC1_KO exhibited a higher proliferation rate and was significantly increased in number than the control cell lines (Figure 4-10).

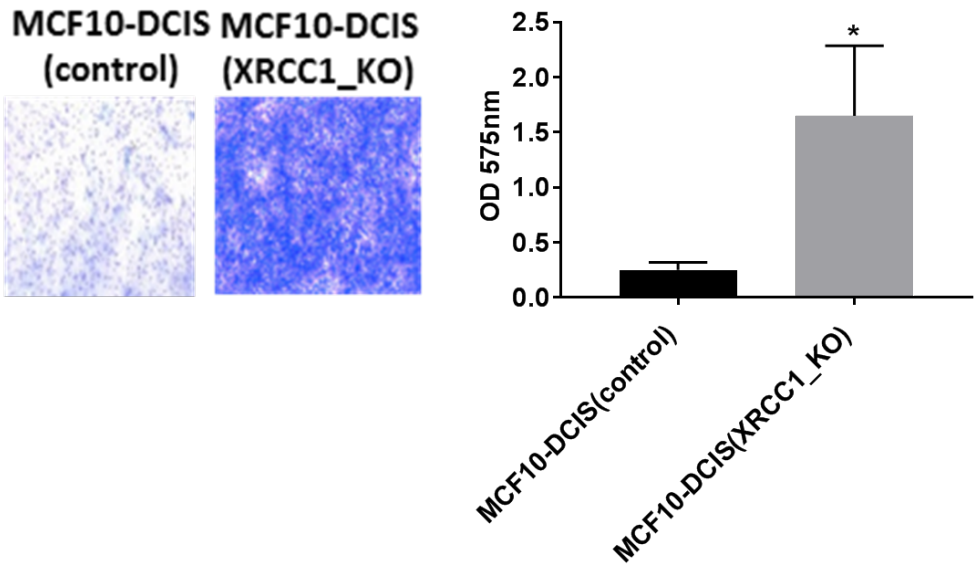


Figure 4-11: Representative images of Invasion assay in MCF10-DCIS control and XRCC1_KO.
Cells were seeded in polycarbonate membrane inserts in 24 well plates (Cell Biolabs, USA) in serum free media and left to invade toward serum containing culture media for 24 hours. The bottoms of the inserts were stained with crystal violet. Images were taken with a Nikon camera microscope at 20X magnification. For quantification, invasive cells were dissociated and absorbances were measured at 575 nm

We evaluated the invasion ability of MCF10-DCIS (XRCC1_KO) in comparison to their controls. Interestingly we found that MCF10-DCIS (XRCC1_KO) acquired an invasive ability that is not present in the control MCF10-DCIS (Figure 4-11).

4.3.2.6 Evaluation of epithelial to mesenchymal phenotype in MCF10-DCIS (XRCC1_KO)

Recent studies have linked the EMT drivers like E-cadherin, N-cadherin, Snail, Vimentin, β-catenin and others to the progression of DCIS to invasive forms of breast cancer (Choi *et al.*, 2013). Therefore, we investigated whether the loss of XRCC1 in MCF10-DCIS enhanced EMT like phenotype in MCF10-DCIS (XRCC1_KO).

We used the Qiagen RT2 Profiler PCR array assay to test the changes in expression of EMT related genes between MCF10-DCIS and MCF10-DCIS (XRCC1_KO). The RT2 profiler is a high throughput assay that can detect the expression of 84 pathway specific mediator genes concurrently. The assay comes in a 96-well plate format; each well is pre-coated with the specific primer. In addition to the 84 EMT specific genes, there are 5 housekeeper genes for data normalisation as well as several quality control measures. The genomic DNA control (GDC) wells assist with the detection of non-transcribed genomic DNA within the isolated mRNA. The positive PCR control (PPC) specifically detects non-transcribed genomic DNA contamination with a high level of sensitivity. The reverse-transcription control (RTC) for determination of the efficacy of the reverse transcription reaction was performed earlier using the RT2 first strand kit (Table 3).

Briefly, $3X10^6$ cells of MCF10-DCIS control and MCF10-DCIS (XRCC1_KO) were collected by trypsinisation. Cells were washed with ice cold PBS and lysised in 350µl of RLT buffer and then the protocol for the Qiagen RNAeasy mini kit (catalogue no. 74104) was followed as per the supplier protocol for RNA purification. The purity and the concentration of the extracted RNA were measured in the nanodrop 2000 (Thermofisher Scientific, UK). We used 0.5µg of RNA to convert to cDNA using the RT2 first strand kit as per the supplier provided protocol. The prepared cDNA was mixed with syber green master mix and nuclease free water and distributed on the EMT RT2 profiler array plates (catalogue no. PAHS-090Z). PCR was done in applied biosciences (ABL-7500 fast block) PCR thermal cycler.

Table 4-3: List of EMT PCR array gene layout.

Position	Unigene	Refseq	Symbol	Description
A01	Hs.502756	NM_024060	AHNAK	AHNAK nucleoprotein
A02	Hs.525622	NM_005163	AKT1	V-akt murine thymoma viral oncogene homolog 1
A03	Hs.1274	NM_006129	BMP1	Bone morphogenetic protein 1
A04	Hs.73853	NM_001200	BMP2	Bone morphogenetic protein 2
A05	Hs.473163	NM_001719	BMP7	Bone morphogenetic protein 7
A06	Hs.490203	NM_004342	CALD1	Caldesmon 1
A07	Hs.731383	NM_018584	CAMK2N1	Calcium/calmodulin-dependent protein kinase II inhibitor 1
A08	Hs.212332	NM_001233	CAV2	Caveolin 2
A09	Hs.461086	NM_004360	CDH1	Cadherin 1, type 1, E-cadherin (epithelial)
A10	Hs.464829	NM_001792	CDH2	Cadherin 2, type 1, N-cadherin (neuronal)
A11	Hs.489142	NM_000089	COL1A2	Collagen, type I, alpha 2
A12	Hs.443625	NM_000090	COL3A1	Collagen, type III, alpha 1
B01	Hs.445827	NM_000393	COL5A2	Collagen, type V, alpha 2
B02	Hs.712929	NM_001904	CTNNB1	Catenin (cadherin-associated protein), beta 1, 88kDa
B03	Hs.95612	NM_004949	DSC2	Desmocollin 2

B04	Hs.519873	NM_004415	DSP	Desmoplakin
B05	Hs.488293	NM_005228	EGFR	Epidermal growth factor receptor
B06	Hs.118681	NM_001982	ERBB3	V-erb-b2 erythroblastic leukemia viral oncogene homolog 3 (avian)
B07	Hs.744830	NM_000125	ESR1	Estrogen receptor 1
B08	Hs.517293	NM_016946	F11R	F11 receptor
B09	Hs.1690	NM_005130	FGFBP1	Fibroblast growth factor binding protein 1
B10	Hs.203717	NM_002026	FN1	Fibronectin 1
B11	Hs.436448	NM_005251	FOXC2	Forkhead box C2 (MFH-1, mesenchyme forkhead 1)
B12	Hs.173859	NM_003507	FZD7	Frizzled family receptor 7
C01	Hs.83381	NM_004126	GNG11	Guanine nucleotide binding protein (G protein), gamma 11
C02	Hs.440438	NM_173849	GSC	Goosecoid homeobox
C03	Hs.445733	NM_002093	GSK3B	Glycogen synthase kinase 3 beta
C04	Hs.462998	NM_001552	IGFBP4	Insulin-like growth factor binding protein 4
C05	Hs.81134	NM_000577	IL1RN	Interleukin 1 receptor antagonist
C06	Hs.706355	NM_004517	ILK	Integrin-linked kinase

C07	Hs.505654	NM_002205	ITGA5	Integrin, alpha 5 (fibronectin receptor, alpha polypeptide)
C08	Hs.436873	NM_002210	ITGAV	Integrin, alpha V (vitronectin receptor, alpha polypeptide, antigen CD51)
C09	Hs.643813	NM_002211	ITGB1	Integrin, beta 1 (fibronectin receptor, beta polypeptide, antigen CD29 includes MDF2, MSK12)
C10	Hs.224012	NM_000214	JAG1	Jagged 1
C11	Hs.654380	NM_000526	KRT14	Keratin 14
C12	Hs.654568	NM_002276	KRT19	Keratin 19
D01	Hs.411501	NM_005556	KRT7	Keratin 7
D02	Hs.335079	NM_005909	MAP1B	Microtubule-associated protein 1B
D03	Hs.513617	NM_004530	MMP2	Matrix metallopeptidase 2 (gelatinase A, 72kDa gelatinase, 72kDa type IV collagenase)
D04	Hs.375129	NM_002422	MMP3	Matrix metallopeptidase 3 (stromelysin 1, progelatinase)
D05	Hs.297413	NM_004994	MMP9	Matrix metallopeptidase 9 (gelatinase B, 92kDa gelatinase, 92kDa type IV collagenase)
D06	Hs.713679	NM_002444	MSN	Moesin
D07	Hs.517973	NM_002447	MST1R	Macrophage stimulating 1 receptor (c-met-related tyrosine kinase)

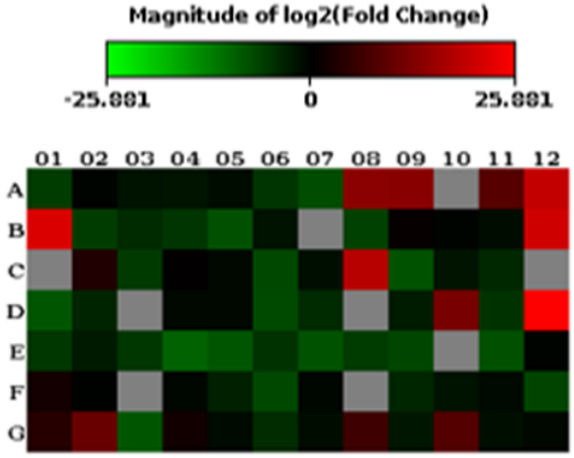
D08	Hs.370414	NM_018055	NODAL	Nodal homolog (mouse)
D09	Hs.495473	NM_017617	NOTCH1	Notch 1
D10	Hs.533657	NM_015901	NUDT13	Nudix (nucleoside diphosphate linked moiety X)-type motif 13
D11	Hs.592605	NM_002538	OCLN	Occludin
D12	Hs.509067	NM_002609	PDGFRB	Platelet-derived growth factor receptor, beta polypeptide
E01	Hs.170473	NM_016445	PLEK2	Pleckstrin 2
E02	Hs.570455	NM_015704	DESI1	PPPDE peptidase domain containing 2
E03	Hs.395482	NM_005607	PTK2	PTK2 protein tyrosine kinase 2
E04	Hs.227777	NM_003463	PTP4A1	Protein tyrosine phosphatase type IVA, member 1
E05	Hs.413812	NM_006908	RAC1	Ras-related C3 botulinum toxin substrate 1 (rho family, small GTP binding protein Rac1)
E06	Hs.78944	NM_002923	RGS2	Regulator of G-protein signalling 2, 24kDa
E07	Hs.414795	NM_000602	SERPINE1	Serpin peptidase inhibitor, clade E (nexin, plasminogen activator inhibitor type 1), member 1
E08	Hs.652307	NM_003616	GEMIN2	Survival of motor neuron protein interacting protein 1
E09	Hs.12253	NM_005901	SMAD2	SMAD family member 2
E10	Hs.48029	NM_005985	SNAI1	Snail homolog 1 (Drosophila)

E11	Hs.360174	NM_003068	SNAI2	Snail homolog 2 (Drosophila)
E12	Hs.673548	NM_178310	SNAI3	Snail homolog 3 (Drosophila)
F01	Hs.376984	NM_006941	SOX10	SRY (sex determining region Y)-box 10
F02	Hs.111779	NM_003118	SPARC	Secreted protein, acidic, cysteine-rich (osteonectin)
F03	Hs.313	NM_000582	SPP1	Secreted phosphoprotein 1
F04	Hs.463059	NM_003150	STAT3	Signal transducer and activator of transcription 3 (acute-phase response factor)
F05	Hs.61635	NM_012449	STEAP1	Six transmembrane epithelial antigen of the prostate 1
F06	Hs.371282	NM_003200	TCF3	Transcription factor 3 (E2A immunoglobulin enhancer binding factors E12/E47)
F07	Hs.742885	NM_003199	TCF4	Transcription factor 4
F08	Hs.438231	NM_006528	TFPI2	Tissue factor pathway inhibitor 2
F09	Hs.645227	NM_000660	TGFB1	Transforming growth factor, beta 1
F10	Hs.133379	NM_003238	TGFB2	Transforming growth factor, beta 2
F11	Hs.713281	NM_003239	TGFB3	Transforming growth factor, beta 3
F12	Hs.522632	NM_003254	TIMP1	TIMP metallopeptidase inhibitor 1
G01	Hs.598100	NM_003692	TMEFF1	Transmembrane protein with EGF-like and two follistatin-like domains 1

G02	Hs.118552	NM_178031	TMEM132A	Transmembrane protein 132A
G03	Hs.364544	NM_014399	TSPAN13	Tetraspanin 13
G04	Hs.66744	NM_000474	TWIST1	Twist homolog 1 (Drosophila)
G05	Hs.643801	NM_004385	VCAN	Versican
G06	Hs.455493	NM_003380	VIM	Vimentin
G07	Hs.459790	NM_033305	VPS13A	Vacuolar protein sorting 13 homolog A (S. cerevisiae)
G08	Hs.108219	NM_004626	WNT11	Wingless-type MMTV integration site family, member 11
G09	Hs.643085	NM_003392	WNT5A	Wingless-type MMTV integration site family, member 5A
G10	Hs.306051	NM_032642	WNT5B	Wingless-type MMTV integration site family, member 5B
G11	Hs.124503	NM_030751	ZEB1	Zinc finger E-box binding homeobox 1
G12	Hs.34871	NM_014795	ZEB2	Zinc finger E-box binding homeobox 2
H01	Hs.520640	NM_001101	ACTB	Actin, beta
H02	Hs.534255	NM_004048	B2M	Beta-2-microglobulin
H03	Hs.592355	NM_002046	GAPDH	Glyceraldehyde-3-phosphate dehydrogenase
H04	Hs.4127	NM_000194	HPRT1	Hypoxanthine

	07			phosphoribosyltransferase 1
H05	Hs.546285	NM_001002	RPLP0	Ribosomal protein, large, P0
H06	N/A	SA_00105	HGDC	Human Genomic DNA Contamination
H07	N/A	SA_00104	RTC	Reverse Transcription Control
H08	N/A	SA_00104	RTC	Reverse Transcription Control
H09	N/A	SA_00104	RTC	Reverse Transcription Control
H10	N/A	SA_00103	PPC	Positive PCR Control
H11	N/A	SA_00103	PPC	Positive PCR Control
H12	N/A	SA_00103	PPC	Positive PCR Control

We identified a differential gene expression in key EMT regulating genes including collagenases *COL1A2, COL3A1, COL5A2* as well as the inhibitors of the canonical WNT pathway WNT11 and WNT5B (Figure 4-12). These changes in gene expression suggest a shift in epithelial to mesenchymal transition phenotype in MCF10-DCIS(XRCC1_KO).



Position	Upregulated Gene
A8	*CAV2*
A9	*CDH1*
A11	*COL1A2*
A12	*COL3A1*
B1	*COL5A2*
B12	*FZD7*
C8	*ITGAV*
D10	*NUDT13*
D12	*PDGFRB*
G2	*TMEM132A*
G8	*WNT11*
G10	*WNT5B*

Figure 4-12: RT2 profiler analysis for EMT in MCF10-DCIS control and XRCC1_KO. Analysis of RT2-PCR profiler was performed in Qiagen website. Normalisation against *GADPH* housekeeper expression was performed. Heat map illustrating up-regulated and down-regulated genes in fold change in MCF10-DCIS (XRCC1_KO) with regard to MCF10-DCIS control cells. The top up-regulated genes are listed here.

4.3.2.7 Morphology of MCF10-DCIS(XRCC1_KO)

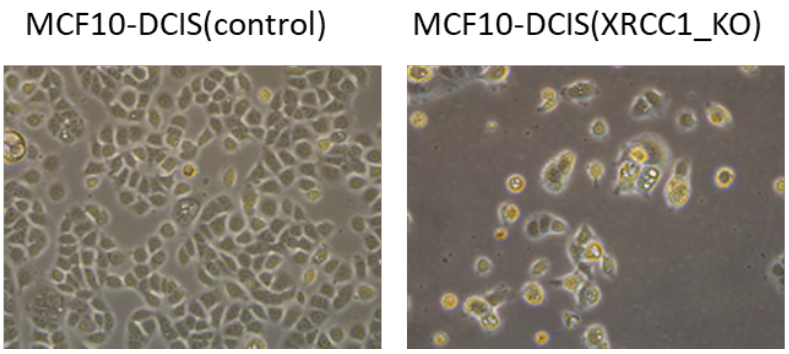


Figure 4-13: Morphology of MCF10-DCIS (control) and MCF10-DCIS (XRCC1_KO). Images were taken using a Nikon microscope camera (20X) objective magnification lens.

Epithelial to mesenchymal transition is associated with many changes in cellular behaviour as well as other morphological changes. Change in morphology from cuboidal epithelial structure into more elongated mesenchymal shaped cells is a hallmark for EMT. That could be attributed to the increase in expression of matrix metalloproteinases (Nelson *et al.*, 2008) and collagenases which allow tumour metastasis and progression (Brinckerhoff, Rutter and Benbow, 2000). We observed changes in MCF10-DCIS (XRCC1_KO) morphology after a few passages for the cells. MCF10-DCIS (XRCC1_KO) lost their cuboidal shape and started to have a more elongated morphology (Figure 4-13).

4.3.2.8 Olaparib as a chemo preventative in MCF10-DCIS(XRCC1_KO) 3D spheres

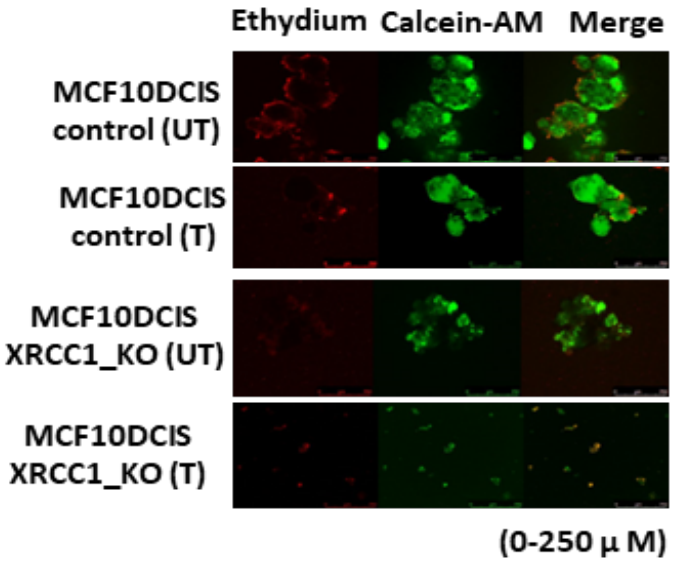


Figure 4-14: Representative photomicrographic images of 3D spheroids. MCF10-DCIS control and XRCC1_KO treated with Olaparib (10µM) from day0. After 14 days the cells were fixed with formaldehyde 3.7% and stained with 2µM calcein AM and 1.5µM ethidium homodimer-1. Imaging was carried out using a Leica SP2 confocal laser scanning microscope.

We observed significant sensitivity to Olaparib in MCF10-DCIS (XRCC1_KO) in the 2D model as demonstrated in the clonogenic and annexinV apoptosis assays. Therefore, we attempted to test the theory that Olaparib could be a potential chemo preventative drug for XRCC1 deficient DCIS. We seeded the MCF10-DCIS control and XRCC1 in tumour sphere medium in ultra-low attachment 6-well plates as described before in the Methods section. Olaparib (10µM) was added from day 0 to both cell lines and refreshed every 3 days. The ability of both cell lines to form spheres was assessed after 14 days. Interestingly, MCF10-DCIS (XRCC1_KO) cells were not able to form any spheres in the presence of Olaparib while MCF10-DCIS (control) retained spheroid forming capacity (Figure 4-14).

4.4 Discussion

DNA instability is a key contributor to cancer development (Yao and Dai, 2014). Previous reports have suggested that there is a possible link between DNA instability and DCIS progression to invasive breast cancers (Heaphy *et al.*, 2009; Pan *et al.*, 2016). Curtis et al. showed an increase in the levels of APE1 in DCIS and IBC compared to normal mammary tissue. Additionally, the same study showed that the loss of nucleoside diphosphate kinase 1 (NM23-H1) and methylpurine DNA glycosylase (MPG) expression is more profound in DCIS and IBC. Both proteins have roles in DNA repair. However, their study used a small cohort of 60 human mammary tissues (Curtis, Thorngren and Nardulli, 2010). Another earlier study linked microsatellite instability to DCIS (Adem *et al.*, 2003). However, the mechanism by which DNA repair defects contribute to DCIS progression is yet to be defined. In our study, we investigated XRCC1 expression in a fairly sizable cohort of DCIS (776 cases) as well as 50 normal breast tissues. Low XRCC1 was associated with high grade DCIS, comedo necrosis and disease local recurrence. Importantly, our analysis shows that higher levels of XRCC1 were expressed in normal breast tissues while that tends to decrease in DCIS and invasive breast cancers. Together, these results suggest a role for XRCC1 in breast cancer progression. XRCC1 plays key roles in BER, single strand break repair (Friedberg, 2003) and nucleotide excision repair (Moser *et al.*, 2007). Here, we also reveal that the loss of XRCC1 is an early event in breast cancer pathogenesis.

The process of progression of DCIS to invasive breast cancers is believed to imply several molecular mechanisms however the exact theory is still not totally

understood (S. Y. Kim *et al.*, 2015). Analysis of biomarkers and genetic signature differences between pure DCIS and invasive DCIS is an important aspect for understanding breast cancer aggressiveness and prognosis (Lee, Kim and Koo, 2018). We investigated invasion phenotype in MCF10-DCIS. Initially, we compared MCF10-DCIS, normal breast tissue MCF-10A as well as triple negative cell line MDA-MB-231. We were able to show a non-invasive phenotype in MCF10-DCIS comparable to that of the normal mammary tissue MCF10A cell line. Therefore, it was a suitable model for studying EMT changes that develop in invasive DCIS (IDC). Interestingly, XRCC1 knock out in MCF10-DCIS (XRCC1_KO) stimulated invasion in those cells, which indicates that low DNA repair capacity is an early mechanism in the development of IDC. Previous studies acknowledged changes in some transcription factors regulating mammary epithelial cell differentiation as an early precursor to invasiveness (Scribner, Behbod and Porter, 2013). Among those, GATA3, ELF5 (Shan *et al.*, 2014), NOTCH (Stylianou, Clarke and Brennan, 2006) and C/EBPβ (Grimm and Rosen, 2003) were recognized. However we did not find a significant variation in those markers in MCF10-DCIS (XRCC1_KO) cells. Of note here is that GATA3, in particular, is an important transcription factor with roles in DNA repair. It interacts with PARP1 and is subject to its parylation (Shan *et al.*, 2014). Additionally, it has functions in the homologous recombination pathway through BRCA1 and the endonuclease RBBP8 (Zhang *et al.*, 2017). These data suggest an indirect role for DNA repair impairment in DCIS progression. Interestingly, Shan *et al.* proved through immune purification of GATA3 that it physically interacts with PARP1, XRCC1, XRCC5 and Ligase (Shan *et al.*, 2014).

These results again provide compelling evidence to the role of DNA repair in breast cancer cell proliferation.

We and others (S. Y. Kim *et al.*, 2015; Pan *et al.*, 2016) are interested in defining biomarkers for DCIS progression to invasive breast cancers and thereby identifying new therapeutic strategies for treating those patients with high risk of progression. Using the high throughput screening RT2 PCR EMT profiler we screened MCF10-DCIS control and MCF10-DCIS (XRCC1_KO) for changes in gene expression that could be regulating the acquired invasive phenotype in MCF10-DCIS (XRCC1_KO).

The collagen family is the main component of the extracellular matrix (Zhang *et al.*, 2017). Changes in collagen levels and collagenases (matrix metalloproteases) have been reported during cellular transformation in EMT (Medici and Nawshad, 2010). Collagen I is the most prominent type in the collagen family. Its role in EMT has been defined in breast, pancreas and lung tumours. It interacts with α2β1 integrin through integrin- binding motifs on its helix structure (Savagner, 2005). Those interactions trigger a downstream signalling cascade. In MCF10-DCIS (XRCC1_KO) we identified significant up-regulation in *COL1A2, COL3A1* and *COL5A2* which indicates a direct role of collagens in MCF10-DCIS (XRCC1_KO) invasion.

Additionally, we found upregulation of the platelet derived growth factor receptor B (*PDGFRB*) in MCF10-DCIS (XRCC1_KO) to be associated with the EMT phenotype acquired in those cells. PDGFRB has been identified before to be a vital element in tumour vascularization and poor outcomes in triple negative breast cancers (D'ippolito *et al.*, 2016). It has already been identified as a therapeutic target,

although clinical trials of PDGFRB inhibitors in combination with tyrosine kinase inhibitors for endocrine responsive breast cancers did not show significant benefit (Criscitiello *et al.*, 2014). In DCIS there are few studies that have compared PDGFRB expression in DCIS and invasive breast cancer (S. Y. Kim *et al.*, 2015; Park, Jung and Koo, 2016; Lee, Kim and Koo, 2018). Park *et al.* showed upregulation of PDGFRα in stromal cells of invasive carcinoma while the elevation of PDGFRB levels was evident in stromal cells of invasive lobular carcinoma tumour micro arrays (Park, Jung and Koo, 2016).

The progression of DCIS to IDC is assumed to be an important facet of breast cancer aggressiveness and poor prognosis (Heaphy *et al.*, 2009). However, the lack of biomarkers for DCIS progression hampers personalization of DCIS therapy and it remains an area of unmet need. Therefore, identification of progression –specific pathways is crucial for the comprehensive treatment of DCIS lesions.

Previously, we investigated Olaparib (PARP1 inhibitor) in XRCC1 deficient triple negative breast cell lines. We observed high sensitivity and synthetic lethality between XRCC1 and PARP1 inhibitors in breast cancer cells. In this study, we explored whether that phenomenon will be applicable to DCIS. We tested the effect of Olaparib on the MCF10-DCIS control and MCF10-DCIS (XRCC1_KO) in a clonogenic survival assay. Interestingly, MCF10-DCIS (XRCC1_KO) was exquisitely sensitive to Olaparib but not MCF10-DCIS (control) cells. The selective toxicity of Olaparib in MCF10-DCIS (XRCC1_KO) was associated with G2/M cell cycle arrest and the accumulation of double strand breaks and apoptotic cells as confirmed by the flow cytometry experiments. These data open up a new area for PARP inhibitors as chemo preventive drugs for DCIS. Olaparib has been approved for the

treatment of BRCA harbouring mutations ovarian cancers (Underhill, Toulmonde and Bonnefoi, 2011). Other generations of PARP inhibitors are being tested in clinical trials for different tumour types (Lee and Gulley, 2017). Our preliminary study shows that PARP inhibitors could have clinical relevance for DCIS patients. That concept requires further investigation through in-vitro and in-vivo studies not only for Olaparib but also for other potent PARP inhibitors such as Talazoparib and Niraparib to understand the detailed mechanism of the response observed here. Importantly, in the 3D-culture model, Olaparib treatment from day 0 totally abolished the spheroid forming capacity of MCF10-DCIS (XRCC1_KO) but not MCF10-DCIS control. This indicated a potent synthetic lethality between XRCC1 and PARP1 that could have important therapeutic applications in the future. The current chemo preventative strategies available for DCIS include endocrine therapy (Tamoxifen and Raloxifene) (Reimers *et al.*, 2015). However, that line of treatment is not available for a broad sector of DCIS patients and also involves serious toxicity (Vogel *et al.*, 2010). Exploiting DNA repair deficiency as a driver for DCIS progression not only can provide an alternative approach for hormone receptor negative DCIS but can also offer more personalized therapeutic modalities. Thus, we conclude that Olaparib could be a novel chemo preventative approach for XRCC1 deficient DCIS lesions.

5 XRCC1 in Ovarian cancers

5.1 Introduction

Ovarian cancer (OC) is the fifth most common cause of cancer-related death in women worldwide (Luvero, Milani and Ledermann, 2014). Epithelial ovarian cancer is considered the most lethal gynaecological malignancy and most patients are diagnosed at an advanced stage. In the UK it is the sixth most common cancer with 7,400 new diagnosed ovarian cancer cases every year (van Zyl, Tang and Bowden, 2018). The standard treatment available for ovarian cancer is surgery and platinum-based chemotherapy including paclitaxel and carboplatin. Tumours mostly recur after 6 months prior to platinum therapy (Luvero, Milani and Ledermann, 2014). The platinum free interval (PFI) is defined as the interval between the completion of the last platinum treatment and the detection of relapse, whereas (PFI) is considered a key predictor of response to consecutive chemotherapy offered after recurrence. According to (PFI) patients are categorized into two categories: 'platinum sensitive' with a PFI of at least 6 months and 'platinum resistant' with a PFI less than 6 months (Luvero, Milani and Ledermann, 2014). Another Biomarker used is cancer antigen 125 (CA125). CA125 was used by the Gynaecological Cancer Inter Group to define recurrence. An elevation in CA125 after first line chemotherapy indicates recurrence (Gupta and Lis, 2009).

Over the last two decades, progression free survival for patients treated with surgery and chemotherapy have not significantly improved. The progression free survival (PFS) has remained static to about 18 months. That is why targeted molecular therapies for treatment of platinum sensitive recurrent ovarian cancers

have emerged (Gaitskell *et al.*, 2011). Angiogenesis is the rate limiting process in tumour progression. Inhibitors of angiogenesis have shown some activity in ovarian cancers. Clinical trials have been conducted on patients at different ovarian cancer stages (H. Wang *et al.*, 2018). Earlier studies showed that bevacizumab decreased the risk of disease progression as a maintenance therapy (Gaitskell *et al.*, 2011). A recent meta-analysis study included data from 8721 patients and revealed that combining angiogenesis inhibitors with chemotherapy decreased the risk of progression of ovarian cancers. However, their analysis concluded that angiogenesis inhibitors did not have any significant survival benefit to patients (H. Wang *et al.*, 2018). Other extensively researched drugs are PARP inhibitors as a targeted therapy for BRCA mutant ovarian cancers (Luvero, Milani and Ledermann, 2014). PARP inhibitors are the first FDA approved DNA repair targeted therapy for ovarian cancer based on personalised genetic background for the patients (Musella *et al.*, 2018). Currently there are three approved PARP inhibitors for the treatment of ovarian cancers (Ison *et al.*, 2018; Musella *et al.*, 2018). In Europe, Olaparib is standardized as a maintenance treatment in platinum-sensitive, relapsed, BRCA1/2 mutated ovarian cancer after a complete or partial response (CR/PR) to platinum-based chemotherapy. In the US, Olaparib is approved as a fourth-line treatment in BRCA1/2 mutated, advanced ovarian cancer. Other PARP inhibitors like Niraparib are approved as maintenance treatment in platinum-sensitive, relapsed, ovarian cancer after a CR/PR to platinum-based chemotherapy in both Europe and United states. Similarly, Rucaparib is approved in both Europe and the US as a third-line treatment in

BRCA1/2 mutated, platinum sensitive, relapsed high-grade ovarian cancer (Jiang *et al.*, 2019).

However, BRCA1/2 mutations occur in only 17% of patients with higher grade disease, making these personalised therapies available for a limited group of patients. The majority however remain with poor overall survival (van Zyl, Tang and Bowden, 2018).

The identification of a BRCA like signature in ovarian cancer has assisted in predicting a response to PARP inhibitors. Whereas mutations affecting the homologous recombination (HR) pathway generate "BRCAness" like phenotype rendering the tumours sensitive to both Olaparib and platinum. Among the key genes coordinating the (HR) pathway are BRCA1, BRCA2, ATM, BARD1, BRIP1, CHEK1, CHEK2, FAM175A, MRE11A, NBN, PALB2, RAD51C and RAD51D (Jiang *et al.*, 2019). To identify tumours with a defective HR pathway a panel of 60-genes was proposed previously as the BRCAness profile. The BRCAness profile was a reliable predictive marker in platinum response in 8 out of 10 patient derived tumour samples. It also predicted PARP inhibitor sensitivity in 4 tested ovarian cell lines as well as being an independent prognostic factor in a public data set of 70 patients (Konstantinopoulos *et al.*, 2010). Another profiling method for the BRCAness phenotype in tumours is the development of a HRD assay to evaluate BRCA1/2 expression and the genomic scarring within the HR pathway. HRD assay comprises three biomarkers: loss of heterozygosity (LOH), telomeric allelic imbalance (TAI) and large-scale state transitions (LSTs). Also, within the assay tumours are given a score between 0-100 with a cut off 42. Tumours with score ≥

42 are considered with impaired HR pathway, while a score of <42 reflected a functional HR pathway (Jiang *et al.*, 2019).

Taken together, these studies demonstrate the efforts to expand the benefit of PARP inhibitors to BRCA proficient patients through personalized mutational profiling. Our group previously showed that XRCC1 expression is associated with highly aggressive ovarian cancers and platinum resistance (Abdel-Fatah *et al.*, 2013). In this work, we investigated the hypothesis of targeting XRCC1 deficient ovarian cancers with PARP inhibitors for a personalised treatment of ovarian cancer and an expansion of PARP inhibitor benefit to more patients in clinics.

5.2 Methodology

The immunohistochemistry of XRCC1 and PARP1 was performed on the TMAs of 525 epithelial ovarian cancer patients who received treatment in Nottingham University Hospitals between 1997 and 2010. The immunohistochemistry protocol and antibody details are described in the Methods chapter. The evaluation of immune staining was performed by calculation of the H-score (range 0–300). For XRCC1, low/negative nuclear expression was identified by the median cut off ≤ 100. Low/negative nuclear PARP1 staining was defined by the median H score of <80.

Transient knock-down of XRCC1 by siRNA and CRISPR knockout of XRCC1 in A2780 was performed as per the described protocol in the Methods section. The clonogenic survival assay of Olaparib and Talazoparib sensitivity in ovarian cell lines is detailed in the Methods section. Functional studies including cell cycle staining with propidium iodide, γH2AX double strand break analysis and apoptosis detection by annexinV was analysed by flow cytometry. Detailed staining and analysis protocol are provided in the Methods section. Invasion and migration assays for studying EMT in the A2780 control and A2780 (XRCC1_KO) were performed using the cytoselect 24-well cell invasion assay and cytoselect 96-well radius cell migration assay respectively as per the supplier protocol. 3D-Spheroids were grown as per the described protocol and imaging was carried out using a Leica SP2 confocal laser scanning microscope. Data analysis was performed in GraphPad Prism-7 software. Error bars represent standard error of mean between

experiments. P-values are indicated as P-values <0.05 =*, p-value <0.01 =** & p-value <0.001=***.

5.3 Results

5.3.1 Clinical Data

5.3.1.1 XRCC1 expression is correlated with patient survival in ovarian cancers

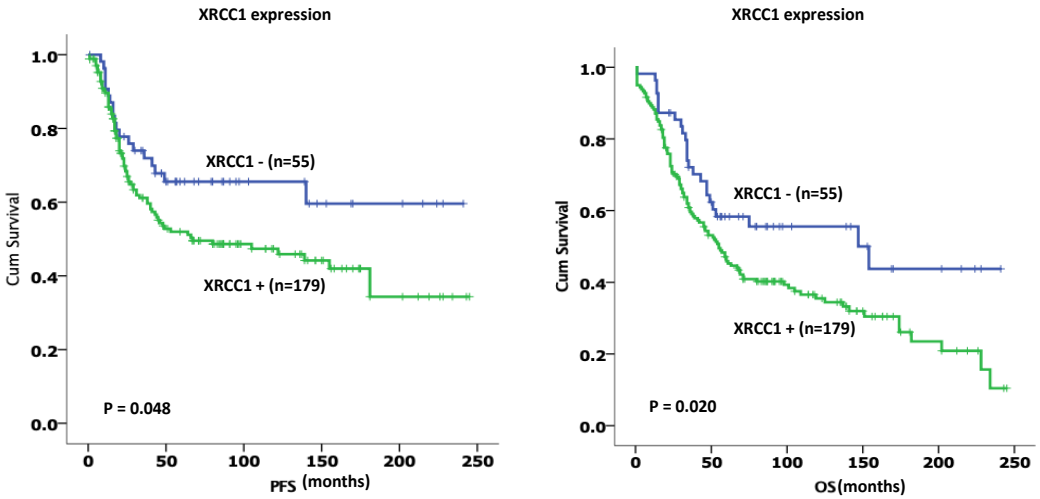


Figure 5-1: Kaplan Meier curve for XRCC1 expression.
The correlation between XRCC1 protein expression and progression free survival (PFS) and ovarian cancer specific survival (OCSS) in the whole cohort.

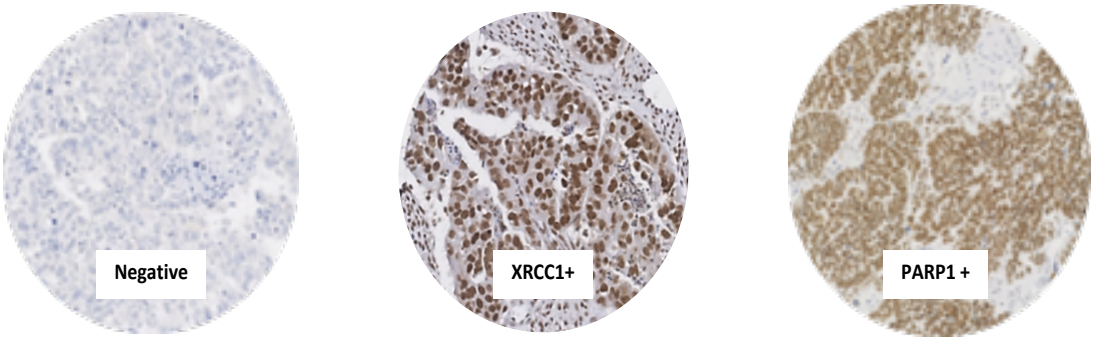


Figure 5-2: Immunohistochemical expression of XRCC1 and PARP1 in ovarian cancers.
Representative images for negative staining, positive XRCC1 nuclear staining and PARP1 positive nuclear staining respectively in ovarian TMAs.

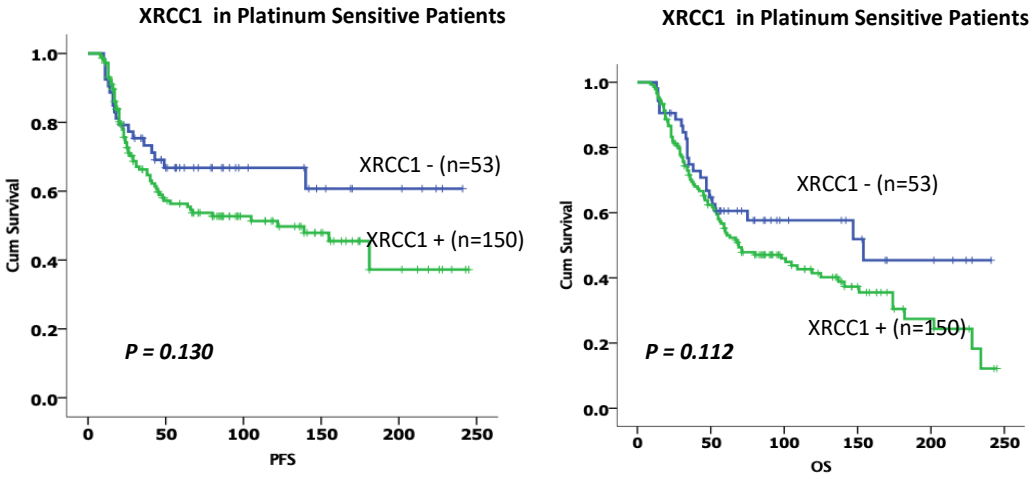


Figure 5-3: Kaplan Meier curve for XRCC1 expression in platinum sensitive patients.
XRCC1 protein expression and PFS and OCSS in the platinum sensitive cohort.

We evaluated XRCC1 and PARP1 expression in a cohort of 525 epithelial ovarian cancers. Immunohistochemical staining of XRCC1 and PARP1 was carried out on tissue microarrays of 525 epithelial ovarian cancer cases treated at Nottingham University Hospitals (NUH) between 1997 and 2010. Tumour staging was done according to the staging system for ovarian cancer of the International Federation of Obstetricians and Gynaecologists (FIGO). Ovarian cancer specific survival (OCSS) was considered from the operation date until the 1st of October 2016 when any remaining survivors were censored. Progression-free survival (PFS) was calculated from the date of the initial surgery to disease progression or from the date of the initial surgery to the last date known to be progression-free for those censored. Patient demographics are summarized in (Table 5-1).

462 cases in total were suitable for analysis of XRCC1 nuclear expression (Figure 5-1). 153/462 (33.1%) tumours were considered low for XRCC1 expression and 309/462 (66.9%) of the TMAs were high in expression. High XRCC1 was associated

with poor PFS survival and OCSS in patient p-values are 0.032 and 0.024 respectively (Figure 5-1). In platinum sensitive patients, high XRCC1 expression was also associated with poor PFS (p=0.130) and poor OCSS (p=0.112), (Figure 5-3). Therefore, XRCC1 expression can be a predictor of patient outcomes in ovarian cancer. Similarly, high XRCC1 was associated with serous cystadenocarcinoma (p <0.0001), higher FIGO stage at diagnosis (p = 0.001), measurable disease before chemotherapy (p= 0.002) and platinum resistance (p = 0.003) (Table 5-2).

Table 5-1: Ovarian cancer patient demographics.

Characteristics	**Number**	**Percentages**
Pathology		
Serous cystadenocarcinoma	290	55.2%
Endometrioid	82	15.6%
Clear cell carcinoma	48	9.1%
Mucinous cystadenocarcinoma	60	11.4%
Others	18	3.4%
Mixed	17	3.2%
Unknown	10	2.1%
Grade		
1	68	12.9%
2	87	16.5%
3	306	58.2%

Unknown	64	12.4%
FIGO Stage		
I	182	34.6%
II	76	14.4%
III	213	40.5%
IV	32	6%
Unknown	22	4.5%
Chemotherapy		
Carboplatin monotherapy	163	31%
Carboplatin + Paclitaxel	177	34%
Other platinum based regimes*	121	23%
No chemotherapy	25	5%
Unknown	39	7%
Platinum sensitivity		
Sensitive	376	71.6%
Resistant	85	16.1%
Unknown	64	11.8%
Relapse status		
Progression-free	238	45.3%
Progressed/relapsed	243	46.2%
Unknown	44	8.3%
Survival status		
Living	199	37.9%

Dead	286	54.4%
Unknown	40	7.6%

*= CAP (Cyclophosphamide, Adriamycin and Cisplatin), ICON5 Trial, SOCTROC Trial, Carboplatin and Endoxan.

Table 5-2: XRCC1 expression and ovarian cancer.

	XRCC1- N(%)	XRCC1+ N(%)	**P- value**
Pathological Type			**<0.0001**
Serous cystadenocarcinoma	66 (24.7)	201 (75.3)	
Mucinous cystadenocarcinoma	23 (47.9)	25 (52.1)	
Endometrioid	30 (41.7)	42 (58.3)	
Clear cell carcinoma	24 (58.5)	17 (41.5)	
Mixed	4 (28.6)	10 (71.4)	
FIGO Stage			**0.001**
I	70 (44.9)	86 (55.1)	
II	18 (26.5)	50 (73.5)	
III	58 (29.7)	137 (70.3)	
IV	5 (16.7)	25 (83.3)	
Tumour Grade			0.105
G1	27 (46.6)	31 (53.4)	
G2	24 (31.6)	52 (68.4)	
G3	90 (32.5)	187 (67.5)	
Measurable Disease pre-*Chemotherapy*			**0.002**

No measurable disease	111 (39.6)	169 (60.4)	
Measurable disease	35 (24.6)	107 (75.4)	
Platinum response			**0.003**
Sensitive	127 (38.6)	202 (61.4)	
Resistant	17 (21.8)	61 (78.2)	

5.3.1.2 PARP1 expression affects ovarian cancer patients' survival in the platinum sensitive cohort.

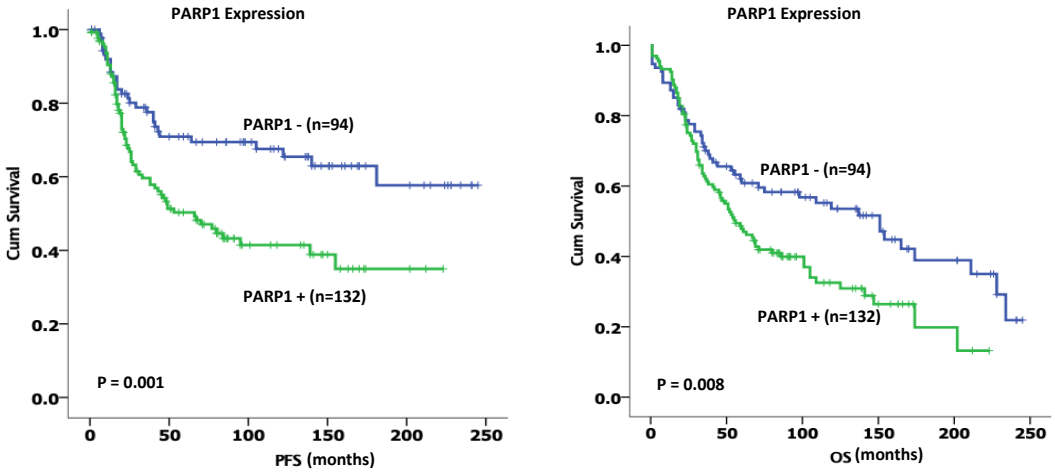


Figure 5-4: Kaplan Meier curve for PARP1 expression.
PARP1 protein expression and PFS and OCSS in the whole cohort.

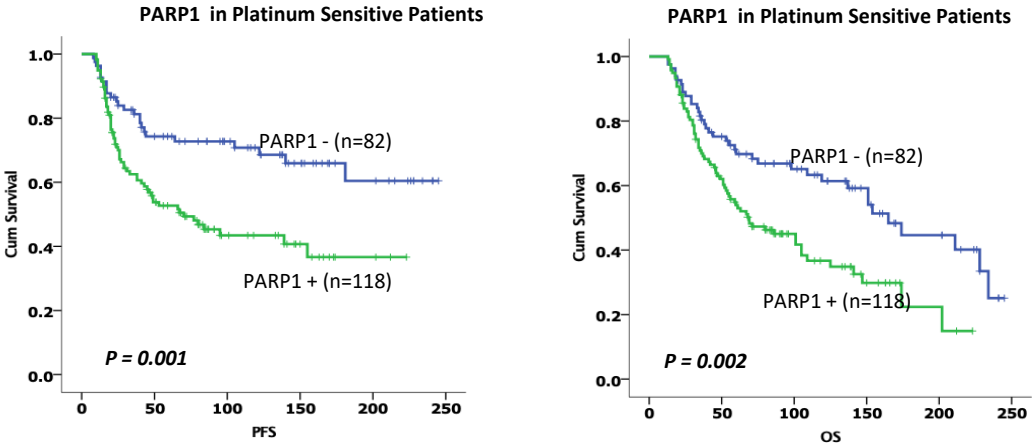


Figure 5-5: Kaplan Meier curve for PARP1 expression in platinum sensitive cohort.
the correlation between PARP1 protein expression and PFS and OS in the platinum sensitive cohort

On the other hand, we investigated PARP1 expression in the same cohort. The number of cases suitable for PARP1 analysis was 424 tumours. 221/424 (52.1%) tumours were high for PARP1 expression and 203/424 (47.9%) of the tumours

were low in expression. High PARP1 expression was associated with poor PFS (p= 0.001) and poor OCSS (p=0.008) in the whole cohort (Figure 5-4). Additionally, high PARP1 expression was associated with low PFS (p=0.001) and poor OCSS (p=0.002) in the platinum sensitive patients (Figure 5-5) whilst in the platinum resistant cohort PARP1 did not significantly affect survival (Figure 5-6). Furthermore, High PARP1 expression was significantly associated with serous cystadenocarcinomas (p <0.00001), higher grade (p = <0.00001), and measurable disease before chemotherapy (p= 0.024) (Table 5-3).

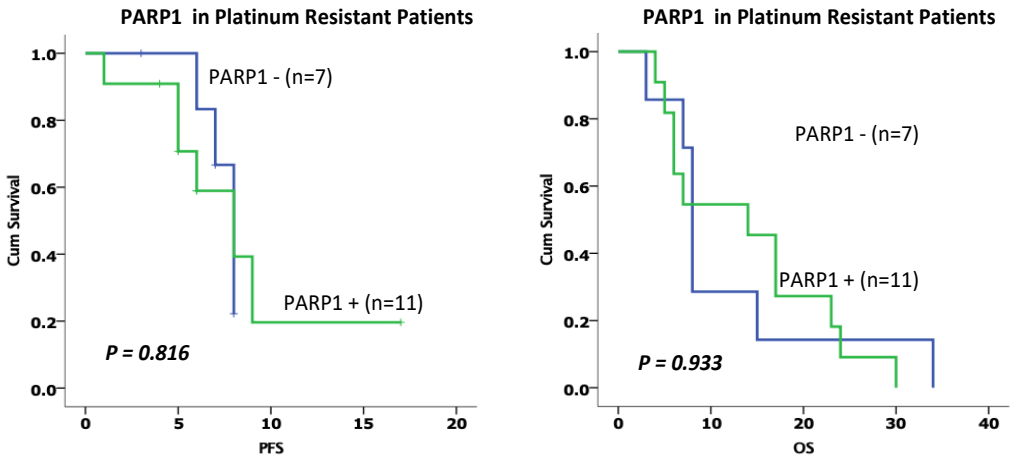


Figure 5-6: Kaplan Meier curve for PARP1 expression in platinum resistant patients.
The correlation between PARP1 protein expression and PFS and OCSS in the platinum resistant cohort.

Table 5-3: PARP1 expression and ovarian cancer.

	PARP1- N(%)	**PARP1+ N(%)**	**P- value**
Pathological Type			
Serous cystadenocarcinoma	84 (35.7)	151 (64.3)	**<0.00001**
Mucinous cystadenocarcinoma	37 (78.7)	10 (21.3)	
Endometrioid	40 (58.0)	29 (42.0)	
Clear cell carcinoma	29 (80.6)	7 (19.4)	
Mixed	3 (21.4)	11 (78.6)	
FIGO Stage			0.443
I	78 (52.3)	71 (47.7)	
II	29 (44.6)	36 (55.4)	
III	74 (43.5)	96 (56.5)	
IV	12 (48.0)	13 (52.0)	
Tumour Grade			**<0.00001**
G1	43 (75.4)	14 (24.6)	
G2	31 (46.3)	36 (53.7)	
G3	104 (41.8)	145 (58.2)	
Measurable Disease pre-chemotherapy			**0.024**
No measurable disease	138 (52.1)	127 (47.9)	
Measurable disease	48 (39.7)	73 (60.3)	

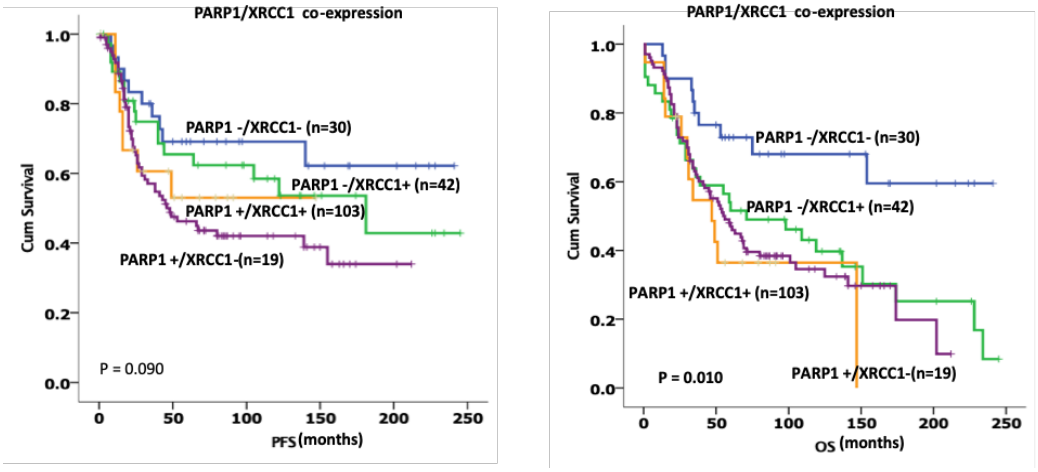


Figure 5-7: Kaplan Meier curve for PARP1 and XRCC1 protein expression. The correlation between PARP1 and XRCC1 co-expression and PFS and OS in ovarian cancers.

Analysis of PARP1/XRCC1 co-expression revealed that tumours with high PARP1/ high XRCC1 have low PFS. Also, high PARP1 /high XRCC1 have a poor OCSS in comparison to PARP1-/XRCC1- tumours (Figure 5-7). High PARP1 and XRCC1 was significantly associated with serous cystadenocarcinoma subtype ($p<0.0001$), high tumour grade ($p=0.002$) and residual disease before chemotherapy ($p=0.004$) (Table 5-4).

Additionally, cox multivariate analysis for XRCC1 and PARP1 showed that platinum sensitivity ($p=0.0001$) and XRCC1 ($p=0.016$) expression were independently associated with PFS, while, platinum sensitivity ($p=0.0001$) and PARP1 expression ($p= 0.023$) influenced OCSS in the studied cohort (Table 5-5).

Table 5-4: XRCC1/PARP1 co-expression in ovarian cancer.

	PARP1-/ XRCC1- N(%)	**PARP1-/ XRCC1+ N(%)**	**PARP1+/ XRCC1 - N(%)**	**PARP1+/ XRCC1 + N(%)**	**P- value**
Pathological Type					***<0.0001***
Serous cystadenocarcinoma	32 (14.3)	45 (20.2)	27 (12.1)	119 (53.4)	
Mucinous cystadenocarcinoma	18 (45.0)	14 (35.0)	1 (2.5)	7 (17.5)	
Endometrioid	21 (34.4)	14 (23.0)	6 (9.8)	20 (32.8)	
Clear cell carcinoma	19 (59.4)	7 (21.9)	1 (3.1)	5 (15.6)	
Mixed	1 (7.7)	2 (15.4)	3 (23.1)	7 (53.8)	
FIGO Stage					0.100
I	46 (34.3)	22 (16.4)	13 (9.7)	53 (39.6)	
II	11 (18.3)	14 (23.3)	7 (11.7)	28 (46.7)	
III	30 (18.9)	40 (25.2)	20 (12.6)	69 (43.4)	
IV	4 (16.7)	7 (29.2)	1 (4.2)	12 (50.0)	
Tumour Grade					***0.002***
G1	22 (44.0)	15 (30.0)	1 (2.0)	12 (24.0)	
G2	15 (24.2)	13 (21.0)	7 (11.3)	27 (43.5)	

G3	48 (20.6)	47 (20.2)	30 (12.9)	108 (46.4)	
Measurable Disease Before Chemotherapy					
No measurable disease	73 (30.5)	47 (19.7)	23 (9.6)	96 (40.2)	***0.004***
Measurable disease	15 (13.0)	30 (26.1)	16 (13.9)	54 (47.0)	

Table 5-5: XRCC1/ PARP1 multivariate analysis.

PFS	Sig.	Exp(B)	95.0% CI for Exp(B)	
			Lower	Upper
Platinum Sensitivity	**0.0001**	13.957	9.572	20.351
XRCC1	**0.016**	1.503	1.078	2.096
PARP1	0.447	1.128	.827	1.539
OCSS				
Platinum Sensitivity	**0.0001**	6.772	4.854	9.448
XRCC1	0.170	1.258	.906	1.748
PARP1	**0.023**	1.421	1.051	1.922

5.3.2 Pre-clinical data

5.3.2.1 XRCC1 SiRNA in ovarian cancer cell lines

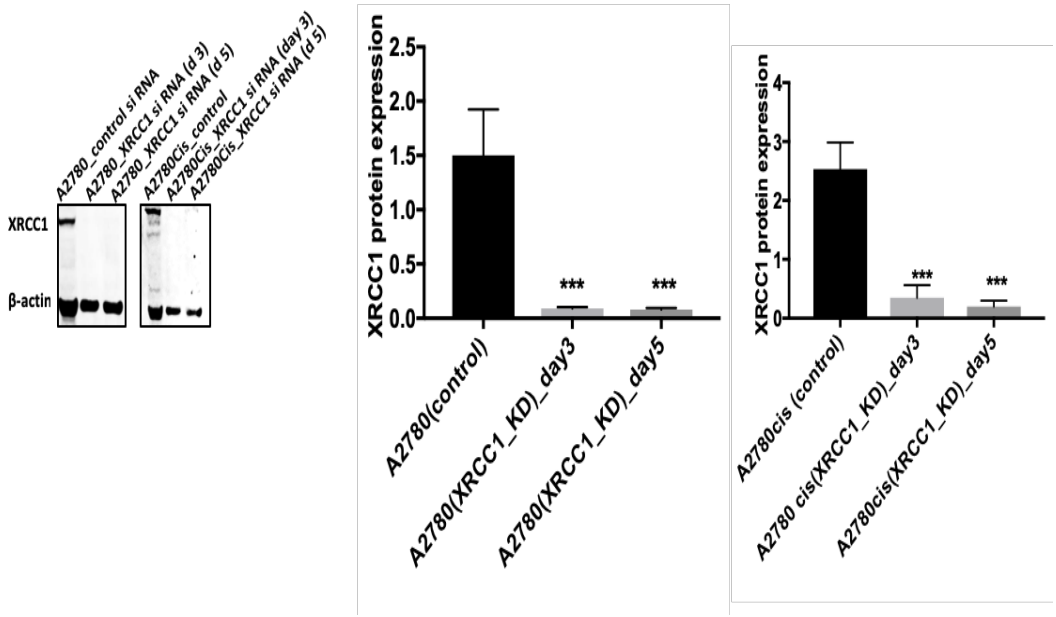


Figure 5-8: XRCC1 SiRNA in ovarian cell lines.
Cells were plated overnight and the next day transfection with XRCC1 siRNA was achieved using Lipofectamine 3000 reagent (Invitrogen, UK) in Opti-mem medium. Cells were incubated with transfection mixture overnight and then the media were changed to fresh media the following day (protocol detailed in the Methods chapter). Lysates were collected for western blot on day 3 and day 5. Quantification of XRCC1 protein levels relative to β-actin (loading control).

To explore further the implication of XRCC1 deficiency in ovarian cancer, we conducted SiRNA studies in ovarian cancer cell lines. A2780 (cisplatin sensitive) and A2780cis cells (cisplatin resistant) were used. XRCC1 siRNA achieved efficient knock down on day 3 and day 5 in the tested cell lines (Figure 5-8).

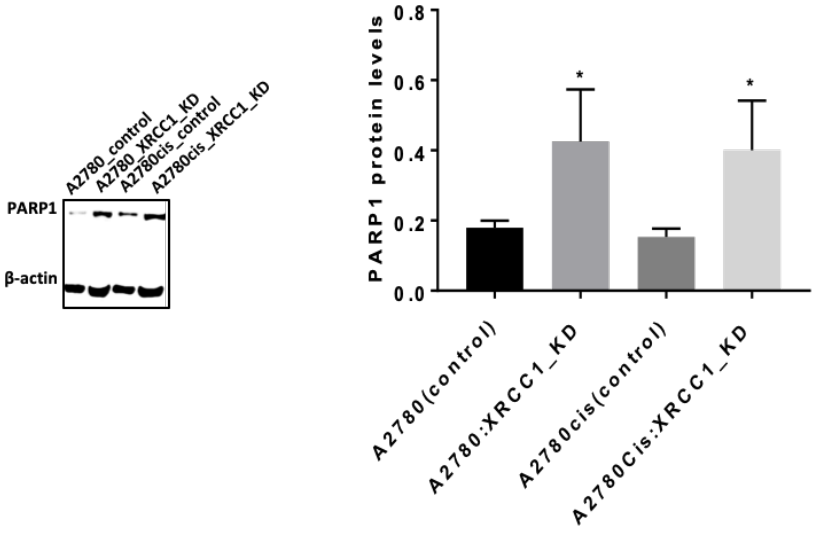


Figure 5-9: PARP1 expression in XRCC1_KD cells.
PARP1 protein levels by western blot in A2780 and A2780cis control and XRCC1_KD on day 3. Quantification of PARP1 protein levels relative to β-actin (loading control).

XRCC1 knock-down cells had induction of PARP1 protein levels in comparison to the control cells as observed in the western blot (Figure 5-9).

5.3.2.2 Olaparib is toxic in XRCC1 deficient cisplatin sensitive ovarian cell lines

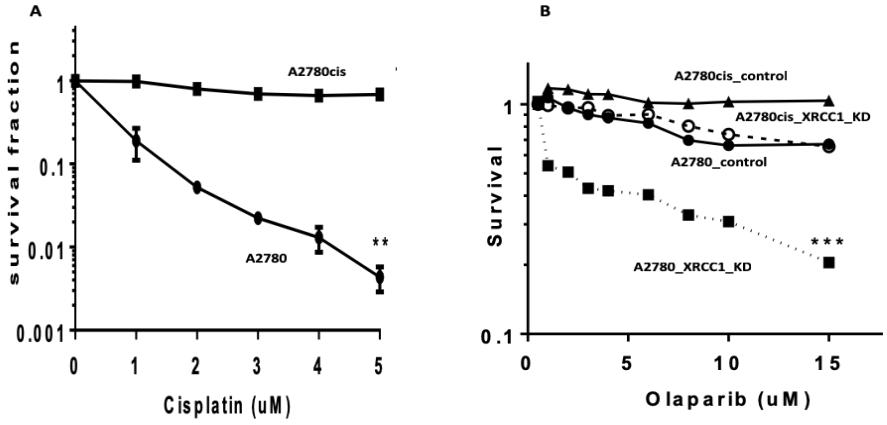


Figure 5-10: Clonogenic survival assay for Cisplatin and Olaparib in ovarian cells. A) Clonogenic survival assay for A2780 and A2780cis in different doses of cisplatin. B) Clonogenic survival assay for A2780, A2780cis controls and XRCC1_KD cells in different doses of Olaparib. Cells were plated in t25 flasks overnight and transfected with XRCC1 SiRNA for 24 hrs. The following day transfection media were changed to culture medium. On day 2, cells were trypsinised and re-plated in 6-well plates at 250 cells/well cell density. Control cells were plated on the same day. Cells were left in the incubator for 14 days to form colonies. Colonies were fixed, stained and counted as described in the Methods section.

As XRCC1 knock-down leads to PARP1 activation in A2780 and A2780cis cells, we hypothesised that PARP1 inhibition with Olaparib will induce toxicity in XRCC1 deficient ovarian cells. Therefore, we tested Olaparib sensitivity in A2780, A2780cis controls and XRCC1_KD cells in a clonogenic survival assay. We observed increased cytotoxicity in A2780 (XRCC1_KD) cells in comparison to XRCC1 depleted A2780cis cells (Figure 5-10). That suggests more sensitivity to Olaparib in cisplatin sensitive cells. We confirmed cisplatin sensitivity in A2780 and A2780cis control cells. As previously published (Beaufort *et al.*, 2014), A2780 cells are more sensitive to cisplatin than A2780cis cells.

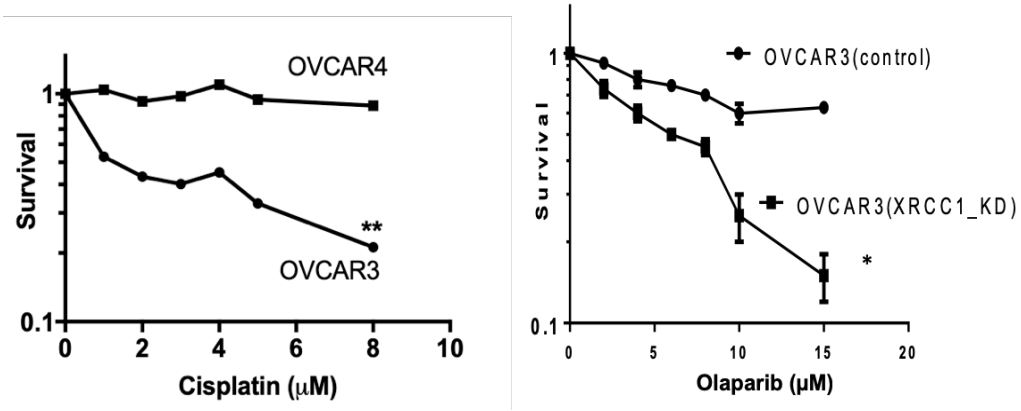


Figure 5-11: Clonogenic survival assay for Cisplatin and Olaparib in OVCAR3 cells. Cisplatin sensitivity in OVCAR3 and OVCAR4 ovarian cell lines. Olaparib sensitivity in OVCAR3 (XRCC1_KD) cells.

We confirmed Olaparib sensitivity in XRCC1 deficient ovarian cells in another cell line model. OVCAR3 cells are cisplatin sensitive in comparison to OVCAR4 cells (Figure 5-11). We depleted XRCC1 with SiRNA in OVCAR3 cells and Olaparib cytotoxicity in OVCAR3 control and XRCC1_KD cells was tested by a clonogenic survival assay. OVCAR3(XRCC1_KD) are more sensitive to Olaparib than the control cells, which emphasizes the results in A2780 (XRCC1_KD) cells.

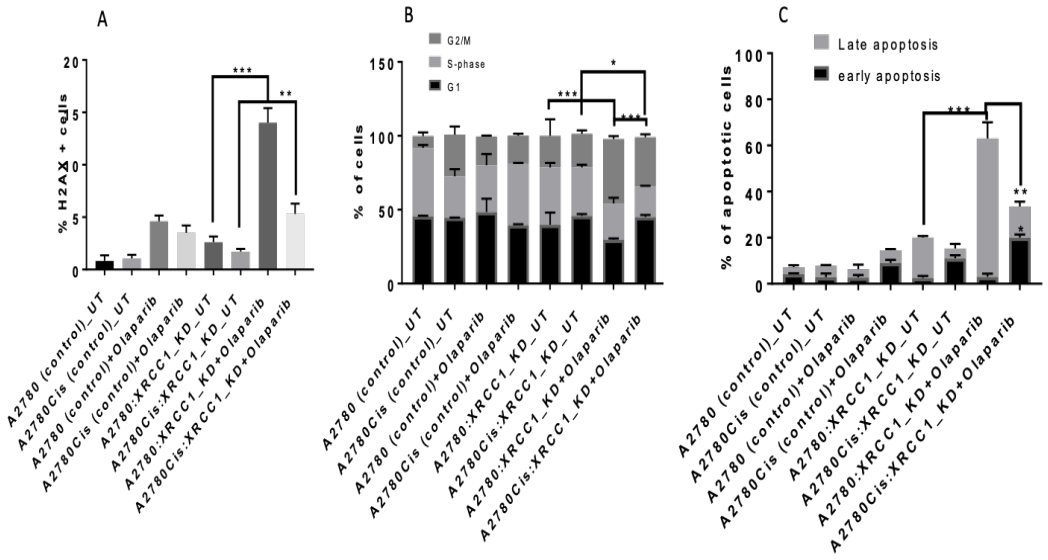


Figure 5-12: Functional studies of Olaparib sensitivity in XRCC1_KD ovarian cells. γH2AX analysis by flow cytometry (A), cell cycle analysis by flow cytometry (B) and annexinV analysis by flow cytometry (C) for A2780 and A2780cis control and XRCC1_KD cells treated with Olaparib. Cells were transfected with XRCC1 SiRNA as described previously. On day 2, cells were trypsinised and re-plated in 6-well plates and treated with Olaparib (10 μM) or left untreated. After 24 hrs of treatment, cells were collected and fixed for at least 30 mins and the propidium iodide/γH2AX staining protocol was followed as described in the Methods sections. For apoptosis analysis by annexinV, cells were collected by trypsinisation and washed with ice cold PBS and re-suspended in the annexinV binding buffer and stained with propidium iodide and annexinV antibody as per the protocol detailed in the Methods section.

Olaparib cytotoxicity led to significant DNA damage in A2780(XRCC1_KD) as observed by increased γH2AX staining. Also, Olaparib led to G2/M cell cycle arrest in both A2780 and A2780cis XRCC1_KD cells, though it was more significant in A2780 cells. γH2AX and cell cycle arrest lead to the increasing accumulation of apoptotic cells in A2780 (XRCC1_KD) cells (Figure5-12).

5.3.2.3 XRCC1 CRISPR knock out in A2780 cells

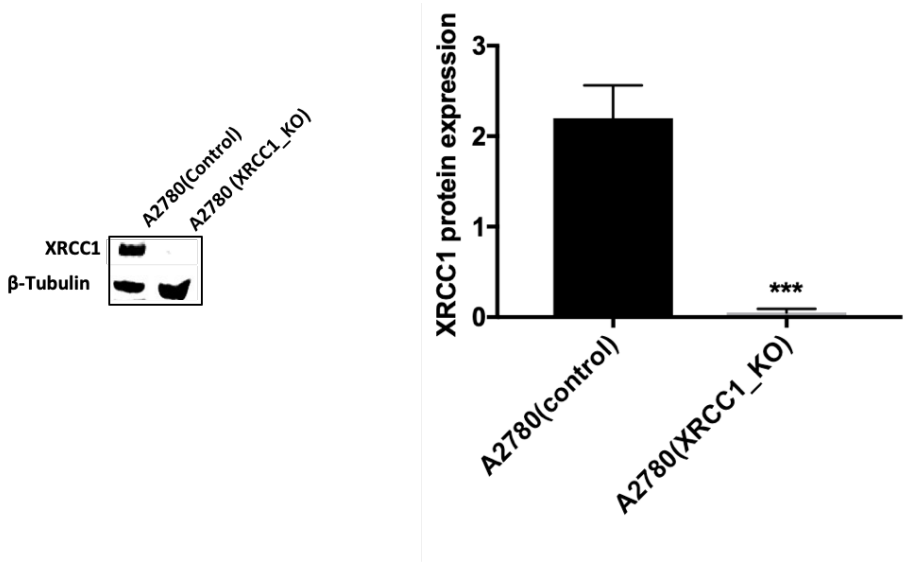


Figure 5-13: Western blot for XRCC1_KO and quantification in A2780 cells. Quantification of XRCC1 protein expression relative to β-tubulin levels.

To validate further the siRNA data, we generated a CRISPR-cas9 knock-out of XRCC1 in A2780 cells. The transfection was delivered as per the described protocol in the Methods chapter. The desired clones were selected in puromycin (10 μg/ml) for 2 weeks. The transfection efficiency was confirmed by western blot (Figure 5-13). The sensitivity of the A2780 (XRCC1_KO) to Olaparib was confirmed using a clonogenic survival assay. As expected, A2780 (XRCC1_KO) was sensitive to Olaparib compared to the control cells (Figure 5-14). Thus, Olaparib sensitivity in XRCC1 deficient platinum sensitive cells was reproduced in different XRCC1 depletion systems.

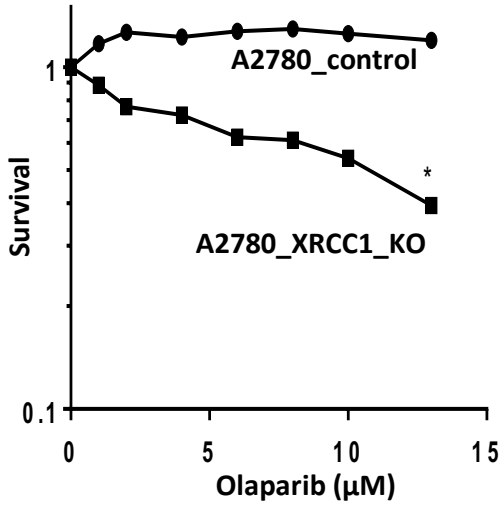


Figure 5-14: Clonogenic survival assay for A2780 (XRCC1_KO) in different doses of Olaparib.
250 cells/well of A2780 control and XRCC1_KO cells were plated in 6-well plates overnight. Then cells were treated with the indicated doses of Olaparib. Cells were left in the incubator for 14 days to form colonies. After incubation, colonies were washed with PBS and stained with crystal violet, acetic acid and methanol mixture.

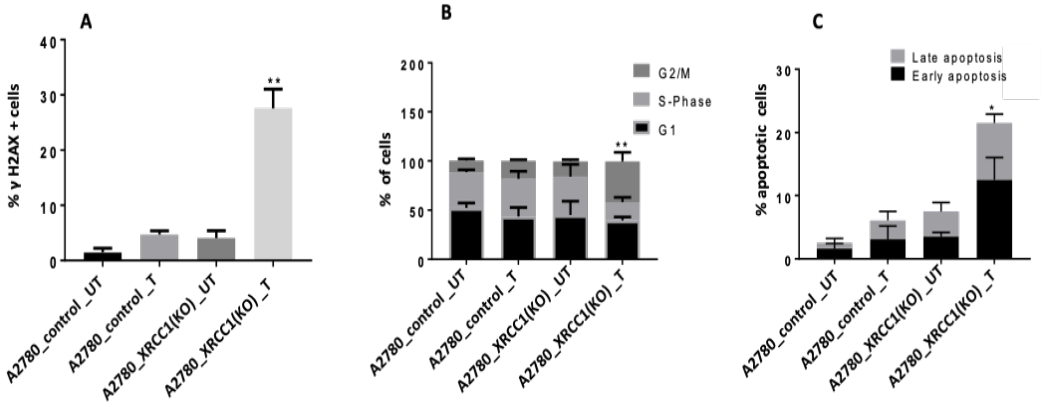


Figure 5-15: Functional studies for Olaparib sensitivity in A2780 (XRCC1_KO). γH2AX analysis by flow cytometry (A), cell cycle analysis by flow cytometry (B) and annexinV analysis by flow cytometry (C) for A2780 control and XRCC1_KO cells. Control and XRCC1_KO cells were plated in 6-well plates overnight and then treated with Olaparib (10μM) for 24 hrs. After treatment cells were collected by trypsinization and the protocol for flow cytometry staining was followed as described in the Methods chapter.

Olaparib treatment in A2780 (XRCC1 _KO) led to the accumulation of double strand breaks and cell cycle arrest in the G2/M phase. Additionally, we observed significant induction of apoptotic cells in A2780 (XRCC1_KO) treated with Olaparib.

5.3.3 Validation of cytotoxicity of PARP inhibitors in XRCC1 deficient ovarian cells using Talazoparib.

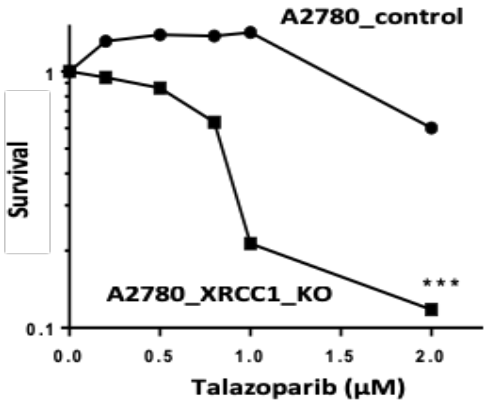


Figure 5-16: Talazoparib sensitivity in A2780 (XRCC1_KO) cells.
Clonogenic survival assay for A2780 control and XRCC1_KO with different doses of Talazoparib. 250 cells/well of A2780 control and XRCC1_KO cells were plated in 6-well plates overnight. Then the cells were treated with the indicated doses of Talazoparib. Cells were left in the incubator for 14 days to form clones. After the incubation period colonies were fixed and stained as described in the Methods chapter.

Talazoparib is another PARP inhibitor. It is at least 50 times more potent than Olaparib in BRCA1/2 deficient cells (B. Wang *et al.*, 2016). To explore whether the cytotoxic effect of Olaparib in XRCC1 deficient cells is mediated by PARP inhibition or PARP trapping, we treated A2780 (XRCC1_KO) with different doses of

Talazoparib. As previously shown, Talazoparib is cytotoxic at much lower doses than Olaparib in the clonogenic survival assay (Figure 5-16). Additionally, Talazoparib treatment led to substantial DNA damage and cell cycle arrest in the G2/M phase and accumulation of apoptotic cells in A2780 (XRCC1_KO) treated with Talazoparib. As expected, Talazoparib at 5μM concentration was more cytotoxic compared to Olaparib (used at 10μM) in the induction of γ H2AX and apoptotic cells as well as the more profound S-phase cell cycle arrest in Talazoparib treated cells compared to Olaparib (Figure 5-17).

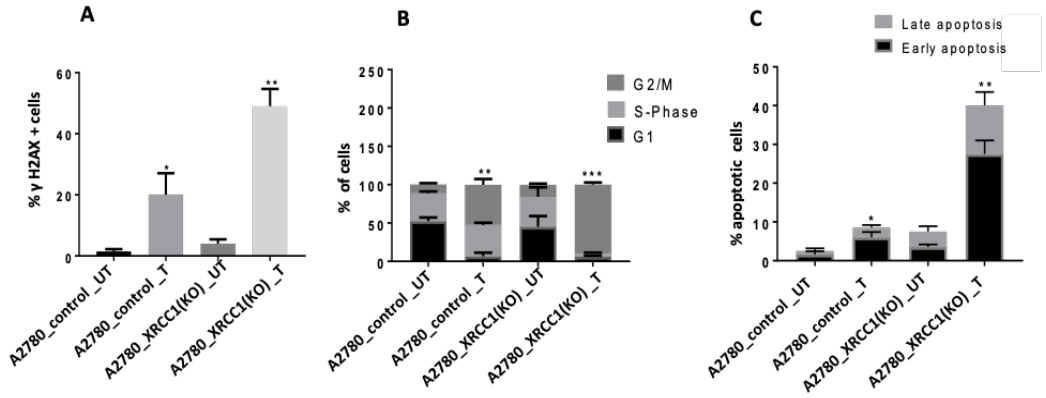


Figure 5-17: Functional studies for Talazoparib sensitivity in A2780 (XRCC1_KO). γH2AX analysis by flow cytometry (A), cell cycle analysis by flow cytometry (B) and annexinV analysis by flow cytometry (C) for A2780 control and XRCC1_KO cells. A2780 control and XRCC1_KO were plated in 6-well plates overnight. Cells were treated with 5μM Talazoparib for 24 hrs. After the incubation time, the cells were trypsinised and the flow cytometry staining protocol was followed as described in the Methods section.

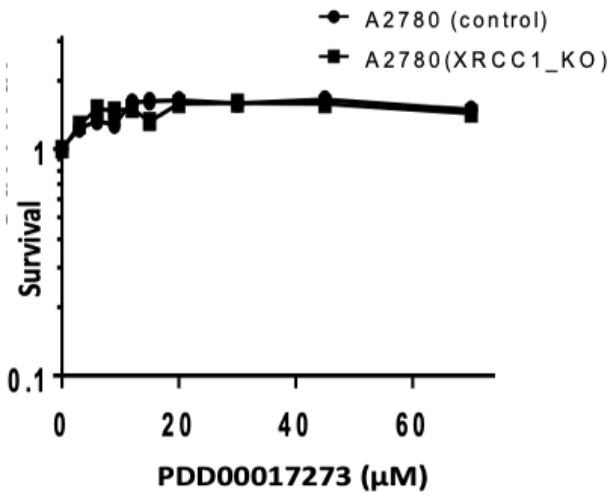


Figure 5-18: Clonogenic survival assay for PARG inhibitor sensitivity in A2780(XRCC1_KO) cells.
A2780 control and XRCC1_KO cells were plated in 6-well plates overnight, then treated with the indicated concentrations of PDD00017273 and left in the incubator to form colonies for 14 days.

PARP1 regulates DNA repair through catalysing the formation of poly (ADP-ribose) (PAR) polymers on itself as well as on other histones and proteins coordinating DNA damage response. The formed (PAR) polymers can be hydrolysed by PAR glycohydrolase (PARG). The balance between PARP1 and PARG levels is essential in cellular homeostasis. The PARG inhibitor PDD00017273 has been recently reported to be synthetically lethal in BRCA1 and BRCA2 deficient cells. Therefore, we tested the sensitivity of the PARG inhibitor (PDD00017273) in XRCC1 deficient cells. However, in the clonogenic survival assay neither the A2780 control nor the XRCC1_KO cells showed any sensitivity to PDD00017273 (Figure 5-18).

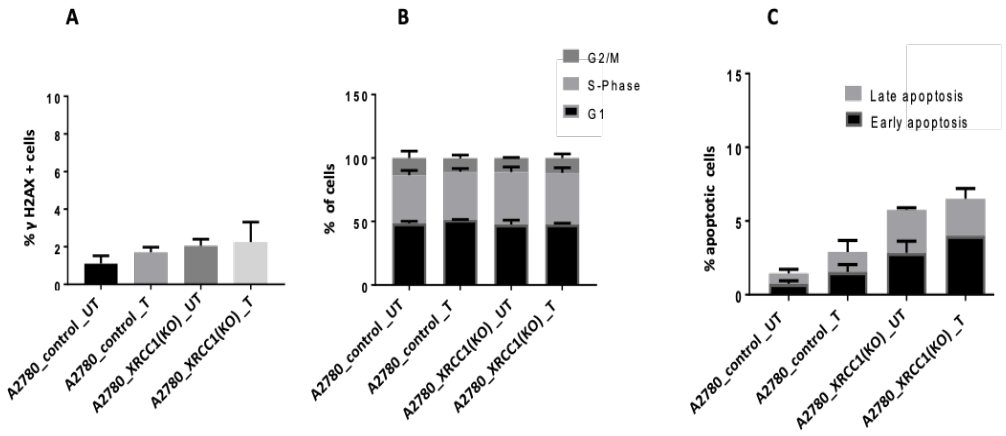


Figure 5-19: Functional studies for PARG inhibitor in A2780 (XRCC1_KO). γH2AX analysis by flow cytometry (A), cell cycle analysis by flow cytometry (B) and annexinV analysis by flow cytometry (C) for A2780 control and XRCC1_KO cells. A2780 control and XRCC1_KO were plated in 6-well plates overnight. Cells were treated with PDD00017273 (10μM) for 24 hrs. After the incubation time, the cells were trypsinised and the flow cytometry staining protocol was followed as described in the Methods section.

Flow cytometry analysis of γH2AX staining did not reveal significant DNA damage in PARG inhibitor treated cells. Similarly, there was no significant cell cycle arrest or significant apoptotic cells formation (Figure 5-19) which confirms that PARG inhibitor is not cytotoxic in XRCC1 deficient ovarian cells.

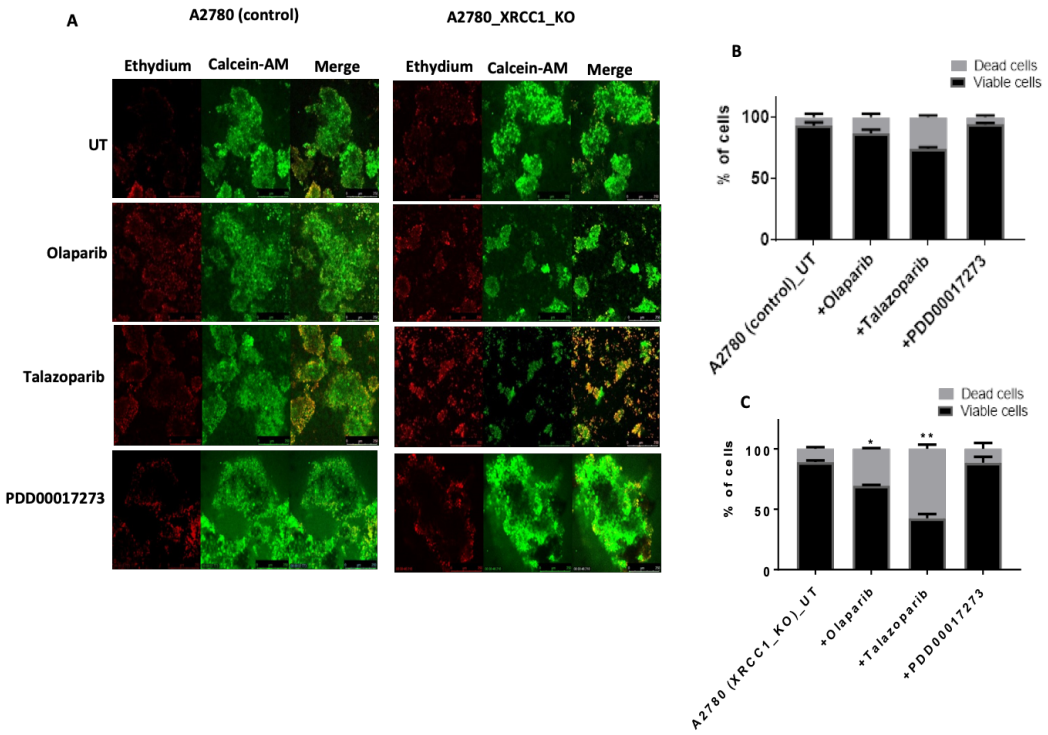


Figure 5-20: Spheroids of ovarian cells treated with Olaparib, Talazoparib and PDD00017273.
(A) Representative photomicrographic images of A2780 control and A2780(XRCC1_KO) spheroids treated with Olaparib (10μM) or Talazoparib (5μM) or PDD00017273 (10μM). (B) Quantification of A2780 cell viability with flow cytometry. (C) Quantification of A2780(XRCC1_KO) cell viability with flow cytometry. $4x10^4$ cells were grown in a tumour sphere medium on ultra-low attachment 6-well plates for 14 days. After spheroid structures formation, spheres were treated with the indicated doses of the inhibitors for 48 hrs. After treatment, spheres were fixed with 37% formaldehyde 1:10 ratio. Then spheres were stained with calcein (2.5μM) and ethydium homodimer (1.5μM).

To mimic the in-vivo system, we generated 3D-spheres for the A2780 control and XRCC1_KO. We tested Olaparib, Talazoparib and PDD00017273 sensitivity in spheroid structures. Similar to the 2D model, Olaparib and Talazoparib were still

sensitive in XRCC1 deficient cells but the PARG inhibitor PDD00017273 did not have significant cytotoxicity in the A2780 control or XRCC1_KO spheres.

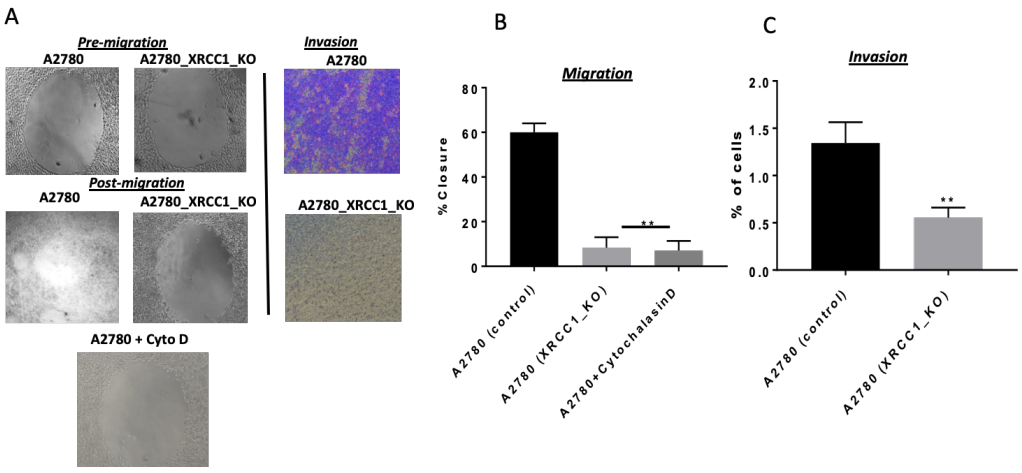


Figure 5-21: Invasion and migration assay in A2780 (XRCC1_KO).
(A) Representative photomicrographic images of invasion and migration assays. (B) Quantification of radius migration area analysed in ImageJ software. (C) Quantification of invasive cells. Invasive cells were stained with crystal violet and extracted with cell extraction solution provided by the supplier. Absorbance were read at a wavelength of 560 nm. The invasion and migration protocols are detailed in the Methods chapter.

Markkanen *et al*. showed that XRCC1 siRNA knock-down leads to deregulation of several genes involved in tissue remodelling and cellular invasion. In their analysis *MMP2, TIMP1, TIMP2* and the collagenases *COL1A1, COL1A2* and *COL3A1* are among the altered genes in XRCC1 deficient cells. This study shed light on a new role for XRCC1 deficiency and impairment of DNA repair in tumour cell remodelling. We tested this hypothesis further in our stable XRCC1_KO A2780. XRCC1 reduced cell invasion and migration ability as demonstrated in the assay results where A2780 control cells have high invasion and migration ability which was significantly reduced in A2780(XRCC1_KO) (Figure 5-21). These preliminary results indicate the indirect role of XRCC1 in EMT gene regulation.

5.4 Discussion

PARP inhibitors are an exciting new strategy for ovarian cancer treatment that has proven to have significant clinical benefits (Fong *et al.*, 2010). The increasingly successful studies of Olaparib accelerated its approval by the FDA for treatment of BRCA germline mutated advanced stage ovarian cancers which received three or more lines of chemotherapy (G. Kim *et al.*, 2015). Currently, other PARP inhibitors are in different stages of clinical trials with promising results so far (Ledermann *et al.*, 2016). Our research group previously investigated the clinicopathological significance of XRCC1 expression in 195 consecutive ovarian cancers. In this study XRCC1 expression was significantly correlated with higher stage ($p = 0.006$), serous type tumours ($p = 0.008$), suboptimal de-bulking ($p = 0.004$) as well as platinum resistance ($p < 0.0001$). Positive XRCC1 tumour patients are at increased risk of ovarian cancer related death by two-fold ($p = 0.007$) and disease progression ($p < 0.0001$) (Abdel-Fatah *et al.*, 2013). In the current study, we investigated XRCC1 and PARP1 expression in a larger cohort of ovarian cancers (n=525). Interestingly, high XRCC1 was associated with aggressive disease and poor survival for patients which concur with the previous study. However, in our cohort XRCC1 expression predicted the outcome of platinum sensitive patients. Hence, XRCC1 subtyping of epithelial ovarian cancer could be as well a predictor of patients' response to platinum.

A previous study aiming to identify defective DNA repair genes that can induce synthetic lethality with PARP inhibitor showed XRCC1 to be a synthetic lethality partner with PARP1 (Lord *et al.*, 2008). We also explored in detail XRCC1/ PARP1

synthetic lethality in the breast cancer model. Here the clinical data shows that XRCC1/ PARP1 synthetic lethality is a useful approach in ovarian cancers.

Our analysis indicates that high PARP1 in ovarian tumours is associated with high grade and poor survival outcome. High PARP1 and XRCC1 expressing tumours also had the worst survival outcome. Our Cox multivariate analysis postulates that XRCC1 and PARP1 correlate significantly with platinum sensitivity.

A published clinical trial for Olaparib in 50 BRCA mutated ovarian tumours revealed that Olaparib sensitivity correlated with platinum sensitivity. The clinical benefit rate was 69% in platinum sensitive patients. That concurs with our findings and suggests that perhaps resistance to platinum and Olaparib involve similar mechanisms (Fong *et al.,* 2010). This may be an area of interesting future investigations.

We showed in our preclinical work sensitivity to Olaparib in XRCC1 deficient ovarian cell lines in different XRCC1 depletion systems. That was more profound in platinum sensitive A2780 ovarian cells. Olaparib reduced cells' ability to form colonies in XRCC1 depleted cells. Olaparib treatment also induced double strand break formation as evidenced by the increase in γH2AX positive cells. Treated XRCC1 deficient cells arrested in the G2/M phase led to the accumulation of apoptotic cells. These data were reproduced in stable CRISPR_KO for XRCC1 in A2780 cells. We also proved Olaparib cytotoxicity in a 3D spheres model of A2780 (XRCC1_KO). Olaparib not only led to an accumulation of dead cells but a reduction in spheroid size.

The ability of PARP inhibitors to trap PARP proteins is believed to be more cytotoxic than PARP inhibition (Murai *et al.*, 2012, 2014). That mechanism of PARP

inhibitors is under intensive exploration. Few studies have explained that more potent PARP inhibitors like Veliparib and Talazoparib exert more cytotoxicity through allosteric stabilizing PARP-DNA complexes (Murai *et al.*, 2012, 2014; Hopkins *et al.*, 2018). These complexes are more toxic than single strand breaks and BER intermediates which persist due to PARP catalytic inhibition. However, Hopkins *et al.* in a recent study were unable to demonstrate an allosteric PARP trapping mechanism for the potent PARP inhibitors. Thus, they suggested that the more likely mechanism to the observed differences in cellular trapping activity may be the extent of DNA damage formed due to inhibition of PARP activity (Hopkins *et al.*, 2015). In our study, we observed an extended DNA damage upon Talazoparib treatment as evidenced by the substantial γH2AX accumulation and G2/M cell cycle arrest and apoptotic cell formation. That DNA damage appears to be substantially more than what is induced with Olaparib treatment. However, our study could not address whether that is due to PARP trapping or PARP catalytic inhibition. More biochemical and mechanistic investigations are required to tackle that question.

Poly (ADP-ribose) glycohydrolase (PARG) can reverse the action of PARP enzymes through its endo and exoglycosidase activity. Removal of PAR by PARG is required for repair of DNA strand breaks and thus, PARG is as important as PARP enzymes in efficient DNA damage response (Gravells, Grant, Kate M Smith, *et al.*, 2017). We screened our XRCC1 deficient and proficient ovarian cells for PARG inhibitor sensitivity. Interestingly, PARG inhibitor did not have any synthetic lethality with XRCC1. A recent study referred to PARG inhibitor synthetic lethality with XRCC1 in a breast cell line model (Martin *et al.*, 2018). That may indicate that different

cancer models have differential sensitivity to PARG inhibitors due to genetic backgrounds and other mutational profiles.

Another detailed study by Pillay *et al.* found differential sensitivity of ovarian cancer cell lines to a PARG inhibitor based on the vulnerability of DNA replication genes. They also confirmed their findings in patient derived ovarian cancer models (Pillay *et al.*, 2019). Therefore, their study, as well as ours, provides evidence that PARG inhibition has a selective cytotoxicity in ovarian cancer cells. Future investigations should address and predict which patient groups can benefit from PARGi in clinics.

In conclusion, PARP inhibitors are an exciting synthetic lethality approach in XRCC1 deficient ovarian cancers. Its clinical potential would need to be further exploited

6 Targeting DNA polymerase Beta in ovarian cancers

6.1 Introduction

DNA polymerase beta (polβ) is the most extensively studied member of the X-family of DNA polymerases (Albertella, Lau and O'Connor, 2005). Members of this family are mainly responsible for gap filling during DNA synthesis and replication. Polβ plays a crucial role in the base excision repair pathway (BER), which is the pathway responsible for repairing base lesions resulting from oxidizing agents and alkylating agents (Dianov and Hübscher, 2013). BER is initiated when DNA glycosylases remove the damaged base and create AP sites in the DNA. Unless repaired, AP sites can be mutagenic and cytotoxic. APE1 endonuclease enzymatic activity processes the phosphodiester bond 5′ to the AP site, thereby generating a nick with 5′-sugar phosphate (dRP) and 3′-hydroxyl group (Dianov and Hübscher, 2013). polβ functions in the BER through its two enzymatic activities; the lyase activity of polβ which eliminates the (dRP) group forming a 5'-phosphate and a one-nucleotide gap. The other enzymatic function is through the nucleotide gap filling and sealing the DNA (Bebenek and Kunkel, 2004). Ligase III- XRCC1 heterodimer will accomplish the repair through the short-batch base excision repair pathway. In the case of oxidized base lesions, the formed 5′ ends are resistant to the lyase activity of polβ, and BER has to proceed through the long batch-BER. That sub-pathway is also polβ dependent initially where it incorporates the first nucleotide into the nick (David, O'Shea and Kundu, 2007). Proliferating cell nuclear antigen (PCNA) and replication factor C along with pol δ/ε then continue strand displacement. The resulting flap of 2-12 nucleotides are removed

by flap endonuclease 1 and DNA ligase I seals the DNA and finishes the long-batch BER pathway (Dianov and Hübscher, 2013).

Thus, polβ functions are rate-limiting steps in the BER. Besides its enzymatic activities it also physically interacts with other members of the BER including XRCC1, Ligase1, and PARP1. Polβ gene encodes a (335 residues 39 KDa) protein (Sykora *et al.*, 2017). It has two functional domains: The N-terminal domain is essential for the dRP lyase activity and the C-terminal domain elemental for polβ nucleotidyl transferase activity during BER. Polβ lacks a 3′ → 5′ exonuclease proofreading activity that distinguishes other replicative polymerases (Sweasy, 2003). In mouse models, loss of polβ causes early embryonic lethality (Sugo *et al.*, 2000). Additionally, 30% out of all the characterized human cancers to date express polβ variant proteins. Of those cancers, 28 types revealed single amino acid mutations, seven had truncated forms of polβ, and eight types had multiple variant mutations of polβ. Swaesey and colleagues have described a few polβ variants affecting gap filling steps in BER and leading to tumour progression. They described the I260M variant of polβ in prostate cancers (Shibani Dalal *et al.*, 2005), the K289M variant of polβ was identified in colon carcinoma (Donigan *et al.*, 2012) and the E295K variant of polβ was described in gastric carcinoma (Lang *et al.*, 2007).

Earlier studies showed the ability of polβ to bypass the cisplatin DNA adduct lesion pt- d-(GCG) (Hoffmann *et al.*, 1995; Starcevic, Dalal and Sweasy, 2004). Comparison of the differential abilities of replicative polymerases to perform translesion synthesis *in vitro* on a substrate containing cisplatin adducted lesion revealed the unique ability of polβ over polymerases ε, η to extend the 3′-OH

opposite the base prior to the lesion (Hoffmann *et al.*, 1995). Polβ was able to restore the arrested replication. These studies pointed to an essential role of polβ in cancer and platinum therapy resistance. In this study, we investigated the influence of polβ expression in platinum sensitivity and prognosis of ovarian cancer patients. We explored the effect of polβ depletion on cisplatin sensitivity *in vitro.* Polβ small molecule inhibitors induced synthetic lethality in BRCA2 deficient cell lines. PARP1 and PARG inhibitors were also screened for sensitivity in polβ deficient cells. We concluded that targeting polβ is a novel therapeutic approach for improving the outcome of ovarian cancer patients.

6.2 Methodology

Immunohistochemical staining of polβ and PARG was carried out on tumour micro arrays (TMA) of 525 ovarian cancer patients treated in Nottingham University Hospitals between 1997 and 2010. The protocol for immunohistochemistry is detailed in the Methods. The TMA slides were incubated with anti-polβ rabbit polyclonal antibody (ab26343, Abcam) at dilution 1:200 or anti-PARG rabbit polyclonal antibody (PA514158, Thermofisher) at dilution 1:100 for 60 min at room temperature. Low/negative nuclear polβ expression was defined by median H-score of ≤180. Low/negative cytoplasmic PARG expression was defined by X-tile H-score of ≤105. *Polβ* mRNA expression was inspected in publicly available ovarian tumour gene expression data sets (http://kmplot.com/analysis/index.php?p=service&cancer=ovar). A test cohort of 107 tumours, validation cohort 1 of 285 tumours, and validation cohort 2 (TCGA) of 465 tumours receiving chemotherapy treatment was used in this study. Polβ inhibitor Pamoic acid and PARGi (PDD00017273) were purchased from (Selleckchem). NSC666719 [4-chloro-5-methyl-N-[5-(naphthalen-2-ylamino)-1H1,2,4-triazol-3-yl]-2-sulfanylbenzenesulfonamide] (polβ small molecule inhibitor) was obtained from the Developmental Therapeutics Program of the National Cancer Institute of the National Institutes of Health (DTP, NCI-NIH). Cell lines used in this study are A2780 (platinum sensitive), A2780cis (platinum resistant), PE01 (BRCA2 deficient), PE04 (BRCA2 proficient), HeLa BRCA2_KD, and HeLa control. SiRNA knock-down of polβ in ovarian cells was carried out as per the siRNA transfection protocol described in the Methods. Nuclear and cytoplasmic

extraction of A2780 and A2780cis cells were carried out using the kit provided by (Thermofisher Scientific) as per the supplier protocol. Clonogenic and flow cytometry analysis for γH2AX, cell cycle, and apoptosis were done as per the protocol described in the Methods. CRISPR-cas9 knock-out of polβ in A2780 and A2780cis were performed as per the Methods chapter. Invasion and migration assays for A2780 and A2780cis control and polβ knock-out were performed as per the supplied protocol from (Cell Biolabs). RT2 PCR profiler for EMT genes in A2780 and A2780cis control and polβ knock-out were done as per Qiagen guided protocol analysis and were performed using the provided software (https://www.qiagen.com/us/shop/genes-and-pathways/data-analysis-center-overview-page/). Western blot and confocal microscopy were performed as detailed in the Methodology section. 3D spheroids for ovarian cell lines as well as HeLa control and HeLa BRCA2_KD cells were grown in Promo Cell tumour spheres XF medium and stained with calcein AM and ethidium bromide as per the detailed protocol in the Methods. Quantification of NAD+ in A2780 and A2780cis control and polβ knock-out following PARGi (20 μM) treatment for 16 h were performed using the NAD+/NADH colorimetric assay kit (catalog ID: ab221821, Abcam, UK) as per manufacturer's protocol. Data analysis was performed on GraphPad Prism-7 software. Error bars represent standard error of mean between experiments. P-values are indicated as P-values <0.05 =*, p-value <0.01 =** & p-value <0.001=***.

6.3 Results

6.3.1 Clinical Data

6.3.1.1 Polβ expression in ovarian tumours

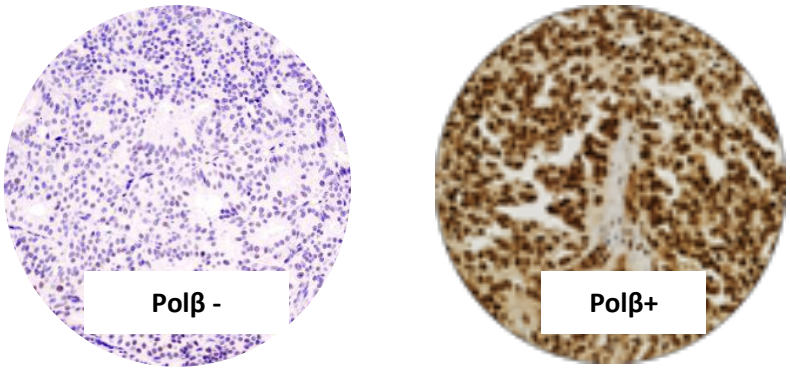


Figure 6-1: Polβ immunohistochemical expression in ovarian tumours. Representative photomicrographic images of negative staining and positive nuclear staining for Polβ in tumour microarrays respectively. Images were taken using Nikon camera microscope at 20x magnification.

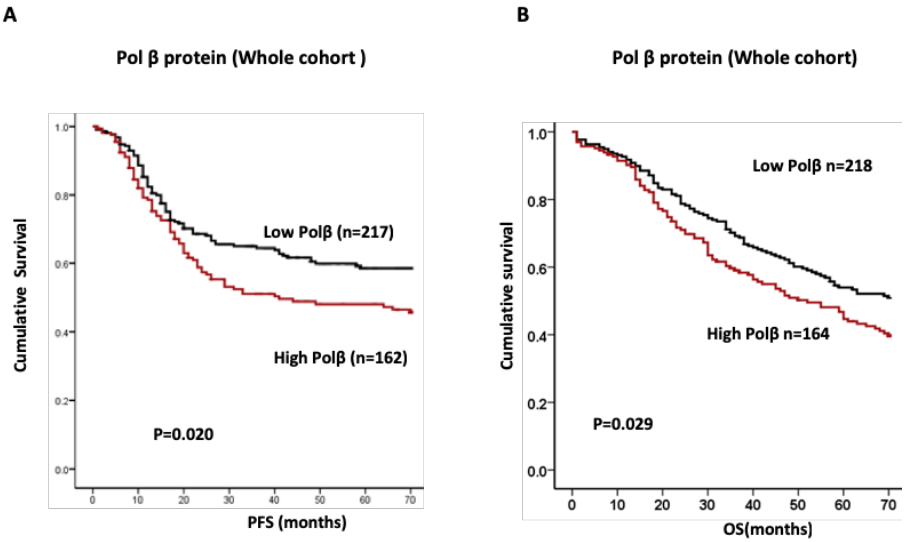


Figure 6-2: Kaplan Meier curve for polβ expression in ovarian tumours. (A)Kaplan-Meier curve showing the correlation between Polβ protein expression and progression-free survival (PFS) in the whole cohort. (B) Kaplan-Meier curve showing the correlation Polβ protein expression and overall survival in the whole cohort.

414 tumours out of the 525 ovarian tumours cohort were positive for polβ nuclear expression (Figure 6-1). High polβ expression was associated with poor progression-free survival (p=0.02) and poor overall survival (0.029) in the whole cohort (Figure 6-2). In the platinum sensitive sub-cohort, high polβ expression was significantly associated with poor progression-free survival (p=0.016) as well as poor overall survival (p=0.013) (Figure 6-3). However, in the platinum resistant tumours polβ expression was not significantly associated with survival outcome in ovarian cancer patients (Figure 6-4).

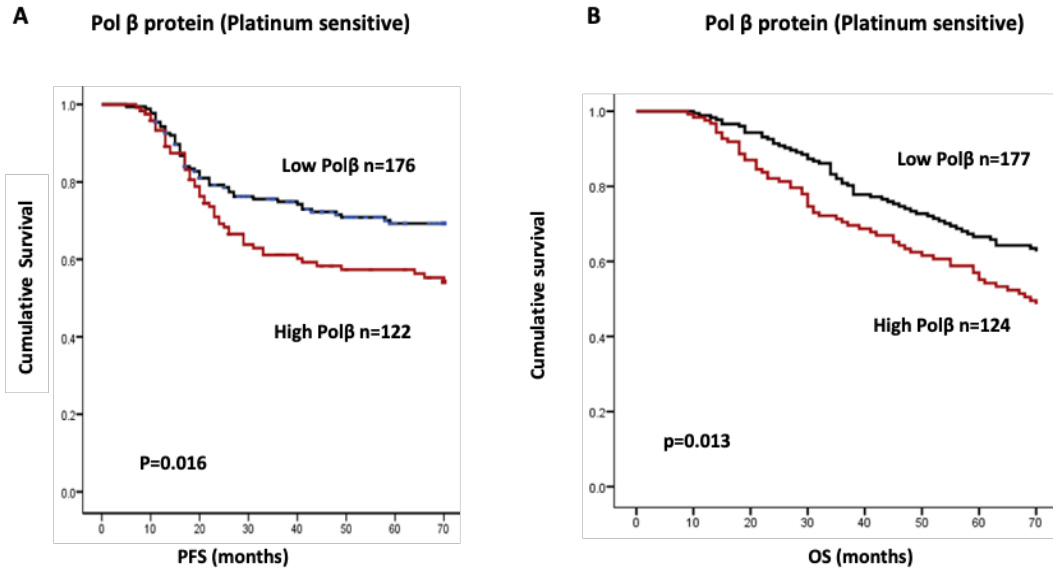


Figure 6-3: Kaplan Meier curve for polβ expression in platinum sensitive tumours. Kaplan Meier curve showing the correlation between polβ protein expression and Progression free survival (A) and overall survival (B) in platinum sensitive ovarian tumours.

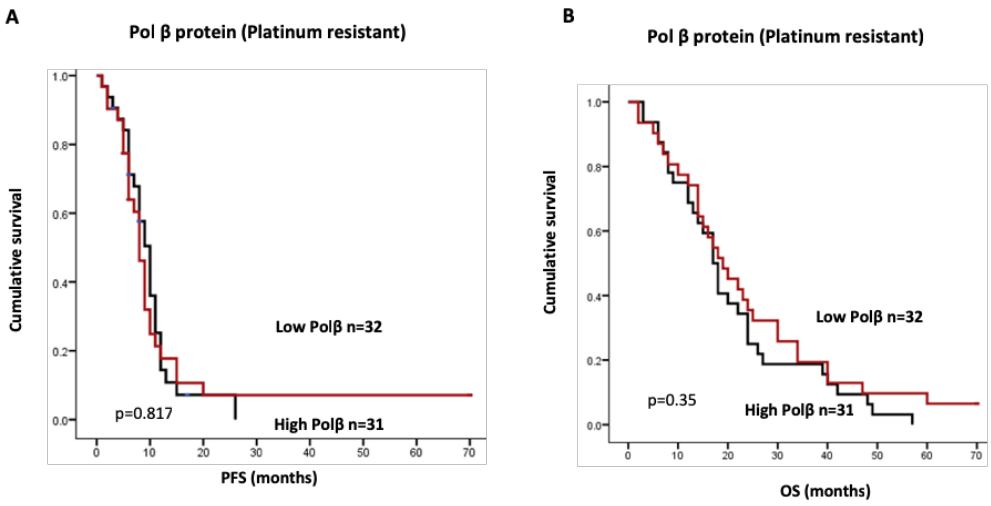


Figure 6-4: Kaplan Meier curve and Polβ expression in platinum resistant tumours. Kaplan Meier curve showing the correlation between polβ protein expression and Progression free survival (A) and overall survival (B) in platinum resistant ovarian tumours.

High Polβ expression was significantly associated with serous cystadenocarcinoma (p=0.001) and surgical sub-optimal debulking (p=0.023). On the other hand, low polβ expression was mostly associated with FIGO stage I disease (p=0.003). Although platinum sensitivity was mostly associated with low polβ expression and platinum resistant tumours were mostly high in polβ expression, it was not statistically significant (p=0.076) (Table 6-1). Taking together these results provides evidence that high polβ expression is associated with aggressive ovarian cancer phenotype.

Table 6-1: Polβ expression and clinico-pathological associations.

	Polβ (Low) N (%)	**Polβ (High) N (%)**	**P-value**
Pathological Type			
Serous cystadenocarcinoma	113 (48.5)	120 (51.5)	**0.001**
Mucinous cystadenocarcinoma	32 (74.4)	11 (25.6)	
Endometrioid	49 (69.0)	22 (31.0)	
Clear cell carcinoma	26 (70.3)	11 (29.7)	
Mixed	6 (50.0)	6 (50.0)	
Other	4 (33.3)	8 (66.7)	
FIGO Stage			
Stage I	101 (67.3)	49 (32.7)	**0.003**
Stage II	25 (41.0)	36 (59.0)	
Stage III	87 (52.4)	79 (47.6)	
Stage IV	15 (55.6)	12 (44.4)	
Tumour Grade			
Grade 1	30 (61.2)	19 (38.8)	0.072
Grade 2	45 (64.3)	25 (35.7)	
Grade 3	124 (50.4)	122 (49.6)	
Platinum sensitivity			
Sensitive	157 (52.0)	145 (48.0)	0.076
Resistant	25 (39.7)	38 (60.3)	

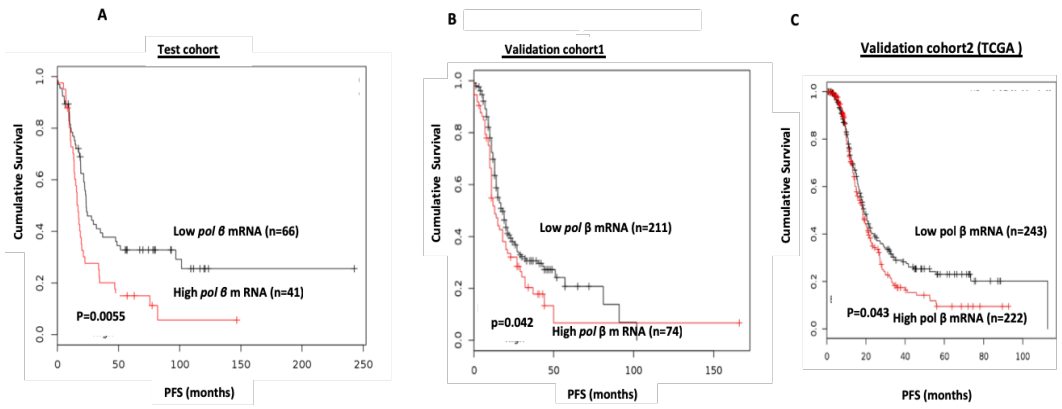


Figure 6-5: *polβ* mRNA expression in ovarian tumours.
Kaplan Meier curve and progression free survival for *polβ* mRNA expression in the test cohort (A), validation cohort1 (B), and validation cohort2 (C).

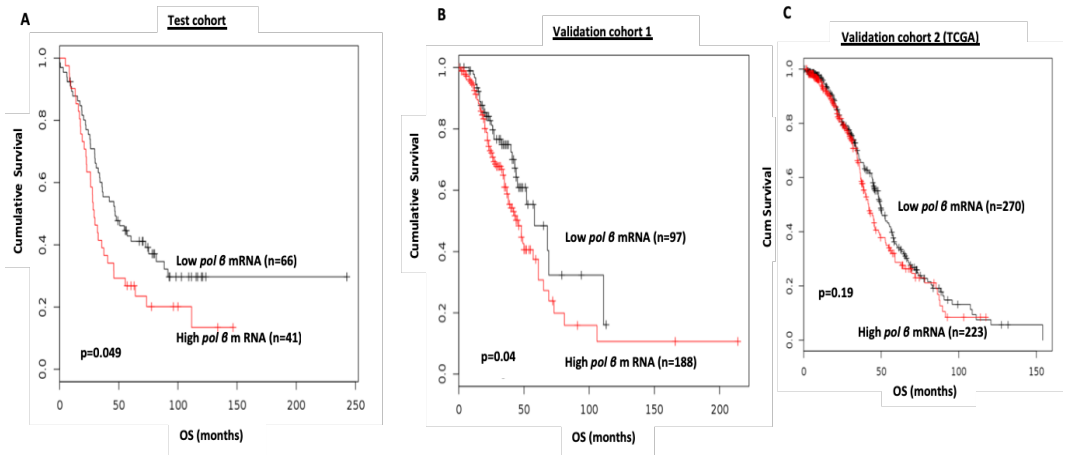


Figure 6-6: *Polβ* mRNA expression and overall survival in ovarian tumours.
Kaplan Meier curve and overall survival for *polβ* mRNA expression in the test cohort (A), validation cohort1 (B) and validation cohort2 (C).

We investigated polβ mRNA expression in publicly available data sets for ovarian tumour gene expression.

(http://kmplot.com/analysis/index.php?p=service&cancer=ovar). A test cohort of 107 tumours, a validation cohort1 of 285 tumours and additional validation cohort2 of 465 tumours available at (https://www.cancer.gov/TCGA) were used.

High *polβ* mRNA expression was significantly associated with poor progression-free survival in the test and validation cohorts (Figure 6-5). Similarly, high *polβ* mRNA expression was associated with poor overall survival in ovarian cancers (Figure 6-6). Thus, the clinical data indicate that polβ expression could be a prognostic factor for ovarian cancer.

6.3.2 Pre-clinical Data

6.3.2.1 Polβ expression in ovarian cell lines

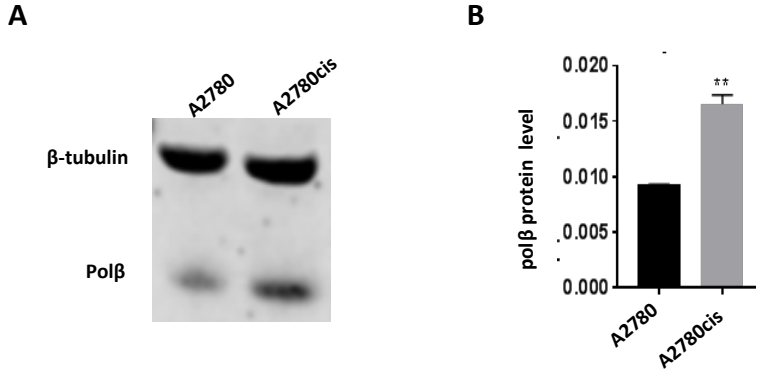


Figure 6-7: Polβ protein expression in A2780 and A2780cis ovarian cell lines.

(A)Western blot showing polβ protein expression in A2780 and A2780cis cells. (B) Relative polβ quantification by western blot. β-tubulin was used as a loading control.

To investigate the influences of polβ expression in the ovarian cancer cell line model we used A2780 cells (platinum sensitive) and its platinum resistant derived cell line model A2780cis (platinum resistant). Interestingly, at the basal levels, A2780cis cells have higher levels of polβ protein expression (Figure 6-7). Upon

cisplatin treatment, we found induction of *polβ* mRNA expression in cisplatin treated A2780cis cells after 48 hrs treatment (Figure 6-8). Additionally, we observed induction of Polβ protein after treatment of 48 hrs in lysates of A2780cis cells treated with cisplatin but not in A2780 cells (Figure 6-9). These results indicate that polβ expression can be induced upon platinum treatment. Immunofluorescence staining for polβ in A2780 and A2780cis cells treated with cisplatin demonstrated significant increase in polβ nuclear fluorescence after 48hr of cisplatin treatment in A2780cis cells but not in A2780 cells (Figure 6-10).

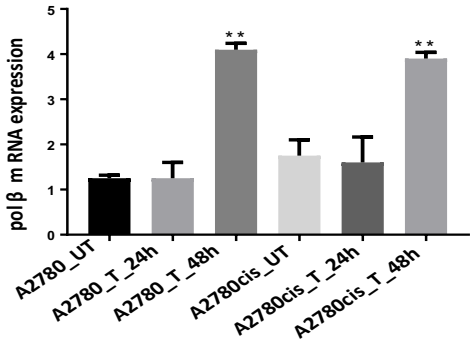


Figure 6-8: *Polβ* mRNA expression in A2780 and A2780cis cells treated with cisplatin.
A2780 and A2780cis cells were plated in T25 flasks overnight and then treated with cisplatin (5μM). Cells were collected in RNA lysis buffer after 24 and 48 hours. Then RNA extraction was performed using the RNA easy-mini kit. RT2 first strand kit was used for cDNA conversion. Real-time PCR was performed on an ABL7500 fast block machine as detailed in the Methods section.

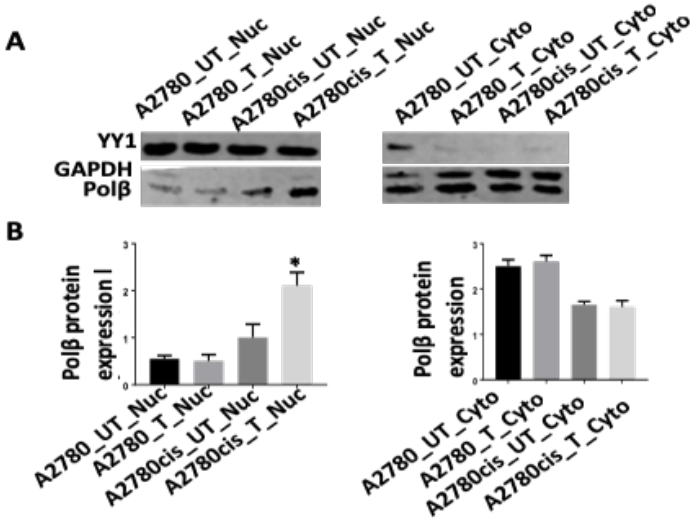


Figure 6-9: Nuclear and cytoplasmic extraction of A2780 and A2780cis cells. (A)Western blot for polβ expression in nuclear and cytoplasmic extracts from A2780 and A2780cis cells untreated and treated with cisplatin for 48 hours. (B) Quantification of polβ protein expression by western blot. GADPH was used as a loading control for cytoplasmic extracts and YY1 was used as the loading control for nuclear extracts.

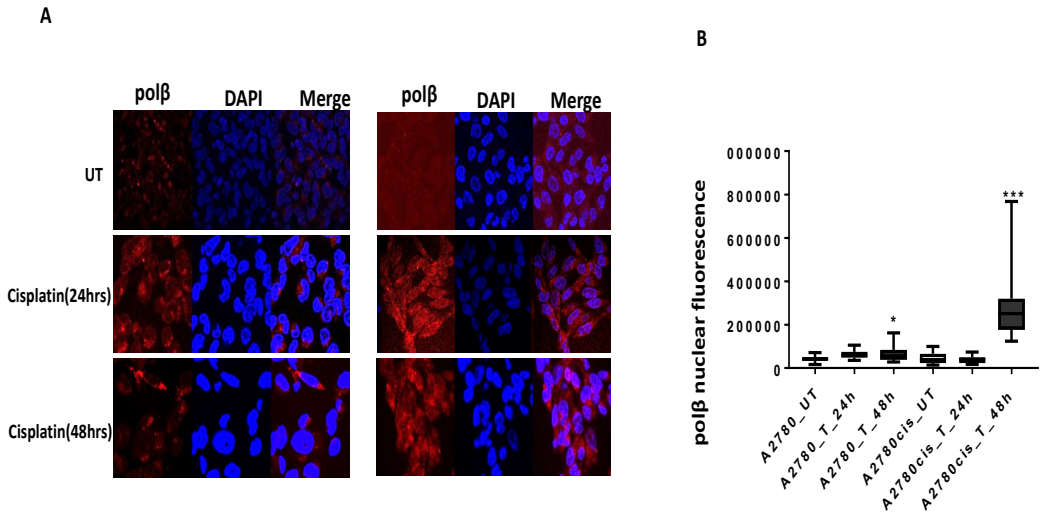


Figure 6-10: Polβ nuclear localization by immunofluorescence. (A)Representative photomicrographic images for polβ nuclear localisation post cisplatin treatment. (B) Quantification of polβ nuclear fluorescence by ImageJ software. Cells were plated on coverslips overnight then treated with 5 μM cisplatin. Cells were fixed at 24 hours and 48 hours post incubation with 4% paraformaldehyde. Then the immunofluorescence staining protocol was followed as described in the Methods.

6.3.2.2 Polβ knock-down in A2780cis cells

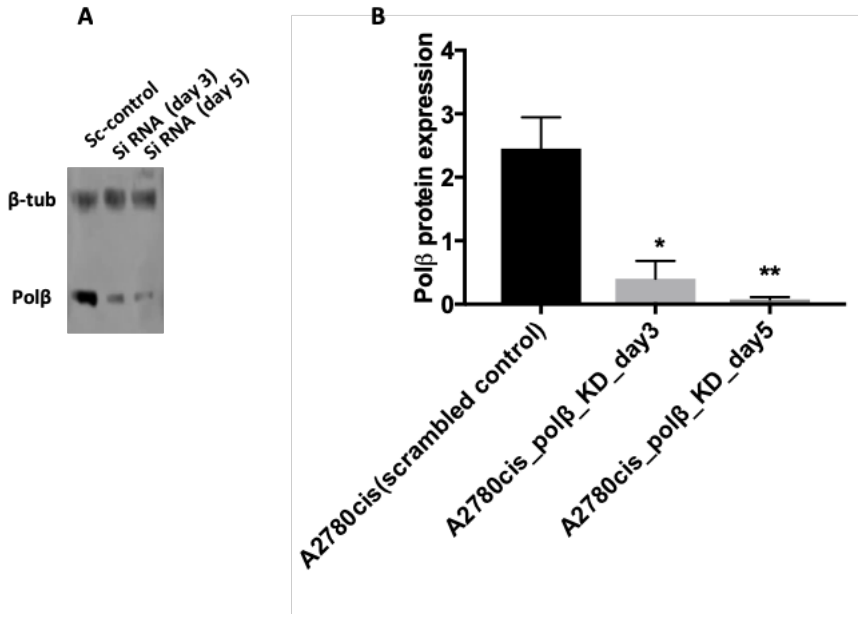


Figure 6-11: Polβ siRNA knock-down.
(A) Polβ western blot and (B) quantification of Polβ protein levels relative to β-tubulin by western blot in A2780cis transfected with negative scrambled control and A2780cis transfected with Polβ siRNA. A2780cis_polβ_KD cells were lysed at day 3 and day 5 to confirm transfection efficiency.

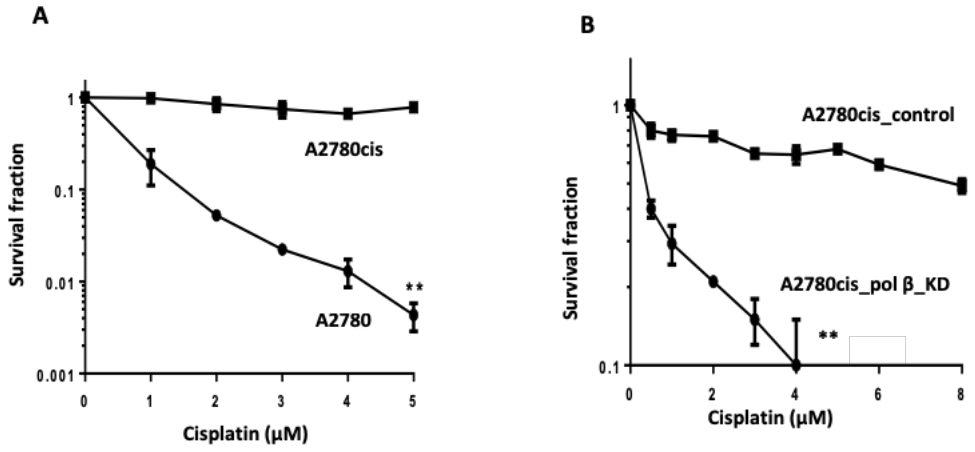


Figure 6-12: Cisplatin sensitivity in A2780cis control and polβ _KD.

(A)Clonogenic survival assay showing cisplatin sensitivity in A2780 and A2780cis. (B)Clonogenic survival assay for A2780cis control and A2780cis_polβ_KD in different doses of cisplatin. A2780cis cells were plated in T25 flasks overnight then transfected with polβ siRNA or negative control in Opti-MEM low serum medium using lipofectamine 3000 reagent. After 48 hours, cells were trypsinised and re-plated in 6-well plates overnight. Then cells were treated with the indicated doses of cisplatin. Cells were left in the incubator to form colonies for 14 days. Colonies were washed with PBS and stained with crystal violet and acetic acid mixture.

When we performed polβ transient knockdown with siRNA we achieved maximum polβ inhibition on day 5 (Figure 6-11). Therefore, we chose day 5 to read all siRNA experimental results. A2780cis cells are resistant to cisplatin in the clonogenic survival assay (Figure 6-12A). However, polβ knock-down re-sensitized A2780cis cells to cisplatin and increased cell killing, as shown in the clonogenic assay (Figure 6-12B).

A2780cis_Polβ_KD cells treated with cisplatin had a greater accumulation of double strand-breaks as evidenced by the accumulation of γH2AX positive cells. Also, cisplatin treatment in A2780cis_polβ_KD cells led to substantial S-phase arrest and increased apoptotic cells in polβ_KD cells but not in scrambled control transfected A2780cis cells (Figure 6-13).

Interestingly, A2780cis_Polβ_KD cells at the basal levels had a significant accumulation of S-phase cells compared to control cells (Figure 6-14A) indicating that polβ knockdown is inducing replication stress in those cells. To confirm these findings, we checked the levels of Ataxia Telangiectasia and Rad3 Related (ATR) protein and its downstream effector phosphorylated checkpoint protein kinase 1 (p-CHK1) levels. ATR and p-CHK1 are crucial responders to cellular replication stress whereas they trigger other proteins including histone H2AX and RAD51 to stabilize the replication fork and prevent its collapse (Awasthi, Foiani and Kumar, 2015; Gupta *et al.*, 2018). A2780cis_polβ_KD cells have increased protein levels of ATR and p-CHK1 which accumulate upon polβ knockdown on day 5 (Figure 6-14).

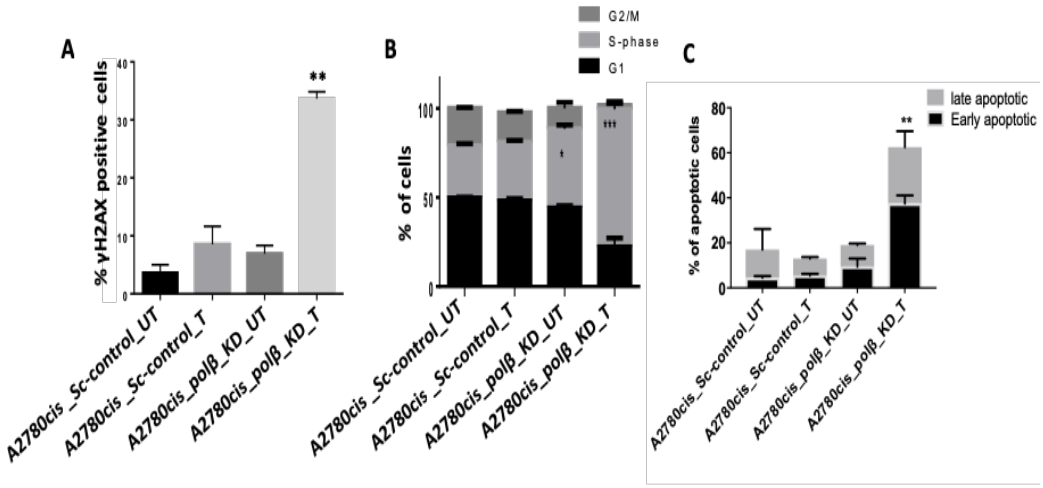


Figure 6-13: Functional studies of cisplatin response in polβ knockdown cells. γH2AX analysis by flow cytometry (A), cell cycle analysis by flow cytometry (B) and annexinV analysis for apoptosis (C) in A2780cis cells scrambled control transfected and A2780cis_polβ_KD treated with 5μM cisplatin for 24 hours. Cells were plated overnight in T25 flasks and transfected with scrambled control or polβ siRNA using lipofectamine3000. On day 3, cells were trypsinised and re-plated in 6-well plates overnight. Cells were treated with 5μM cisplatin or left untreated. On day 5 cells were collected and stained according to the flow cytometry protocol described in the Methods.

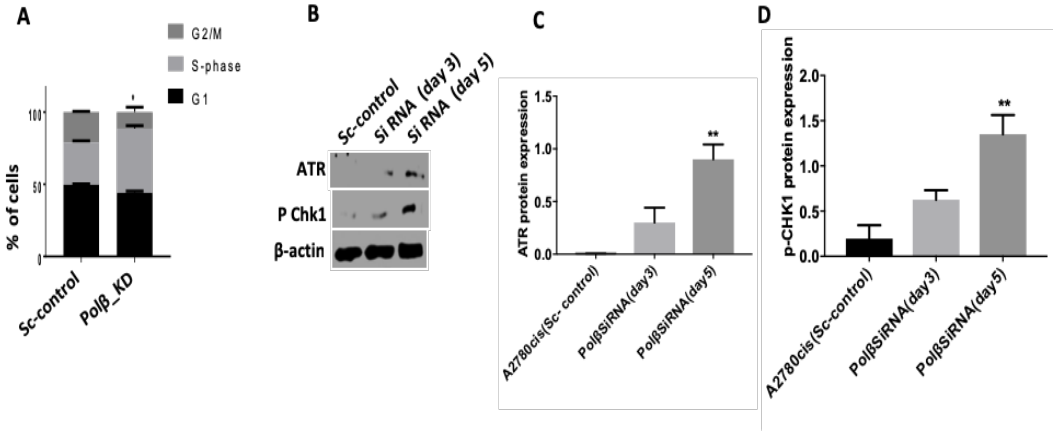


Figure 6-14: Replication stress in A2780cis_polβ _KD cells.
(A)Cell cycle analysis by flow cytometry for A2780cis (scrambled control) and polβ_KD cells. Western blot images (B) and protein quantification (C) and (D) for A2780cis scrambled control transfected and A2780cis_ polβ_KD cells collected on day 3 and day 5.

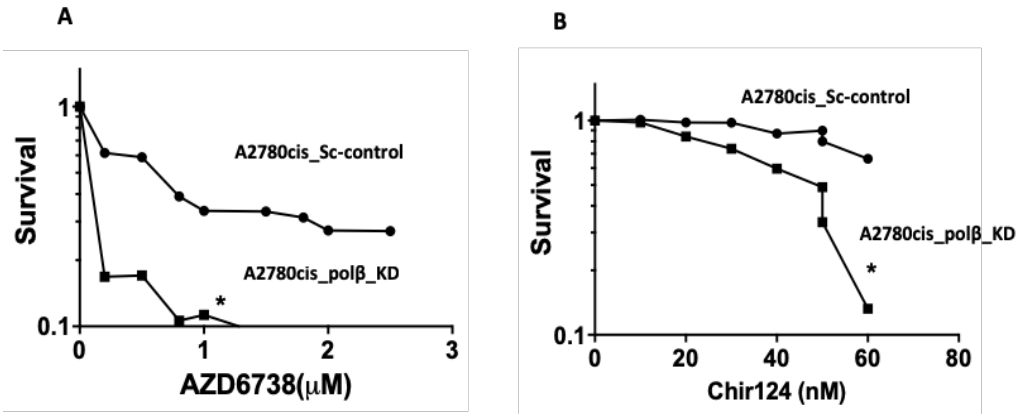


Figure 6-15: Clonogenic survival assay for ATRi and CHK1i in polβ _KD cells. (A)AZD6738 (ATR inhibitor) sensitivity in A2780cis scrambled control cells and A2780cis polβ_KD cells. (B) Chir124 (CHK1 inhibitor) in A2780cis_polβ_KD cells.

The overexpression in ATR and p-CHK1 protein levels was associated with increased sensitivity to ATR inhibition by AZD6738 and CHK1 inhibition by Chir124 in A2780cis_polβ_KD cells in comparison to the control cells (Figure 6-15). These data confirm a fundamental role for ATR and CHK1 in the survival of polβ deficient cells.

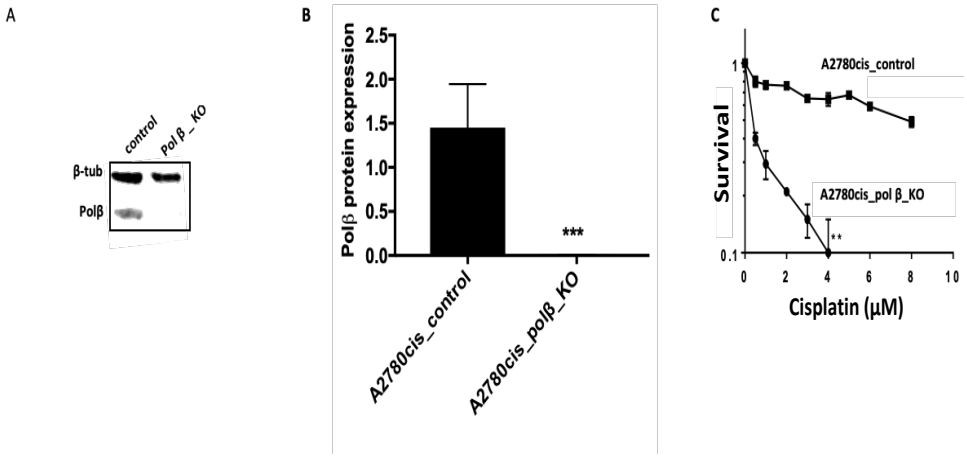


Figure 6-16: Polβ knock-out in A2780cis cells.
(A)Western blot showing polβ_KO by CRISPRcas9 in A2780cis cells. (B) Quantification of polβ protein levels relative to β-tubulin by western blot. (C)Clonogenic survival assay for A2780cis control and polβ_knock out in different doses of cisplatin.

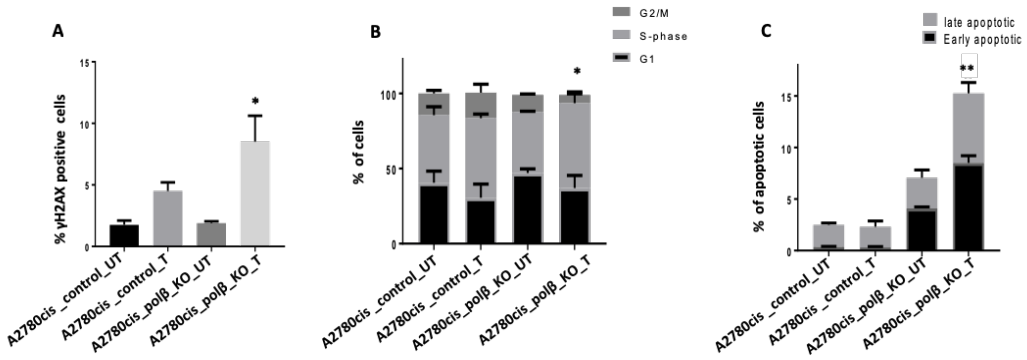


Figure 6-17: Functional studies for cisplatin sensitivity in A2780cis polβ _KO.

γH2AX analysis by flow cytometry (A), cell cycle analysis by flow cytometry (B) and annexin V apoptosis analysis (C) for A2780cis cells control and polβ_knock-out cells treated with 5μM cisplatin for 24 hours. A2780cis control and A2780cis_polβ_KO cells were plated in 6-well plates overnight. Cells were treated with cisplatin(5μM) for 24 hours. After incubation with cisplatin, cells were collected by trypsinization and stained as per the flow cytometry staining protocol described previously in the Methods section.

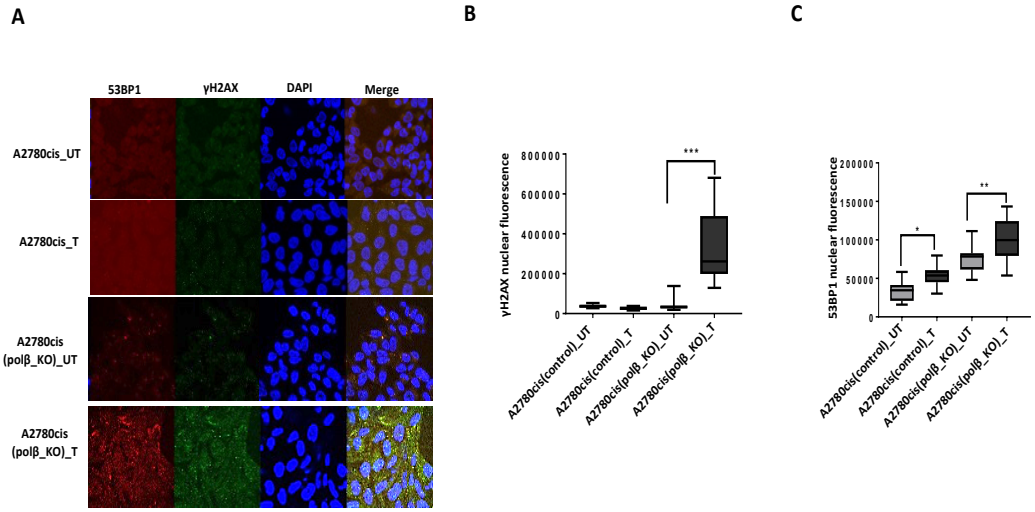


Figure 6-18: Immunofluorescence staining for γH2AX and 53BP1 in A2780cis cells. (A)Representative photomicrographic images for γH2AX and 53BP1 staining in A2780cis control and polβ KO treated with cisplatin for 24 hrs. (B) Quantification of γH2AX nuclear fluorescence by ImageJ software. (C) Quantification of 53BP1 nuclear fluorescence by ImageJ software. A2780cis control and polβ KO cells were plated on coverslips overnight, then treated with cisplatin 5μM for 24 hrs. After incubation with platinum, cells were fixed with 4% paraformaldehyde and stained with 53BP1 and γH2AX antibodies as per the immunofluorescence protocol described in the Methods. For analysis, minimum of 50 cells were counted. Images and quantification are representative of three independent experiments.

We aimed to validate the finding of cisplatin sensitivity in A2780cis_polβ_KD in another polβ deficient model. Therefore, we generated polβ CRISPR knock-out in A2780cis. The knockout efficiency was validated by western blot (Figure 6-16). A2780cis_polβ_KO cells are sensitive to cisplatin, as shown in the clonogenic survival assay (Figure 6-16). Cisplatin treatment in A2780cis_polβ_KO led to the accumulation of double strand breaks and cell cycle arrest in S-phase as well as apoptotic cell accumulation (Figure 6-17). We confirmed DSBs accumulation by immunofluorescence staining for γH2AX and 53BP1 in A2780cis control and polβ KO treated with cisplatin. We observed an increase in γH2AX and 53BP1 nuclear fluorescence after 24 hrs of cisplatin treatment in A2780cis_polβ_KO cells but not in control cells (Figure 6-18).

These results imply the potential of polβ inhibition in the sensitization of ovarian cancer cells to cisplatin. We used additional platinum resistant ovarian cell line (PEO4) cells and evaluated the effect of polβ knock-down by siRNA on cisplatin response. As shown in (Figure 6-19), polβ knock-down sensitizes PEO4 cells to cisplatin compared to control cells. Functional analysis of PEO4_polβ_KD cells treated with cisplatin revealed the accumulation of γH2AX positive cells, which indicated an increase of double strand breaks as well as cell cycle arrest in the S-phase. Unrepaired double strand-breaks and cell cycle arrest lead to cell death by apoptosis as observed in annexin V assay analysis (Figure 6-20). We confirmed DSBs accumulation by immunofluorescence staining for γH2AX and 53BP1 in PE04

control and polβ KD treated with cisplatin. We observed an increase in γH2AX and 53BP1 nuclear fluorescence after 24 hrs of cisplatin treatment in PE04_polβ_KD cells but not in control cells (Figure 6-21).

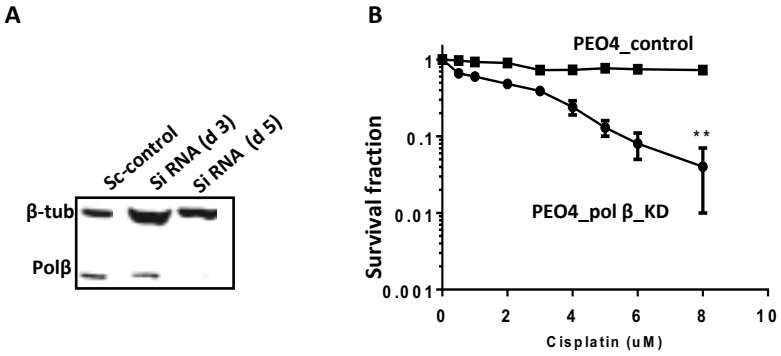


Figure 6-19: Polβ knockdown in PEO4 ovarian cells.
(A)Western blot for polβ siRNA in PEO4 cells on day 3 and day 5. β-tubulin was used as a loading control. (B) Clonogenic survival assay for cisplatin sensitivity in PEO4 polβ_KD cells.

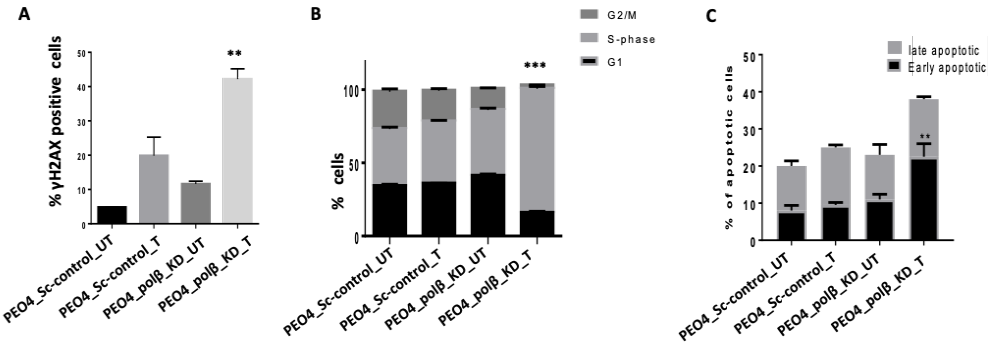


Figure 6-20: Functional studies for cisplatin sensitivity in PEO4_polβ_KD cells. γH2AX analysis by flow cytometry (A), cell cycle analysis by flow cytometry (B) and annexin V apoptosis analysis (C) for PEO4 control and polβ_KD cells treated with 5μM cisplatin for 24 hours. Cells were plated overnight inT25 flasks and transfected with scrambled control or polβ siRNA using lipofectamine3000. On day 3, cells were trypsinised and re-plated in 6-well plates overnight. Cells were treated with 5μM cisplatin or left untreated. On day 5, cells were collected and stained according to the flow cytometry protocol described in the Methods section.

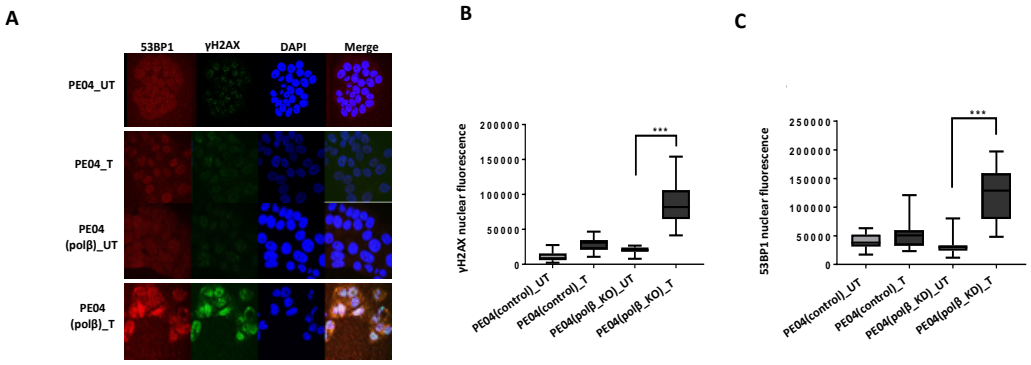


Figure 6-21: Immunofluorescence for γH2AX and 53BP1 nuclear staining in PE04 cells.

(A)Representative photomicrographic images for γH2AX and 53BP1 staining in PE04 control and polβ KD treated with cisplatin for 24 hrs. (B) Quantification of γH2AX nuclear fluorescence by ImageJ software. (C) Quantification of 53BP1 nuclear fluorescence by ImageJ software. PE04 control and polβ KD cells were plated on coverslips overnight, then treated with cisplatin 5μM for 24 hrs. After incubation, cells were fixed with 4% paraformaldehyde and stained with 53BP1 and γH2AX antibodies as per the immunofluorescence protocol described in the Methods. For analysis, a minimum of 50 cells were counted. Images and quantifications are representative of three independent experiments.

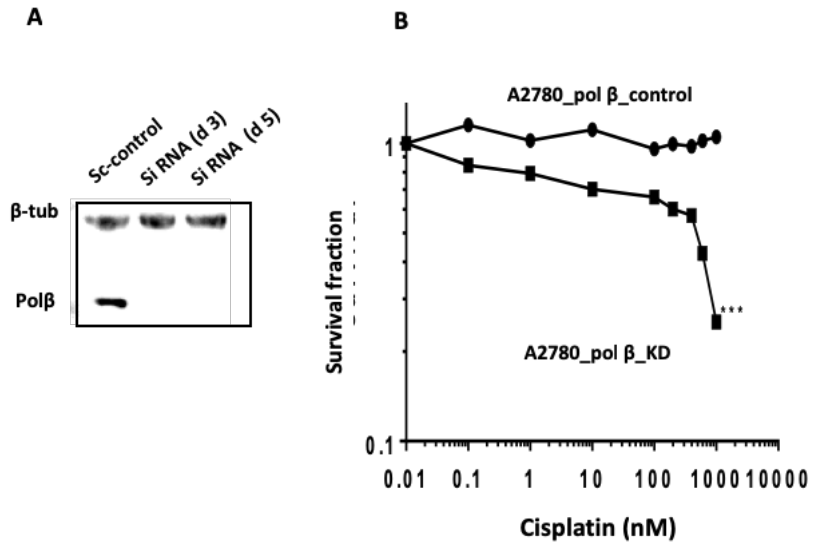


Figure 6-22: Polβ siRNA knockdown in A2780 cells.

(A)Western blot for polβ siRNA in A2780 cells. β-tubulin was used as a loading control. (B) Clonogenic survival assay for cisplatin sensitivity in A2780 control and polβ_KD cells.

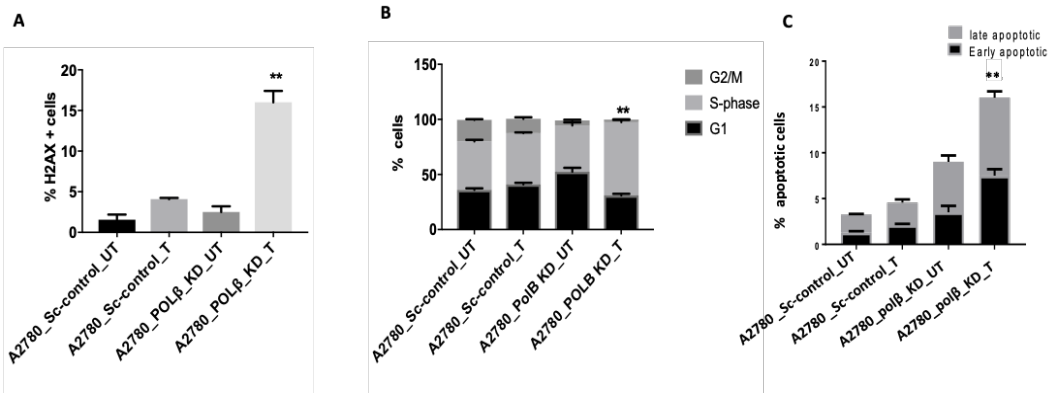


Figure 6-23: Functional studies for cisplatin sensitivity in A2780_polβ_KD cells. γH2AX analysis by flow cytometry (A), cell cycle analysis by flow cytometry (B) and annexin V apoptosis analysis (C) for A2780 control and polβ_KD cells treated with 1μM cisplatin for 24 hours.

To study the effect of polβ knockdown on cisplatin-sensitive ovarian cell lines, we knocked down polβ by siRNA in A2780 (platinum sensitive) cells. A robust knockdown was achieved as seen in (figure 6-22). A2780_polβ_KD cells are sensitive to cisplatin even at nanomolar concentrations in clonogenic assays (Figure 6-22). Flow cytometry analysis showed substantial S-phase cell cycle arrest in A2780_polβ_KD cells treated with 1μM cisplatin. Low dose cisplatin treatment (1μM) led to significant γH2AX formation and the accumulation of apoptotic cells (Figure 6-23). Similar to A2780cis, we generated CRISPR cas9 knock-out of polβ in A2780 cells and confirmed cisplatin sensitivity in A2780_polβ_KO. As expected, A2780_polβ_KO cells are sensitive to cisplatin (Figure 6-24) and have a similar phenotype to transient knockdown cells (Figure 6-25).

We confirmed DSB accumulation by immunofluorescence staining for γH2AX and 53BP1 in A2780 control and polβ KO cells treated with cisplatin. We observed an increase in γH2AX and 53BP1 nuclear fluorescence after 24 hrs of cisplatin treatment in A2780_polβ_KO cells but not in control cells (Figure 6-26).

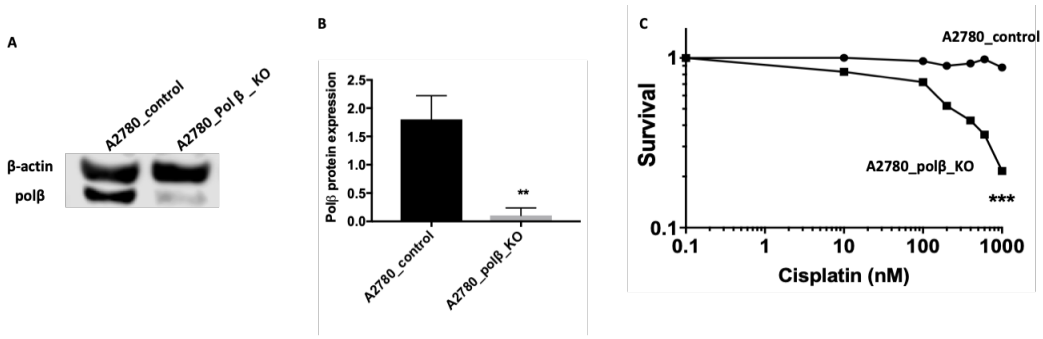


Figure 6-24: Polβ CRISPR_KO in A2780 cells.
(A)Western blot for polβ CRISPR_KO in A2780 cells. (B) Quantification of polβ protein expression by western blot. (C) Clonogenic survival assay for cisplatin sensitivity in A2780_polβ_KO cells.

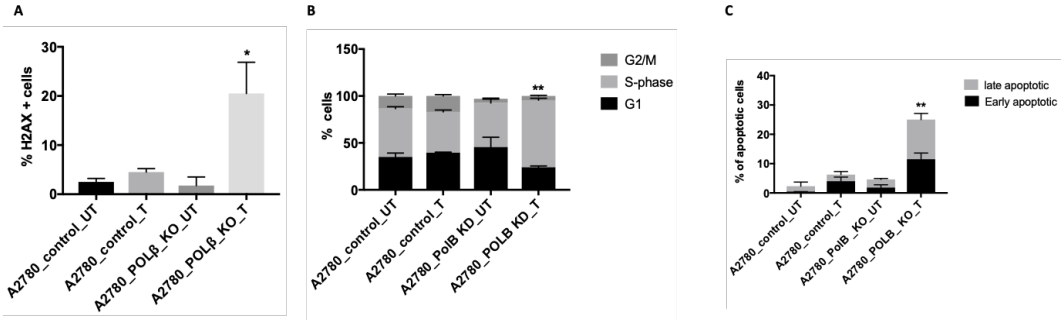


Figure 6-25: Functional studies of cisplatin sensitivity in A2780_polβ _KO cells. γH2AX analysis by flow cytometry (A), cell cycle analysis by flow cytometry (B) and annexin V apoptosis analysis (C) for A2780 control and polβ_KO cells treated with 1μM cisplatin for 24 hours.

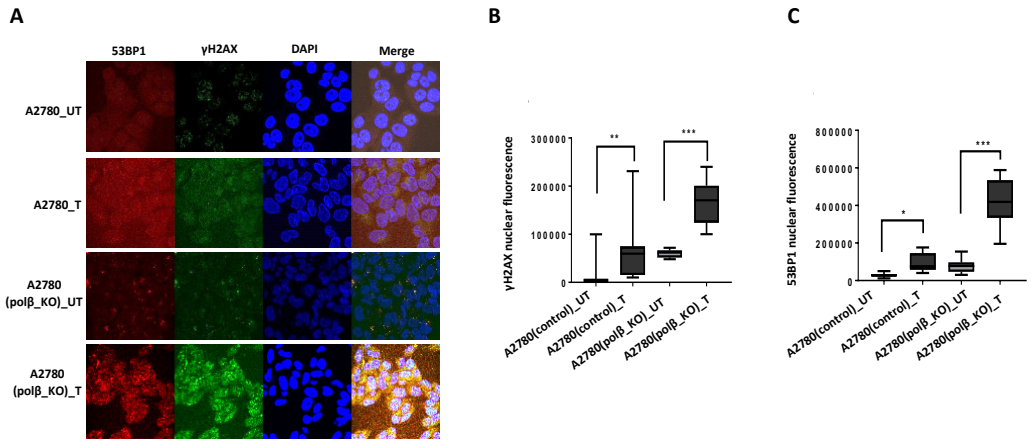


Figure 6-26: Immunofluorescence for γH2AX and 53BP1 nuclear staining in A2780 cells.
(A)Representative photomicrographic images for γH2AX and 53BP1 staining in A2780 control and polβ KO treated with cisplatin for 24 hrs. (B) Quantification of γH2AX nuclear fluorescence by ImageJ software. (C) Quantification of 53BP1 nuclear fluorescence by ImageJ software. A2780 control and polβ KO cells were plated on coverslips overnight, then treated with cisplatin 5μM for 24 hrs. After incubation with platinum, the cells were fixed with 4% paraformaldehyde and stained with 53BP1 and γH2AX antibodies as per the immunofluorescence protocol described in the Methods. For analysis, a minimum of 50 cells were counted. Images and quantification are representative of three independent experiments.

6.3.2.3 Mesenchymal to epithelial transition phenotype in polβ_knock out cells.

Invasion of ovarian cancer cells from the primary tumour site to the distal organs is a hallmark of ovarian cancer, where ovarian cancer multicellular spheroids passively move within the peritoneal fluid or ascites (Awasthi, Foiani and Kumar, 2015). We observed the effect of polβ inhibition on re-sensitization of ovarian cancer cell lines to cisplatin. Thus, we hypothesised that polβ inhibition could reduce the invasive phenotype of ovarian cancer cell lines. Comparison of

A2780_polβ_KO to control A2780 cells showed that polβ_KO reduced A2780 cells' ability to invade (Figure 6-27). Although A2780cis cells have lower invasion ability than A2780 cells (Figure 6-27), Polβ_KO in those cells significantly reduced their invasion ability compared to control A2780cis cells.

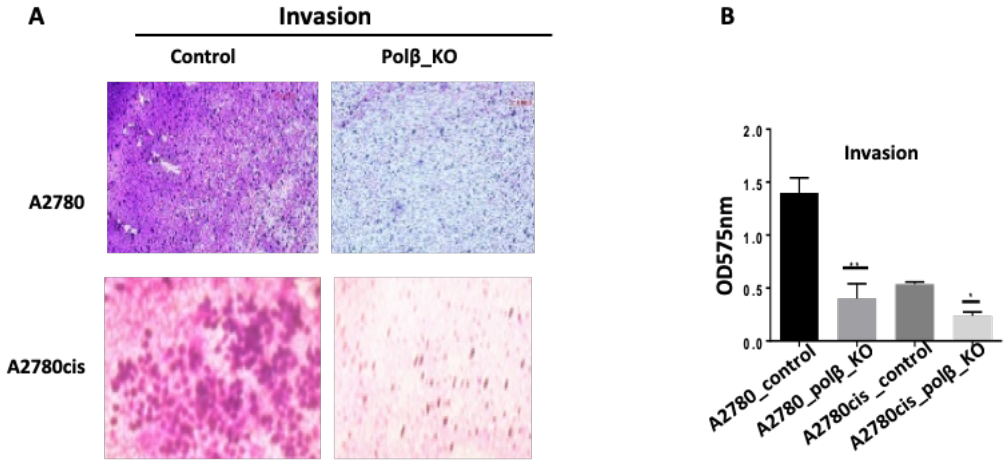


Figure 6-27: Invasion assay in polβ KO cells.
(A)Representative photomicrographic images of invasion assay in A2780 and A2780cis control and polβ_KO cells. Invasive cells were stained with crystal violet and images were taken with Nikon camera microscope (20X magnification). (B) Quantification of stained invasive cells at optical density (575 nm). Invasive cells were dissociated from the inserts using cell extraction solution (provided by the kit) then 100μL were transferred to a 96-well plate, and absorbance were measured using microplate reader.

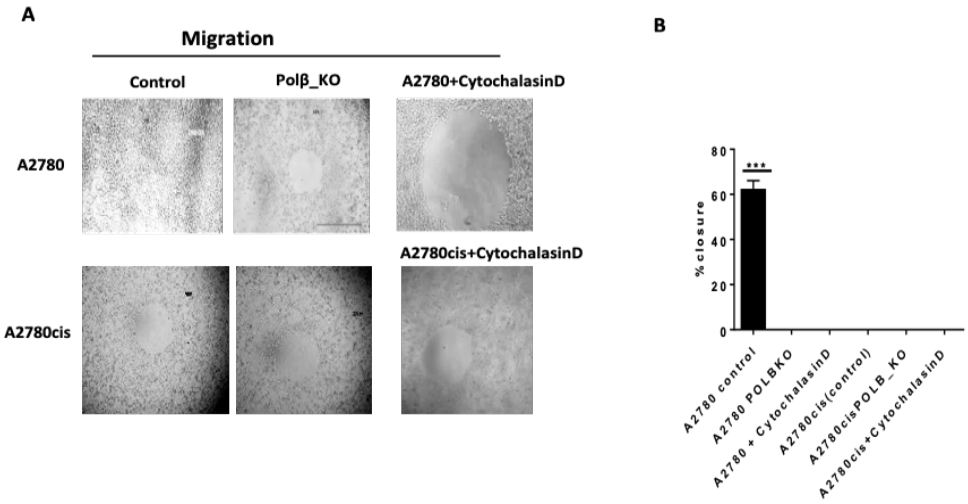


Figure 6-28: Migration assay in polβ _KO cells.
A) Representative photomicrographic images of migration assay in A2780 and A2780cis control and polβ_KO cells. (B) Percentage closure quantification by ImageJ software in A2780 and A2780cis control and polβ_KO cells. Cells treated with Cytochalasin D (1.5μM) were used as a negative control.

We evaluated polβ_KO cells' migration ability. A2780_polβ_KO cells have a substantial reduction in migration compared to A2780 control cells (Figure 6-28). Interestingly, A2780cis have no migration ability (Figure 6-28). Thus, we could not confirm the effect of polβ _KO on their migration capacity.

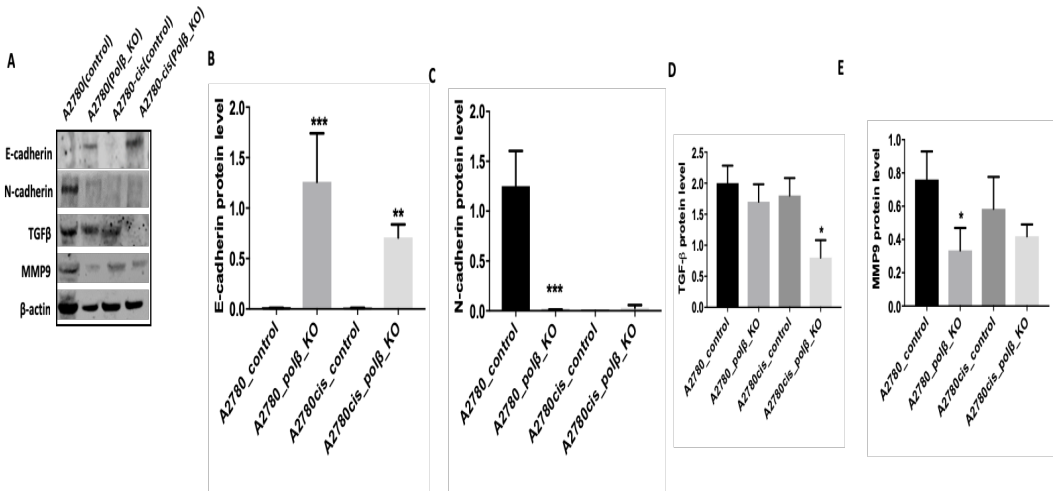
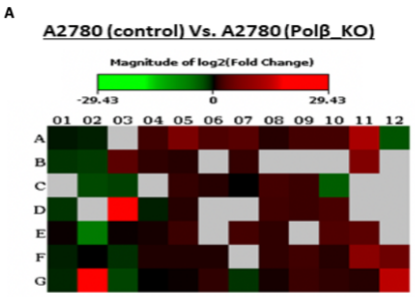


Figure 6-29: Western blots for E-cadherin, N-cadherin, TGFβ and MMP-9 in A2780 and A2780cis control and polβ _KO cells.
(A)Representative images for western blot showing E-cadherin, N-cadherin, TGFβ and MMP-9 protein levels in A2780 and A2780cis control and polβ _KO. Quantification of protein levels by western blot for: E-cadherin (B), N-cadherin (C), TGFβ (D) and MMP-9 (E) in A2780 and A2780cis control and polβ_KO. β-actin was used as a loading control.



B

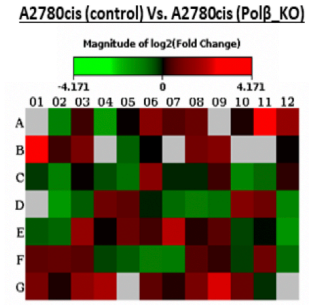
Grid position	Down-regulated
A12	COL3A1
B1	COL5A2
B2	CTNNB1
C02	GSC
C03	GSK3B
C10	JAG1
D01	KRT7
E02	DESI1
F03	SPP1
G03	TSPAN13
G07	VPS13A
H02	B2M

C

Grid position	Up-regulated
A05	BMP7
A11	COL1A2
B11	FOXC2
D03	MMP2
E10	SNAI1
E11	SNAI2
F11	TGFB3
F12	TIMP1
G02	TMEM132A
G12	ZEB2
H01	ACTB
H10	RTC
H11	PPC

Figure 6-30: RT2 PCR profiler for EMT genes in A2780 control and polβ_KO.
(A)Heat map demonstrating up-regulated and down-regulated genes in fold change in A2780_polβ_KO cells compared to control cells. (B) List of the top down-regulated genes in A2780_polβ_KO cells. (C) List of the top up-regulated genes in A2780_polβ_KO cells. RT2-PCR analysis and normalisation against *GADPH* housekeeper expression was performed in Qiagen website.

A



B

Grid position	Down-regulated
A04	BMP2
D02	MAP1B
E11	SNAI3
F07	TCF4

C

Grid position	Up-regulated
A11	COL1A2
B01	COL5A2
E07	SERPINE1
G09	WNT5A

Figure 6-31: RT2 PCR profiler in A2780cis control and polβ _KO cells. (A)Heat map demonstrating up-regulated and down-regulated genes in fold change in A2780_polβ_KO cells compared to control cells. (B) List of the top down-regulated genes in A2780_polβ_KO cells. (C) List of the top up-regulated genes in A2780_polβ_KO cells. RT2-PCR analysis and normalisation against *GADPH* housekeeper expression was performed in Qiagen website

Altered cadherin levels in epithelial to mesenchymal transition (EMT) phenotype have been extensively reported before (Fang *et al.*, 2017). Also, TGFβ and matrix metalloproteinase signalling have direct roles in EMT regulation (Alsina-Sanchís *et al.*, 2017). Therefore, we anticipated that polβ depletion leads to an alteration in the levels of these genes and affects the invasion and migration phenotype of the polβ_KO cells. Western blot analysis showed an increase in E-cadherin levels in both A2780_polβ_KO and A2780cis_polβ_KO cells, while N-cadherin protein levels were only detected in A2780 control cells and significantly diminished in A2780_polβ_KO cells. TGFβ and MMP-9 levels significantly decreased in both A2780_polβ_KO and A2780cis_polβ_KO cells (Figure 6-29).

To confirm whether these changes in protein levels are associated with changes at mRNA levels, RT2-PCR profiler arrays for EMT genes were used. The RT2-PCR profiler arrays are a high throughput screening assay that detects the mRNA levels

of 84 pathway specific related genes simultaneously (detailed in the Methods chapter). EMT gene screening analysis comparing A2780_polβ_KO cells to their parental control cells revealed down-regulation of some key EMT genes including (*COL3A1, COL5A2, CTNNB1, GSC* and *GSK3B*) (Figure 6-30B). Besides, we observed up-regulation in other EMT regulators including (*COl1A2, BMP7, MMP2, SNAI1, SNAI2* and *TGFB3*) (Figure 6-30C). A2780cis control cells showed previously low invasion and migration ability. RT2-PCR profiling of EMT genes in A2780cis_polβ_KO demonstrated down-regulation of fewer essential genes including (*BMP2, MAP1B, SNAI3& TCF4*) (Figure 6-31B) as well as up-regulation of other EMT drivers including (*COL1A2, COL5A2, SERPINE1 &WNT5A*) (Figure 6-31C). Taken together, these data suggest a complex role for polβ in the regulation of EMT phenotype.

6.3.2.4 Polβ depletion induces synthetic lethality in BRCA2 deficient ovarian cells

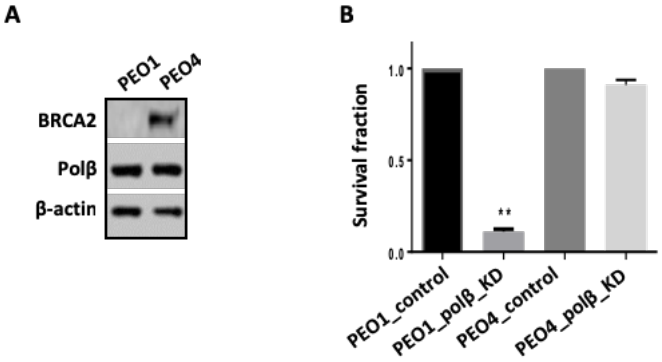


Figure 6-32: Synthetic lethality of polβ knockdown in BRCA2 deficient cells.

(A) Western blot showing the levels of BRCA2 and polβ in PE01 and PE04 cells. (B) MTS proliferation assay for PE01 and PE04 control and polβ_ KD cells. PE01 and PE04 cells were plated overnight in T25 flasks. Cells were transfected with scrambled control or polβ siRNA using lipofectamine3000 reagent in Opti-mem low serum medium. On day 2, cells were trypsinised and re-plated in 96-well plates overnight. On day 7, cell viability was determined using MTS cell Titer 96-Aqueous one solution (Promega).

Targeting BRCA2 deficient ovarian tumours with PARP inhibitors is a very successful application for synthetic lethality in clinic. However, different resistance mechanisms to PARP inhibitors have been reported. Therefore, exploiting other synthetic lethality approaches is an un-met need. We explored the concept of synthetic lethality of polβ depletion in BRCA2 deficient ovarian cell lines. PEO1 cells derived from a patient who had BRCA2 mutation and was platinum sensitive. After recurrence, the patient had another mutation reverted BRCA2 expression and became platinum resistant and the PE04 cell line was taken from the recurrent tumour. Polβ knockdown in PE01 cells led to a significant reduction in cell viability while polβ depletion did not affect PE04 cell viability (Figure 6-32).

Polβ depletion leads to impairment of the base excision repair pathway and formation of single strand breaks. BRCA2 deficient cells have impaired homologous recombination, and therefore, double strand breaks will persist and cause lethality. PE01 _polβ_KD cells have an accumulation of double strand breaks as evidenced by the increase in γH2AX levels. PE01_polβ_KD cells arrest substantially in the S-phase, leading to apoptotic cell death as observed in annexin V analysis (Figure 6-33).

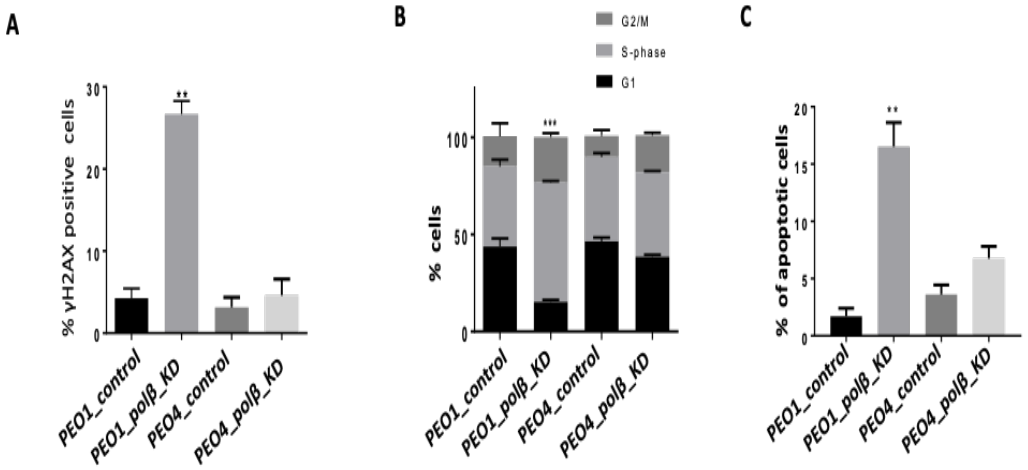


Figure 6-33: Functional studies of polβ synthetic lethality with BRCA2.

γH2AX analysis by flow cytometry (A), cell cycle analysis by flow cytometry (B) and annexin V apoptosis analysis (C) for PE01 and PE04 control and polβ_KD cells.

6.3.2.5 Synthetic lethality of pamoic acid in BRCA2 deficient PE01 cells

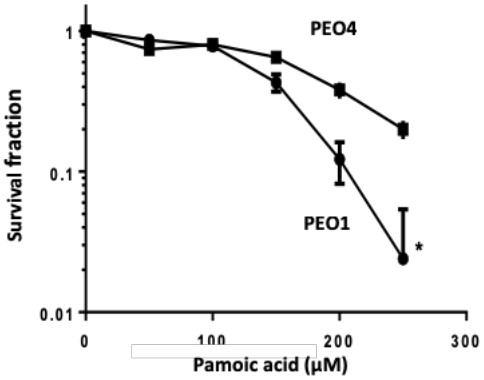


Figure 6-34: Pamoic acid sensitivity in PE01 and PE04.

Clonogenic survival assay for PE01 and PE04 treated with different doses of pamoic acid. Cells were plated in 6-well plates overnight. For PE01 cells, 1000 cells/well were plated. For PE04 cells, 350 cells/well were plated. Cells were treated the following day with the indicated doses of pamoic acid and left in the incubator for three weeks to form colonies.

Pamoic acid is a previously described small molecule inhibitor for polβ (Jaiswal *et al.*, 2015). We tested the synthetic lethality of pamoic acid in BRCA2 deficient (PE01) and BRCA2 proficient cells (Figure 6-34). Similar to polβ knock-down, polβ inhibition has a comparable synthetic lethality effect in BRCA2 deficient PE01 cells. PE01 cells were more sensitive to pamoic acid than PE04 as it reduced its ability to form colonies (Figure 6-34) Pamoic acid treatment led to increased DNA damage, S-phase cell cycle arrest and formation of apoptotic cells in PE01 cells but not in PE04 cells (Figure 6-35).

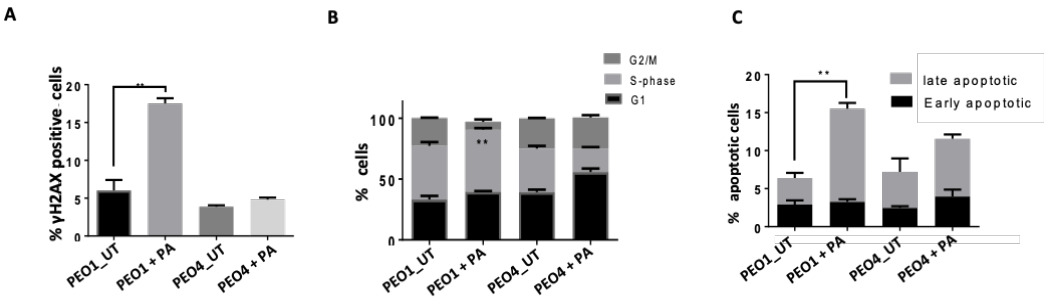


Figure 6-35: Functional study of pamoic acid synthetic lethality in PE01 cells. γH2AX analysis by flow cytometry (A), cell cycle analysis by flow cytometry (B) and AnnexinV apoptosis analysis by flow cytometry in PE01 and PE04 treated with pamoic acid for 24 hrs. PE01 and PE04 cells were plated in 6-well plates overnight. Cells were treated with pamoic acid (250μM) for 24 hours. After incubation, cells were trypsinised, and the flow cytometry staining protocol was followed, as described in the Methods section.

6.3.2.6 Evaluation of pamoic acid synthetic lethality in HeLa BRCA2 deficient cells

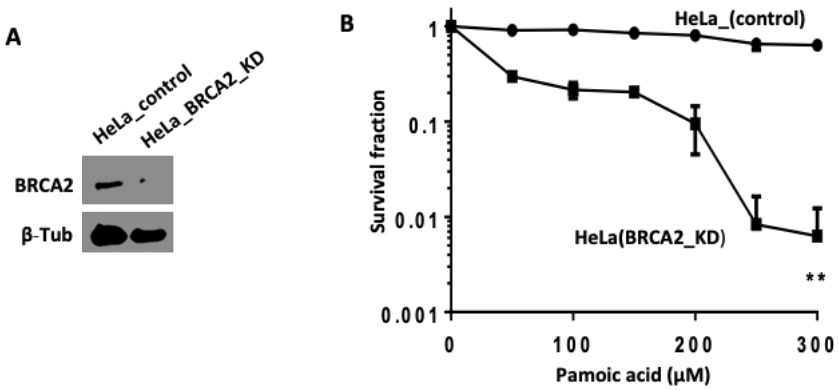


Figure 6-36: Pamoic acid sensitivity in HeLa BRCA2 deficient cells. (A)Western blot showing BRCA2 protein levels relative to β-tubulin in HeLa control and HeLa BRCA2 SilenciX cells. (B) Clonogenic survival assay for HeLa control and HeLa BRCA2 deficient treated with the indicated doses of pamoic acid.

To further validate the synthetic lethality of polβ inhibition in BRCA2 deficient cells, we used HeLa BRCA2 silenciX cells. HeLa BRCA2 is sensitive to polβ inhibition

by pamoic acid, as shown in the clonogenic survival assay (Figure 6-36). Pamoic acid sensitivity in HeLa BRCA2 deficient cells was also associated with the accumulation of double strand breaks, S-phase cell cycle arrest and apoptosis (Figure 6-37).

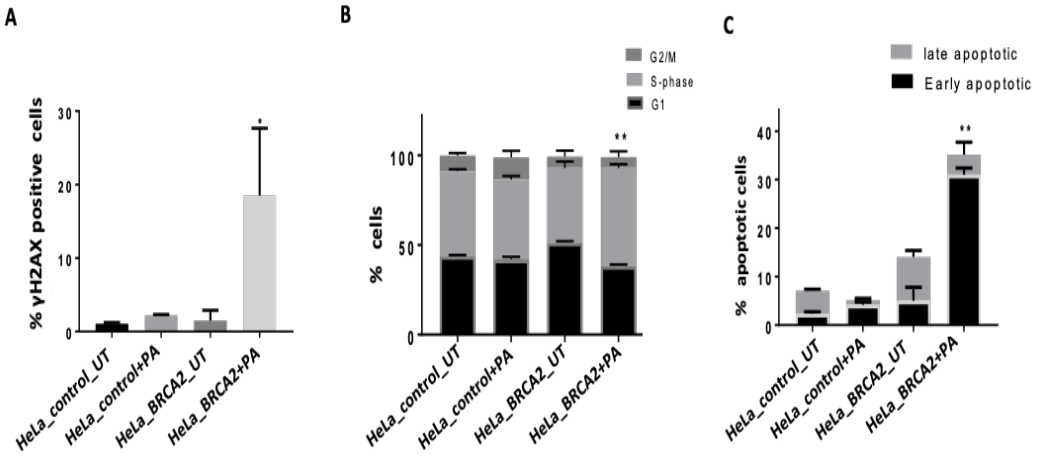


Figure 6-37: Functional studies for pamoic acid sensitivity in HeLa BRCA2 deficient cells.
γH2AX analysis by flow cytometry (A), cell cycle analysis by flow cytometry (B) and AnnexinV apoptosis analysis by flow cytometry (C) in HeLa control and HeLa BRCA2 deficient cells. HeLa control and HeLa BRCA2_KD cells were plated in 6-well plates overnight. The following day cells were treated with pamoic acid (250μM) for 24 hours. After incubation with the drug, cells were collected by trypsinization and stained as described in the flow cytometry staining protocol described in the Methods.

6.3.2.7 Evaluation of NSC666719 polβ small molecule inhibitor for synthetic lethality in BRCA2 deficient cells

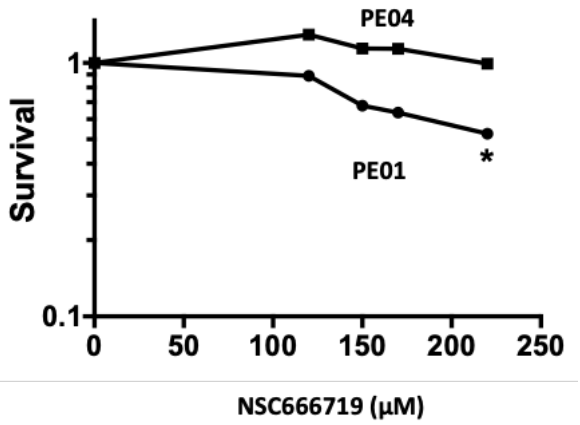


Figure 6-38: NSC666719 sensitivity in PE01 and PE04 cells.

PE01 and PE04 were plated in 6-well plates overnight for clonogenic survival assay. Cells were treated with the indicated doses of NSC666719 then left to form colonies for three weeks. Colonies were washed with PBS and stained with crystal violet, methanol and acetic acid mixture.

We further validated another small molecule inhibitor for polβ NSC666719 [4-chloro-5-methyl-N-[5-(naphthalen-2-ylamino)-1H1,2,4-triazol-3-yl]-2 sulfanylbenzenesulfonamide for synthetic lethality in BRCA2 deficient PE01 cells. NSC666719 affected PE01 cell survival in the clonogenic survival assay compared to BRCA2 proficient PE04 cells (Figure 6-38). Flow cytometry staining of γH2AX demonstrated a significant DNA damage in PE01 cells treated with NSC666719 but not in treated PE04 cells. Treated PE01 cell arrest in the G2/M phase leads to significant apoptotic cell death (Figure: 6-39).

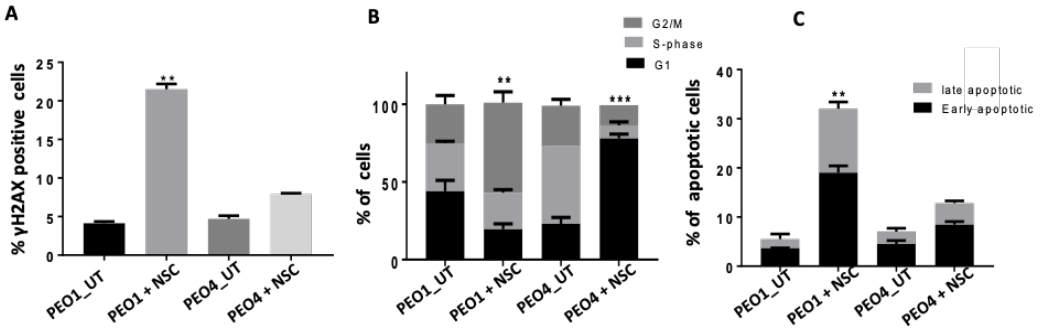


Figure 6-39: Functional study of NSC666719 synthetic lethality in PE01 cells. γH2AX analysis by flow cytometry (A), cell cycle analysis by flow cytometry (B) and annexin V apoptosis analysis by flow cytometry (C) in PE01 and PE04 cells treated with NSC666719 (250 μM) for 24 hours.

6.3.2.8 Synthetic lethality of polβ inhibitors in 3D spheroid models of BRCA2 deficient cells

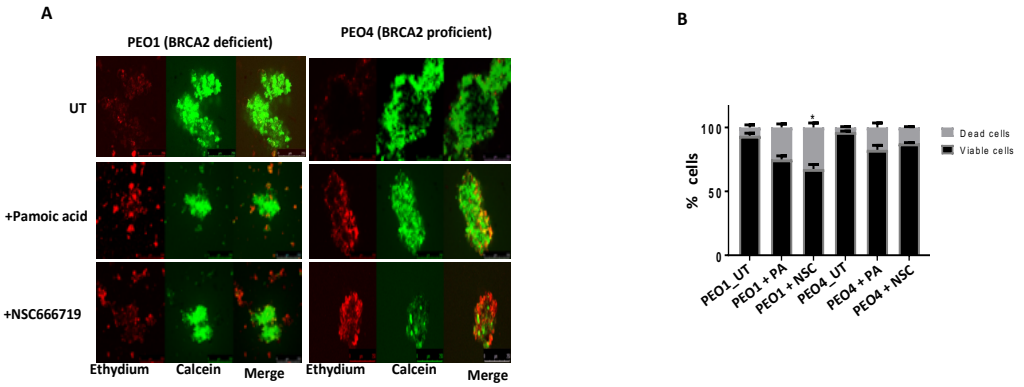


Figure 6-40: Polβ inhibitors in 3D spheroids of PE01 and PE04 cells. (A)Representative photomicrographic images of 3D spheroids of PE01 and PE04 treated with Pamoic acid (250 μM) or NSC666719 (250 μM). (B) Quantification of viable and dead cells with flow cytometry. PE01 and PE04 cells (5 x10^4 cells /well) were seeded in ultra-low attachment 6-well plates. Cells were left to form spheres for three weeks. 3D-structures were treated with the indicated doses of polβ inhibitors for 48 hours. Then structures were fixed with 37% formaldehyde for 30 mins and stained with calcein AM (2.5μM) and ethidium homodimer (1.5μM). Imaging was performed on a Leica SP2 confocal microscope. ImageJ software was used for analysis.

To verify the observed synthetic lethality of polβ inhibitors in BRCA2 deficient cells, we tested polβ inhibitors in 3D spheroids of BRCA2 deficient (PE01 and HeLa BRCA2_KD cells) and BRCA2 proficient (PE04 and HeLa control cells) 3D spheroids to mimic an *in vivo* tumour model. 3D spheroids were treated with pamoic acid (250μM) or NSC666719 (250μM). Interestingly, polβ inhibitors increased cell death in BRCA2 deficient 3D spheroids, PE01 (Figure 6-40) and HeLa_BRCA2_KD (Figure 6-41), while also leading to a visible reduction in spheroid size. Flow cytometry quantification of viable/dead cells using calcein AM and ethidium homodimer respectively demonstrated an increase in ethidium staining in PE01 and HeLa_BRCA2_KD cells treated with pamoic acid or NSC666719.

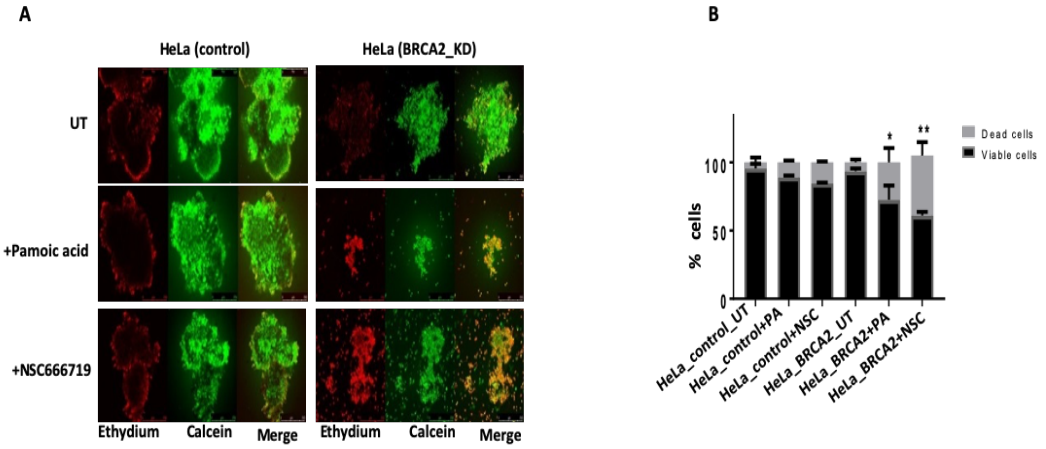


Figure 6-41: polβ inhibitors in 3D spheroids of HeLa control and HeLa_BRCA2_KD. (A)Representative photomicrographic images of 3D spheroids of HeLa control and HeLa_BRCA2_KD treated with Pamoic acid (250 μM) or NSC666719 (250 μM). (B) Quantification of viable and dead cells by flow cytometry.

6.3.2.9 Evaluation of Olaparib effect in polβ deficient ovarian cancer cells

PARP inhibitors have proven their efficacy in tackling BRCA deficient ovarian cancers. Several studies have concluded that Olaparib treatment significantly improved patient outcomes. Therefore, many studies are trying to identify which group of patients will benefit from PARP inhibitors. We investigated whether Olaparib can have a synthetic lethality application in polβ deficient tumours. A2780 and A2780cis control and polβ_KO were treated with different doses of Olaparib in a clonogenic survival assay. Surprisingly, both platinum sensitive and platinum resistant polβ_KO cells did not have any sensitivity to Olaparib treatment (Figure 6-42). Upon DNA damage, PARP1 catalyses the addition of poly (ADP) ribose polymers (PAR) on itself and on key nuclear proteins including histones, DNA polymerases, topoisomerases and DNA ligase-2 to coordinate DNA repair (Underhill, Toulmonde and Bonnefoi, 2011). The formed (PAR) polymers can be hydrolysed by poly (ADP) ribose glycohydrolase (PARG) (Andrabi *et al.*, 2006). PDD00017273 is a previously described PARG inhibitor. We tested PDD00017273 (hereafter PARGi) sensitivity in polβ_KO cells. Interestingly, PARGi was selectively toxic in A2780 control and A2780cis polβ_KO cells (Figure 6-43). We validated that further in PE04 polβ siRNA_KD cells and they were selectively sensitive to PARGi more that control cells (Figure 6-43). We explored PAR polymer levels in A2780 and A2780cis control and polβ _KO. Western blot revealed that polβ _KO cells have a reduction in PAR polymers at the basal levels (Figure 6-44). PARP1 levels showed no significant difference between control and polβ _KO cells

(Figure 6-44). It is therefore anticipated that the difference in PAR polymer formation could be due to alterations in PARG activity in polβ _KO cells.

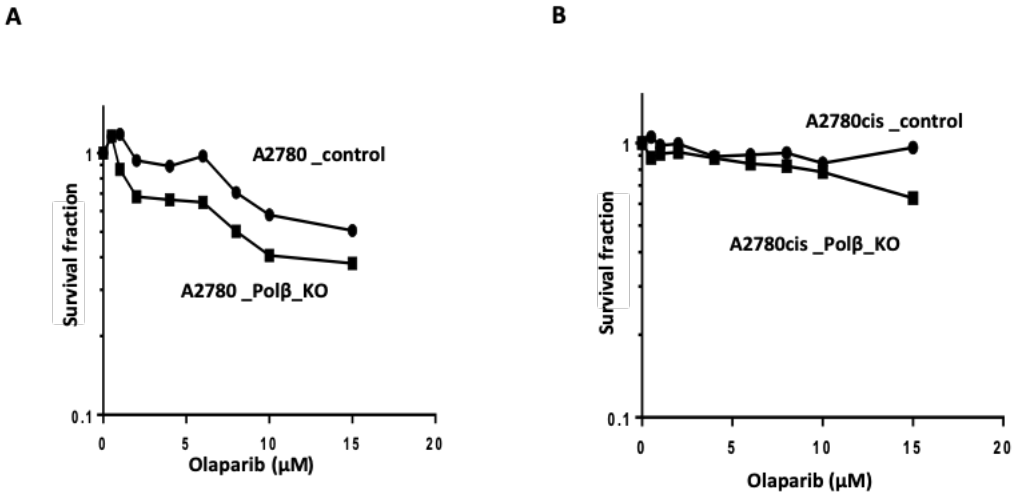


Figure 6-42: Olaparib treatment in polβ _KO cells.
(A)Clonogenic survival assay for A2780 control and polβ_KO in different doses of Olaparib. (B) Clonogenic survival assay for A2780cis control and polβ_KO treated with various doses of Olaparib.

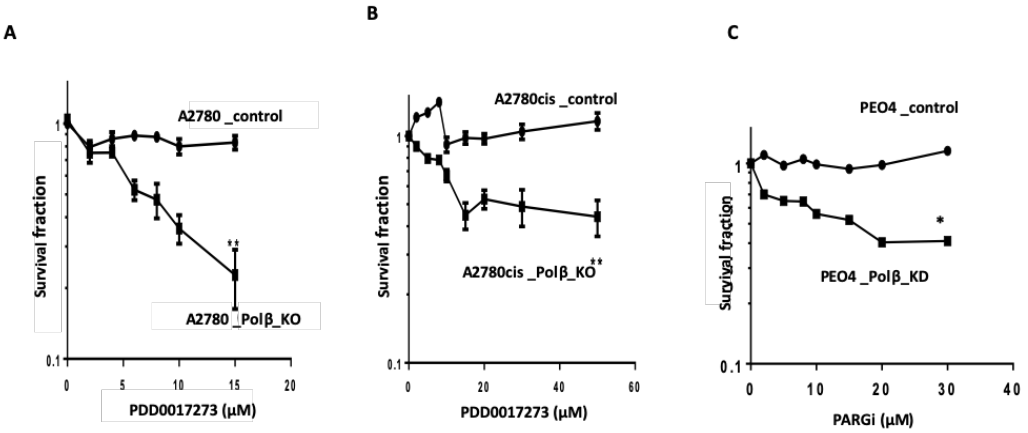


Figure 6-43: PDD0017273 sensitivity in Polβ deficient cells.
Clonogenic survival assay for A2780 control and polβ_KO (A), A2780cis control and polβ_KO (B) PE04 control and polβ _KD (C) in different doses of PARGi.

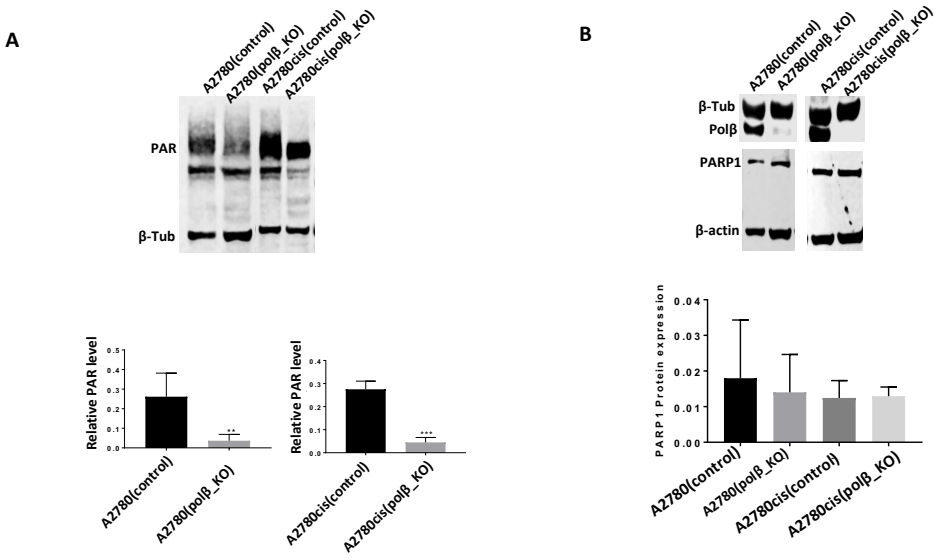


Figure 6-44: PAR and PARP1 protein levels in polβ _KO cells.
(A)Western blot and quantification of poly (ADP) ribose (PAR) polymers levels relative to β-tubulin, in A2780 and A2780cis control and polβ _KO cells. (B) Western blot and quantification of polβ and PARP1 protein levels relative to β-actin, in A2780 and A2780cis control and polβ _KO cells.

PAR polymer accumulation could be a death signal (Andrabi *et al.*, 2006). Therefore, we checked PAR levels upon Olaparib or PARGi treatment. PARP1 inhibition by Olaparib decreased PAR formation in both control and polβ_KO cells while PARGi increased the formation of PAR polymers, which manifested as a dark smear in the western blot (Figure 6-45). However, quantification of PAR levels showed more PAR accumulation in KO cells treated with PARGi.

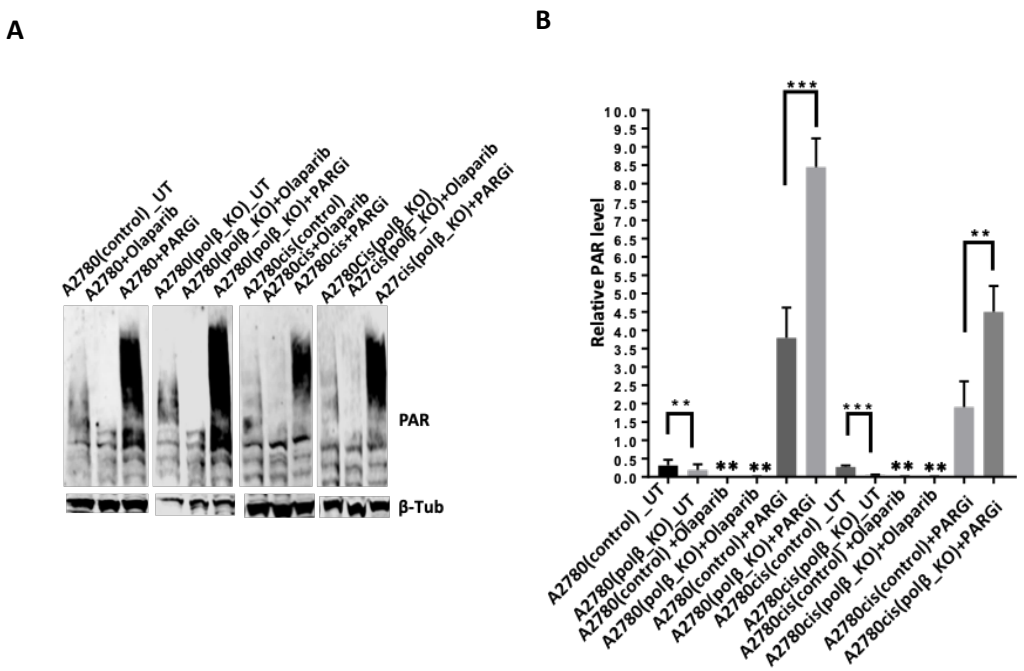


Figure 6-45: Western blot for PAR levels in treated polβ _KO cells.
(A)Western blot showing PAR polymer levels in A2780 and A2780cis control and polβ _KO cells untreated or treated with Olaparib (10μM) or with PARGi (20μM) for 16 hours. (B)PAR level quantification by western blot in A2780 and A2780cis control and polβ _KO cells untreated or treated with Olaparib or with PARGi. β-tubulin was used as a loading control.

We conducted an immunofluorescence study to monitor the formation of PAR polymers in A2780 control and A2780 (polβ_KO) cells. Following PARGi treatment, both A2780 control and A2780 (polβ_KO) accumulated PAR polymers at 6 hrs. However, that accumulation was transient in control cells, whereas PAR fluorescence decreased significantly at 24 hrs treatment. On the other hand, in polβ_KO cells PAR levels persisted at 24 hrs (Figure 6-46).

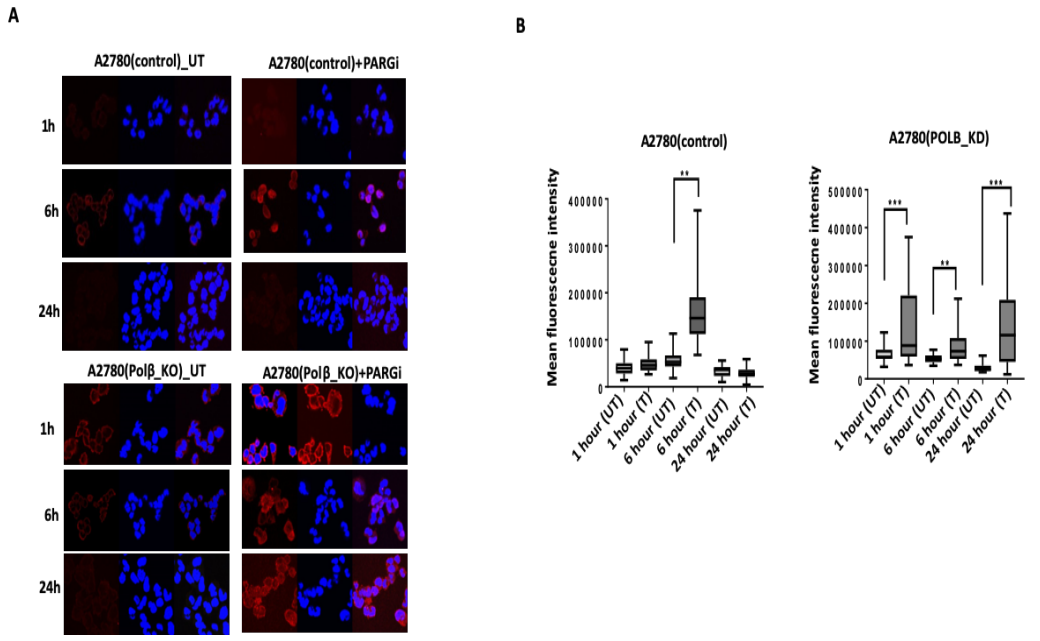


Figure 6-46: Immunofluorescence of PAR in A2780 control and A2780(polβ _KO) cells.

(A)Immunofluorescence staining for poly (ADP) ribose polymers in A2780 control and Polβ_knockout cells untreated or treated with PARGi (20 μM) for 1 h, 6 h and 24 h. (B) Quantification of Poly (ADP) ribose polymers fluorescence by ImageJ software. A2780 control and polβ_KO cells were seeded on coverslips overnight then treated with PARGi (20 μM). Cells were fixed with 4% paraformaldehyde (w/v) at 1h, 6h, and 24h as indicated. Cells were stained with anti-poly (ADP) ribose polymers antibody (1:500) dilution at 4°C overnight. Images were taken using a Leica SP2 confocal laser scanning microscope. For analysis, a minimum of 100 cells per slide were counted.

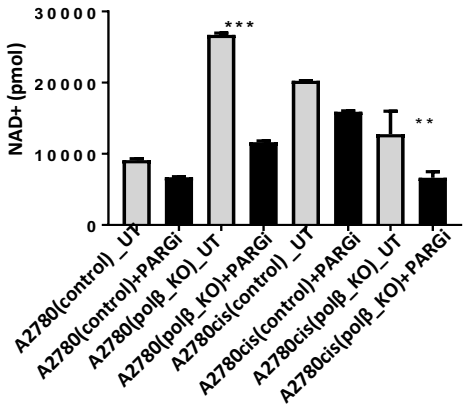


Figure 6-47: NAD+ assay in polβ deficient and proficient cells treated with PARGi. A2780 and A2780cis control and polβ _KO cells were treated with PARGi (20μM) for 16 hours. After incubation, cells were extracted as per the NAD+/NADH colourimetric kit (Abcam) protocol.

PARP1 catalyses the formation of PAR polymers utilising NAD+ to complete that process; thus, NAD+ level homeostasis is directly linked to PAR formation (Surjana, Halliday and Damian, 2010). We evaluated NAD+ levels in A2780 control and polβ_KO cells treated with PARGi. Significant reduction in NAD+ was observed in polβ_KO cells treated with PARGi (Figure 6-47). NAD+ depletion is known to affect cell survival and DNA damage response (Ying *et al.*, 2005). We confirmed the effect of PARGi treatment on cell cycle progression. PARGi led to S-phase cell cycle arrest in both A2780 and A2780cis polβ_KO cells. Additionally, PARGi induced double-strand break formation and lead to an increase in apoptotic cells in both A2780 (Figure 6-48) and A2780cis polβ_KO cells (Figure 6-49).

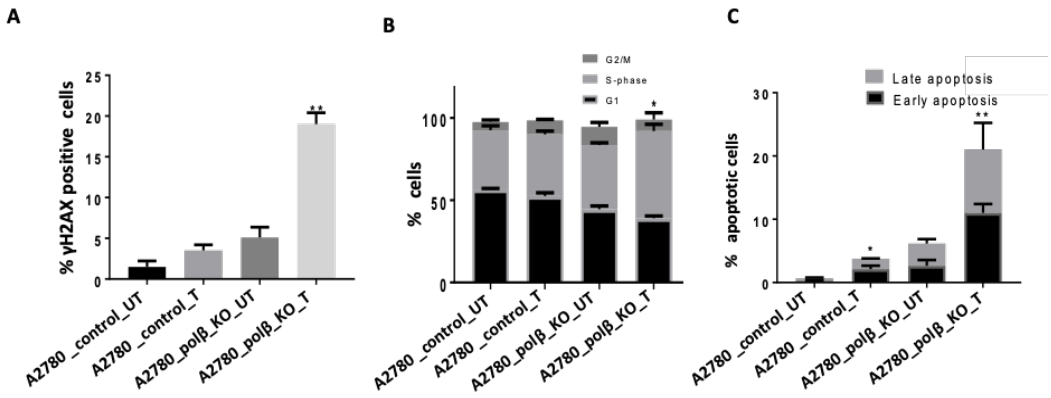


Figure 6-48: Functional studies of PARGi sensitivity in A2780 control and polβ _KO cells.
γH2AX analysis by flow cytometry (A), cell cycle analysis by flow cytometry (B) and annexin V apoptosis analysis by flow cytometry (C) for A2780 control and polβ _KO cells treated with PARGi (20μM).

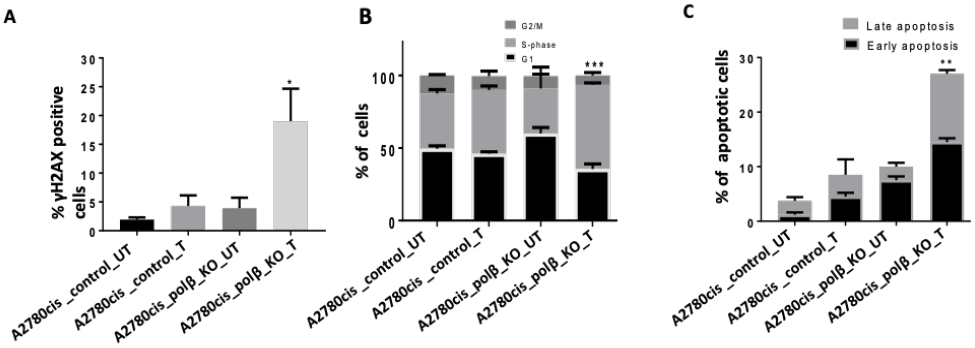


Figure 6-49: Functional studies for PARGi sensitivity in A2780cis (polβ_KO) cells.
γH2AX analysis by flow cytometry (A), cell cycle analysis by flow cytometry (B) and annexin V apoptosis analysis by flow cytometry (C) for A2780cis control and polβ _KO cells treated with PARGi (20μM).

We tested PARGi and Olaparib sensitivity in A2780 and A2780cis control and polβ_KO 3D spheroids. PARGi led to increased cell death and a reduction in spheroid size in both A2780 (polβ_KO) and A2780cis (polβ_KO) cells. However,

Olaparib did not affect cell viability, as demonstrated by the flow cytometry analysis of cell viability (Figure 6-50).

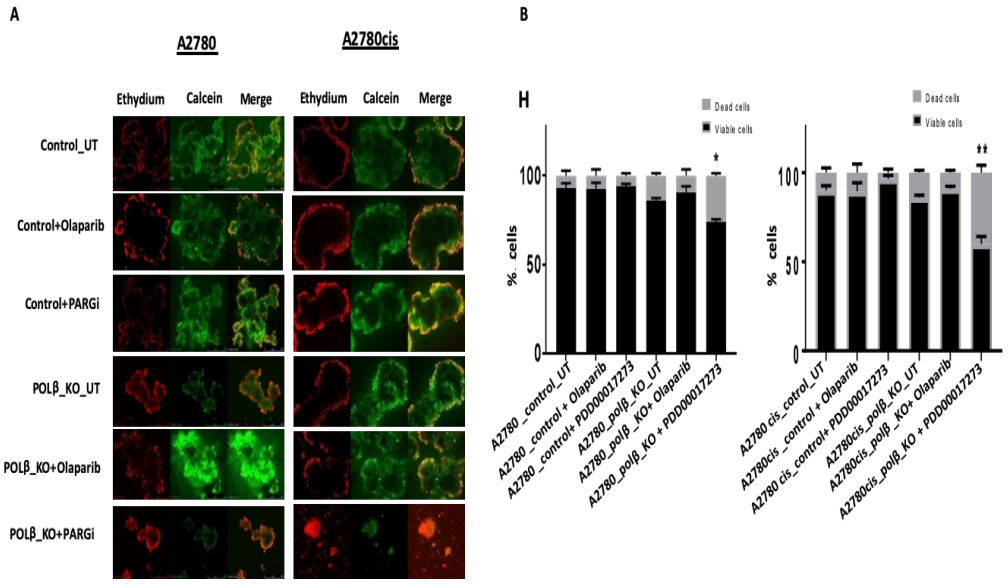


Figure 6-50: PARGi and Olaparib response in 3D spheroids.
(A)Representative photomicrographic images of 3D spheroids of A2780 and A2780cis control and polβ_KO treated with Olaparib (10μM) or PARGi (20μM).

6.3.2.10 Clinicopathological significance of PARG expression in human ovarian tumours

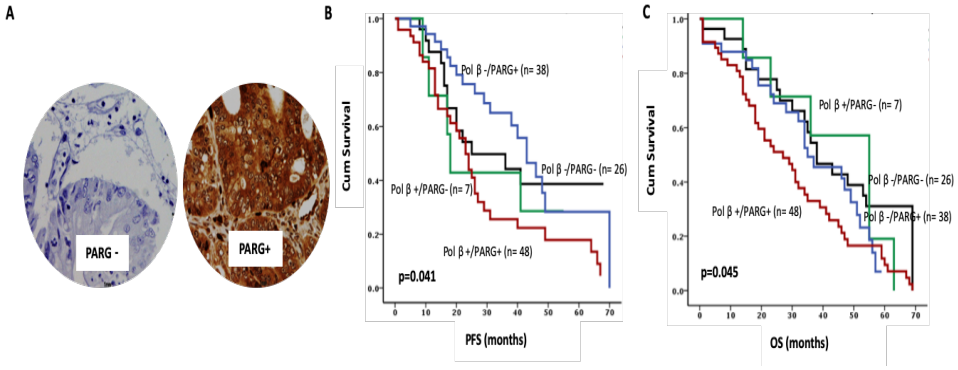


Figure 6-51: PARG expression in human ovarian cancers.
(A)Immunohistochemical expression of cytoplasmic PARG protein in ovarian tumour microarrays. Polβ and PARG co-expression and Kaplan-Meier curve for ovarian cancer progression-free survival (PFS) (B) and overall survival (C).

Table 6-2: Polβ /PARG co-expression and clinicopathological associations.

	Polβ-/PARG-	**Polβ+/PARG-**	**Polβ-/PARG+**	**Polβ+/PARG+**	**P-value**
Pathological Type					
Serous cystadenocarcinoma	17(42.5%)	4(50.0%)	43(54.4%)	65(68.4%)	**0.017**
Mucinous cystadenocarcinoma	6(15.0%)	2(25.0%)	16(20.3%)	4(14.3%)	
Endometrioid	7(17.5%)	0(0%)	12(15.2%)	11(11.6%)	
Clear cell carcinoma	7(17.5%)	2(25.0%)	2(2.5%)	6(6.3%)	
Mixed	2(5%)	0(0%)	4(5.1%)	4(4.2%)	
Other	1(2.5%)	0(0%)	2(2.5%)	5(5.3%)	
Surgical pathology Stage					
Stage I	20(51.3%)	3(37.5%)	39(51.3%)	26(28.3%)	**0.004**
Stage II	1(2.6%)	1(12.5%)	9(11.8%)	24(26.1%)	
Stage III	17(43.6%)	4(50%)	28(36.8%)	36(39.1%)	
Stage IV	1(2.6%)	0(0%)	0(0%)	6(6.5%)	
Tumour Grade					
Low	5(16.7%)	1(12.5%)	14(20.6%)	12(14.1%)	0.377
Intermediate	4(13.3%)	2(25.0%)	20(29.4%)	16(18.8%)	
High	21(70.0%)	5(62.5%)	34(50.0%)	57(67.1%)	
Platinum sensitivity					
Sensitive	36(94.7%)	8(100%)	63(96.9%)	70(89.7%)	0.285
Resistant	2(5.3%)	0(0%)	2(3.1%)	8(10.3%)	

Table 6-3: Multivariate analysis for polβ , PARG and platinum sensitivity.

PFS								
	B	SE	Wald	df	Sig.	Exp(B)	95.0% CI for Exp(B)	
							Lower	Upper
Platinum Sensitivity	3.662	0.489	56.109	1	**0.0001**	38.930	14.934	101.484
Polβ	0.626	0.249	6.328	1	**0.012**	1.870	1.148	3.046
PARG	-0.555	0.284	3.824	1	0.051	0.574	0.329	1.001
OS								
	B	SE	Wald	df	Sig.	Exp(B)	95.0% CI for Exp(B)	
							Lower	Upper
Platinum Sensitivity	2.525	0.352	51.457	1	**0.0001**	12.495	6.267	24.911
Polβ	0.367	0.215	2.921	1	0.087	1.444	0.948	2.199
PARG	-0.468	0.245	3.639	1	0.056	0.626	0.387	1.013

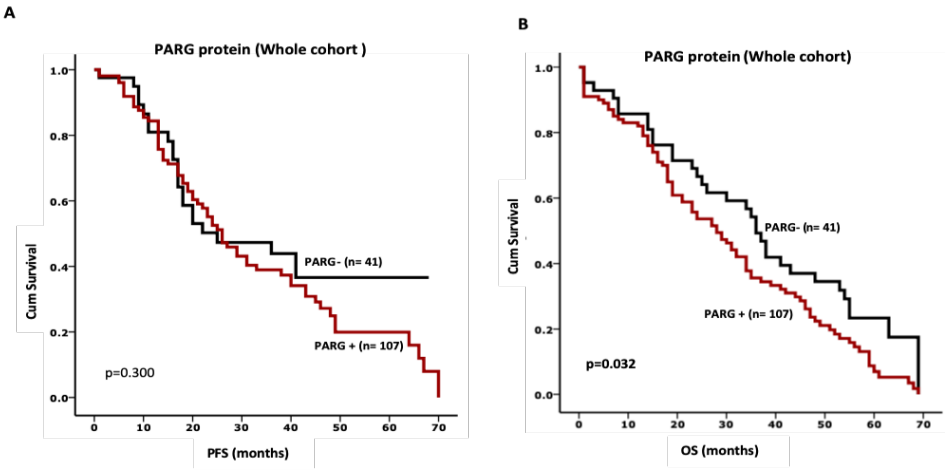


Figure 6-52: Kaplan Meier curve for PARG expression in the whole cohort.
(A) PARG expression and Kaplan Meier curves for PFS (A) and overall survival (B) in the whole cohort.

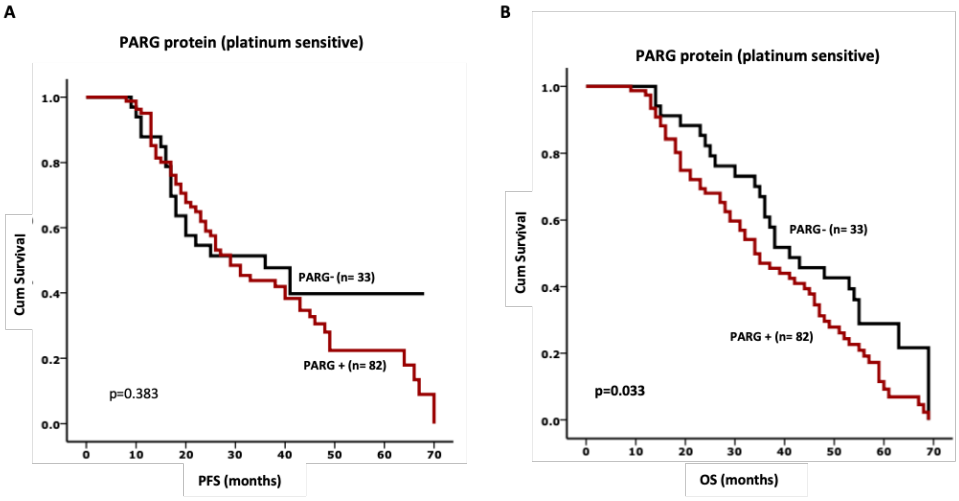


Figure 6-53: Kaplan Meier curve and PARG expression in the platinum sensitive cohort.
(A) PARG expression and Kaplan Meier curves for PFS (A) and overall survival (B) in the platinum sensitive cohort.

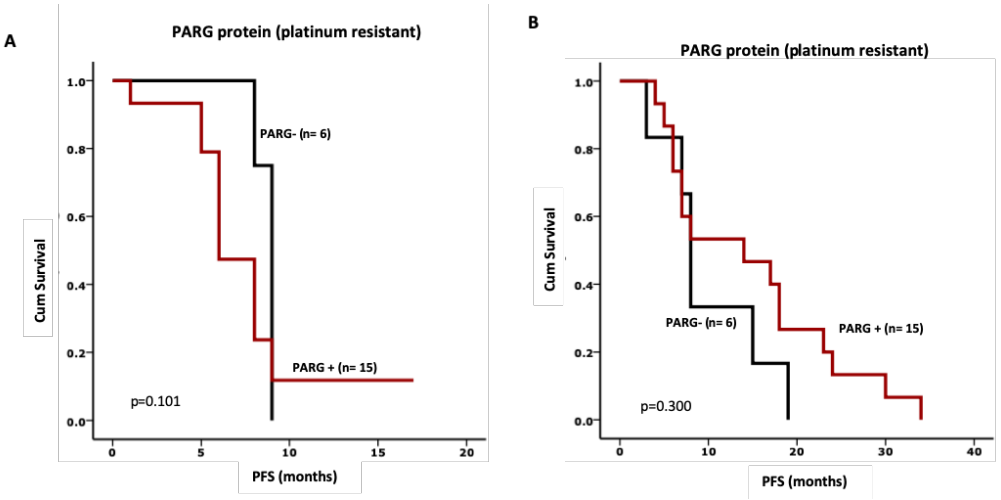


Figure 6-54: Kaplan Meier curve and PARG expression in the platinum resistant cohort.
(A) PARG expression and Kaplan Meier curves for PFS (A) and overall survival (B) in the platinum resistant cohort.

The data suggest that the PARG inhibitor is selectively toxic in polβ deficient ovarian cell lines. Thus, we evaluated polβ/PARG co-expression in ovarian cancer tumours. High polβ/PARG co-expression has poor PFS (p= 0.041) as well as OS (p=0.045) as shown in the Kaplan Meier curves (Figure 6-51). Clinicopathological correlations revealed that Polβ/PARG co-expression was associated with serous cystadenocarcinomas (p=0.017) as well as higher stage (p=0.004) (Table 6-2). In multivariate analysis polβ (p=0.012) and platinum sensitivity (0.0001) independently affected PFS while PARG expression was borderline non-significant in multivariate analysis (p= 0.051 & 0.056 respectively). Platinum sensitivity was independently associated with OS (p=0.0001) (Table 6-3). Although PARG protein expression did not influence PFS, high PARG expression was associated with poor overall survival in ovarian cancer patients (p=0.032) (Figure 6-52). Similar to polβ expression, high PARG expression was also associated with poor overall survival in the platinum sensitive cohort (Figure 6-53) but not in the platinum resistant cohort (Figure 6-54). Analysis of clinic-pathological features showed that high PARG expression was significantly associated with serous cystadenocarcinomas (p=0.011) (Table 6-4).

Table 6-4: PARG expression and clinico-pathological associations.

	PARG (Low) (%)	**PARG (High) (%)**	**P-value**
Pathological Type			
Serous cystadenocarcinoma	25 (41.7%)	129(60.3%)	**0.011**
Mucinous cystadenocarcinoma	11(18.3%)	26(12.1%)	
Endometrioid	9(15.0%)	30(14.0%)	
Clear cell carcinoma	10(16.7%)	9(4.2%)	
Mixed	2(3.3%)	10(4.7%)	
Other	3(5.0%)	10(4.7%)	
Surgical pathology Stage			
Stage I	26(45.6%)	79(38.5%)	0.149
Stage II	4(7.0%)	38(18.5%)	
Stage III	26(45.6%)	80(3.9%)	
Stage IV	1(1.8%)	8(3.9%)	
Tumour Grade			
Low	8(16.7%)	29(15.4%)	0.559
Intermediate	8(16.7%)	45(23.9%)	
High	32(66.7%)	114(60.6%)	
Platinum sensitivity			
Sensitive	51(89.5%)	161(91.5%)	0.646
Resistant	6(10.5%)	15(8.5%)	

6.4 Discussion

DNA polymerase beta (polβ) plays a fundamental role during the base excision repair pathway (David, O'Shea and Kundu, 2007). Recent reports have shown that polβ localises in the mitochondria and functions in mammalian base excision repair pathway (Kaufman and Van Houten, 2017). The Bohr group showed polβ immunoreactivity in mitochondrial extracts from murine brain and kidney only, but not in any of the mitochondrial liver, heart or skeletal muscles (Sykora *et al.*, 2017). In this study, we investigated polβ expression in 525 ovarian cancer and showed that high polβ expression was associated with poor prognosis in platinum sensitive ovarian tumours. Correspondingly, at mRNA levels polβ expression influenced the outcome of ovarian cancer patients implying the significance of polβ expression as a prognostic factor and a predictor of platinum response. Previous studies showed high polβ expression in colorectal (Iwatsuki *et al.*, 2009) and prostatic tumours (Dobashi *et al.*, 1994) more than normal tissue. Suppression of polβ sensitised colorectal cells to platinum treatment *in vitro* model (Iwatsuki *et al.*, 2009). In ovarian cancer cell lines, we showed up-regulation of polβ expression in cisplatin resistant cells (A2780cis) more than A2780 control cells. Cisplatin treatment induced polβ expression at mRNA levels and protein levels. Nuclear and cytoplasmic extraction showed induction of polβ expression in the nuclear extracts of A2780cis cells treated with cisplatin but not in platinum sensitive A2780 cells. Immunofluorescence studying of polβ in untreated and platinum treated cells revealed the nuclear localization of polβ in platinum resistant cells (A2780cis) after 48 hours of treatment. Taken together,

the data from our study and previous studies provide evidence that polβ has a direct role in platinum response.

Cisplatin is the first line of therapy in ovarian cancers (van Zyl, Tang and Bowden, 2018). Although it was quite effective, the development of an intrinsic and extrinsic resistance mechanism rendered tumour resistance and recurrence a major challenge in ovarian cancer treatment. Cisplatin targets the nucleus leading to the formation of platinum DNA adducts, which are intra-strand cross-links. The most predominant lesion formed by cisplatin is the 1,2-d(GpG) which activates the nucleotide excision repair pathway (NER) (Iwatsuki *et al.*, 2009). However, replicative polymerases cannot overcome the intra-strand crosslink cisplatin lesion which should conventionally block replication leading to cellular apoptosis. Some polymerases can bypass the intra-strand crosslink lesion - these are the so-called translesion polymerases (Srivastava *et al.*, 2015). Translesion polymerases catalyse DNA synthesis using the adducted DNA as a template, and then replicative polymerases can resume replication. Hence, translesion polymerases can overcome the replicative block of cisplatin and generate resistance (Nemec *et al.*, 2017). Emerging data has shown that polβ and polη can bypass the pt-GG lesions and act as translesion polymerases (Srivastava *et al.*, 2015). A recent study reported that Polβ P242R variant, which is actually present in 2.4% of the human population, could act as a translesion polymerase (Nemec *et al.*, 2017). Another report showed that (T889C) variant in *POLβ* gene was associated with resistance to 5-fluorouracil, cisplatin and epirubicin in gastric cancer (Tan *et al.*, 2015). Therefore, polβ can be a predictor of cisplatin response in platinum-treated human cancers. We showed that polβ depletion by siRNA and CRISPR-cas9

sensitizes different ovarian cancer cells to cisplatin. This is consistent with previous reports that polβ knockdown delayed repair of oxaliplatin lesions in colon cancer cells (Yang *et al.*, 2010). Cisplatin-treated polβ depleted cells accumulated double strand breaks and S-phase cell cycle arrest and increased apoptosis in the different tested models. That confirms the role of polβ in cisplatin resistance mechanisms and the possibility of overcoming it by polβ inhibition. Importantly we elucidated a novel role of polβ in regulating EMT phenotype in ovarian cancer cell lines. Polβ knock-out cells had less ability to invade and migrate. A2780 (polβ_KO) and A2780cis (polβ_KO) cells had lower protein levels of N-cadherin, TGFβ and MMP-9. These are well-identified genes that mark the EMT phenotype. A2780 (polβ_KO) cells had an induction in E-cadherin expression. These results indicate a reversion to mesenchymal phenotype in polβ deficient cells. EMT phenotype is associated with aggressiveness in ovarian cancers as well as other malignancies. Additionally, RT2-PCR profiler analysis of EMT genes in polβ knock-out and control cells identified dysregulation of crucial EMT genes including *COL3A1, COL5A2, CTNNB1* and *SNAI3*. The data illustrates a complex role for polβ in EMT regulation. However, it suggests that polβ inhibitors could have a potential role in tackling tumour invasion and metastasis.

We investigated the sensitivity of polβ small molecule inhibitors (pamoic acid and NSC666719) in BRCA2 deficient cells. polβ inhibitors induced selective toxicity in BRCA2 deficient cells (PE01 and HeLa_BRCA2_KD). Polβ inhibitors induced cell death in BRCA2 deficient cells in 2D and 3D cell line models. Polβ depletion will lead to impairment of BER and single strand break repair (SSBR). SSBs if

unrepaired will convert to double-strand break lesions during replication. BRCA2 deficient cells are known to have homologous recombination deficiency, and the DSBs would persist, while BRCA2 proficient cells will activate the homologous recombination repair pathway and the cells will survive polβ depletion. Our data provide the first evidence that polβ inhibitors can have a synthetic lethality application in BRCA2 deficient tumours.

Although PARP inhibitors have great success in the induction of synthetic lethality in BRCA deficient ovarian cancers (Ding *et al.*, 2016), Olaparib did not show significant lethality in polβ_KO cells. This is perhaps due to the fact that both PARP1 and polβ are mainly responsible for processing SSBR. Remarkably, PARGi (PDD00017273) had significant toxicity in polβ knock-out cells. Few explanations to that observation can be drawn from our study. Immunofluorescence experiments demonstrated that PARGi treatment leads to the accumulation of PAR polymers in both A2780 control and A2780 polβ_KO cells. However, after 24 hours treatment, A2780 cells were able to restore normal PAR levels while it persisted in A2780_polβ KO cells. PAR polymers signal the release of apoptosis-inducing factor (AIF), a mitochondrial oxidoreductase that is liberated to the cytoplasm to mark cell death (Yu *et al.*, 2006). Moreover, high molecular weight PAR polymer was reported to act as a nuclear death (Andrabi *et al.*, 2006; Yu *et al.*, 2006). We observed the accumulation of high molecular weight PAR polymers selectively in polβ knock out cells treated with PARGi. PARGi treatment was associated with reduced cellular levels of NAD+. NAD+ depletion leads to Sirtuin level alterations and DNA repair impairment (Ying *et al.*, 2005). The Sirtuin family are NAD+ consumers. In particular, SIRT1 and SIRT6 are involved in DNA repair

(Lombard, 2009) whereas SIRT6 interacts with PARP1 in the base excision repair. Thus, PAR accumulation and NAD+ depletion contribute directly and indirectly to impairment of DNA repair machinery and cell death (Surjana, Halliday and Damian, 2010; Fouquerel and Sobol, 2014; Croteau *et al.*, 2017).

Our study provides evidence that polβ expression is a crucial predictor of platinum response in ovarian tumours. Polβ inhibitors can have a clinical impact in platinum sensitive and BRCA deficient ovarian cancers. PARGi is a novel therapeutic approach in polβ deficient ovarian cancers.

7 General Discussion

Breast and ovarian cancers are the most lethal malignancies affecting women worldwide (Minchom, Aversa and Lopez, 2018; Damia and Broggini, 2019) despite the recent advances in genomics and proteomic studies that have led to identifying some molecular drivers and prognostic biomarkers. However, understanding of tumour escape and resistance mechanisms to therapy remains unclear. In breast cancer the advent of genomic technologies has led to comprehensive profiling of the genomic landscape of some breast cancers sub-types (Curtis, 2015). That understanding was translated into identifying personalised targeted therapies for certain breast subtypes. For instance, HER2 expressing breast tumours can benefit from HER2 blockage treatment like trastuzumab, neratinib and pertuzumab. Nevertheless, there is a lack in personalised targeted therapies for certain subtypes of breast cancers, particularly triple negative tumours (Green, 2017). Characterisation of biomarkers for targeting triple negative breast cancers remains an area of un-met need. Additionally, further categorising of predictive and prognostic biomarkers for response to therapies is crucial to circumvent resistance mechanisms in tumours. In ovarian cancers, the standardised treatment is cytoreductive surgery followed by platinum-based chemotherapy (Kim, Cho and Song, 2017). In general, there is a lag in genomic profiling of ovarian cancers compared to breast cancers. Previous molecular studies of ovarian cancers have broadly classified tumours into two categories based on their main genetic aberrations. Type I tumours which include low grade serous, mucinous, endometrioid, clear cell cancers, and Brenner tumours are characterised with *KRAS* mutations which is thought to be the driver mutations in type I tumours. The other type II tumours include high grade serous,

high grade endometrioid, malignant mixed mesodermal tumours and other undifferentiated tumours and are specified by *TP53* mutations, *BRCA1/2* mutations as well as other homologous recombination pathway deficiencies (Previs *et al.*, 2016). Olaparib is the first biomarker directed therapy for ovarian cancers. Other PARP inhibitors like Niraparib and Veliparib are also approved for BRCA mutated ovarian carcinomas (Jiang *et al.*, 2019). Despite the success of PARP inhibitors in tackling *BRCA1/2* mutated ovarian cancers by inducing synthetic lethality, identification of more molecular targeted therapies is urgently needed. *BRCA1* and *BRCA2* germline mutations account for only about 15% of ovarian cancers. Additionally, mechanisms for resistance for PARP inhibitors including reactivation of BRCA mediated HR have already been described (Dhillon and Taniguchi, 2015). However, another crucial aspect in designing molecular targeted therapies is the intra-tumour heterogeneity and the pattern and timing of mutation evolution. The characterisation of mutations that cause tumour initiation (driver mutations) and those particularly conferring to metastatic sites and representing the newly progressive tumour clones require further investigations in ovarian cancers (Minchom, Aversa and Lopez, 2018).

The main aim of our study was to identify new synthetic lethality interactions that can be of clinical relevance to breast and ovarian patients, thereby inhibiting the base excision repair pathway. We aimed to expand the benefit of PARP inhibitors to new patient groups through identifying new biomarkers of response. In our breast cohort, low XRCC1 and high PARP1 expression were associated with high grade, high mitotic index, high pleomorphism, ER-/PR- and high-risk Nottingham

Prognostic Index and poor breast cancer specific survival. The data implies the significance of the XRCC1/PARP1 signature as prognostic biomarkers for breast cancers. Olaparib treatment induced selective toxicity in XRCC1 deficient cells in the different isogenic cell line models that we tested. Olaparib treatment led to cell cycle arrest dependant on the p53 genetic background of the cells. Cell cycle stallation led to substantial DNA damage and apoptosis in Olaparib treated XRCC1 deficient cells. Previous work by Horton and colleagues proposed a model for PARP inhibitor synthetic lethality. PARP1 binds to the sites of DNA damage, however, in the presence of PARP inhibitors synthesis of poly (ADP) ribose polymers by PARP1 is prevented. Thus, modifications of PARP1 and other BER key enzymes such as polβ and XRCC1 are impaired (Horton *et al.*, 2014). PARP1 trapping to DNA complexes are more cytotoxic than unrepaired SSBs caused by PARP inhibition That hypothesis was proposed in few studies before (Murai *et al.*, 2012; Hopkins *et al.*, 2019). We investigated PARP trapping mediated cytotoxicity in our XRCC1 deficient and proficient models. Comparison between Talazoparib and Olaparib mediated PARP recruitment to the nucleus revealed earlier accumulation of PARP foci in Talazoparib treated XRCC1 knock-out cells. Moreover, greater accumulation of γH2AX at earlier time points compared to Olaparib treated cells was observed. Together the data indicates that Talazoparib exerts its potent cytotoxicity through PARP trapping in addition to PARP inhibition. In the DCIS cohort, we showed that the loss of XRCC1 is an early event in breast cancer pathogenesis. Knock-out of XRCC1 in MCF10-DCIS cells increased its proliferation activity, cellular invasion and migration suggesting a more aggressive phenotype to XRCC1 deficient DCIS lesions. A recent study suggested a role for

DNA damage repair dysregulation in the progression of DCIS to invasive breast cancers through the loss of SIM2 ATM phosphorylation that mediates HR deficiency and EMT (Pearson *et al.*, 2019). Similarly, we found upregulation of several EMT genes in MCF10-DCIS_XRCC1 KO suggesting that down-regulation of XRCC1 promotes an EMT phenotype.

In ovarian cancer, high XRCC1 expression was associated with high grade, higher FIGO staging and poor PFS. In the platinum sensitive cohort, high XRCC1 expression was associated with poor PFS and OCSS. However, there was no significant associations between XRCC1 and survival outcomes in platinum resistant patients. Similarly, PARP1 expression was significantly associated with aggressive ovarian cancer phenotype. A previous study by our group showed that XRCC1 expression in ovarian tumours was significantly associated with higher stage, increased risk of disease progression and platinum resistance in ovarian cancers (Abdel-Fatah *et al.*, 2013). Together the data suggests a role for BER pathway upregulation and platinum resistance. Given that platinum therapy mainly induces DNA damage, it is conceivable that alterations of a specific DNA repair pathway will directly affect the platinum response. Preclinical evidence relating mutations in DNA repair key players and sensitivity or resistance to platinum are already emerging (Dai *et al.*, 2015; Damia and Broggini, 2019). Olaparib and Talazoparib treatment were associated with selective cytotoxicity in XRCC1 deficient ovarian cancer cells. PARPi toxicity was associated with cell cycle arrest, DNA damage and apoptosis. The data suggests a new synthetic lethality interaction between PARP1 and XRCC1 that is applicable in the ovarian cancer model. A recent report has suggested the presence of BRCA1/2 somatic mutations

in circulating free DNA of platinum refractory breast and ovarian tumours and with known resistance to PARPi (Ratajska *et al.*, 2017). Therefore our, data provides evidence that XRCC1 expression in ovarian cancers could be an alternative predictive biomarker for PARPi response.

We expanded the hypothesis of inhibition of the BER pathway to induce lethality in ovarian cancers through investigating polβ expression which processes a rate limiting step in the BER pathway. High polβ expression was more associated with higher FIGO staging, high grade cystadenocarcinoma, poor PFS and OS in ovarian cancer patients. Polβ has low fidelity compared to other polymerases in the Y-family of DNA polymerases and no known 5'-3' proofreading mechanism. Therefore, it is suggested that polβ over expression can lead to mismatched nucleotide insertion and mutational increase (Starcevic, Dalal and Sweasy, 2004). Polβ variants have been reported previously in oesophageal cancers (Zheng *et al.*, 2013), lung cancers (Nemec *et al.*, 2017) and prostate cancers (Dalal *et al.*, 2005), supporting the hypothesis that over-expression of polβ increases tumorigenesis. Preclinically, we observed that polβ depletion re-sensitizes ovarian cancer cells to cisplatin, increases DNA damage and reduces aggressiveness through reducing invasion and migration ability. The data provides evidence that polβ inhibition can be an exciting approach to reducing ovarian cancer aggressiveness. Polβ is involved in repairing cisplatin DNA adducts through extending the replication DNA synthesised by polymerases α and δ and restoring stalled replication (Vaisman and Chaney, 2000). P242R polβ variant was previously reported to function as a translesion polymerase and activate the NER pathway to remove DNA crosslinks and repair platinum lesion (Nemec *et al.*, 2017). That could possibly explain why

polβ inhibition led to cisplatin re-sensitization in our study. However, the exact role for polβ in the EMT process requires further investigations.

Polβ inhibition by small molecule inhibitors induced selective toxicity in BRCA2 deficient cells, implying a synthetic lethality interaction between polβ and BRCA2. Polβ inserts a nucleotide to fill the DNA gap and accomplish the short batch BER pathway. Also, it initiates the long-batch BER pathway by inserting a single nucleotide then a switch to polymerases δ &ε to incorporate the missing nucleotides (Dianov and Hübscher, 2013). Thus, Polβ inhibition will ultimately impair the BER pathway and lead to the accumulation of SSBs which will eventually become DSBs when they encounter the replication fork. In BRCA2 deficient cells there is dysfunction in the HR pathway initiation and thus persistent DSBs will lead to cell death. Additionally, Polβ knock-out cells were selectively sensitive to PARG inhibitor (PARGi). PARGi induced accumulation of poly (ADP) ribose (PAR) polymers, DSBs and cell cycle arrest. Interestingly, polβ knock-out cells were resistant to Olaparib treatment which also reduced PAR formation in the cells. A recent report proposed that loss of PARG activity is a possible mechanism for PARPi resistance in BRCA2 deficient tumours. PARG works in the same direction as PARPi and preventing PAR accumulation. Hence, decreased PARG activity can allow tumour cells to escape the PARPi lethal mechanism (Gogola *et al.*, 2018). These finding are in concordance with our observations in polβ deficient ovarian cancer cells. Together the data implies that endogenous PARG levels could predict the Olaparib response in HR deficient as well as polβ deficient ovarian cancers. Another recent study by Pillay *et al*. has revealed that ovarian cancer cells respond differently to PARG inhibitor (PDD00017273)

compared to PARP inhibitor (Olaparib) dependant on DNA replication vulnerabilities in the cells (Pillay *et al.*, 2019).

We confirmed Polβ/ PARG co-expression in our ovarian cancer cohort, with it being associated with high grade tumours and poor PFS in ovarian cancer patients. Thus, the results imply a role for the dysregulation of PARG levels in ovarian cancer prognosis dependant on polβ expression.

7.1 Limitations of the study

We comprehensively investigated XRCC1 as a new biomarker for PARPi sensitivity in breast and ovarian cancers. We validated XRCC1 and PARP1 correlation with survival outcome and clinicopathological features in invasive breast cancers as well as ovarian cancers. We used various models for XRCC1 depletion such as SiRNA, CRISPR-cas9 knock out, ShRNA and XRCC1 hypomethylation. XRCC1 deficiency was synthetically lethal with PARPi in all the model system that we used. However, our analysis did not suggest whether XRCC1 deficiency is a driver mutation in breast and ovarian cancer or being a secondary mechanism for tumour adaptation. In that context investigating XRCC1 depletion in normal breast tissue or cells would have been beneficial. Although we studied XRCC1 depletion in MCF10-DCIS cell line model, yet they are known to be of non-invasive malignant origin. Additionally, comparing PARPi cytotoxicity in normal breast and ovarian tissue would be useful for further clinical applications aimed to be achieved from our work. Nevertheless, the limited availability of normal breast and ovarian cell lines or tissue models available to us is a limitation of our study. Another potential limitation for our work is that the specificity of Polβ inhibitors against other DNA repair enzymes as well as other polymerases have not been validated. Thus, we emphasised that our study with Polβ inhibitors is preliminary and aimed to draw the attention to the clinical benefit of developing Polβ inhibitors for personalising treatment of ovarian cancers.

7.2 Future directions and conclusions

Targeted or precision medicine in oncology is rapidly evolving due to the advent of genomic and transcriptomic studies. Approaches to stratifying patients according to their genetic alterations rather than by their tumour site are ongoing (Minchom, Aversa and Lopez, 2018). The balance between genomic instability and DNA damage response in cancer cells represents an exciting field for therapy design. Drugs targeting DNA damage repairing pathways through inducing synthetic lethality have already shown clinical benefit (Gavande *et al.*, 2016). PARP inhibitor approval demonstrated the success of that approach. However, other DNA repair inhibitors are under development such as ATM inhibitors, ATR inhibitors, WEE1 inhibitors, CHK1 inhibitors DNA-PK inhibitors. Nevertheless, identifying reliable biomarkers of response to the available DNA repair inhibitors are yet to be defined (Pearl *et al.*, 2015; Minchom, Aversa and Lopez, 2018). The wide availability of genomic screening for patients' DNA is expected to provide meaningful directions in that respect. A recent *in vivo* study has explored a combination strategy of Olaparib and WEE1 inhibitor (AZD1775) to augment HR deficiency in BRCA2 deficient cells and maximize the benefit of Olaparib (Karnak *et al.*, 2014). In gastric cancer cell lines and xenograft model AZD1775 combination with Olaparib blocked the activation of several HR related proteins and induced more DNA damage compared to Olaparib alone treatment (Lin *et al.*, 2018). Another study on circulating tumour cell patients derived explants of small cell lung cancer (SCLC) confirmed that WEE1 combination with Olaparib can induce HR defects and replication stress that can lead to lethality in malignant cells (Lallo *et*

al., 2018). Thus, a combination strategy of Olaparib with other DNA repair inhibitors is an exciting area for future investigations.

In our study, we provided a novel response biomarker to PARP inhibitors. Nevertheless, more predictive biomarkers still need to be identified to expand the success of PARP inhibitors to more patients. Our study highlighted how polβ inhibitors can have a synthetic lethality application in BRCA2 deficient ovarian cancers and therefore could provide a new synthetic lethality interaction to overcome the resistance to PARP inhibitors already being reported. Thus, more focused research toward developing polβ inhibitors could be of clinical benefit. The role of immune response modulation in tumour progression and therapeutic outcomes is more appreciated. The profile of somatic mutations differs between tumour types whereas the presentation of mutant proteins by MHC class I activates T-cells and stimulates the immune response against malignant cells carrying those proteins. Functional mutations lead to neoantigen load on MHC class and therefore better immune response (Zhang *et al.*, 2019). Recently, defects in the DNA damage response have been shown to increase neoantigen load in tumours. BRCA1/2 inactivation are associated with unique mutational signature in tumours (Alexandrov *et al.*, 2013). Our group recently showed that low XRCC1/ ATM / BRCA1 expression in breast cancers were associated with higher grades, high proliferation indexes and CD8+ tumour infiltrating lymphocytes. Additionally, PD-1/PD-L1 expression in XRCC1 deficient breast cancers was associated with aggressive phenotype and poor survival, implying a link between DNA repair deficient and immune response modulations (Green *et*

al., 2017). Remarkably, a recent report demonstrated PARPi upregulated PD-L1 expression in breast cancer cell lines and a xenografts model through inactivation of GSK3β (Jiao *et al.*, 2017). While in ovarian cancer, early phase clinical trials are currently exploring a combination of Olaparib and durvalumab (PDL-1) in BRCA germline mutated ovarian cancer (clinicaltrials.gov) (NCT02734004), (NCT02953457). Nevertheless, there are other trials exploring Olaparib and durvalumab combinations in platinum resistant advanced ovarian cancers. One study reported promising results in non-BRCA deficient ovarian cancers (Lee *et al.*, 2017), emphasising that there are other response biomarkers to PARPi as well as immune checkpoint upregulation in cancers. Thus, the compelling research question at the advent of the DNA repair targeted therapy field should be what are the response biomarkers to therapies (Zhang *et al.*, 2019). DNA repair pathways are an ideal field for the development of personalised medicine, yet more genomic, preclinical and clinical studies are needed to provide DNA repair targeted inhibitors at the patient's bedside.

8 References

References

Abdel-Fatah, T. *et al.* (2013) 'Clinicopathological and functional significance of XRCC1 expression in ovarian cancer', *International Journal of Cancer*. John Wiley & Sons, Ltd, 132(12), pp. 2778–2786. doi: 10.1002/ijc.27980.

Abdel-Fatah, Tarek M A *et al.* (2014) 'DNA polymerase b deficiency is linked to aggressive breast cancer: A comprehensive analysis of gene copy number, mRNA and protein expression in multiple cohorts'. doi: 10.1016/j.molonc.2014.01.001.

Abdel-Fatah, Tarek M.A. *et al.* (2014) 'DNA polymerase β deficiency is linked to aggressive breast cancer: A comprehensive analysis of gene copy number, mRNA and protein expression in multiple cohorts', *Molecular Oncology*. No longer published by Elsevier, 8(3), pp. 520–532. doi: 10.1016/J.MOLONC.2014.01.001.

Adem, C. *et al.* (2003) 'Microsatellite instability in hereditary and sporadic breast cancers', *International Journal of Cancer*. John Wiley & Sons, Ltd, 107(4), pp. 580–582. doi: 10.1002/ijc.11442.

Al-Attar, A. *et al.* (2010) 'Human apurinic/apyrimidinic endonuclease (APE1) is a prognostic factor in ovarian, gastro-oesophageal and pancreatico-biliary cancers', *British Journal of Cancer*. Nature Publishing Group, 102(4), pp. 704–709. doi: 10.1038/sj.bjc.6605541.

Alano, C. C. *et al.* (2010) 'NAD+ depletion is necessary and sufficient for poly(ADP-ribose) polymerase-1-mediated neuronal death.', *The Journal of neuroscience : the official journal of the Society for Neuroscience*. NIH Public Access, 30(8), pp. 2967–78. doi: 10.1523/JNEUROSCI.5552-09.2010.

Alba, E. *et al.* (2018) 'Integrative cluster classification to predict pathological

complete response to neoadjuvant chemotherapy in early breast cancer.', *Journal of Clinical Oncology*. American Society of Clinical Oncology, 36(15_suppl), pp. 579–579. doi: 10.1200/JCO.2018.36.15_suppl.579.

Albarakati, N. *et al.* (2015) 'Targeting BRCA1-BER deficient breast cancer by ATM or DNA-PKcs blockade either alone or in combination with cisplatin for personalized therapy', *Molecular Oncology*, 9(1), pp. 204–217. doi: 10.1016/j.molonc.2014.08.001.

Albertella, M. R., Lau, A. and O'Connor, M. J. (2005) 'The overexpression of specialized DNA polymerases in cancer', *DNA Repair*, 4(5), pp. 583–593. doi: 10.1016/j.dnarep.2005.01.005.

Alexandrov, L. B. *et al.* (2013) 'Signatures of mutational processes in human cancer', *Nature*. Nature Publishing Group, 500(7463), pp. 415–421. doi: 10.1038/nature12477.

Alnajjar, K. S. *et al.* (2017) 'DNA Polymerase β Cancer-Associated Variant I260M Exhibits Nonspecific Selectivity toward the β-γ Bridging Group of the Incoming dNTP.', *Biochemistry*. NIH Public Access, 56(40), pp. 5449–5456. doi: 10.1021/acs.biochem.7b00713.

Alsina-Sanchís, E. *et al.* (2017) 'TGFβ Controls Ovarian Cancer Cell Proliferation.', *International journal of molecular sciences*. Multidisciplinary Digital Publishing Institute (MDPI), 18(8). doi: 10.3390/ijms18081658.

Amin, M. B. *et al.* (2017) 'The Eighth Edition AJCC Cancer Staging Manual: Continuing to build a bridge from a population-based to a more "personalized"

approach to cancer staging', *CA: A Cancer Journal for Clinicians*. American Cancer Society, 67(2), pp. 93–99. doi: 10.3322/caac.21388.

Andrabi, S. A. *et al.* (2006) *Poly(ADP-ribose) (PAR) polymer is a death signal*. Available at: www.pnas.orgcgidoi10.1073pnas.0606526103 (Accessed: 4 May 2019).

Andree, H. A. *et al.* (1990) 'Binding of vascular anticoagulant alpha (VAC alpha) to planar phospholipid bilayers.', *The Journal of biological chemistry*, 265(9), pp. 4923–8. Available at: http://www.ncbi.nlm.nih.gov/pubmed/2138622 (Accessed: 20 June 2018).

De Angelis, R. *et al.* (2014) 'Cancer survival in Europe 1999-2007 by country and age: results of EUROCARE--5-a population-based study.', *The Lancet. Oncology*. Elsevier, 15(1), pp. 23–34. doi: 10.1016/S1470-2045(13)70546-1.

Armstrong, D. K. *et al.* (2006) 'Intraperitoneal Cisplatin and Paclitaxel in Ovarian Cancer', *New England Journal of Medicine*. Massachusetts Medical Society, 354(1), pp. 34–43. doi: 10.1056/NEJMoa052985.

Aure, M. R. *et al.* (2017) 'Integrative clustering reveals a novel split in the luminal A subtype of breast cancer with impact on outcome', *Breast Cancer Research*, 19(1), p. 44. doi: 10.1186/s13058-017-0812-y.

Awasthi, P., Foiani, M. and Kumar, A. (2015) 'ATM and ATR signaling at a glance', *J Cell Sci*. The Company of Biologists Ltd, 128(23), pp. 4255–4262. doi: 10.1242/JCS.169730.

Bai, P. (2015) 'Biology of Poly(ADP-Ribose) Polymerases: The Factotums of Cell

Maintenance'. doi: 10.1016/j.molcel.2015.01.034.

Balaji, K. *et al.* (2017) 'AXL Inhibition Suppresses the DNA Damage Response and Sensitizes Cells to PARP Inhibition in Multiple Cancers.', *Molecular cancer research : MCR*. NIH Public Access, 15(1), pp. 45–58. doi: 10.1158/1541-7786.MCR-16-0157.

Band, V. and Sager, R. (1989) 'Distinctive traits of normal and tumor-derived human mammary epithelial cells expressed in a medium that supports long-term growth of both cell types.', *Proceedings of the National Academy of Sciences of the United States of America*, 86(4), pp. 1249–53. Available at: http://www.ncbi.nlm.nih.gov/pubmed/2919173 (Accessed: 19 March 2019).

Bane, A. (2013) 'Ductal carcinoma in situ: what the pathologist needs to know and why.', *International journal of breast cancer*. Hindawi Limited, 2013, p. 914053. doi: 10.1155/2013/914053.

Beaufort, C. M. *et al.* (2014) 'Ovarian Cancer Cell Line Panel (OCCP): Clinical Importance of In Vitro Morphological Subtypes', *PLoS ONE*. Edited by R. Pearson. Public Library of Science, 9(9), p. e103988. doi: 10.1371/journal.pone.0103988.

Bebenek, K. and Kunkel, T. A. (2004) 'Functions of DNA Polymerases', *Advances in Protein Chemistry*. Academic Press, 69, pp. 137–165. doi: 10.1016/S0065-3233(04)69005-X.

Beijersbergen, R. L., Wessels, L. F. A. and Bernards, R. (2017) 'Synthetic Lethality in Cancer Therapeutics', *Annual Review of Cancer Biology*. Annual Reviews , 1(1), pp. 141–161. doi: 10.1146/annurev-cancerbio-042016-073434.

References

Benjamini, Y. and Yekutieli, D. (2005) 'False Discovery Rate–Adjusted Multiple Confidence Intervals for Selected Parameters', *Journal of the American Statistical Association*. Taylor & Francis, 100(469), pp. 71–81. doi: 10.1198/016214504000001907.

Bitler, B. G. *et al.* (2015) 'Synthetic lethality by targeting EZH2 methyltransferase activity in ARID1A-mutated cancers', *Nature Medicine*, 21(3), pp. 231–238. doi: 10.1038/nm.3799.

Blamey, R. W. *et al.* (2007) 'Survival of invasive breast cancer according to the Nottingham Prognostic Index in cases diagnosed in 1990–1999', *European Journal of Cancer*. Pergamon, 43(10), pp. 1548–1555. doi: 10.1016/J.EJCA.2007.01.016.

Bowtell, D. D. L. (2010) 'The genesis and evolution of high-grade serous ovarian cancer', *Nature Reviews Cancer*, 10(11), pp. 803–808. doi: 10.1038/nrc2946.

Brandão, M., Pondé, N. and Piccart-Gebhart, M. (2019) 'Mammaprint™: a comprehensive review', *Future Oncology*. Future Medicine Ltd London, UK , 15(2), pp. 207–224. doi: 10.2217/fon-2018-0221.

Bray, F. *et al.* (2018) 'Global cancer statistics 2018: GLOBOCAN estimates of incidence and mortality worldwide for 36 cancers in 185 countries', *CA: A Cancer Journal for Clinicians*. American Cancer Society, 68(6), pp. 394–424. doi: 10.3322/caac.21492.

Brem, R. *et al.* (2006) 'The XRCC1 -77T->C variant: haplotypes, breast cancer risk, response to radiotherapy and the cellular response to DNA damage', *Carcinogenesis*. Oxford University Press, 27(12), pp. 2469–2474. doi:

10.1093/carcin/bgl114.

Brinckerhoff, C. E., Rutter, J. L. and Benbow, U. (2000) 'Interstitial collagenases as markers of tumor progression.', *Clinical cancer research : an official journal of the American Association for Cancer Research*, 6(12), pp. 4823–30. Available at: http://www.ncbi.nlm.nih.gov/pubmed/11156241 (Accessed: 5 March 2019).

ter Brugge, P. *et al.* (2016) 'Mechanisms of Therapy Resistance in Patient-Derived Xenograft Models of BRCA1-Deficient Breast Cancer', *Journal of the National Cancer Institute*. Oxford University Press, 108(11), p. djw148. doi: 10.1093/jnci/djw148.

Brunen, D. and Bernards, R. (2017) 'Drug therapy: Exploiting synthetic lethality to improve cancer therapy', *Nature Reviews Clinical Oncology*. Nature Publishing Group, 14(6), pp. 331–332. doi: 10.1038/nrclinonc.2017.46.

Bu, T. *et al.* (2014) 'XRCC1 Arg399Gln polymorphism confers risk of breast cancer in American population: a meta-analysis of 10846 cases and 11723 controls.', *PloS one*. Public Library of Science, 9(1), p. e86086. doi: 10.1371/journal.pone.0086086.

Caldon, C. E. and Musgrove, E. A. (2010) 'Distinct and redundant functions of cyclin E1 and cyclin E2 in development and cancer.', *Cell division*. BioMed Central, 5, p. 2. doi: 10.1186/1747-1028-5-2.

Cancer Genome Atlas Research Network (2011) 'Integrated genomic analyses of ovarian carcinoma', *Nature*, 474(7353), pp. 609–615. doi: 10.1038/nature10166.

Canitrot, Y. *et al.* (1998) 'Overexpression of DNA polymerase beta in cell results in

a mutator phenotype and a decreased sensitivity to anticancer drugs.', *Proceedings of the National Academy of Sciences of the United States of America*. National Academy of Sciences, 95(21), pp. 12586–90. doi: 10.1073/pnas.95.21.12586.

Chan, K. *et al.* (2007) 'Overexpression of DNA polymerase b results in an increased rate of frameshift mutations during base excision repair', *Mutagenesis*, 22(3), pp. 183–188. doi: 10.1093/mutage/gel070.

Chang, H. H. Y. *et al.* (2017) 'Non-homologous DNA end joining and alternative pathways to double-strand break repair', *Nature Reviews Molecular Cell Biology*. Nature Publishing Group, 18(8), pp. 495–506. doi: 10.1038/nrm.2017.48.

Chasle, J. *et al.* (2003) 'Immunohistochemical study of cell cycle regulatory proteins in intraductal breast carcinomas--a preliminary study.', *European journal of cancer (Oxford, England : 1990)*, 39(10), pp. 1363–9. Available at: http://www.ncbi.nlm.nih.gov/pubmed/12826038 (Accessed: 12 June 2019).

Chehab, N. H. *et al.* (2000) 'Chk2/hCds1 functions as a DNA damage checkpoint in G(1) by stabilizing p53.', *Genes & development*. Cold Spring Harbor Laboratory Press, 14(3), pp. 278–88. Available at: http://www.ncbi.nlm.nih.gov/pubmed/10673500 (Accessed: 16 June 2019).

Chen, K. *et al.* (1998) 'Up-regulation of base excision repair correlates with enhanced protection against a DNA damaging agent in mouse cell lines', *Nucleic Acids Research*, 26(8), pp. 2001–2007. doi: 10.1093/nar/26.8.2001.

Choi, Y. *et al.* (2013) 'Epithelial-mesenchymal transition increases during the

progression of in situ to invasive basal-like breast cancer', *Human Pathology*, 44(11), pp. 2581–2589. doi: 10.1016/j.humpath.2013.07.003.

Choi, Y. E. *et al.* (2016) 'Platinum and PARP Inhibitor Resistance Due to Overexpression of MicroRNA-622 in BRCA1 -Mutant Ovarian Cancer', *Cell Reports*, 14(3), pp. 429–439. doi: 10.1016/j.celrep.2015.12.046.

Claus, E. B. *et al.* (2005) 'Prevalence of <EMPH TYPE="ITAL">BRCA1</EMPH> and <EMPH TYPE="ITAL">BRCA2</EMPH> Mutations in Women Diagnosed With Ductal Carcinoma In Situ', *JAMA*, 293(8), p. 964. doi: 10.1001/jama.293.8.964.

Constantin, N. *et al.* (2005) 'Human mismatch repair: reconstitution of a nick-directed bidirectional reaction.', *The Journal of biological chemistry*. American Society for Biochemistry and Molecular Biology, 280(48), pp. 39752–61. doi: 10.1074/jbc.M509701200.

Criscitiello, C. *et al.* (2014) 'Investigational platelet-derived growth factor receptor kinase inhibitors in breast cancer therapy', *Expert Opinion on Investigational Drugs*. Taylor & Francis, 23(5), pp. 599–610. doi: 10.1517/13543784.2014.895323.

Croteau, D. L. *et al.* (2017) 'NAD+ in DNA repair and mitochondrial maintenance.', *Cell cycle (Georgetown, Tex.)*. Taylor & Francis, 16(6), pp. 491–492. doi: 10.1080/15384101.2017.1285631.

Curtin, N. J. (2012) 'DNA repair dysregulation from cancer driver to therapeutic target', *Nature Reviews Cancer*. Nature Publishing Group, 12(12), pp. 801–817.

doi: 10.1038/nrc3399.

Curtis, C. (2015) 'Genomic profiling of breast cancers.', *Current opinion in obstetrics & gynecology*. NIH Public Access, 27(1), pp. 34–9. doi: 10.1097/GCO.0000000000000145.

Curtis, C. D., Thorngren, D. L. and Nardulli, A. M. (2010) 'Immunohistochemical analysis of oxidative stress and DNA repair proteins in normal mammary and breast cancer tissues', *BMC Cancer*. BioMed Central, 10(1), p. 9. doi: 10.1186/1471-2407-10-9.

Cuzick, J. *et al.* (2011) 'Effect of tamoxifen and radiotherapy in women with locally excised ductal carcinoma in situ: long-term results from the UK/ANZ DCIS trial', *The Lancet Oncology*, 12(1), pp. 21–29. doi: 10.1016/S1470-2045(10)70266-7.

D'ippolito, E. *et al.* (2016) 'Tumor and Stem Cell Biology miR-9 and miR-200 Regulate PDGFRb-Mediated Endothelial Differentiation of Tumor Cells in Triple-Negative Breast Cancer'. doi: 10.1158/0008-5472.CAN-16-0140.

Dai, C.-H. *et al.* (2015) 'RNA interferences targeting the Fanconi anemia/BRCA pathway upstream genes reverse cisplatin resistance in drug-resistant lung cancer cells', *Journal of Biomedical Science*, 22(1), p. 77. doi: 10.1186/s12929-015-0185-4.

Dalal, S. *et al.* (2005) 'Prostate-Cancer-Associated I260M Variant of DNA Polymerase β Is a Sequence-Specific Mutator †', *Biochemistry*, 44(48), pp. 15664–15673. doi: 10.1021/bi051179z.

Dalal, S. *et al.* (2007) 'The Leu22Pro tumor-associated variant of DNA polymerase

beta is dRP lyase deficient', *Nucleic Acids Research*, 36(2), pp. 411–422. doi: 10.1093/nar/gkm1053.

Damia, G. and Broggini, M. (2019) 'Platinum Resistance in Ovarian Cancer: Role of DNA Repair.', *Cancers*. Multidisciplinary Digital Publishing Institute (MDPI), 11(1). doi: 10.3390/cancers11010119.

David, S. S., O'Shea, V. L. and Kundu, S. (2007) 'Base-excision repair of oxidative DNA damage', *Nature*, 447(7147), pp. 941–950. doi: 10.1038/nature05978.

Debnath, J., Muthuswamy, S. K. and Brugge, J. S. (2003) 'Morphogenesis and oncogenesis of MCF-10A mammary epithelial acini grown in three-dimensional basement membrane cultures', *Methods*, 30(3), pp. 256–268. doi: 10.1016/S1046-2023(03)00032-X.

Deng, C.-X. and Wang, R.-H. (2003) 'Roles of BRCA1 in DNA damage repair: a link between development and cancer', *Human Molecular Genetics*. Narnia, 12(90001), pp. 113R – 123. doi: 10.1093/hmg/ddg082.

Dhillon, K. K. and Taniguchi, T. (2015) 'Resistance to PARP Inhibitors Mediated by Secondary BRCA1/2 Mutations', in. Humana Press, Cham, pp. 431–452. doi: 10.1007/978-3-319-14151-0_18.

Dianov, G. L. (2011) 'Base excision repair targets for cancer therapy.', *American journal of cancer research*. e-Century Publishing Corporation, 1(7), pp. 845–51. Available at: http://www.ncbi.nlm.nih.gov/pubmed/22016832 (Accessed: 19 June 2019).

Dianov, G. L. and Hübscher, U. (2013) 'Mammalian base excision repair: the

forgotten archangel.', *Nucleic acids research*. Oxford University Press, 41(6), pp. 3483–90. doi: 10.1093/nar/gkt076.

Dianov, G. and Lindahl, T. (1994) 'Reconstitution of the DNA base excision—repair pathway', *Current Biology*. Cell Press, 4(12), pp. 1069–1076. doi: 10.1016/S0960-9822(00)00245-1.

Dietlein, F., Thelen, L. and Reinhardt, H. C. (2014) 'Cancer-specific defects in DNA repair pathways as targets for personalized therapeutic approaches', *Trends in Genetics*, 30, pp. 326–339. doi: 10.1016/j.tig.2014.06.003.

Ding, X. *et al.* (2016) 'Synthetic viability by BRCA2 and PARP1/ARTD1 deficiencies', *Nature Communications*, 7, p. 12425. doi: 10.1038/ncomms12425.

Dobashi, Y. *et al.* (1994) 'DNA polymerase beta gene mutation in human prostate cancer.', *Cancer research*. American Association for Cancer Research, 54(11), pp. 2827–9. Available at: http://www.ncbi.nlm.nih.gov/pubmed/8187060 (Accessed: 4 May 2019).

Donigan, K. A. *et al.* (2012) 'Human POLB gene is mutated in high percentage of colorectal tumors.', *The Journal of biological chemistry*. American Society for Biochemistry and Molecular Biology, 287(28), pp. 23830–9. doi: 10.1074/jbc.M111.324947.

Dörr, J. R. *et al.* (2013) 'Synthetic lethal metabolic targeting of cellular senescence in cancer therapy', *Nature*. Nature Publishing Group, 501(7467), pp. 421–425. doi: 10.1038/nature12437.

Drost, R. *et al.* (2011) 'BRCA1 RING Function Is Essential for Tumor Suppression

but Dispensable for Therapy Resistance', *Cancer Cell*. Cell Press, 20(6), pp. 797–809. doi: 10.1016/J.CCR.2011.11.014.

Drost, R. *et al.* (2016) 'BRCA1185delAG tumors may acquire therapy resistance through expression of RING-less BRCA1.', *The Journal of clinical investigation*. American Society for Clinical Investigation, 126(8), pp. 2903–18. doi: 10.1172/JCI70196.

Du, Y. *et al.* (2016) 'Blocking c-Met-mediated PARP1 phosphorylation enhances anti-tumor effects of PARP inhibitors.', *Nature medicine*. NIH Public Access, 22(2), pp. 194–201. doi: 10.1038/nm.4032.

Edwards, S. L. *et al.* (2008) 'Resistance to therapy caused by intragenic deletion in BRCA2', *Nature*. Nature Publishing Group, 451(7182), pp. 1111–1115. doi: 10.1038/nature06548.

Eiring, A. M. *et al.* (2015) 'Combined STAT3 and BCR-ABL1 inhibition induces synthetic lethality in therapy-resistant chronic myeloid leukemia', *Leukemia*, 29(3), pp. 586–597. doi: 10.1038/leu.2014.245.

ELLIS, I. O. *et al.* (2007) 'Pathological prognostic factors in breast cancer. II. Histological type. Relationship with survival in a large study with long-term follow-up', *Histopathology*. John Wiley & Sons, Ltd (10.1111), 20(6), pp. 479–489. doi: 10.1111/j.1365-2559.1992.tb01032.x.

Ellis, M. J. *et al.* (2012) 'Whole-genome analysis informs breast cancer response to aromatase inhibition', *Nature*. Nature Publishing Group, 486(7403), pp. 353–360. doi: 10.1038/nature11143.

References

Elston, C. W. and Ellis, I. O. (1991) 'Pathological prognostic factors in breast cancer. I. The value of histological grade in breast cancer: experience from a large study with long-term follow-up.', *Histopathology*, 19(5), pp. 403–10. Available at: http://www.ncbi.nlm.nih.gov/pubmed/1757079 (Accessed: 30 June 2019).

Emdin, S. O. *et al.* (2006) 'SweDCIS: Radiotherapy after sector resection for ductal carcinoma in situ of the breast. Results of a randomised trial in a population offered mammography screening', *Acta Oncologica*, 45(5), pp. 536–543. doi: 10.1080/02841860600681569.

Eng-Wong, J., Costantino, J. P. and Swain, S. M. (2010) 'The impact of systemic therapy following ductal carcinoma in situ.', *Journal of the National Cancer Institute. Monographs*. Oxford University Press, 2010(41), pp. 200–3. doi: 10.1093/jncimonographs/lgq021.

Etemadmoghadam, D. *et al.* (2009) 'Integrated genome-wide DNA copy number and expression analysis identifies distinct mechanisms of primary chemoresistance in ovarian carcinomas.', *Clinical cancer research : an official journal of the American Association for Cancer Research*. NIH Public Access, 15(4), pp. 1417–27. doi: 10.1158/1078-0432.CCR-08-1564.

Facchetti, G., Zampieri, M. and Altafini, C. (2012) 'Predicting and characterizing selective multiple drug treatments for metabolic diseases and cancer', *BMC Systems Biology*. BioMed Central, 6(1), p. 115. doi: 10.1186/1752-0509-6-115.

Fang, D. *et al.* (2017) 'Epithelial-mesenchymal transition of ovarian cancer cells is sustained by Rac1 through simultaneous activation of MEK1/2 and Src signaling pathways.', *Oncogene*. NIH Public Access, 36(11), pp. 1546–1558. doi:

10.1038/onc.2016.323.

Farmer, H. *et al.* (2005) 'Targeting the DNA repair defect in BRCA mutant cells as a therapeutic strategy', *Nature*. Nature Publishing Group, 434(7035), pp. 917–921. doi: 10.1038/nature03445.

Ferlay, J. *et al.* (2010) 'Estimates of worldwide burden of cancer in 2008: GLOBOCAN 2008', *International Journal of Cancer*, 127(12), pp. 2893–2917. doi: 10.1002/ijc.25516.

Ferlay, J. *et al.* (2015) 'Cancer incidence and mortality worldwide: Sources, methods and major patterns in GLOBOCAN 2012', *International Journal of Cancer*. John Wiley & Sons, Ltd, 136(5), pp. E359–E386. doi: 10.1002/ijc.29210.

Fong, P. C. *et al.* (2010) 'Poly(ADP)-ribose polymerase inhibition: frequent durable responses in BRCA carrier ovarian cancer correlating with platinum-free interval.', *Journal of clinical oncology : official journal of the American Society of Clinical Oncology*, 28(15), pp. 2512–9. doi: 10.1200/JCO.2009.26.9589.

Fouquerel, E. and Sobol, R. W. (2014) 'ARTD1 (PARP1) activation and NAD(+) in DNA repair and cell death.', *DNA repair*. NIH Public Access, 23, pp. 27–32. doi: 10.1016/j.dnarep.2014.09.004.

Frezza, C. *et al.* (2011) 'Haem oxygenase is synthetically lethal with the tumour suppressor fumarate hydratase', *Nature*. Nature Publishing Group, 477(7363), pp. 225–228. doi: 10.1038/nature10363.

Friedberg, E. C. (2003) 'DNA damage and repair', *Nature*, 421(6921), pp. 436–440. doi: 10.1038/nature01408.

References

Gaitskell, K. *et al.* (2011) 'Angiogenesis inhibitors for the treatment of ovarian cancer', *Cochrane Database of Systematic Reviews*, (9), p. CD007930. doi: 10.1002/14651858.CD007930.pub2.

Galea, M. H. *et al.* (1992) 'The Nottingham Prognostic Index in primary breast cancer.', *Breast cancer research and treatment*, 22(3), pp. 207–19. Available at: http://www.ncbi.nlm.nih.gov/pubmed/1391987 (Accessed: 30 June 2019).

Gavande, N. S. *et al.* (2016) 'DNA repair targeted therapy: The past or future of cancer treatment?', *Pharmacology & Therapeutics*. Pergamon, 160, pp. 65–83. doi: 10.1016/J.PHARMTHERA.2016.02.003.

Giuliano, A. E. *et al.* (2017) 'Breast Cancer-Major changes in the American Joint Committee on Cancer eighth edition cancer staging manual', *CA: A Cancer Journal for Clinicians*. American Cancer Society, 67(4), pp. 290–303. doi: 10.3322/caac.21393.

Gogola, E. *et al.* (2018) 'Selective Loss of PARG Restores PARylation and Counteracts PARP Inhibitor-Mediated Synthetic Lethality', *Cancer Cell*. Cell Press, 33(6), pp. 1078-1093.e12. doi: 10.1016/J.CCELL.2018.05.008.

Gorringe, K. L. and Fox, S. B. (2017) 'Ductal Carcinoma In Situ Biology, Biomarkers, and Diagnosis.', *Frontiers in oncology*. Frontiers Media SA, 7, p. 248. doi: 10.3389/fonc.2017.00248.

Gravells, P., Grant, E., Smith, Kate M, *et al.* (2017) 'Specific killing of DNA damage-response deficient cells with inhibitors of poly(ADP-ribose) glycohydrolase.', *DNA repair*. Elsevier, 52, pp. 81–91. doi: 10.1016/j.dnarep.2017.02.010.

References

Gravells, P., Grant, E., Smith, Kate M., *et al.* (2017) 'Specific killing of DNA damage-response deficient cells with inhibitors of poly(ADP-ribose) glycohydrolase', *DNA Repair*. Elsevier, 52, pp. 81–91. doi: 10.1016/J.DNAREP.2017.02.010.

Green, A. R. *et al.* (2015) 'Biological and clinical significance of PARP1 protein expression in breast cancer', *Breast Cancer Research and Treatment*, 149(2), pp. 353–362. doi: 10.1007/s10549-014-3230-1.

Green, A. R. *et al.* (2016) 'Nottingham prognostic index plus (NPI+) predicts risk of distant metastases in primary breast cancer', *Breast Cancer Research and Treatment*. Springer, 157(1), pp. 65–75. doi: 10.1007/s10549-016-3804-1.

Green, A. R. *et al.* (2017) 'Clinical Impact of Tumor DNA Repair Expression and T-cell Infiltration in Breast Cancers', *Cancer Immunology Research*. American Association for Cancer Research, 5(4), pp. 292–299. doi: 10.1158/2326-6066.CIR-16-0195.

Green, A. R. (2017) 'Molecular classification of breast cancer: what the pathologist needs to know', *Pathology*. Elsevier, 49(2), pp. 111–119. doi: 10.1016/J.PATHOL.2016.10.012.

Grimm, S. L. and Rosen, J. M. (2003) 'The Role of C/EBPβ in Mammary Gland Development and Breast Cancer', *Journal of Mammary Gland Biology and Neoplasia*. Kluwer Academic Publishers-Plenum Publishers, 8(2), pp. 191–204. doi: 10.1023/A:1025900908026.

Gupta, D. *et al.* (2018) 'ATR-Chk1 activation mitigates replication stress caused by mismatch repair-dependent processing of DNA damage', *Proceedings of the*

National Academy of Sciences, 115(7), pp. 1523–1528. doi: 10.1073/pnas.1720355115.

Gupta, D. and Lis, C. G. (2009) 'Role of CA125 in predicting ovarian cancer survival - a review of the epidemiological literature', *Journal of Ovarian Research*. BioMed Central, 2, p. 13. doi: 10.1186/1757-2215-2-13.

H. Nicolay, N., Helleday, T. and A. Sharma, R. (2012) 'Biological Relevance of DNA Polymerase Beta and Translesion Synthesis Polymerases to Cancer and its Treatment', *Current Molecular Pharmacology*, 5(1), pp. 54–67. doi: 10.2174/1874467211205010054.

Hagting, A. *et al.* (1999) 'Translocation of cyclin B1 to the nucleus at prophase requires a phosphorylation-dependent nuclear import signal', *Current Biology*. Cell Press, 9(13), pp. 680–689. doi: 10.1016/S0960-9822(99)80308-X.

Hansen, A. B. *et al.* (2006) 'Mitochondrial DNA integrity is not dependent on DNA polymerase-β activity', *DNA Repair*. Elsevier, 5(1), pp. 71–79. doi: 10.1016/J.DNAREP.2005.07.009.

Heaphy, C. M. *et al.* (2009) 'Genomic instability demonstrates similarity between DCIS and invasive carcinomas.', *Breast cancer research and treatment*. NIH Public Access, 117(1), pp. 17–24. doi: 10.1007/s10549-008-0165-4.

Hoch, N. C. *et al.* (2017) 'XRCC1 mutation is associated with PARP1 hyperactivation and cerebellar ataxia', *Nature*. Nature Publishing Group, 541(7635), pp. 87–91. doi: 10.1038/nature20790.

Hoffmann, J.-S. *et al.* (1995) *DNA polymerase (3 bypasses in vitro a single d(GpG)-*

cisplatin adduct placed on codon 13 of the HRAS gene [calf thymus DNA polymerases a, 13, 6, and £/cis-diamminedichloroplatinum(II)/lesion bypass], *Biochemistry*. Available at: https://www.pnas.org/content/pnas/92/12/5356.full.pdf (Accessed: 6 May 2019).

Holmberg, L. *et al.* (2008) 'Absolute Risk Reductions for Local Recurrence After Postoperative Radiotherapy After Sector Resection for Ductal Carcinoma In Situ of the Breast', *Journal of Clinical Oncology*, 26(8), pp. 1247–1252. doi: 10.1200/JCO.2007.12.7969.

Hopkins, T. A. *et al.* (2015) 'Mechanistic Dissection of PARP1 Trapping and the Impact on In Vivo Tolerability and Efficacy of PARP Inhibitors', *Molecular Cancer Research*. American Association for Cancer Research, 13(11), pp. 1465–1477. doi: 10.1158/1541-7786.MCR-15-0191-T.

Hopkins, T. A. *et al.* (2018) 'PARP1 trapping by PARP inhibitors drives cytotoxicity both in cancer cells and healthy bone marrow'. doi: 10.1158/1541-7786.MCR-18-0138.

Hopkins, T. A. *et al.* (2019) 'PARP1 Trapping by PARP Inhibitors Drives Cytotoxicity in Both Cancer Cells and Healthy Bone Marrow', *Molecular Cancer Research*. American Association for Cancer Research, 17(2), pp. 409–419. doi: 10.1158/1541-7786.MCR-18-0138.

Horton, J. K. *et al.* (2014) 'Base Excision Repair Defects Invoke Hypersensitivity to PARP Inhibition', *Molecular Cancer Research*, 12(8), pp. 1128–1139. doi: 10.1158/1541-7786.MCR-13-0502.

References

Hsieh, P. and Yamane, K. (2008) 'DNA mismatch repair: molecular mechanism, cancer, and ageing.', *Mechanisms of ageing and development*. NIH Public Access, 129(7–8), pp. 391–407. doi: 10.1016/j.mad.2008.02.012.

Huang, M.-J. *et al.* (2006) 'A small-molecule c-Myc inhibitor, 10058-F4, induces cell-cycle arrest, apoptosis, and myeloid differentiation of human acute myeloid leukemia', *Experimental Hematology*, 34(11), pp. 1480–1489. doi: 10.1016/j.exphem.2006.06.019.

Huang, Y., Li, L. and Yu, L. (2009) 'XRCC1 Arg399Gln, Arg194Trp and Arg280His polymorphisms in breast cancer risk: a meta-analysis', *Mutagenesis*. Oxford University Press, 24(4), pp. 331–339. doi: 10.1093/mutage/gep013.

Hwang, E. S. *et al.* (2004) *Patterns of Chromosomal Alterations in Breast Ductal Carcinoma In situ*. Available at: http://clincancerres.aacrjournals.org/content/clincanres/10/15/5160.full.pdf (Accessed: 18 March 2019).

Ibrahim, E. E. *et al.* (2012) 'Embryonic NANOG Activity Defines Colorectal Cancer Stem Cells and Modulates through AP1- and TCF-dependent Mechanisms', *STEM CELLS*. John Wiley & Sons, Ltd, 30(10), pp. 2076–2087. doi: 10.1002/stem.1182.

Ison, G. *et al.* (2018) 'FDA Approval Summary: Niraparib for the Maintenance Treatment of Patients with Recurrent Ovarian Cancer in Response to Platinum-Based Chemotherapy', *Clinical Cancer Research*, 24(17), pp. 4066–4071. doi: 10.1158/1078-0432.CCR-18-0042.

Iwatsuki, M. *et al.* (2009) 'A platinum agent resistance gene, *POLB* , is a prognostic

indicator in colorectal cancer', *Journal of Surgical Oncology*. John Wiley & Sons, Ltd, 100(3), pp. 261–266. doi: 10.1002/jso.21275.

Jaiswal, A. S. *et al.* (2009) 'A Novel Inhibitor of DNA Polymerase Enhances the Ability of Temozolomide to Impair the Growth of Colon Cancer Cells', *Molecular Cancer Research*, 7(12), pp. 1973–1983. doi: 10.1158/1541-7786.MCR-09-0309.

Jaiswal, A. S. *et al.* (2011) 'DNA Polymerase β as a Novel Target for Chemotherapeutic Intervention of Colorectal Cancer', *PLoS ONE*. Edited by B. Ko. Public Library of Science, 6(2), p. e16691. doi: 10.1371/journal.pone.0016691.

Jaiswal, A. S. *et al.* (2015) 'NSC666715 and Its Analogs Inhibit Strand-Displacement Activity of DNA Polymerase β and Potentiate Temozolomide-Induced DNA Damage, Senescence and Apoptosis in Colorectal Cancer Cells', *PLOS ONE*. Edited by R. W. Sobol. Public Library of Science, 10(5), p. e0123808. doi: 10.1371/journal.pone.0123808.

Jallepalli, P. V *et al.* (2003) 'The Chk2 tumor suppressor is not required for p53 responses in human cancer cells.', *The Journal of biological chemistry*. American Society for Biochemistry and Molecular Biology, 278(23), pp. 20475–9. doi: 10.1074/jbc.M213159200.

Jelinic, P. and Levine, D. A. (2014) 'New Insights into PARP Inhibitors' Effect on Cell Cycle and Homology-Directed DNA Damage Repair', *Molecular Cancer Therapeutics*, 13(6), pp. 1645–1654. doi: 10.1158/1535-7163.MCT-13-0906-T.

Jiang, X. *et al.* (2019) 'PARP inhibitors in ovarian cancer: Sensitivity prediction and resistance mechanisms', *Journal of Cellular and Molecular Medicine*, 23(4), pp.

2303–2313. doi: 10.1111/jcmm.14133.

Jiao, S. *et al.* (2017) 'PARP Inhibitor Upregulates PD-L1 Expression and Enhances Cancer-Associated Immunosuppression.', *Clinical cancer research : an official journal of the American Association for Cancer Research*. NIH Public Access, 23(14), pp. 3711–3720. doi: 10.1158/1078-0432.CCR-16-3215.

Jiricny, J. (2006) 'The multifaceted mismatch-repair system', *Nature Reviews Molecular Cell Biology*. Nature Publishing Group, 7(5), pp. 335–346. doi: 10.1038/nrm1907.

Jirström, K. *et al.* (2003) 'Tissue microarray analyses of G1/S-regulatory proteins in ductal carcinoma in situ of the breast indicate that low cyclin D1 is associated with local recurrence', *British Journal of Cancer*, 89(10), pp. 1920–1926. doi: 10.1038/sj.bjc.6601398.

Johnson, N. *et al.* (2013) 'Stabilization of mutant BRCA1 protein confers PARP inhibitor and platinum resistance.', *Proceedings of the National Academy of Sciences of the United States of America*. National Academy of Sciences, 110(42), pp. 17041–6. doi: 10.1073/pnas.1305170110.

Karnak, D. *et al.* (2014) 'Combined Inhibition of Wee1 and PARP1/2 for Radiosensitization in Pancreatic Cancer', *Clinical Cancer Research*, 20(19), pp. 5085–5096. doi: 10.1158/1078-0432.CCR-14-1038.

Kauff, N. D. *et al.* (2003) 'Epithelial lesions in prophylactic mastectomy specimens from women withBRCA mutations', *Cancer*, 97(7), pp. 1601–1608. doi: 10.1002/cncr.11225.

References

Kaufman, B. A. and Van Houten, B. (2017) 'POLB: A new role of DNA polymerase beta in mitochondrial base excision repair', *DNA Repair*. Elsevier, 60, pp. A1–A5. doi: 10.1016/J.DNAREP.2017.11.002.

Kelley, M. R. *et al.* (2001) 'Elevated and altered expression of the multifunctional DNA base excision repair and redox enzyme Ape1/ref-1 in prostate cancer.', *Clinical cancer research : an official journal of the American Association for Cancer Research*, 7(4), pp. 824–30. Available at: http://www.ncbi.nlm.nih.gov/pubmed/11309329 (Accessed: 19 June 2019).

Kelly, Z. L. *et al.* (2011) 'HOX genes in ovarian cancer.', *Journal of ovarian research*. BioMed Central, 4, p. 16. doi: 10.1186/1757-2215-4-16.

Kerlikowske, K. *et al.* (2010) 'Biomarker expression and risk of subsequent tumors after initial ductal carcinoma in situ diagnosis.', *Journal of the National Cancer Institute*. Oxford University Press, 102(9), pp. 627–37. doi: 10.1093/jnci/djq101.

Kerlikowske, K. (2010) 'Epidemiology of ductal carcinoma in situ.', *Journal of the National Cancer Institute. Monographs*. Oxford University Press, 2010(41), pp. 139–41. doi: 10.1093/jncimonographs/lgq027.

Kiessling, A. *et al.* (2006) 'Selective Inhibition of c-Myc/Max Dimerization and DNA Binding by Small Molecules', *Chemistry & Biology*. Cell Press, 13(7), pp. 745–751. doi: 10.1016/J.CHEMBIOL.2006.05.011.

Kim, G. *et al.* (2015) 'FDA Approval Summary: Olaparib Monotherapy in Patients with Deleterious Germline BRCA-Mutated Advanced Ovarian Cancer Treated with Three or More Lines of Chemotherapy', *Clinical Cancer Research*. American

Association for Cancer Research, 21(19), pp. 4257–4261. doi: 10.1158/1078-0432.CCR-15-0887.

Kim, J. Y., Cho, C. H. and Song, H. S. (2017) 'Targeted therapy of ovarian cancer including immune check point inhibitor', *The Korean Journal of Internal Medicine*. Korean Association of Internal Medicine, 32(5), p. 798. doi: 10.3904/KJIM.2017.008.

Kim, M. Y., Zhang, T. and Kraus, W. L. (2005) 'Poly(ADP-ribosyl)ation by PARP-1: "PAR-laying" NAD+ into a nuclear signal.', *Genes & development*. Cold Spring Harbor Laboratory Press, 19(17), pp. 1951–67. doi: 10.1101/gad.1331805.

Kim, S. Y. *et al.* (2015) 'Genomic differences between pure ductal carcinoma in situ and synchronous ductal carcinoma in situ with invasive breast cancer', *Oncotarget*. Impact Journals, LLC, 6(10), p. 7597. doi: 10.18632/ONCOTARGET.3162.

King, B. *et al.* (2013) 'The Ubiquitin Ligase FBXW7 Modulates Leukemia-Initiating Cell Activity by Regulating MYC Stability', *Cell*, 153(7), pp. 1552–1566. doi: 10.1016/j.cell.2013.05.041.

Kojima, K. *et al.* (2006) 'Mdm2 inhibitor Nutlin-3a induces p53-mediated apoptosis by transcription-dependent and transcription-independent mechanisms and may overcome Atm-mediated resistance to fludarabine in chronic lymphocytic leukemia.', *Blood*. American Society of Hematology, 108(3), pp. 993–1000. doi: 10.1182/blood-2005-12-5148.

Koll, T. T. *et al.* (2008) 'HSP90 inhibitor, DMAG, synergizes with radiation of lung

cancer cells by interfering with base excision and ATM-mediated DNA repair', *Molecular Cancer Therapeutics*, 7(7), pp. 1985–1992. doi: 10.1158/1535-7163.MCT-07-2104.

Kononen, J. *et al.* (1998) 'Tissue microarrays for high-throughput molecular profiling of tumor specimens.', *Nature medicine*, 4(7), pp. 844–7. Available at: http://www.ncbi.nlm.nih.gov/pubmed/9662379 (Accessed: 14 July 2019).

Konstantinopoulos, P. A. *et al.* (2010) 'Gene Expression Profile of *BRCA* ness That Correlates With Responsiveness to Chemotherapy and With Outcome in Patients With Epithelial Ovarian Cancer', *Journal of Clinical Oncology*, 28(22), pp. 3555–3561. doi: 10.1200/JCO.2009.27.5719.

Koopman, G. *et al.* (1994) 'Annexin V for flow cytometric detection of phosphatidylserine expression on B cells undergoing apoptosis.', *Blood*, 84(5), pp. 1415–20. Available at: http://www.ncbi.nlm.nih.gov/pubmed/8068938 (Accessed: 20 June 2018).

Krejci, L. *et al.* (2012) 'Homologous recombination and its regulation', *Nucleic Acids Research*. Narnia, 40(13), pp. 5795–5818. doi: 10.1093/nar/gks270.

Kroiss, R. *et al.* (2008) 'Prevalence of pre-malignant and malignant lesions in prophylactic mastectomy specimens of BRCA1 mutation carriers: comparison with a control group', *Journal of Cancer Research and Clinical Oncology*. Springer-Verlag, 134(10), pp. 1113–1121. doi: 10.1007/s00432-008-0383-5.

Kurman, R. J. and Shih, I.-M. (2016) 'The Dualistic Model of Ovarian Carcinogenesis', *The American Journal of Pathology*, 186(4), pp. 733–747. doi:

10.1016/j.ajpath.2015.11.011.

Lalani, N. and Rakovitch, E. (2017) 'Improving Therapeutic Ratios with the Oncotype DX® Ductal Carcinoma In Situ (DCIS) Score.', *Cureus*. Cureus Inc., 9(4), p. e1185. doi: 10.7759/cureus.1185.

Lallo, A. *et al.* (2018) 'The Combination of the PARP Inhibitor Olaparib and the WEE1 Inhibitor AZD1775 as a New Therapeutic Option for Small Cell Lung Cancer', *Clinical Cancer Research*, 24(20), pp. 5153–5164. doi: 10.1158/1078-0432.CCR-17-2805.

Lamarche, B. J., Orazio, N. I. and Weitzman, M. D. (2010) 'The MRN complex in double-strand break repair and telomere maintenance.', *FEBS letters*. NIH Public Access, 584(17), pp. 3682–95. doi: 10.1016/j.febslet.2010.07.029.

Landen, C. N., Kinch, M. S. and Sood, A. K. (2005) 'EphA2 as a target for ovarian cancer therapy', *Expert Opinion on Therapeutic Targets*, 9(6), pp. 1179–1187. doi: 10.1517/14728222.9.6.1179.

Lang, T. *et al.* (2007) 'The E295K DNA Polymerase Beta Gastric Cancer-Associated Variant Interferes with Base Excision Repair and Induces Cellular Transformation', *Molecular and Cellular Biology*, 27(15), pp. 5587–5596. doi: 10.1128/MCB.01883-06.

Lange, S. S., Takata, K. and Wood, R. D. (2011) 'DNA polymerases and cancer.', *Nature reviews. Cancer*. NIH Public Access, 11(2), pp. 96–110. doi: 10.1038/nrc2998.

Langhans, S. A. (2018) 'Three-Dimensional in Vitro Cell Culture Models in Drug

Discovery and Drug Repositioning.', *Frontiers in pharmacology*. Frontiers Media SA, 9, p. 6. doi: 10.3389/fphar.2018.00006.

Lari, S. A. and Kuerer, H. M. (2011) 'Biological Markers in DCIS and Risk of Breast Recurrence: A Systematic Review', *Journal of Cancer*, 2, pp. 232–261. doi: 10.7150/jca.2.232.

Ledermann, J. A. *et al.* (2016) 'Overall survival in patients with platinum-sensitive recurrent serous ovarian cancer receiving olaparib maintenance monotherapy: an updated analysis from a randomised, placebo-controlled, double-blind, phase 2 trial', *The Lancet Oncology*. Elsevier, 17(11), pp. 1579–1589. doi: 10.1016/S1470-2045(16)30376-X.

Lee, J.-M. *et al.* (2017) 'Safety and Clinical Activity of the Programmed Death-Ligand 1 Inhibitor Durvalumab in Combination With Poly (ADP-Ribose) Polymerase Inhibitor Olaparib or Vascular Endothelial Growth Factor Receptor 1-3 Inhibitor Cediranib in Women's Cancers: A Dose-Escalation, Phase I Study', *Journal of Clinical Oncology*, 35(19), pp. 2193–2202. doi: 10.1200/JCO.2016.72.1340.

Lee, J.-M. and Gulley, J. L. (2017) 'Checkpoint and PARP inhibitors, for whom and when.', *Oncotarget*. Impact Journals, LLC, 8(56), pp. 95036–95037. doi: 10.18632/oncotarget.20852.

Lee, J. H., Kim, H. M. and Koo, J. S. (2018) 'Differential Expression of Cancer-Associated Fibroblast-Related Proteins in Ductal Carcinoma in situ According to Molecular Subtype and Stromal Histology', *Pathobiology*. Karger Publishers, 85(5–6), pp. 311–321. doi: 10.1159/000492392.

References

Lehmann, A R *et al.* (1975) 'Xeroderma pigmentosum cells with normal levels of excision repair have a defect in DNA synthesis after UV-irradiation.', *Proceedings of the National Academy of Sciences of the United States of America*. National Academy of Sciences, 72(1), pp. 219–23. doi: 10.1073/pnas.72.1.219.

Li, C. I. (2003) 'Relationship Between Long Durations and Different Regimens of Hormone Therapy and Risk of Breast Cancer', *JAMA*, 289(24), p. 3254. doi: 10.1001/jama.289.24.3254.

Li, C. I., Daling, J. R. and Malone, K. E. (2005) 'Age-Specific Incidence Rates of In situ Breast Carcinomas by Histologic Type, 1980 to 2001', *Cancer Epidemiology Biomarkers & Prevention*. American Association for Cancer Research, 14(4), pp. 1008–1011. doi: 10.1158/1055-9965.EPI-04-0849.

Li, H. *et al.* (2010) 'PIK3CA mutations mostly begin to develop in ductal carcinoma of the breast', *Experimental and Molecular Pathology*, 88(1), pp. 150–155. doi: 10.1016/j.yexmp.2009.09.016.

Li, H., Ha, T. C. and Tai, B. C. (2009) 'XRCC1 gene polymorphisms and breast cancer risk in different populations: A meta-analysis', *The Breast*, 18(3), pp. 183–191. doi: 10.1016/j.breast.2009.03.008.

Li, S. K. H. and Martin, A. (2016) 'Mismatch Repair and Colon Cancer: Mechanisms and Therapies Explored'. doi: 10.1016/j.molmed.2016.02.003.

Li, X. and Heyer, W.-D. (2008) 'Homologous recombination in DNA repair and DNA damage tolerance.', *Cell research*. NIH Public Access, 18(1), pp. 99–113. doi: 10.1038/cr.2008.1.

References

Lim, S. and Kaldis, P. (2013) 'Cdks, cyclins and CKIs: roles beyond cell cycle regulation', *Development*, 140(15), pp. 3079–3093. doi: 10.1242/dev.091744.

Lin, X. *et al.* (2018) 'Augmented antitumor activity by olaparib plus AZD1775 in gastric cancer through disrupting DNA damage repair pathways and DNA damage checkpoint', *Journal of Experimental & Clinical Cancer Research*. BioMed Central, 37(1), p. 129. doi: 10.1186/s13046-018-0790-7.

Liu, L. *et al.* (2017) 'Variant 2 of KIAA0101, antagonizing its oncogenic variant 1, might be a potential therapeutic strategy in hepatocellular carcinoma', *Oncotarget*. Impact Journals, 8(27), pp. 43990–44003. doi: 10.18632/oncotarget.16702.

Lombard, D. B. (2009) 'Sirtuins at the breaking point: SIRT6 in DNA repair.', *Aging*. Impact Journals, LLC, 1(1), pp. 12–6. doi: 10.18632/aging.100014.

London, R. E. (2015) 'The structural basis of XRCC1-mediated DNA repair', *DNA Repair*. Elsevier, 30, pp. 90–103. doi: 10.1016/J.DNAREP.2015.02.005.

Lord, C. J. *et al.* (2008) 'A high-throughput RNA interference screen for DNA repair determinants of PARP inhibitor sensitivity.', *DNA repair*, 7(12), pp. 2010–9. doi: 10.1016/j.dnarep.2008.08.014.

Lord, C. J. and Ashworth, A. (2017) 'PARP inhibitors: Synthetic lethality in the clinic', *Science*, 355(6330), pp. 1152–1158. doi: 10.1126/science.aam7344.

Luvero, D., Milani, A. and Ledermann, J. A. (2014) 'Treatment options in recurrent ovarian cancer: latest evidence and clinical potential.', *Therapeutic advances in medical oncology*. SAGE Publications, 6(5), pp. 229–39. doi:

10.1177/1758834014544121.

Lynge, E. *et al.* (2014) 'Variation in detection of ductal carcinoma in situ (DCIS) during screening mammography A survey within the International Cancer Screening Network (ICSN)', *European journal of cancer (Oxford, England : 1990)*. NIH Public Access, 50(1). doi: 10.1016/J.EJCA.2013.08.013.

Madhusudan, S. *et al.* (2005) 'Isolation of a small molecule inhibitor of DNA base excision repair', *Nucleic Acids Research*, 33(15), pp. 4711–4724. doi: 10.1093/nar/gki781.

Manavathi, B. *et al.* (2013) 'Derailed estrogen signaling and breast cancer: an authentic couple.', *Endocrine reviews*. The Endocrine Society, 34(1), pp. 1–32. doi: 10.1210/er.2011-1057.

Maréchal, A. and Zou, L. (2013) 'DNA damage sensing by the ATM and ATR kinases.', *Cold Spring Harbor perspectives in biology*. Cold Spring Harbor Laboratory Press, 5(9). doi: 10.1101/cshperspect.a012716.

Marteijn, J. A. *et al.* (2014) 'Understanding nucleotide excision repair and its roles in cancer and ageing', *Nature Reviews Molecular Cell Biology*. Nature Publishing Group, 15(7), pp. 465–481. doi: 10.1038/nrm3822.

Martin, L. *et al.* (2018) 'Abstract 1943: PARG inhibitors exhibit synthetic lethality with XRCC1 deficiency and a cellular mechanism of action that is distinct from PARP inhibition', *Cancer Research*. American Association for Cancer Research, 78(13 Supplement), pp. 1943–1943. doi: 10.1158/1538-7445.AM2018-1943.

Martin, S. A. (2016) 'The DNA mismatch repair pathway', *DNA Repair in Cancer*

Therapy. Academic Press, pp. 151–177. doi: 10.1016/B978-0-12-803582-5.00006-1.

Matos, J. and West, S. C. (2014) 'Holliday junction resolution: Regulation in space and time', *DNA Repair*. Elsevier, 19, pp. 176–181. doi: 10.1016/J.DNAREP.2014.03.013.

McKinnon, P. J. (2004) 'ATM and ataxia telangiectasia.', *EMBO reports*. European Molecular Biology Organization, 5(8), pp. 772–6. doi: 10.1038/sj.embor.7400210.

McLornan, D. P., List, A. and Mufti, G. J. (2014) 'Applying Synthetic Lethality for the Selective Targeting of Cancer', *New England Journal of Medicine*, 371(18), pp. 1725–1735. doi: 10.1056/NEJMra1407390.

McShane, L. M. *et al.* (2005) 'Reporting Recommendations for Tumor Marker Prognostic Studies (REMARK)', *JNCI: Journal of the National Cancer Institute*, 97(16), pp. 1180–1184. doi: 10.1093/jnci/dji237.

Medici, D. and Nawshad, A. (2010) 'Type I collagen promotes epithelial-mesenchymal transition through ILK-dependent activation of NF-kappaB and LEF-1.', *Matrix biology : journal of the International Society for Matrix Biology*. NIH Public Access, 29(3), pp. 161–5. doi: 10.1016/j.matbio.2009.12.003.

Metallo, C. M. (2013) 'Profiling metabolic networks to study cancer metabolism', *Current Opinion in Biotechnology*. Elsevier Current Trends, 24(1), pp. 60–68. doi: 10.1016/J.COPBIO.2012.11.001.

Miller, F. R. *et al.* (2000) 'MCF10DCIS.com Xenograft Model of Human Comedo Ductal Carcinoma In Situ', *JNCI: Journal of the National Cancer Institute*. Oxford

University Press, 92(14), pp. 1185a – 1186. doi: 10.1093/jnci/92.14.1185a.

Minchom, A., Aversa, C. and Lopez, J. (2018) 'Dancing with the DNA damage response: next-generation anti-cancer therapeutic strategies.', *Therapeutic advances in medical oncology*. SAGE Publications, 10, p. 1758835918786658. doi: 10.1177/1758835918786658.

Modrich, P. (2006) 'Mechanisms in eukaryotic mismatch repair.', *The Journal of biological chemistry*. American Society for Biochemistry and Molecular Biology, 281(41), pp. 30305–9. doi: 10.1074/jbc.R600022200.

Moelans, C. B., Verschuur-Maes, A. H. and van Diest, P. J. (2011) 'Frequent promoter hypermethylation of BRCA2, CDH13, MSH6, PAX5, PAX6 and WT1 in ductal carcinoma in situ and invasive breast cancer', *The Journal of Pathology*, 225(2), pp. 222–231. doi: 10.1002/path.2930.

Moore, D. H. *et al.* (2000) 'Alterations in the expression of the DNA repair/redox enzyme APE/ref-1 in epithelial ovarian cancers.', *Clinical cancer research : an official journal of the American Association for Cancer Research*, 6(2), pp. 602–9. Available at: http://www.ncbi.nlm.nih.gov/pubmed/10690545 (Accessed: 19 June 2019).

Moser, J. *et al.* (2007) 'Sealing of Chromosomal DNA Nicks during Nucleotide Excision Repair Requires XRCC1 and DNA Ligase IIIα in a Cell-Cycle-Specific Manner', *Molecular Cell*. Cell Press, 27(2), pp. 311–323. doi: 10.1016/J.MOLCEL.2007.06.014.

Moullan, N. *et al.* (2003) 'Polymorphisms in the DNA repair gene XRCC1, breast

cancer risk, and response to radiotherapy.', *Cancer epidemiology, biomarkers & prevention : a publication of the American Association for Cancer Research, cosponsored by the American Society of Preventive Oncology*. American Association for Cancer Research, 12(11 Pt 1), pp. 1168–74. Available at: http://www.ncbi.nlm.nih.gov/pubmed/14652276 (Accessed: 27 June 2018).

Murai, J. *et al.* (2012) 'Trapping of PARP1 and PARP2 by Clinical PARP Inhibitors.', *Cancer research*. NIH Public Access, 72(21), pp. 5588–99. doi: 10.1158/0008-5472.CAN-12-2753.

Murai, J. *et al.* (2014) 'Stereospecific PARP Trapping by BMN 673 and Comparison with Olaparib and Rucaparib', *Molecular Cancer Therapeutics*. American Association for Cancer Research, 13(2), pp. 433–443. doi: 10.1158/1535-7163.MCT-13-0803.

Musella, A. *et al.* (2018) 'Rucaparib: An emerging parp inhibitor for treatment of recurrent ovarian cancer', *Cancer Treatment Reviews*, 66, pp. 7–14. doi: 10.1016/j.ctrv.2018.03.004.

Nakayama, N. *et al.* (2010) 'Gene amplification *CCNE1* is related to poor survival and potential therapeutic target in ovarian cancer', *Cancer*, 116(11), p. NA-NA. doi: 10.1002/cncr.24987.

Nelson, C. M. *et al.* (2008) 'Change in cell shape is required for matrix metalloproteinase-induced epithelial-mesenchymal transition of mammary epithelial cells.', *Journal of cellular biochemistry*. NIH Public Access, 105(1), pp. 25–33. doi: 10.1002/jcb.21821.

References

Nemec, A. A. *et al.* (2017) 'DNA Polymerase Beta Germline Variant Confers Cellular Response to Cisplatin Therapy', *Molecular Cancer Research*, 15(3), pp. 269–280. doi: 10.1158/1541-7786.MCR-16-0227-T.

Nielsen-Preiss, S. M. and Low, R. L. (2000) 'Identification of a β-like DNA Polymerase Activity in Bovine Heart Mitochondria', *Archives of Biochemistry and Biophysics*, 374(2), pp. 229–240. doi: 10.1006/abbi.1999.1590.

O'Connor, M. J. (2015) 'Targeting the DNA Damage Response in Cancer', *Molecular Cell*. Cell Press, 60(4), pp. 547–560. doi: 10.1016/J.MOLCEL.2015.10.040.

Pan, A. *et al.* (2016) 'Detection of gene copy number alterations in DCIS and invasive breast cancer by QM-FISH.', *American journal of translational research*. e-Century Publishing Corporation, 8(11), pp. 4994–5004. Available at: http://www.ncbi.nlm.nih.gov/pubmed/27904700 (Accessed: 11 March 2019).

Pang, J.-M. B., Dobrovic, A. and Fox, S. B. (2013) 'DNA methylation in ductal carcinoma in situof the breast', *Breast Cancer Research*. BioMed Central, 15(3), p. 206. doi: 10.1186/bcr3420.

Park, C. K., Jung, W. H. and Koo, J. S. (2016) 'Expression of cancer-associated fibroblast-related proteins differs between invasive lobular carcinoma and invasive ductal carcinoma', *Breast Cancer Research and Treatment*, 159(1), pp. 55–69. doi: 10.1007/s10549-016-3929-2.

Pearl, L. H. *et al.* (2015) 'Therapeutic opportunities within the DNA damage response', *Nature Reviews Cancer*. Nature Publishing Group, 15(3), pp. 166–180.

doi: 10.1038/nrc3891.

Pearson, S. J. *et al.* (2019) 'ATM-dependent activation of SIM2s regulates homologous recombination and epithelial–mesenchymal transition', *Oncogene*, 38(14), pp. 2611–2626. doi: 10.1038/s41388-018-0622-4.

Perou, C. M. *et al.* (2000) 'Molecular portraits of human breast tumours', *Nature*. Nature Publishing Group, 406(6797), pp. 747–752. doi: 10.1038/35021093.

Petridis, C. *et al.* (2016) 'Genetic predisposition to ductal carcinoma in situ of the breast', *Breast Cancer Research*. BioMed Central, 18(1), p. 22. doi: 10.1186/s13058-016-0675-7.

Pillay, N. *et al.* (2019) 'DNA Replication Vulnerabilities Render Ovarian Cancer Cells Sensitive to Poly(ADP-Ribose) Glycohydrolase Inhibitors', *Cancer Cell*. Cell Press, 35(3), pp. 519-533.e8. doi: 10.1016/J.CCELL.2019.02.004.

Powell, S. N. and Kachnic, L. A. (2003) 'Roles of BRCA1 and BRCA2 in homologous recombination, DNA replication fidelity and the cellular response to ionizing radiation', *Oncogene*. Nature Publishing Group, 22(37), pp. 5784–5791. doi: 10.1038/sj.onc.1206678.

Prakash, A. and Doublié, S. (2015) 'Base Excision Repair in the Mitochondria.', *Journal of cellular biochemistry*. NIH Public Access, 116(8), pp. 1490–9. doi: 10.1002/jcb.25103.

Prakash, R. *et al.* (2015) 'Homologous recombination and human health: the roles of BRCA1, BRCA2, and associated proteins.', *Cold Spring Harbor perspectives in biology*. Cold Spring Harbor Laboratory Press, 7(4), p. a016600. doi:

10.1101/cshperspect.a016600.

Prasad, R. *et al.* (2017) 'DNA polymerase β: A missing link of the base excision repair machinery in mammalian mitochondria', *DNA Repair*. Elsevier, 60, pp. 77–88. doi: 10.1016/J.DNAREP.2017.10.011.

Prat, J. (2015) 'Abridged republication of FIGO's staging classification for cancer of the ovary, fallopian tube, and peritoneum', *Cancer*. John Wiley and Sons Inc., 121(19), pp. 3452–3454. doi: 10.1002/cncr.29524.

Previs, R. A. *et al.* (2016) 'The rise of genomic profiling in ovarian cancer.', *Expert review of molecular diagnostics*. NIH Public Access, 16(12), pp. 1337–1351. doi: 10.1080/14737159.2016.1259069.

Provenzano, E. *et al.* (2003) 'Biological markers that predict clinical recurrence in ductal carcinoma in situ of the breast.', *European journal of cancer (Oxford, England : 1990)*, 39(5), pp. 622–30. Available at: http://www.ncbi.nlm.nih.gov/pubmed/12628841 (Accessed: 12 June 2019).

Punglia, R. S. *et al.* (2018) 'Epidemiology, Biology, Treatment, and Prevention of Ductal Carcinoma In Situ (DCIS)', *JNCI Cancer Spectrum*. Oxford University Press, 2(4). doi: 10.1093/jncics/pky063.

Rakha, E. A. *et al.* (2014) 'Nottingham Prognostic Index Plus (NPI+): a modern clinical decision making tool in breast cancer', *British Journal of Cancer*. Nature Publishing Group, 110(7), pp. 1688–1697. doi: 10.1038/bjc.2014.120.

Rakha, E. A., Reis-Filho, J. S. and Ellis, I. O. (2008) 'Basal-Like Breast Cancer: A Critical Review'. doi: 10.1200/JCO.2007.13.1748.

References

Ratajska, M. *et al.* (2017) 'Detection of BRCA1/2 mutations in circulating tumor DNA from patients with ovarian cancer.', *Oncotarget*. Impact Journals, LLC, 8(60), pp. 101325–101332. doi: 10.18632/oncotarget.20722.

Ray Chaudhuri, A. and Nussenzweig, A. (2017) 'The multifaceted roles of PARP1 in DNA repair and chromatin remodelling', *Nature Reviews Molecular Cell Biology*. Nature Publishing Group, 18(10), pp. 610–621. doi: 10.1038/nrm.2017.53.

Reid, B. M., Permuth, J. B. and Sellers, T. A. (2017) 'Epidemiology of ovarian cancer: a review.', *Cancer biology & medicine*. Chinese Anti-Cancer Association, 14(1), pp. 9–32. doi: 10.20892/j.issn.2095-3941.2016.0084.

Reid, R. J. D. *et al.* (2016) 'A Synthetic Dosage Lethal Genetic Interaction Between CKS1B and PLK1 Is Conserved in Yeast and Human Cancer Cells.', *Genetics*. Genetics, 204(2), pp. 807–819. doi: 10.1534/genetics.116.190231.

Reimers, L. L. *et al.* (2015) 'Breast Cancer Chemoprevention among High-risk Women and those with Ductal Carcinoma In Situ.', *The breast journal*. NIH Public Access, 21(4), pp. 377–86. doi: 10.1111/tbj.12418.

Reinhardt, H. C. and Schumacher, B. (2012) 'The p53 network: cellular and systemic DNA damage responses in aging and cancer.', *Trends in genetics : TIG*. Europe PMC Funders, 28(3), pp. 128–36. doi: 10.1016/j.tig.2011.12.002.

Ricci, F. *et al.* (2018) 'Recent Insights into Mucinous Ovarian Carcinoma.', *International journal of molecular sciences*. Multidisciplinary Digital Publishing Institute (MDPI), 19(6). doi: 10.3390/ijms19061569.

Ringberg, A. *et al.* (2001) 'Cell biological factors in ductal carcinoma in situ (DCIS)

of the breast-relationship to ipsilateral local recurrence and histopathological characteristics.', *European journal of cancer (Oxford, England : 1990)*, 37(12), pp. 1514–22. Available at: http://www.ncbi.nlm.nih.gov/pubmed/11506959 (Accessed: 12 June 2019).

Robertson, A. B. *et al.* (2009) 'DNA Repair in Mammalian Cells', *Cellular and Molecular Life Sciences*, 66(6), pp. 981–993. doi: 10.1007/s00018-009-8736-z.

Roka, S. *et al.* (2004) 'High nuclear grade and negative estrogen receptor are significant risk factors for recurrence in DCIS', *European Journal of Surgical Oncology (EJSO)*, 30(3), pp. 243–247. doi: 10.1016/j.ejso.2003.11.004.

Roy, R., Chun, J. and Powell, S. N. (2011) 'BRCA1 and BRCA2: different roles in a common pathway of genome protection.', *Nature reviews. Cancer*. NIH Public Access, 12(1), pp. 68–78. doi: 10.1038/nrc3181.

Russnes, H. G. *et al.* (2017) 'Breast Cancer Molecular Stratification: From Intrinsic Subtypes to Integrative Clusters', *The American Journal of Pathology*. Elsevier, 187(10), pp. 2152–2162. doi: 10.1016/J.AJPATH.2017.04.022.

Sajish, M. and Schimmel, P. (2015) 'A human tRNA synthetase is a potent PARP1-activating effector target for resveratrol', *Nature*. Nature Publishing Group, 519(7543), pp. 370–373. doi: 10.1038/nature14028.

Saldivar, J. S., Wu, X. and Gershenson, D. (2007) 'Nucleotide excision repair pathway review I: Implications in ovarian cancer and platinum sensitivity', *Gynecologic Oncology*. Academic Press, 107(1), pp. S56–S71. doi: 10.1016/J.YGYNO.2007.07.043.

References

Sänger, N. *et al.* (2014) 'Molecular Markers as Prognostic Factors in DCIS and Small Invasive Breast Cancers.', *Geburtshilfe und Frauenheilkunde*. Thieme Medical Publishers, 74(11), pp. 1016–1022. doi: 10.1055/s-0034-1383033.

Sanjari Moghaddam, A. *et al.* (2016) 'XRCC1 Gene Polymorphisms and Breast Cancer Risk: A Systematic Review and Meta- Analysis Study.', *Asian Pacific journal of cancer prevention : APJCP*, 17(S3), pp. 323–30. Available at: http://www.ncbi.nlm.nih.gov/pubmed/27165246 (Accessed: 27 June 2018).

Savagner, P. (2005) *Rise and fall of epithelial phenotype : concepts of epithelial-mesenchymal transition*. Landes Bioscience/Eurekah.com. Available at: https://books.google.co.uk/books?id=DHmA12sU4n0C&pg=PA129&lpg=PA129&dq=Alpha+2+beta+1+integrin+is+required+for+the+collagen+and+FGF-1+induced+cell+dispersion+in+a+rat+bladder+carcinoma+cell+line&source=bl&ots=_JzZTxXeuw&sig=ACfU3U3i74W5d-A8TbYw5a2fjLhFAnRUHQ&hl=en&sa=X&ved=2ahUKEwjl3obP1_rgAhUQM-wKHXEhB0gQ6AEwAnoECAIQAQ#v=onepage&q=Alpha 2 beta 1 integrin is required for the collagen and FGF-1 induced cell dispersion in a rat bladder carcinoma cell line&f=false (Accessed: 11 March 2019).

Schwartz, G. F. *et al.* (2000) 'Consensus Conference on the Treatment of In Situ Ductal Carcinoma of the Breast, April 22-25, 1999.', *Cancer*, 88(4), pp. 946–54. Available at: http://www.ncbi.nlm.nih.gov/pubmed/10679665 (Accessed: 19 March 2019).

Scribner, K. C., Behbod, F. and Porter, W. W. (2013) 'Regulation of DCIS to invasive breast cancer progression by Singleminded-2s (SIM2s).', *Oncogene*. NIH Public

Access, 32(21), pp. 2631–9. doi: 10.1038/onc.2012.286.

Seibold, P. *et al.* (2015) 'XRCC1 Polymorphism Associated With Late Toxicity After Radiation Therapy in Breast Cancer Patients', *International Journal of Radiation Oncology*Biology*Physics*. Elsevier, 92(5), pp. 1084–1092. doi: 10.1016/J.IJROBP.2015.04.011.

Seki, M. *et al.* (2004) 'High-efficiency bypass of DNA damage by human DNA polymerase Q', *The EMBO Journal*. European Molecular Biology Organization, 23(22), p. 4484. doi: 10.1038/SJ.EMBOJ.7600424.

Shah, F. *et al.* (2017) 'Exploiting the Ref-1-APE1 node in cancer signaling and other diseases: from bench to clinic', *npj Precision Oncology*. Nature Publishing Group, 1(1), p. 19. doi: 10.1038/s41698-017-0023-0.

Shah, R., Rosso, K. and Nathanson, S. D. (2014) 'Pathogenesis, prevention, diagnosis and treatment of breast cancer.', *World journal of clinical oncology*. Baishideng Publishing Group Inc, 5(3), pp. 283–98. doi: 10.5306/wjco.v5.i3.283.

Shan, L. *et al.* (2014) 'GATA3 cooperates with PARP1 to regulate CCND1 transcription through modulating histone H1 incorporation', *Oncogene*. Nature Publishing Group, 33(24), pp. 3205–3216. doi: 10.1038/onc.2013.270.

Shen, J. *et al.* (2015) 'ARID1A Deficiency Impairs the DNA Damage Checkpoint and Sensitizes Cells to PARP Inhibitors', *Cancer Discovery*, 5(7), pp. 752–767. doi: 10.1158/2159-8290.CD-14-0849.

Sherbenou, D. W. and Druker, B. J. (2007) 'Applying the discovery of the Philadelphia chromosome.', *The Journal of clinical investigation*. American Society

for Clinical Investigation, 117(8), pp. 2067–74. doi: 10.1172/JCI31988.

Shibani Dalal, ‡ *et al.* (2005) ‘Prostate-Cancer-Associated I260M Variant of DNA Polymerase β Is a Sequence-Specific Mutator†’. American Chemical Society . doi: 10.1021/BI051179Z.

Shih, I.-M. and Kurman, R. J. (2004) ‘Ovarian tumorigenesis: a proposed model based on morphological and molecular genetic analysis.’, *The American journal of pathology*, 164(5), pp. 1511–8. doi: 10.1016/s0002-9440(10)63708-x.

Shirai, H. *et al.* (2013) ‘PARG dysfunction enhances DNA double strand break formation in S-phase after alkylation DNA damage and augments different cell death pathways’, *Cell Death & Disease*. Nature Publishing Group, 4(6), pp. e656–e656. doi: 10.1038/cddis.2013.133.

Simpson, J. F. and Page, D. L. (2000) ‘The p53 tumor suppressor gene in ductal carcinoma in situ of the breast.’, *The American journal of pathology*. Elsevier, 156(1), pp. 5–6. doi: 10.1016/S0002-9440(10)64698-6.

Solin, L. J. *et al.* (2013) ‘A Multigene Expression Assay to Predict Local Recurrence Risk for Ductal Carcinoma In Situ of the Breast’, *JNCI Journal of the National Cancer Institute*. Narnia, 105(10), pp. 701–710. doi: 10.1093/jnci/djt067.

Soni, D. V. *et al.* (2008) ‘Cyclin B1 is rate limiting but not essential for mitotic entry and progression in mammalian somatic cells’, *Cell Cycle*. doi: 10.4161/cc.7.9.5711.

Sørlie, T. *et al.* (2001) ‘Gene expression patterns of breast carcinomas distinguish tumor subclasses with clinical implications.’, *Proceedings of the National Academy of Sciences of the United States of America*. National Academy of Sciences, 98(19),

pp. 10869–74. doi: 10.1073/pnas.191367098.

Srivastava, A. K. *et al.* (2015) ‘Enhanced expression of DNA polymerase eta contributes to cisplatin resistance of ovarian cancer stem cells.’, *Proceedings of the National Academy of Sciences of the United States of America*. National Academy of Sciences, 112(14), pp. 4411–6. doi: 10.1073/pnas.1421365112.

Starcevic, D., Dalal, S. and Sweasy, J. B. (2004) ‘Is there a link between DNA polymerase beta and cancer?’, *Cell cycle (Georgetown, Tex.)*, 3(8), pp. 998–1001. Available at: http://www.ncbi.nlm.nih.gov/pubmed/15280658 (Accessed: 5 May 2019).

Stephens, P. J. *et al.* (2012) ‘The landscape of cancer genes and mutational processes in breast cancer’, *Nature*. Nature Publishing Group, 486(7403), pp. 400–404. doi: 10.1038/nature11017.

Stylianou, S., Clarke, R. B. and Brennan, K. (2006) ‘Aberrant Activation of Notch Signaling in Human Breast Cancer’, *Cancer Research*, 66(3), pp. 1517–1525. doi: 10.1158/0008-5472.CAN-05-3054.

Sugo, N. *et al.* (2000) ‘Neonatal lethality with abnormal neurogenesis in mice deficient in DNA polymerase beta’, *The EMBO Journal*. EMBO Press, 19(6), pp. 1397–1404. doi: 10.1093/emboj/19.6.1397.

Sultana, Rebeka *et al.* (2013) ‘Targeting XRCC1 deficiency in breast cancer for personalized therapy.’, *Cancer research*. American Association for Cancer Research, 73(5), pp. 1621–34. doi: 10.1158/0008-5472.CAN-12-2929.

Sultana, R. *et al.* (2013) ‘Targeting XRCC1 Deficiency in Breast Cancer for

Personalized Therapy', *Cancer Research*, 73(5), pp. 1621–1634. doi: 10.1158/0008-5472.CAN-12-2929.

Sun, C. *et al.* (2014) 'Phosphorylation of ribosomal protein S6 confers PARP inhibitor resistance in BRCA1-deficient cancers', *Oncotarget*, 5(10), pp. 3375–85. doi: 10.18632/oncotarget.1952.

Surjana, D., Halliday, G. M. and Damian, D. L. (2010) 'Role of nicotinamide in DNA damage, mutagenesis, and DNA repair.', *Journal of nucleic acids*. Hindawi, 2010. doi: 10.4061/2010/157591.

Sutherland, R. L. and Musgrove, E. A. (2004) 'Cyclins and Breast Cancer', *Journal of Mammary Gland Biology and Neoplasia*, 9(1), pp. 95–104. doi: 10.1023/B:JOMG.0000023591.45568.77.

Sweasy, J. B. (2003) 'Fidelity mechanisms of DNA polymerase beta.', *Progress in nucleic acid research and molecular biology*, 73, pp. 137–69. doi: 10.1016/S0079-6603(03)01005-5.

Sykora, P. *et al.* (2017) 'DNA Polymerase Beta Participates in Mitochondrial DNA Repair.', *Molecular and cellular biology*. American Society for Microbiology Journals, 37(16), pp. e00237-17. doi: 10.1128/MCB.00237-17.

Szántó, M. *et al.* (2012) 'Poly(ADP-ribose) polymerase-2: emerging transcriptional roles of a DNA-repair protein', *Cellular and Molecular Life Sciences*, 69(24), pp. 4079–4092. doi: 10.1007/s00018-012-1003-8.

Tan, X. *et al.* (2015) 'Clinical significance of a point mutation in DNA polymerase beta (POLB) gene in gastric cancer.', *International journal of biological sciences*.

Ivyspring International Publisher, 11(2), pp. 144–55. doi: 10.7150/ijbs.10692.

Tebbs, R. S. *et al.* (1999) 'Requirement for theXrcc1DNA Base Excision Repair Gene during Early Mouse Development', *Developmental Biology*, 208(2), pp. 513–529. doi: 10.1006/dbio.1999.9232.

Teicher, B. A., Linehan, W. M. and Helman, L. J. (2012) 'Targeting Cancer Metabolism', *Clinical Cancer Research*. American Association for Cancer Research, 18(20), pp. 5537–5545. doi: 10.1158/1078-0432.CCR-12-2587.

Tewari, K. S. *et al.* (2016) 'Early initiation of chemotherapy following complete resection of advanced ovarian cancer associated with improved survival: NRG Oncology/Gynecologic Oncology Group study', *Annals of Oncology*, 27(1), pp. 114–121. doi: 10.1093/annonc/mdv500.

To, T. *et al.* (2014) 'Is carcinoma *in situ* a precursor lesion of invasive breast cancer?', *International Journal of Cancer*, 135(7), pp. 1646–1652. doi: 10.1002/ijc.28803.

Trowbridge, K. *et al.* (2007) 'Synthetic lethality of Drosophila in the absence of the MUS81 endonuclease and the DmBlm helicase is associated with elevated apoptosis.', *Genetics*. Genetics Society of America, 176(4), pp. 1993–2001. doi: 10.1534/genetics.106.070060.

Uchiyama, Y. *et al.* (2009) 'Distribution and roles of X-family DNA polymerases in eukaryotes', *Biochimie*, 91(2), pp. 165–170. doi: 10.1016/j.biochi.2008.07.005.

Underhill, C., Toulmonde, M. and Bonnefoi, H. (2011) 'A review of PARP inhibitors: from bench to bedside', *Annals of Oncology*. Oxford University Press, 22(2), pp.

268–279. doi: 10.1093/annonc/mdq322.

Vaisman, A. and Chaney, S. G. (2000) ‘The efficiency and fidelity of translesion synthesis past cisplatin and oxaliplatin GpG adducts by human DNA polymerase beta.’, *The Journal of biological chemistry*. American Society for Biochemistry and Molecular Biology, 275(17), pp. 13017–25. doi: 10.1074/jbc.275.17.13017.

Villalonga-Planells, R. *et al.* (2011) ‘Activation of p53 by Nutlin-3a Induces Apoptosis and Cellular Senescence in Human Glioblastoma Multiforme’, *PLoS ONE*. Edited by M. Lesniak. Public Library of Science, 6(4), p. e18588. doi: 10.1371/journal.pone.0018588.

Vincent-Salomon, A. *et al.* (2008) ‘Integrated Genomic and Transcriptomic Analysis of Ductal Carcinoma In situ of the Breast’, *Clinical Cancer Research*. American Association for Cancer Research, 14(7), pp. 1956–1965. doi: 10.1158/1078-0432.CCR-07-1465.

Vogel, V. G. *et al.* (2010) ‘Update of the National Surgical Adjuvant Breast and Bowel Project Study of Tamoxifen and Raloxifene (STAR) P-2 Trial: Preventing Breast Cancer’, *Cancer Prevention Research*, 3(6), pp. 696–706. doi: 10.1158/1940-6207.CAPR-10-0076.

Wallace, S. S., Murphy, D. L. and Sweasy, J. B. (2012) ‘Base excision repair and cancer.’, *Cancer letters*. NIH Public Access, 327(1–2), pp. 73–89. doi: 10.1016/j.canlet.2011.12.038.

Wang, B. *et al.* (2016) ‘Discovery and Characterization of (8S,9R)-5-Fluoro-8-(4-fluorophenyl)-9-(1-methyl-1H-1,2,4-triazol-5-yl)-2,7,8,9-tetrahydro-3H-

pyrido[4,3,2-de]phthalazin-3-one (BMN 673, Talazoparib), a Novel, Highly Potent, and Orally Efficacious Poly(ADP-ribose) Polymer', *Journal of medicinal chemistry*, 59(1), pp. 335–57. doi: 10.1021/acs.jmedchem.5b01498.

Wang, C. *et al.* (2018) 'Estrogen promotes estrogen receptor negative BRCA1-deficient tumor initiation and progression', *Breast Cancer Research*. BioMed Central, 20(1), p. 74. doi: 10.1186/s13058-018-0996-9.

Wang, D., Luo, M. and Kelley, M. R. (2004) 'Human apurinic endonuclease 1 (APE1) expression and prognostic significance in osteosarcoma: enhanced sensitivity of osteosarcoma to DNA damaging agents using silencing RNA APE1 expression inhibition.', *Molecular cancer therapeutics*, 3(6), pp. 679–86. Available at: http://www.ncbi.nlm.nih.gov/pubmed/15210853 (Accessed: 19 June 2019).

Wang, H. *et al.* (2018) 'Angiogenesis Inhibitors for the Treatment of Ovarian Cancer: An Updated Systematic Review and Meta-analysis of Randomized Controlled Trials.', *International journal of gynecological cancer : official journal of the International Gynecological Cancer Society*. Wolters Kluwer Health, 28(5), pp. 903–914. doi: 10.1097/IGC.0000000000001258.

Wang, Y. *et al.* (2016) 'RING domain-deficient BRCA1 promotes PARP inhibitor and platinum resistance.', *The Journal of clinical investigation*. American Society for Clinical Investigation, 126(8), pp. 3145–57. doi: 10.1172/JCI87033.

Wang, Y. K. *et al.* (2017) 'Genomic consequences of aberrant DNA repair mechanisms stratify ovarian cancer histotypes', *Nature Genetics*. Nature Publishing Group, 49(6), pp. 856–865. doi: 10.1038/ng.3849.

References

Wheler, J. J. *et al.* (2016) 'TP53 Alterations Correlate with Response to VEGF/VEGFR Inhibitors: Implications for Targeted Therapeutics', *Molecular Cancer Therapeutics*, 15(10), pp. 2475–2485. doi: 10.1158/1535-7163.MCT-16-0196.

Winzer, K.-J. *et al.* (2016) 'Improving the Prognostic Ability through Better Use of Standard Clinical Data - The Nottingham Prognostic Index as an Example', *PLOS ONE*. Edited by Y. St-Pierre. Public Library of Science, 11(3), p. e0149977. doi: 10.1371/journal.pone.0149977.

Wyman, C. and Kanaar, R. (2006) 'DNA Double-Strand Break Repair: All's Well that Ends Well', *Annual Review of Genetics*, 40(1), pp. 363–383. doi: 10.1146/annurev.genet.40.110405.090451.

Yamtich, J. and Sweasy, J. B. (2010) 'DNA polymerase family X: function, structure, and cellular roles.', *Biochimica et biophysica acta*. NIH Public Access, 1804(5), pp. 1136–50. doi: 10.1016/j.bbapap.2009.07.008.

Yang, J. *et al.* (2010) 'Cells deficient in the base excision repair protein, DNA polymerase beta, are hypersensitive to oxaliplatin chemotherapy', *Oncogene*, 29(3), pp. 463–468. doi: 10.1038/onc.2009.327.

Yang, L. *et al.* (2013) 'Identification of Poly(ADP-Ribose) Polymerase-1 as a Cell Cycle Regulator through Modulating Sp1 Mediated Transcription in Human Hepatoma Cells', *PLoS ONE*. Edited by S. A. Andrabi. Public Library of Science, 8(12), p. e82872. doi: 10.1371/journal.pone.0082872.

Yang, R. L. *et al.* (2015) 'DCIS in BRCA1 and BRCA2 mutation carriers: prevalence, phenotype, and expression of oncodrivers C-MET and HER3', *Journal of*

Translational Medicine, 13(1), p. 335. doi: 10.1186/s12967-015-0698-3.

Yao, Y. and Dai, W. (2014) 'Genomic Instability and Cancer.', *Journal of carcinogenesis & mutagenesis*. NIH Public Access, 5. doi: 10.4172/2157-2518.1000165.

Ying, W. *et al.* (2005) 'NAD+ as a metabolic link between DNA damage and cell death', *Journal of Neuroscience Research*, 79(1–2), pp. 216–223. doi: 10.1002/jnr.20289.

Yu, S.-W. *et al.* (2006) 'Apoptosis-inducing factor mediates poly(ADP-ribose) (PAR) polymer-induced cell death.', *Proceedings of the National Academy of Sciences of the United States of America*. National Academy of Sciences, 103(48), pp. 18314–9. doi: 10.1073/pnas.0606528103.

Yuan, Z. *et al.* (2015) 'Predictive assessment in pharmacogenetics of XRCC1 gene on clinical outcomes of advanced lung cancer patients treated with platinum-based chemotherapy', *Scientific Reports*. Nature Publishing Group, 5(1), p. 16482. doi: 10.1038/srep16482.

Yue, P. Y. K. *et al.* (2010) 'A Simplified Method for Quantifying Cell Migration/Wound Healing in 96-Well Plates', *Journal of Biomolecular Screening*, 15(4), pp. 427–433. doi: 10.1177/1087057110361772.

Zannini, L., Delia, D. and Buscemi, G. (2014) 'CHK2 kinase in the DNA damage response and beyond', *Journal of Molecular Cell Biology*. Oxford University Press, 6(6), p. 442. doi: 10.1093/JMCB/MJU045.

Zecchini, V. and Frezza, C. (2017) 'Metabolic synthetic lethality in cancer therapy',

Biochimica et Biophysica Acta (BBA) - Bioenergetics. Elsevier, 1858(8), pp. 723–731. doi: 10.1016/J.BBABIO.2016.12.003.

Zhang, F. *et al.* (2017) 'The transcription factor GATA3 is required for homologous recombination repair by regulating CtIP expression', *Oncogene*, 36(36), pp. 5168–5176. doi: 10.1038/onc.2017.127.

Zhang, G. *et al.* (2019) 'Combinatorial therapy of immune checkpoint and cancer pathways provides a novel perspective on ovarian cancer treatment (Review)', *Oncology Letters*. Spandidos Publications, 17(3), pp. 2583–2591. doi: 10.3892/ol.2019.9902.

Zhang, X. *et al.* (2016) 'Predictors for local invasive recurrence of ductal carcinoma in situ of the breast: a meta-analysis.', *European journal of cancer prevention : the official journal of the European Cancer Prevention Organisation (ECP)*. Wolters Kluwer Health, 25(1), pp. 19–28. doi: 10.1097/CEJ.0000000000000131.

Zhang, Y. and Hunter, T. (2014) 'Roles of Chk1 in cell biology and cancer therapy', *International Journal of Cancer*, pp. 1013–1023. doi: 10.1002/ijc.28226.

Zhao, X. *et al.* (2017) 'Cell cycle-dependent control of homologous recombination', *Acta Biochimica et Biophysica Sinica*, 49(8), pp. 655–668. doi: 10.1093/abbs/gmx055.

Zheng, H. *et al.* (2013) 'DNA polymerase beta overexpression correlates with poor prognosis in esophageal cancer patients', *Chinese Science Bulletin*. Springer Berlin Heidelberg, 58(26), pp. 3274–3279. doi: 10.1007/s11434-013-5956-2.

Zhou, B.-B. S. and Elledge, S. J. (2000) 'The DNA damage response: putting

checkpoints in perspective', *Nature*. Nature Publishing Group, 408(6811), pp. 433–439. doi: 10.1038/35044005.

Zhou, W. *et al.* (2010) 'Long-term survival of women with basal-like ductal carcinoma in situ of the breast: a population-based cohort study', *BMC Cancer*. BioMed Central, 10(1), p. 653. doi: 10.1186/1471-2407-10-653.

van Zyl, B., Tang, D. and Bowden, N. A. (2018) 'Biomarkers of platinum resistance in ovarian cancer: what can we use to improve treatment', *Endocrine-Related Cancer*, 25(5), pp. R303–R318. doi: 10.1530/ERC-17-0336.